

Targeted Delivery of Arsenic Compounds to Tumor Cells Using Polymeric Micelles

by

Qi Zhang

A thesis submitted in partial fulfillment of the requirements for the degree of

Doctor of Philosophy

Medical Sciences – Laboratory Medicine and Pathology

University of Alberta

© Qi Zhang, 2016

## Abstract

Arsenic trioxide (ATO), dissolved in water as arsenous acid or inorganic arsenite ( $\text{As}^{\text{III}}$ ), is an effective chemotherapeutic agent against acute promyelocytic leukemia (APL). It has been investigated as a potential treatment for a variety of solid tumors although with much poorer efficacy than for APL. The toxicity of  $\text{As}^{\text{III}}$  and its derivatives has limited its use. Nano drug delivery systems such as polymeric micelles with the capability to deliver the drug into targeted tumor areas are expected to improve the therapeutic efficacy of arsenic therapy for solid tumor treatment and alleviate its adverse side effects. The ultimate goal of this study is to develop a polymeric micelle system for targeted delivery of arsenicals to specific tumor cells. Towards this goal, a strategy involving thiol functionalization of polymer chains was developed to effectively encapsulate trivalent arsenic compounds into polymeric micelles. The mercaptohexylamino group was conjugated to methoxy poly(ethylene oxide)-*block*-poly( $\alpha$ -carboxylate- $\epsilon$ -caprolactone) (PEO-*b*-PCCL) via an amide bond, forming thiolated methoxy poly(ethylene oxide)-*block*-poly[ $\alpha$ -(6-mercaptohexyl amino)carboxylate- $\epsilon$ -caprolactone] [PEO-*b*-P(CCLC<sub>6</sub>-SH)]. A higher arsenic loading content was achieved with thiolated micelles compared to micelles without thiol groups in the micelle core. The weight percentage of encapsulated arsenic element in the micelles was in the range of 2.5 ~ 4.0 wt% depending on the total thiol amount in the micelles, which corresponded with ~ 0.65 mole of arsenic per mole of thiol groups. The formation of the As-S bond in the micelle core slowed down the arsenic release from the micelles. The arsenic release could be triggered by addition of thiol-containing small molecules such as glutathione (GSH), which compete with polymer chains for arsenic binding. Mixed micelles formed from a mixture of PEO-*b*-PCCL and PEO-*b*-P(CCLC<sub>6</sub>-SH) polymers with surface modification of affinity ligands, i.e. RGD-containing peptides, were prepared to facilitate the targeted delivery of arsenic to targeting tumor cells.

Although the peptide modification enhanced the cytotoxicity and cellular uptake of arsenic encapsulated in mixed micelles, the high arsenic burst release (~50% of initially encapsulated As<sup>III</sup>) from mixed micelles diminished the targeting activity of affinity ligands, and peptide-decorated mixed micelles did not exhibit superior targeting performance than non-mixed micelles or free As<sup>III</sup>. The arsenic burst release can be reduced by enhancing the micelle stability. Mixed micelles formed from a mixture of PEO-*b*-PBCL and PEO-*b*-P(CCLC<sub>6</sub>-SH) and terpolymeric micelles formed from PEO-*b*-P(CCLC<sub>6</sub>-SH)-*b*-PCL both had reduced As<sup>III</sup> burst release (~20% of initially encapsulated As<sup>III</sup>). The incorporation of the PCL block into the PEO-*b*-P(CCLC<sub>6</sub>-SH) polymer not only enhanced the micelle stability, but also added extra complexity to the micelle structure. The chain arrangement of the polyester block influenced the micelle surface charge by affecting the micelle structure, which further affected the cellular uptake of encapsulated arsenic. The results revealed in this thesis demonstrate that polymeric micelles are a versatile carrier with great tunable properties and have great potential for the successful targeted delivery of arsenic chemotherapeutic agents to solid tumors.

## Preface

Contents in **Sections 1.1.1, 1.1.2.3, and 1.1.4.2 in Chapter 1** of this thesis has been published in the review “Therapeutic and analytical applications of arsenic binding to proteins,” *Metallomics*, 2015, 7, 39–55, authored by Chen BB, Liu QQ, Popowich A, Shen SW, Yan XW, Zhang Q, Li X-F, Weifeld M, Cullen WR, and Le XC. I was responsible for the literature review on the “Arsenic-based drugs” section. Chen BB and Popowich A were responsible for the literature review on the “Purification of specific proteins” section. Liu QQ was responsible for the literature review on the “Arsenic biosensors” section. Yan XW was responsible for the literature review on the “Imaging of cellular events” section. Shen SW contributed to the scope definition of the review and overall manuscript structure. Li X-F, Weifeld M, and Cullen WR contributed to manuscript edits. Le XC was the corresponding author and was involved with concept formation and manuscript composition.

**Chapter 2** of this thesis has been published as Zhang Q, Vakili MR, Li X-F, Lavasanifar A, Le XC, “Polymeric micelles for GSH-triggered delivery of arsenic species to cancer cells,” *Biomaterials*, 2014, 35, 7088–7100. I was responsible for the study design, experiment conduction, data collection and analysis as well as manuscript composition. Vakili MR assisted with polymer synthesis and contributed to NMR spectrum interpretation and manuscript edits. Li X-F contributed to manuscript edits. Lavasanifar A and Le XC were corresponding authors and were involved with concept formation and manuscript composition.

## **Acknowledgements**

I would like to express my most sincere gratitude to my supervisor Dr. X. Chris Le and my co-supervisor Dr. Afsaneh Lavasanifar for their support, guidance, inspiration, motivation, and insight throughout my whole PhD program. Dr. Le understands my research interests and strengths better than I myself do. I am grateful that Dr. Le initiated this interdisciplinary arsenic delivery project, allowing me to explore the massive material world with one focused objective. Without Dr. Le's patient guidance, I would have been lost in miscellaneous problems encountered during the research and have completed or achieved nothing. Dr. Lavasanifar offers me her strong support in study design and manuscript publishing. My PhD research project would not be accomplished without her expertise in polymeric micelle research. Dr. Lavasanifar sets a great role model as a successful female scientist and entrepreneur. I always marvel at her great personality and strong leadership.

I would like to thank my supervisory committee members, Dr. Xing-Fang Li and Dr. Michael Weinfeld, for their insightful discussion, comments, and suggestions.

My appreciation goes to Dr. Mohammad Reza Vakili for training me and helping me with polymer synthesis, and for his advice and encouragement when my research progress was extremely slow. I also thank Ms. Xiufen Lu for training me and helping me with the ICP-MS and arsenic analysis; Dr. Nazila Safaei Nikouei, Dr. Shyam Garg, and Ms. Hoda Soleymani Abyaneh for discussions about micelle preparation and characterization; Dr. Shengwen Shen, Dr. Yanming Liu, and Ms. Jinhua Li for discussions about cell biology and cell culture; Dr. Hongquan Zhang, Dr. Zhixin Wang, Dr. Xiaowen Yan, and Dr. Hanyong Peng for discussions about experiment design.

Thank you to Ms. Katerina Carastathis and Ms. Dianne Sergy, for their support and for organizing so many enjoyable seasonal parties. Thank you to all my friends in both the AET division and in Dr. Lavasanifar's group for sharing this wonderful journey with me.

Finally, I wish to thank my partner Lei and my cat Don for keeping my company. My deep gratitude and regret goes to my dear mom and dad for bearing with me being away from home for these years and caring for me by showering me with all their understanding and encouragement, and sending me annual New Year's goods from home.

# TABLE OF CONTENTS

## CHAPTER 1. INTRODUCTION ..... 1

1.1	THERAPEUTIC APPLICATION OF ARSENIC COMPOUNDS .....	1
1.1.1	<i>History of therapeutic application of arsenic compounds</i> .....	1
1.1.2	<i>Mechanism of action</i> .....	2
1.1.3	<i>Toxicity and adverse side effects of arsenic therapy</i> .....	13
1.1.4	<i>Development of arsenic therapy</i> .....	15
1.2	POLYMERIC MICELLES AS NANO DRUG DELIVERY CARRIERS .....	29
1.2.1	<i>Nanomedicine</i> .....	29
1.2.2	<i>Advantages of micelles derived from the versatile polymer structures</i> .....	31
1.2.3	<i>PEO-b-PCL based polymeric micelles</i> .....	43
1.3	SCOPE OF THIS THESIS.....	45
1.4	REFERENCES.....	47

## CHAPTER 2. STRATEGY DEVELOPMENT FOR ENHANCED ARSENIC ENCAPSULATION AND GSH-TRIGGERED

## ARSENIC RELEASE IN POLYMERIC MICELLES ..... 75

2.1	INTRODUCTION .....	75
2.2	MATERIALS AND METHODS .....	76
2.2.1	<i>Materials and cell line information</i> .....	76
2.2.2	<i>Synthesis of thiol-functionalized copolymer PEO-b-P(CCLC<sub>6</sub>-SH)</i> .....	77
2.2.3	<i>Synthesis of alkyl substituted PEO-b-PCCL copolymer without thiol functional group PEO-b-P(CCLC<sub>6</sub>)</i> 78	
2.2.4	<i>Preparation of micelles loaded with phenylarsine oxide (PAO)</i> .....	79
2.2.5	<i>Determination of arsenic loading in the micelles</i> .....	79

2.2.6	<i>Characterization of polymers and their self-assembled structures</i> .....	80
2.2.7	<i>In vitro polymer stability study</i> .....	82
2.2.8	<i>In vitro release of arsenic from the polymer micelles</i> .....	82
2.2.9	<i>In vitro cell cytotoxicity of arsenic before and after encapsulation in micelles</i> .....	83
2.2.10	<i>Data analysis</i> .....	84
2.3	RESULTS .....	84
2.3.1	<i>Polymer synthesis and characterization</i> .....	84
2.3.2	<i>Optimization of PAO loading into polymeric micelles</i> .....	87
2.3.3	<i>Characterization of the assembly of block polymers</i> .....	88
2.3.4	<i>Stability study</i> .....	94
2.3.5	<i>In vitro release study</i> .....	95
2.3.6	<i>In vitro cytotoxicity study of block polymers</i> .....	98
2.4	DISCUSSION .....	99
2.5	CONCLUSION .....	105
2.6	REFERENCES.....	106

## **CHAPTER 3. MIXED MICELLES FOR TARGETED DELIVERY OF ARSENIC COMPOUNDS .....109**

3.1	INTRODUCTION .....	109
3.2	GRGDS-PEO <sup>6000</sup> -B-PCCL <sub>15</sub> /PEO <sup>5000</sup> -B-PCCL <sub>15</sub> MIXED MICELLE SYSTEM FOR ARSENIC ENCAPSULATION .....	111
3.2.1	<i>Materials and Methods</i> .....	111
3.2.2	<i>Results</i> .....	120
3.3	DIFFERENT MIXED MICELLES FOR ARSENIC ENCAPSULATION.....	140
3.3.1	<i>Methods</i> .....	140
3.3.2	<i>Results</i> .....	141
3.4	DISCUSSION .....	150

3.5	CONCLUSION .....	153
3.6	REFERENCES.....	154

## **CHAPTER 4. TERPOLYMERIC MICELLES FOR ARSENIC DELIVERY WITH ENHANCED MICELLE STABILITY AND INCREASED ARSENIC CELLULAR UPTAKE .....156**

4.1	INTRODUCTION .....	156
4.2	MATERIALS AND METHODS .....	157
4.2.1	<i>Materials and cell information.....</i>	<i>157</i>
4.2.2	<i>Terpolymer synthesis and thiol functionalization.....</i>	<i>158</i>
4.2.3	<i>Encapsulation of As<sup>III</sup>.....</i>	<i>162</i>
4.2.4	<i>Characterization of micelles .....</i>	<i>162</i>
4.2.5	<i>Micelle <sup>1</sup>H-NMR in D<sub>2</sub>O.....</i>	<i>163</i>
4.2.6	<i>In vitro arsenic release from the micelles .....</i>	<i>163</i>
4.2.7	<i>Cellular uptake of iAs<sup>III</sup>-encapsulated micelles.....</i>	<i>164</i>
4.2.8	<i>Data analysis.....</i>	<i>165</i>
4.3	RESULTS .....	165
4.3.1	<i>Synthesis, thiol-functionalization, and As<sup>III</sup> encapsulation.....</i>	<i>165</i>
4.3.2	<i>The effect of terpolymer structure on micellar stability .....</i>	<i>174</i>
4.3.3	<i>The effect of terpolymer structure on micelle surface charge at different pH.....</i>	<i>177</i>
4.3.4	<i>Investigations on the block arrangement in the micellar structure by <sup>1</sup>H-NMR .....</i>	<i>180</i>
4.3.5	<i>Morphology of iAs<sup>III</sup>-loaded micelles. ....</i>	<i>185</i>
4.3.6	<i>In vitro arsenic release from micelles .....</i>	<i>186</i>
4.3.7	<i>Cellular uptake of encapsulated As<sup>III</sup>.....</i>	<i>189</i>
4.4	DISCUSSION .....	193
4.5	CONCLUSIONS .....	197
4.6	REFERENCES.....	197

**CHAPTER 5. GENERAL DISCUSSION AND CONCLUSIONS 200**

5.1 GENERAL DISCUSSION .....200

5.2 CONCLUSIONS .....204

5.3 FUTURE WORK AND PERSPECTIVES .....205

5.4 REFERENCES.....206

**BIBLIOGRAPHY .....208**

## List of Tables

<b>Table 1.1. Chemical structures of GSAO, PENAO, and ZIO-101.....</b>	<b>20</b>
<b>Table 2.1. Molecular weight of block polymers .....</b>	<b>85</b>
<b>Table 4.1. Molecular weight, composition, critical micelle concentration (CMC) and size of block polymers.....</b>	<b>173</b>
<b>Table 4.2. Ratio of CL, CCL, and CCL-C6-SH components in terpolymers calculated from <sup>1</sup>H-NMR spectra obtained in CDCl<sub>3</sub> and D<sub>2</sub>O.....</b>	<b>183</b>

## List of Schemes

<b>Scheme 2.1. Synthesis of thiol-containing polymer PEO-<i>b</i>-P(CCLC<sub>6</sub>-SH) and the control polymer without thiol groups PEO-<i>b</i>-P(CCLC<sub>6</sub>).....</b>	<b>78</b>
<b>Scheme 2.2. Encapsulation of PAO into PEO-<i>b</i>-P(CCLC<sub>6</sub>-SH) and PEO-<i>b</i>-P(CCLC<sub>6</sub>) micelles. ....</b>	<b>79</b>
<b>Scheme 2.3. The dissociation of PAO from PEO-<i>b</i>-P(CCLC<sub>6</sub>-S-PAO) (A) in buffer without GSH, and (B) the competition reaction between GSH and PEO-<i>b</i>-P(CCLC<sub>6</sub>-S-PAO). ....</b>	<b>97</b>
<b>Scheme 3.1. Synthesis of acetal-PEO and acetal-PEO-<i>b</i>-PCCL. ....</b>	<b>113</b>
<b>Scheme 4.1. Synthesis of PEO/PCL/PCCL terpolymers and thiol-functionalized terpolymers. ....</b>	<b>161</b>
<b>Scheme 4.2. Proposed structures of micelles. ....</b>	<b>184</b>

## List of Equations

$M_n = \Sigma(n_i M_i) / \Sigma n_i$	Equation 3-1 .....	120
$M_w = \Sigma(n_i M_i^2) / \Sigma(n_i M_i)$	Equation 3-2 .....	120
$PD = M_w / M_n$	Equation 3-3 .....	121

## List of Figures

Figure 1.1. Schema illustrating proposed sites of action of ATO in interrupting a reciprocal feedback loop between leukemic cells and endothelium.....	12
Figure 1.2. Metabolism and transportation of GSAO, PENAO and ZIO-101 by endothelial cells.....	24
Figure 1.3. Structure of micelles.....	30
Figure 1.4. Structure of doxorubicin (DOX). .....	32
Figure 1.5. Stimuli-triggered release. ....	35
Figure 1.6 Schema illustrating H <sub>2</sub> O <sub>2</sub> -triggered degradation of polymers containing boronic ester.....	38
Figure 1.7. Targeting with affinity ligands. ....	43
Figure 2.1. <sup>1</sup> H NMR spectra of PEO- <i>b</i> -PCCL (A), PEO- <i>b</i> -P(CCLC <sub>6</sub> ) (B), PEO- <i>b</i> -P(CCLC <sub>6</sub> -SH) (C), and PEO- <i>b</i> -P(CCLC <sub>6</sub> -S-PAO) (D) in CDCl <sub>3</sub> . ....	86
Figure 2.2. FT-IR spectra of PEO- <i>b</i> -PCCL, PEO- <i>b</i> -P(CCLC <sub>6</sub> -SH), and PEO- <i>b</i> -P(CCLC <sub>6</sub> -S-PAO) in KBr pellets.....	87
Figure 2.3. Arsenic loading in PEO- <i>b</i> -P(CCLC <sub>6</sub> ) and PEO- <i>b</i> -P(CCLC <sub>6</sub> -SH) micelles with different PAO amounts added.....	88
Figure 2.4. CMC determination of PEO- <i>b</i> -PCCL, PEO- <i>b</i> -P(CCLC <sub>6</sub> -SH), and PEO- <i>b</i> -P(CCLC <sub>6</sub> -S-PAO). ....	91
Figure 2.5. Size distribution of (A) PEO- <i>b</i> -P(CCLC <sub>6</sub> SH) and (B) PEO- <i>b</i> -P(CCLC <sub>6</sub> -S-PAO) (10 mg/mL) in toluene, DMAc, and water.....	92
Figure 2.6. TEM pictures of micelles prepared from PEO- <i>b</i> -PCCL (A), PEO- <i>b</i> -P(CCLC <sub>6</sub> -SH) (B), and PEO- <i>b</i> -P(CCLC <sub>6</sub> -S-PAO) (C and D).....	93
Figure 2.7. TEM picture of PAO.....	93
Figure 2.8. Size distribution of (A) PEO- <i>b</i> -P(CCLC <sub>6</sub> -SH) and (B) PEO- <i>b</i> -P(CCLC <sub>6</sub> -S-PAO) micelles (1 mg/mL) in water and SDS solution after incubation in a 37 °C water bath over time. ....	96
Figure 2.9. <i>In vitro</i> release profile of PEO- <i>b</i> -P(CCLC <sub>6</sub> -S-PAO) in CH <sub>3</sub> COONH <sub>4</sub> buffer (pH 7.4) with different GSH concentrations at 37 °C. ....	97
Figure 2.10. Cytotoxicity of (A) PEO- <i>b</i> -P(CCLC <sub>6</sub> -SH) and (B) free PAO and PEO- <i>b</i> -P(CCLC <sub>6</sub> -S-PAO) to MDA-MB-435 cell line using neutral red assay.....	101

Figure 2.11. Cytotoxicity of mercaptohexylamine against MDA-MB-435 cells. ....	102
Figure 3.1. Scheme illustrating peptide conjugation onto the distal end of PEO. ....	110
Figure 3.2. Preparation of As <sup>III</sup> -encapsulated micelles. ....	117
Figure 3.3. <sup>1</sup> H-NMR spectrum of acetal-PEO <sup>6000</sup> . ....	121
Figure 3.4. MALDI -MS spectrum of acetal-PEO <sup>6000</sup> . ....	122
Figure 3.5. <sup>1</sup> H-NMR of acetal-PEO <sup>6000</sup> - <i>b</i> -PCCL <sub>17</sub> . ....	122
Figure 3.6. Monitoring GRGDS-amide conjugation to acetal-PEO- <i>b</i> -PCCL polymers using HPLC-UV chromatography. ....	124
Figure 3.7. Calibration curve for free GRGDS-amide. ....	124
Figure 3.8. <sup>1</sup> H-NMR spectra of micelles (1 mg/mL, prepared in D <sub>2</sub> O) with and without GRGDS-amide. ....	125
Figure 3.9. Arsenic loading in PEO- <i>b</i> -P(CCLC <sub>6</sub> -SH) micelles without incubation at 37 °C (A) and with incubation at 37 °C (B). ....	128
Figure 3.10. Arsenic loading and As/S molar ratio in PMM, CMM, and non-mixed PEO- <i>b</i> -P(CCLC <sub>6</sub> -S-As <sup>III</sup> ) micelles. ....	129
Figure 3.11. Size distribution by intensity of micelles (1 mg/mL) before and after sequential filtration through membranes of different pore sizes. ....	130
Figure 3.12. Percentage of remaining arsenic after filtration compared to the same sample before filtration. ....	130
Figure 3.13. <i>In vitro</i> arsenic release from micelles in RPMI-1640 cell culture medium supplemented with 10% FBS at 37 °C. ....	131
Figure 3.14. <i>In vitro</i> cytotoxicity of free and encapsulated As <sup>III</sup> against the control cell line, MCF10A cells. ....	133
Figure 3.15. <i>In vitro</i> cytotoxicity of free and encapsulated As <sup>III</sup> against the target cell line, MDA-MB-435 cells. ....	134
Figure 3.16. Cellular uptake of free and encapsulated As <sup>III</sup> by control cell line MCF10A cells, with and without 1 h pretreatment of free GRGDS-amide (1 mg/mL). ....	138
Figure 3.17. Cellular uptake of free and encapsulated As <sup>III</sup> by target cell line MDA-MB-435 cells at 24 h treatment. ....	138

Figure 3.18. Cellular uptake of free and encapsulated As <sup>III</sup> (10 μM) by MDA-MB-435 cells at different treatment concentration and treatment duration. ....	139
Figure 3.19. Cellular uptake of free and encapsulated As <sup>III</sup> (10 μM) by MDA-MB-435 cells with or without 1 h pretreatment of free GRGDS-amide (1 mg/mL) after 24 h arsenic treatment duration. ....	139
Figure 3.20. <sup>1</sup> H-NMR of PEO <sup>5000</sup> - <i>b</i> -PCL <sub>6</sub> in CDCl <sub>3</sub> . ....	142
Figure 3.21. <sup>1</sup> H-NMR of PEO <sup>5000</sup> - <i>b</i> -PCL <sub>10</sub> in CDCl <sub>3</sub> . ....	143
Figure 3.22. <sup>1</sup> H-NMR of PEO <sup>5000</sup> - <i>b</i> -PBCL <sub>6</sub> in CDCl <sub>3</sub> . ....	143
Figure 3.23. <sup>1</sup> H-NMR of PEO <sup>5000</sup> - <i>b</i> -P(D,L-LA) <sub>4</sub> in CDCl <sub>3</sub> . ....	144
Figure 3.24. <sup>1</sup> H-NMR of PEO <sup>5000</sup> - <i>b</i> -P(D,L-LA) <sub>8</sub> in CDCl <sub>3</sub> . ....	144
Figure 3.25. <sup>1</sup> H-NMR of PEO <sup>5000</sup> - <i>b</i> -PCCL <sub>10</sub> in CDCl <sub>3</sub> . ....	145
Figure 3.26. Arsenic loading in different mixed micelles. ....	146
Figure 3.27. Sulfur content of different mixed micelles. ....	146
Figure 3.28. <i>In vitro</i> arsenic release from PEO- <i>b</i> -PCCL/PEO- <i>b</i> -P(CCLC <sub>6</sub> -S-As <sup>III</sup> ) mixed micelle. ....	148
Figure 3.29. <i>In vitro</i> arsenic release from PEO- <i>b</i> -P(D,L-LA)/PEO- <i>b</i> -(CCLC <sub>6</sub> -S-As <sup>III</sup> ) mixed micelles with different DP of P(D,L-LA). ....	148
Figure 3.30. <i>In vitro</i> arsenic release from PEO- <i>b</i> -PCL/PEO- <i>b</i> -P(CCLC <sub>6</sub> -S-As <sup>III</sup> ) mixed micelles with different DP of PCL. ....	149
Figure 3.31. <i>In vitro</i> arsenic release from PEO- <i>b</i> -PBL <sub>6</sub> /PEO- <i>b</i> -P(CCLC <sub>6</sub> -S-As <sup>III</sup> ) mixed micelle. ....	149
Figure 4.1. <sup>1</sup> H-NMR spectrum of PEO- <i>b</i> -PCL- <i>b</i> -PCCL in CDCl <sub>3</sub> (A) and D <sub>2</sub> O (B). ....	167
Figure 4.2. <sup>1</sup> H-NMR spectrum of PEO- <i>b</i> -PCL- <i>b</i> -P(CCLC <sub>6</sub> -SH) in CDCl <sub>3</sub> (A) and D <sub>2</sub> O (B). ....	168
Figure 4.3. <sup>1</sup> H-NMR spectrum of PEO- <i>b</i> -(PCL- <i>co</i> -PCCL) in CDCl <sub>3</sub> (A) and D <sub>2</sub> O (B). ....	169
Figure 4.4. <sup>1</sup> H-NMR spectrum of PEO- <i>b</i> -(PCL- <i>co</i> -P(CCLC <sub>6</sub> -SH)) in CDCl <sub>3</sub> (A) and D <sub>2</sub> O (B). ....	170
Figure 4.5. <sup>1</sup> H-NMR spectrum of PEO- <i>b</i> -PCCL- <i>b</i> -PCL in CDCl <sub>3</sub> (A) and D <sub>2</sub> O (B). ....	171
Figure 4.6. <sup>1</sup> H-NMR spectrum of PEO- <i>b</i> -P(CCLC <sub>6</sub> -SH)- <i>b</i> -PCL in CDCl <sub>3</sub> (A) and D <sub>2</sub> O (B). ....	172
Figure 4.7. Arsenic loading and As/S molar ratio in thiol-functionalized terpolymeric micelles encapsulated with As <sup>III</sup> . ....	174
Figure 4.8. CMC of polymer 1, polymer 2, polymer 3, and PEO- <i>b</i> -PCCL <sub>17</sub> . ....	176

<b>Figure 4.9. Size distribution of arsenic-loaded micelles (0.1 mg/mL) in water and PBS using DLS technology..</b>	177
<b>Figure 4.10. Zeta potential of micelles prepared from 1 mg/mL starting polymers (A), thiol-containing polymers (B), and iAs<sup>III</sup>-loaded polymers (C) at different pH values..</b>	178
<b>Figure 4.11. Zeta-potential of micelles (1 mg/mL) in phosphate buffer (0.1 M, pH 7).</b>	180
<b>Figure 4.12. TEM of arsenic-loaded micelles.</b>	185
<b>Figure 4.13. TEM of micelle 1b (A) and micelle 3b (B) taken at 80 kV with magnification of 28,000.</b>	186
<b>Figure 4.14. <i>In vitro</i> As<sup>III</sup> release from micelles at 37 °C in (A) water, (B) RPMI-1640 cell culture medium, and (C) RPMI-1640 medium supplemented with 10% FBS.</b>	188
<b>Figure 4.15. <i>In vitro</i> cytotoxicity of free and encapsulated arsenic formulations against MDA-MB-435 cells.</b>	191
<b>Figure 4.16. <i>In vitro</i> cellular uptake of arsenic by MDA-MB-435 cells after 24 h treatment of free and encapsulated arsenic formulations.</b>	192

## List of Acronyms

$\gamma$ GT	$\gamma$ -glutamyltranspeptidase
AA	Ascorbic acid
ABL1	Abelson murine leukemia viral oncogene homolog 1
Akt	Protein kinase B
AML	Acute myeloid leukemia
ANT	Adenine nucleotide translocase
AP-1	Activator protein 1
APL	Acute promyelocytic leukemia
As <sup>III</sup>	As(OH) <sub>3</sub> , or AsO <sub>2</sub> <sup>-</sup>
Atg	Autophagy-related protein
ATO	Arsenic trioxide
ATRA	All-trans retinoic acid
BCR	Breakpoint cluster region protein
BSO	L-buthionine sulfoximine
CML	Chronic myeloid leukaemia
CMC	Critical micellar concentration
CMM	Control mixed micelles
DCA	Dichloroacetate
DLS	Dynamic light scattering
DMA <sup>III</sup>	Dimethylarsonous acid
DMAc	N,N-dimethylacetamide
DOX	Doxorubicin

DP	Degree of polymerization
ECM	Extracellular matrix
EPR	Enhanced permeation and retention
ER	Endoplasmic reticulum
FBS	Fetal bovine serum
GSH	Glutathione
HCC	Hepatocellular carcinoma
HK	Hexokinase
HUVEC	Human umbilical vein endothelial cell
ICP	Inductively coupled plasma
MDR	Multidrug resistance
miRNA	microRNA
MM	Multiple myeloma
MMA <sup>III</sup>	Monomethylarsonous acid
MMP	Matrix metalloproteinase
MS	Mass spectrometry
mTOR	Mammalian target of rapamycin
NF- $\kappa$ B	Nuclear factor- $\kappa$ B
NP	Nanoparticle
PAO	Phenylarsine oxide
PBCL	poly( $\alpha$ -benzylcarbonyl- $\epsilon$ -caprolactone)
PCCL	poly( $\alpha$ -carbonyl- $\epsilon$ -caprolactone)
PCL	poly( $\epsilon$ -caprolactone)

PdI	Polydispersity index
PDK	Pyruvate dehydrogenase kinase
PDLLA	poly(D,L-lactide)
PEO	poly(ethylene oxide)
PGA	polyglycolide
PI3K	Phosphatidylinositol 3 kinase
PML	Promyelocytic leukaemia protein
PMM	Peptide-decorated mixed micelles
RAR $\alpha$	Retinoic acid receptor- $\alpha$
RGD	Arginine-glycine-aspartic acid
ROS	Reactive oxygen species
RXR	Retinoid X receptor
SDS	Sodium dodecyl sulfate
TEM	Transmission electron microscopy
TGF- $\beta$	Transforming growth factor $\beta$
TNF- $\alpha$	Tumor necrosis factor $\alpha$
TRAIL	Tumor necrosis factor-related apoptosis-inducing ligand
Trx	Thioredoxin
TrxR	Thioredoxin reductase
VEGF	Vascular endothelial growth factor

# Chapter 1. Introduction

## 1.1 Therapeutic application of arsenic compounds

### 1.1.1 History of therapeutic application of arsenic compounds

Arsenic compounds, or arsenicals, though known as potent toxins and carcinogens, have been used therapeutically for more than 2400 years (Doyle 2009; Waxman and Anderson 2001). Ancient Chinese alchemists prepared elixirs with orpiment ( $\text{As}_4\text{S}_6$ ) and realgar ( $\text{As}_4\text{S}_4$ ) as ingredients, which were prescribed for various imbalances in the soul, health, and discipline (Sarquis 1979). A number of traditional Chinese medicines contain mineral arsenicals, and several formulations are still in use today (J Liu et al. 2008). Hippocrates (460-375 B.C.) used orpiment and realgar to treat tumors and cancerous ulcers (Cullen 2008). Medicinal uses of arsenic reached their peak in the eighteenth and nineteenth centuries. Arsenic was used mainly externally until the development of Fowler's solution during the late eighteenth century, which is a solution of 1% potassium arsenite ( $\text{KAsO}_2$ ) in alcohol and water. Fowler's solution became one of the principal therapeutic drugs of the time, and was prescribed for epilepsy, asthma, eczema, Hodgkin's disease, leukemia, anemia, rheumatism, and psoriasis (Dilda and Hogg 2007). In the early 1900s, the first organic arsenical used therapeutically, Salvarsan (arsphenamine), was introduced to treat syphilis and African trypanosomiasis (sleeping sickness). It quickly became the most widely prescribed drug in the world. Melarsoprol, a trivalent organoarsenical developed in 1949, is still being used for the treatment of sleeping sickness (Williams 2009).

In the 1970s, Chinese researchers found that dissolved arsenic trioxide ( $\text{As}_2\text{O}_3$ , ATO), forming arsenic acid [ $\text{As}(\text{OH})_3$ ,  $\text{As}^{\text{III}}$ ] in aqueous solution, was a relatively safe and effective treatment for relapsed and refractory acute promyelocytic leukemia (APL) (Dilda and Hogg 2007;

Shen et al. 1997; Sun et al. 1992; Waxman and Anderson 2001). The success of As<sub>2</sub>O<sub>3</sub> (intravenous injection of its aqueous solution) in APL treatment led to its approval as a first-line treatment for APL by the United States Food and Drug Administration (FDA) in September 2000 (Cullen 2008).

Encouraged by the great success of ATO therapy in APL treatment, interest was aroused to extend the application of ATO therapy to other hematopoietic and non-hematopoietic malignancies. With the goal to develop arsenic therapy in cancer treatment, studies on the mechanisms of arsenic-induced cell death and development of arsenic therapies including combination therapy, novel organoarsenicals, and targeted delivery of arsenicals, are on the rise during the recent decade.

### **1.1.2 Mechanism of action**

ATO can induce cell growth inhibition, cell cycle arrest, and cell death among a wide range of cancer cell types, including breast cancer, colon cancer, myeloma, ovarian cancer, prostate cancer, renal cancer, hepatocellular carcinoma (HCC), lung cancer, Laryngeal squamous cell carcinoma, and cholangiocarcinoma (BH Cheng et al. 2008; Li et al. 2004; Liu et al. 2010; Walker et al. 2010; Zhong et al. 2010). Phase I/II clinical trials were conducted to evaluate the safety and efficacy of ATO monotherapy in patients with advanced metastatic melanoma (Kim et al. 2005; Tarhini et al. 2008), recurrent urothelial cancer (Bajorin et al. 2009), advanced HCC (Lin et al. 2007), metastatic renal cell carcinoma (Vuky et al. 2002), and refractory germ cell malignancies (Beer et al. 2006). Although ATO monotherapy was found to be well tolerated, its activity in most cancer patients was limited. Combination therapy of ATO and other chemotherapy or agents that can sensitize the tumor cells to ATO treatment is suggested. Therefore, it is important to understand the mode of action in ATO-induced tumor suppression.

#### **1.1.2.1 Arsenic-induced apoptosis**

Apoptosis can be initiated by the death receptor (extrinsic) pathway and/or the mitochondrial (intrinsic) pathway. (Elmore 2007) The extrinsic pathway involves the interaction between

external signals or ligands and their transmembrane death receptors (DRs), which can transmit the death signals from the cell surface to the intracellular signaling pathway. The death receptor/ligand pairs include but are not limited to Fas (or CD95)/FasL, tumor necrosis factor receptor 1 (TNF-R1)/tumor necrosis factor  $\alpha$  (TNF- $\alpha$ ), TNF-R2/TNF- $\alpha$ , DR3/Apo3L, DR4/Apo2L, and DR5/Apo2L. The intrinsic pathway involves mitochondrial membrane depolarization and loss of mitochondrial transmembrane potential ( $\psi_M$ ) induced by non-receptor-mediated stimuli, such as increased reactive oxygen species (ROS) generation, accumulation of DNA damage, and induction of endoplasmic reticulum (ER) stress (Elmore 2007). Both the extrinsic and intrinsic pathways end at the point of the execution phase, when execution caspases activate cytoplasmic endonuclease and proteases that degrade nuclear material and cytoskeletal proteins, and final morphological and biochemical changes occur in apoptotic cells.

Reports showing that ATO can induce cell apoptosis via the intrinsic pathway have been well documented (Gazitt and Akay 2005; Sanchez et al. 2010). Arsenic treatment results in elevated ROS and induces oxidative stress, which is attributed to the perturbation of the glutathione (GSH) and thioredoxin (Trx) systems. The GSH and Trx systems play pivotal roles in maintaining the oxidative homeostasis in cells. Due to the high affinity of trivalent arsenic species for thiol groups, ATO and its trivalent methylated metabolites [monomethylarsonous acid (MMA<sup>III</sup>) and dimethylarsonous acid (DMA<sup>III</sup>)] can bind directly to GSH to form As–GS complexes, which are the substrates of multidrug resistance (MDR) proteins, resulting in efflux of arsenic from cell cytosol to the extracellular medium (S Shen et al. 2013; Leslie 2012). High concentration of ATO (>10  $\mu$ M) can inhibit the activity of glutathione reductase (GR), which reduces the conversion of the oxidant GSSG to the reductive GSH (Nikaido et al. 2003; Ray et al. 2014). The formation of As–GS complexes and the inhibition of GR activity leads to GSH depletion. Thioredoxin reductase

(TrxR) is more sensitive than GR to the activity inhibition induced by arsenic (Lu et al. 2007). The MALDI-MS analysis revealed that arsenic at sub  $\mu\text{M}$  concentration can irreversibly inhibit the TrxR activity by forming a (Cys)–S–As(OH)–Se–(Sec) crosslinking loop at the Cys-Sec active site of TrxR, where Sec is a selenium (Se)-containing selenocysteine (Lu et al. 2007). GSH was slightly protective for the TrxR activity inhibition when the treated arsenic concentration was low ( $<0.5 \mu\text{M}$ ). However, when the treated arsenic concentration exceeded  $0.5 \mu\text{M}$ , GSH could not protect TrxR from activity inhibition.

Rojewski et al. (2004) observed ATO-induced loss of  $\psi_M$  in a variety of myelogenic and lymphatic cell lines and demonstrated that the loss of  $\psi_M$  could not be prevented by blocking the ATO-induced caspase activation. Consequent release of cytochrome c from mitochondria to cytosol and activation of caspase-9 and caspase-3 were observed in cells where ATO treatment triggered the intrinsic apoptotic pathway. The level of Bcl-2 protein is closely related to the mitochondrial pathway of ATO-induced apoptosis. Arsenic treatment can down-regulate Bcl-2 expression in treated cells, such as human gastrointestinal cancer cells (Ma et al. 2014; L Zhang et al. 2015b) and B-cell lymphoma cells (L Wang et al. 2015). And overexpression of Bcl-2 in cells can protect the cells from ATO-induced apoptosis (Scholz et al. 2005). Combination of metformin and ATO can synergistically down-regulate Bcl-2 expression in HCC cells (Yang et al. 2015).

ATO can induce cell apoptosis via the extrinsic pathway as well. ATO was reported to induce apoptosis of ovarian cancer cells (Kong et al. 2005), osteosarcoma cells (Yang et al. 2010), and keratinocytes (Liao et al. 2004) by upregulating the expression of Fas with consequent downstream activation of caspase-8 and caspase-3. How ATO treatment up-regulates Fas expression remains to be clarified. Woo et al. (2004) observed up-regulated Fas expression in HeLa cells treated with ATO, which sensitized HeLa cells to the treatment of an anti-Fas antibody, CH11, via Fas-induced

apoptosis. Woo et al. (2004) further demonstrated that the Fas expression was up-regulated at the transcriptional level through ROS-mediated nuclear factor- $\kappa$ B (NF- $\kappa$ B) activation. ATO treatment induced ROS production in a dose- and time-dependent manner. Increased ROS levels activated NF- $\kappa$ B and increased its binding ability to the Fas promoter, which up-regulated *Fas* gene expression. In the study by Liao et al. (2004), low doses of ATO ( $\leq 1 \mu\text{M}$ ) induced proliferation of keratinocytes with enhanced NF- $\kappa$ B and activator protein 1 (AP-1) activity; while high doses of ATO ( $\geq 5 \mu\text{M}$ ) induced apoptosis with increased Fas expression and further enhanced AP-1 activity, but NF- $\kappa$ B activity was not enhanced.

Like Fas upregulation, ATO treatment increased the expression of another death receptor, DR5 (or tumor necrosis factor-related apoptosis-inducing ligand receptor 2, TRAIL-R2) in glioma cells (Kim et al. 2008), multiple myeloma (MM) cells (Byun et al. 2003), and malignant hematopoietic cells (Szegezdi et al. 2006), which either enhanced TRAIL (or Apo2L)-induced apoptosis or restored the sensitivity of cells to TRAIL treatment. Szegezdi et al. (2006) found that inhibition of the phosphatidylinositol 3 kinase (PI3K) was equally efficient in sensitizing leukemic cells to TRAIL with similar effects on DR5 expression, and proposed that ATO may in part act through inhibition of the PI3K/protein kinase B (or Akt) signaling pathway.

A recent study by Wu et al. (2010) suggested that whether ATO-induced apoptosis in MM cells occurred through the extrinsic or the intrinsic signaling pathway depended on the genetic background of p53. Wu et al. (2010) tested four MM cell lines, three with mutant p53 and one with wild-type p53. After ATO treatment, mutated p53 myeloma cells had increased expression levels of both DR5 and TRAIL and activation of caspase-8 and caspase-3 with no activation of Bax, Bcl-xL, and caspase-9, indicating the extrinsic apoptotic pathway; while wild-type p53 myeloma cells had activation of caspase-9 and caspase-3 with no activation of caspase-8, indicating the intrinsic

apoptotic pathway. Meanwhile, ATO treatment induced G2/M arrest in mutated p53 myeloma cells and G0/G1 arrest in wild-type p53 myeloma cells. Silencing the p53 gene in wild-type p53 myeloma cells would result in a transition from the intrinsic apoptotic pathway to the extrinsic apoptotic pathway with an activation of caspase-8 and expression of DR5.

Recently Zhang et al. (2015) observed ER dilation, upregulation of glucose-regulated protein 78 (also known as binding immunoglobulin protein, BiP, an ER resident chaperone protein), and CCAAT/enhancer-binding protein (CHOP) homologous protein in HepG2 and SMMC-7721 human HCC cells treated with ATO, indicating the ER stress was induced. The treatment of 4-phenylbutyric acid, an ER stress inhibitor, can alleviate the ATO-induced cell apoptosis. Therefore, ATO-induced cell apoptosis could be partially mediated by ER stress.

#### **1.1.2.2 Arsenic-induced autophagic cell death**

Autophagy is a degradation process that recycles damaged cellular organelles and proteins and can result in both tumor suppression and promotion (Duffy et al. 2015). Kanzawa et al. (2003) first observed ATO induced autophagy in U373 glioma cells. This process could not be inhibited by blocking the activation of caspases. A follow-up study confirmed the ATO-induced autophagy in glioma cells with the translocation of the microtubule-associated protein light chain 3 (LC3), an autophagy-specific marker, from the cytosol to autophagosome membrane (Kanzawa et al. 2005). In this same study, Kanzawa et al. (2005) further demonstrated that Bcl-2/adenovirus E1B 19-kDa-interacting protein 3 (BNIP3), which was up-regulated after ATO treatment, played an important role in ATO-induced autophagy. The autophagic cell death involved damage of mitochondrial membrane integrity but not caspase activation.

ATO-induced autophagy was observed in a variety of lymphoma and leukemia cell lines (J Cheng et al. 2012; Goussetis et al. 2010; Han et al. 2012; Li et al. 2014; Qian et al. 2007; Yang et

al. 2008). Qian et al. (2007) discovered that ATO treatment enhanced phosphorylation of Akt and up-regulated the expression of Beclin-1 in Molt-4 and Mutz-1 cells. Both Akt and Beclin-1 play a pivotal role in autophagy regulation. (Duffy et al. 2015) Akt is the upstream regulator of mammalian target of rapamycin (mTOR). The phosphorylation of Akt will activate mTOR and ultimately inhibit autophagy. Beclin-1 is a promoter of autophagy. Once Beclin-1 binds to vacuolar sorting protein 34 (Vpa34) to form the Beclin-1 complex, the complex will further bind to other autophagy-related proteins (Atgs) to start the early steps of autophagosome formation. In the study by Qian et al. (2007), the promotion of autophagy resulting from Beclin-1 upregulation outweighed the inhibition of autophagy resulting from Akt phosphorylation. The ATO-induced Beclin-1 upregulation was observed in KT1 (Goussetis et al. 2010), U939 (Goussetis et al. 2010; Han et al. 2012), and K562 (Cheng et al. 2012) leukemic cells as well.

The Beclin-1-independent pathway was observed in ATO-induced autophagy by Smith et al. (2010) The knockdown of Beclin-1 gene did not affect the translocation of CL3 induced by ATO in ovarian carcinoma cells. Unlike Molt-4 and Mutz-1 cells in which cells Qian et al.(2007) observed enhanced activation of Akt induced by ATO, HOS and HT1080 sarcoma cells (Chiu et al. 2015), HepG2 and Huh7 HCC cells (Zhai et al. 2015), HT29 and HCT116 colon carcinoma cells (XY Cai et al. 2015), and SW1353 chondrosarcoma cells (Jiao et al. 2015) experienced inhibited activity of Akt and mTOR, indicating ATO-induced autophagy by the regulation of the PI3K/Akt/mTOR pathway.

### **1.1.2.3 Target degradation of PML-RAR $\alpha$ oncogenic protein in APL**

APL is characterized by a specific t(15;17)(q22;q12) gene translocation, an accumulation of abnormal promyelocytes in blood and bone marrow, occurrence of fibrinogenopenia, and disseminated intravascular coagulation (Chen et al. 2011; Dethe et al. 1990). The t(15;17)(q22;q12)

translocation generates an oncogenic fused protein that is a structural hybrid of the promyelocytic leukemia (PML) protein and the retinoic acid receptor- $\alpha$  (RAR $\alpha$ ), namely, PML-RAR $\alpha$ . The formation of the oncogenic fusion protein PML-RAR $\alpha$  causes APL with two mechanisms (Zhu et al. 1997; Zhu et al. 2002). On one hand, this fusion protein displaces PML from the nuclear matrix to nucleoplasm, disrupts the PML nuclear-body formation, and therefore blocks apoptosis. On the other hand, the homodimers of the fusion PML-RAR $\alpha$  protein have much stronger interaction with transcriptional corepressors than wild-type RAR $\alpha$  heterodimers with the retinoid X receptor (RXR), which blocks cell differentiation.

ATO is especially effective for APL treatment because it can trigger the modification of PML-RAR $\alpha$  with small ubiquitin-like modifier (SUMO). The SUMOylation of PML-RAR $\alpha$  further triggers the ubiquitination of PML-RAR $\alpha$ , which promotes the degradation of the oncogenic protein. The molecular interaction between ATO and PML-RAR $\alpha$  was studied by Zhang et al. (2010) In brief, arsenic tends to replace zinc from a zinc finger ring structure (PML-R-ZF), which is contained in the RING domain of PML located at the N-terminus of PML-RAR $\alpha$ . Arsenic is coordinated with “three sulphur atoms from the three conserved cysteines” in PML-R-ZF. Upon replacement of zinc by arsenic, the conformation of PML-R-ZF changes from a tetrahedral structure to a pyramid cone structure. The conformational change induces the oligomerization of PML-RAR $\alpha$  and subsequent SUMOylation by enhancing the molecular interaction between PML and UBC9 and SUMO-2. The PML-RAR $\alpha$  oligomers are quickly degraded after being tagged with ubiquitin.

Since the fusion protein PML-RAR $\alpha$  blocks both apoptosis and cell differentiation, the protein degradation is expected to induce both apoptosis and cell differentiation. Interestingly, treatment with ATO resulted primarily in apoptosis and to a lesser extent in cell differentiation, which is in

contrast to treatment with all-*trans* retinoic acid (ATRA), which was the first line therapy for APL before ATO was approved for application in APL treatment. This phenomenon can be explained by different active sites of ATO and ATRA (Ablain and de The 2011). ATRA acts on the RAR $\alpha$  moiety, activates the transcription of target genes and induces cell differentiation. ATO acts on the PML moiety and triggers PML-RAR $\alpha$  degradation, inducing PML re-localization on nuclear bodies (NBs), which results in cell apoptosis. The combination of ATO and ATRA results in synergistic action in APL treatment, leading to both high clinical remission and low relapse rates (Burnett et al. 2015). Recently, the direct binding of arsenic to cysteine residues in zinc fingers located in the PML-RAR $\alpha$  was demonstrated to be one of the plausible modes of action leading to APL remission (Jeanne et al. 2010; Zhang et al. 2010).

#### **1.1.2.4 Target degradation of BCR-ABL1 oncogenic protein**

A majority of chronic myeloid leukemia (CML) and Philadelphia chromosome positive acute lymphoblastic leukemia (Ph<sup>+</sup> ALL) cases express the oncogenic BCR-ABL1 fusion protein, which is short for breakpoint cluster region protein-Abelson murine leukemia viral oncogene homolog 1 fusion protein. (Arana-Trejo et al. 2002) The formation of BCR-ABL1 fusion protein is caused by a gene translocation of t(9;22)(q35;q11). BCR-ABL1 has increased tyrosine kinase activity compared to normal ABL1 protein and its activity cannot be regulated by the molecules that control the activity of normal ABL protein. (Salesse and Verfaillie 2002) Thus, BCR-ABL1 fusion protein causes malignant transformation by interfering with several cell signal pathways that closely regulate cell proliferation, differentiation, and survival. Tyrosine kinase inhibitors such as Imatinib, Nilotinib and Dasatinib are used as the first line therapy in CML treatment to suppress the activity of BCR-ABL1 protein (Kujak and Kolesar 2016). Unfortunately, resistance to tyrosine kinase inhibitors is easily developed in CML cells (Jabbour and Kantarjian 2016).

Previous studies reviewed by Hu et al. (2005) showed that BCR-ABL1 positive CML cells are sensitive to ATO and As<sub>4</sub>S<sub>4</sub> treatment and the effect of arsenicals is independent of BCR-ABL1 kinase activity. Therefore the combination of arsenicals and tyrosine kinase inhibitors can generate a synergistic effect targeting the BCR-ABL1 protein. Recent studies revealed two mechanisms of arsenic-induced degradation of BCR-ABL1 oncogenic protein.

Zhang et al. (2009) treated the BCR-ABL1-positive K562 CML cell line with As<sub>4</sub>S<sub>4</sub> and/or Imatinib and found that many mRNA transcripts and proteins related to the ubiquitin proteasome pathway (UPP), especially the E3 ubiquitin ligase, were significantly up-regulated in the As<sub>4</sub>S<sub>4</sub>-treated and co-treated cells compared to Imatinib-treated cells. A follow-up study demonstrated that arsenic can directly bind to the RING finger domain of c-CBL, an E3 ligase that mediates the ubiquitination of BCR-ABL1 protein (Mao et al. 2010). The binding of arsenic on c-CBL inhibits the self-ubiquitination/degradation of c-CBL, thus up-regulating c-CBL. The up-regulated c-CBL increases the ubiquitination/degradation of the oncogenic BCR/ABL1 protein.

Goussetis et al. (2012) proposed that the degradation of BCR-ABL1 protein in ATO-treated K562 cells was an autophagic degradation process, as they observed p62/SQSTM1-mediated translocation of BCR/ABL1 protein to the autolysosomes and BCR-ABL1 degradation mediated by protease cathepsin B. The role that ATO played in this context was to induce the cell autophagy.

#### **1.1.2.5 Anti-Angiogenesis effect of inorganic arsenic**

Angiogenesis, the formation of new capillaries from pre-existing blood vessels, plays an important role in the proliferation of both liquid and solid tumors (Folkman and Shing 1992). Angiogenesis facilitates the delivery of nutrients and the removal of wastes from the tumor tissue. Angiogenesis is linked to metastasis and recurrence of cancers. At sub  $\mu$ M concentrations arsenic can promote the proliferation of human umbilical vein endothelial cells (HUVECs) *in vitro* (Kao et al. 2003)

and can stimulate angiogenesis *in vivo* (Soucy et al. 2003). However, Alimoghaddam et al. (2006) observed a significant reduction in bone marrow hot-spot vascular density in 17 APL patients after treatment with ATO, demonstrating that ATO is an effective anti-angiogenesis in APL. Once again, arsenic is demonstrated to be among the most controversial therapeutic agents.

#### **1.1.2.5.1 Vascular endothelial growth factor (VEGF) expression inhibition**

VEGF includes a family of multifunctional cytokines that are widely expressed by tumor cells. By acting through receptors expressed on vascular endothelial cells, VEGF promotes endothelial cell migration, proliferation, and differentiation, which therefore induces angiogenesis. (Dvorak 2002) Roboz et al. (2000) evaluated the effect of ATO treatment on the reciprocal stimulatory loop between the endothelial cell line HUVECs and the leukemic cell line HEL. Although resting HUVECs could be activated after 5 days of incubation with 0.5  $\mu$ M ATO with a cell morphology transformation from cobblestone appearance to spindle shape and an elevated binding activity for HEL cells, the VEGF-induced capillary tubule and branch formation in HUVECs was prevented by ATO treatment, which inhibited the differentiation of HUVECs. Furthermore, ATO suppressed the VEGF expression in HEL cells. Roboz et al. (2000) proposed the hypothesis that ATO inhibits angiogenesis by interrupting the reciprocal stimulatory loop between leukemic cells and endothelial cells (**Figure 1.1**).

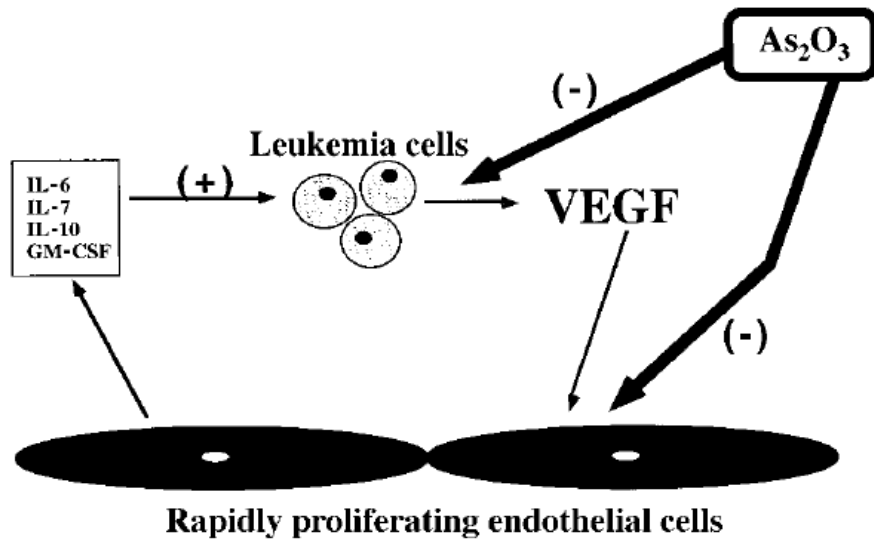


**Figure 1.1. Schema illustrating proposed sites of action of ATO in interrupting a reciprocal feedback loop between leukemic cells and endothelium.** (Reprinted with the permission from reference Roboz et al. 2000. Copyright 2011 by The American Society of hematology.)

The expression of VEGF is closely related to NF- $\kappa$ B and TNF- $\alpha$ . NF- $\kappa$ B promotes the expression of TNF- $\alpha$ , and TNF- $\alpha$  promotes the expression of VEGF. The NF- $\kappa$ B-induced TNF- $\alpha$  activation can further up-regulate NF- $\kappa$ B. Xie et al. (2015) demonstrated ATO down-regulated VEGF expression via inhibition of NF- $\kappa$ B, which resulted in effective volume reduction of malignant pleural effusion caused by pleural metastasis of lung cancer in a mouse model study.

With the fast development of molecular biology techniques, more recent studies have examined the regulation of microRNA (miRNA) expression induced by ATO treatment. ATO metabolism in cells involves methylation (Thomas et al. 2004), which could result in a deficiency in methyl donors in cells. Ji et al. (2014) observed decreased methylation levels of miRNA-155 (miR-155) promoter in PC-3 and LNCaP prostate cancer cells treated with ATO, which was most probably due to the methyl donor deficiency. Decreased methylation levels of miRNA-155 promoter triggered the increased expression of miR-155, which targets SMAD2 mRNA and inhibits the expression/activation of SMAD2. The transforming growth factor beta (TGF-

$\beta$ )/SMAD signal pathway was therefore blocked. The blocked TGF- $\beta$ /SMAD signal significantly attenuated the expression of NF- $\kappa$ B. A similar mechanism of action was demonstrated in the MHCC97 human HCC cell line (Jiang et al. 2014; Y Li et al. 2015). In MHCC97 cells treated with ATO, the expression of miRNA-491 was up-regulated, which down-regulated the expression/activation of SMAD3.

In HUVECs, ATO treatment increased the expression of VEGFA, VEGFA mRNA, miRNA-126 (miR-126), and the E26 transformation-specific sequence (Ets) factor 2 (Ets-2) by upregulating the expression of Ets-2 mRNA (Ge et al. 2015). Although the association of Ets-2 with miR-126 and VEGF is not clear, Ets-2 siRNA can down-regulate both the expression of Ets-2 mRNA and miR-126, and miR-126 inhibitor treatment can down-regulate VEGFA mRNA.

#### **1.1.2.5.2 Matrix metalloproteinases (MMPs) expression and activity inhibition**

MMPs play an important role in the invasion of tumors into surrounding normal tissues, because they catalyze the degradation of multiple elements of the extracellular matrix (ECM) (Coussens and Werb 1996). MMPs, such as MMP-2 and MMP-9, are overexpressed in several aggressive malignancies such as malignant glioblastoma (GBM) and invasive MM phenotypes.

Inorganic arsenic (ATO and As<sub>4</sub>S<sub>4</sub>) treatment inhibits MMP-2 activity in several MM cell lines (Hiwatashi et al. 2011; Khorramizadeh et al. 2006), GBM cell lines (Gwak et al. 2014), and gastric cancer cell lines (L Zhang et al. 2015a). In addition to MMP-2 activity inhibition, Gwak et al. (2014) observed the inhibition of Akt phosphorylation, MT1-MMP expression and MMP-2 expression when GBM cell lines were treated with low concentration of ATO (1–10  $\mu$ M).

#### **1.1.3 Toxicity and adverse side effects of arsenic therapy**

The toxicity of arsenic, both acute poisoning and chronic exposure, has been scientifically studied ever since the early twenties century (Lecoq 1910). The minimum lethal dose of ATO is between

100 mg and 200 mg (Hindmarsh and McCurdy 1986). Large scale epidemiology studies showed that ATO is a human carcinogen and is associated with elevated risks for vascular disease at high exposure levels (100–400 µg/L) (Sidhu et al. 2015). The effect of chronic arsenic exposure on renal injury and progressive chronic kidney disease remains unclear (Robles-Osorio et al. 2015). However, co-exposure to inorganic arsenic and cadmium is associated with pronounced renal toxicity greater than exposure to each of the agents alone (Buchet et al. 2003).

Due to improper application of arsenic-containing folk medicine and poor quality control of arsenic-containing homeopathic medications, clinical toxicity of arsenic therapy has been observed from time to time. Zhu and Zheng (2012) reported a case of verrucous carcinoma in a psoriasis patient who ingested orally an illegally produced folk drug containing arsenicals for one year. Chakraborti et al. (2003) reported three poisoned patients who deliberately ingested orally arsenic-containing homeopathic medicines with the intention to treat white dermal patches or liver problems. Different grades of melanosis and skin lesions were observed in these three patients. More severe symptoms, such as acute gastrointestinal illness and quadriparesis, resulting from polyneuropathy, occurred to one patient who consumed a total of 144 mg of trivalent arsenic over 6 days.

The dosage of arsenic is properly controlled in the hospital setting, and therefore the risk of arsenic therapy is partly negated. Most case studies of arsenic treatment for APL reported that side effects of the administration of arsenic were mild and transient. The main side effects include skin rashes, musculoskeletal pain, nausea or vomiting, and headaches, most of which are tolerable. However, some patients did experience leukocytosis, neutropenia, and liver dysfunction. And physicians observed occasional Pseudotumor cerebri in APL patients receiving arsenic therapy recently (Smith et al. 2014). Some patients died of pulmonary hemorrhage, intracranial

hemorrhage, or without a defined reason during ATO treatment (Westervelt et al. 2001; Zhou et al. 2010). Case studies indicate the diversity in individual tolerance to ATO toxicity, which can be influenced by factors including age, physical condition, *de novo* APL vs refractory APL, and prior treatment.

#### **1.1.4 Development of arsenic therapy**

##### **1.1.4.1 Combination therapy**

The idea of combining two active drugs or combining an active drug with its adjuvant in cancer treatment is not new (De Vita et al. 1975). Arsenic therapies combined with ATRA (Ravandi et al. 2010), cisplatin (Dogra et al. 2015; Suzuki et al. 2015), Bortezomib (LL Zhao et al. 2015), and even transarterial chemoembolization therapies (H Wang et al. 2015), have been tested both *in vitro* and *in vivo*, where they demonstrated additive or synergistic anti-tumor effects. Here, selected arsenic combination therapies that modulate specific cellular pathways are reviewed.

###### **1.1.4.1.1 Combination therapy targeting GSH systems**

The GSH system plays a crucial role in maintaining the oxidative homeostasis in cells by scavenging ROS and maintaining several antioxidants in reduced states. Modulation of the GSH and Trx systems may sensitize the cells to ATO treatment.

Ascorbic acid (AA) can deplete intracellular GSH, which can enhance ATO-induced apoptosis in multiple lymphoma cell lines (Dai et al. 1999). A phase II clinical trial of the combination therapy of AA and ATO was tested in patients with relapsed or refractory lymphoid malignancies; however, it revealed limited activity (Chang et al. 2009).

L-buthionine sulfoximine (BSO) is an inhibitor of GSH synthesis. Pereira et al. (2015) discovered that BSO sensitized ATO-induced autophagy of Hep-2 cells but did not increase ROS generation. Pereira et al. (2015) proposed that the decreased synthesis reduced the efflux of ATO in the form of As-GS complex.

#### **1.1.4.1.2 Combination therapy targeting glucose metabolism**

Transformed metabolism pathways are observed in the majority of cancer cells and provide the huge amounts of energy, proteins, lipids, and nucleic acids needed to support rapid cell proliferation (Chiche et al. 2010; Miller et al. 2012). Both the hypoxic tumor microenvironment and the expression of oncogenes such as *c-MYC* gene contribute to the metabolic transformation (Dang 1999; Miller et al. 2012). The Warburg effect (aerobic glycolysis), a shift from glycolysis followed by oxidation of pyruvate in mitochondria to glycolysis followed by lactate formation in cytosol, was discovered in the late 1920s (Warburg et al. 1926). This glycolytic shift is accompanied by increased expression of an array of proteins including glucose transporters (Iwasaki et al. 2015), hexokinase-2 (HK-2) (Chen et al. 2014), lactate dehydrogenase A (LDH-A) (Y Yu et al. 2014), and pyruvate dehydrogenase kinase (PDK) (Newington et al. 2012; Y Yu et al. 2014). Through this glycolytic shift, cancer cells can decrease ROS generation and develop resistance to some anti-cancer treatment (Newington et al. 2012; Thornalley and Rabbani 2011). A recent study on systematic profiling of arsenic-binding proteins revealed that arsenic can inhibit the activity of HK-2 by binding to Cys256 and Cys704, each of which is in close proximity to one of the two active sites of HK-2 (HN Zhang et al. 2015). Although arsenic can inhibit HK-2, overexpression of HK-2 can reverse the ATO-induced apoptosis in cancer cells (HN Zhang et al. 2015). Therefore, combinations of ATO and agents that can target the metabolism pathways could potentially overcome the arsenic-resistance in the tumor cells which undergo aerobic glycolysis.

The PI3K/Akt/mTOR pathway controls glycolysis in addition to autophagy regulation (Shimobayashi and Hall 2014). Inhibition of mTOR activity can decrease the aerobic glycolysis. Decollogne et al. (2015) demonstrated that a combination of Temsirolimus, a mTOR inhibitor, and *P*-(N-(S-penicillaminylacetyl)amino) phenylarsonous acid (PEANO), a novel arsenic-based pro-

drug, can synergistically inhibit cell proliferation and induce cell death in SKOV-3 cells, a PEANO-resistant ovarian cancer cell line.

Dichloroacetate (DCA) is a PDK inhibitor, and can bind to the active site of PDK and inhibit its activity to inactivate pyruvate dehydrogenase (PDH). PDH plays a central role in glucose metabolism by converting pyruvate to acetyl-CoA. PDK overexpression contributes to the Warburg effect by reducing the conversion of pyruvate to acetyl-CoA. DCA treatment induces PDK inhibition and promotes the conversion of pyruvate to acetyl-CoA, helping shunt pyruvate to mitochondria to resume the tricarboxylic acid cycle and increase ROS generation. Co-treatment of DCA and ATO has been demonstrated with a synergistic effect on cell growth inhibition in MDA-MB-468 and MDA-MB-231 breast cancer cells (Sun et al. 2011).

As DCA and ATO target two different sets of pathways in cells, the sequence of administration of these two agents may affect the final cell death outcome. Emadi et al. (2015) compared the apoptosis of acute myeloid leukemia (AML) cells induced by co-treatment of DCA and ATO with and without DCA priming for 24 hours and found that the DCA priming increased cell apoptosis by 77.3%.

#### **1.1.4.1.3 Combination therapy targeting Bcl-2 protein downregulation**

Bcl-2 protein is an anti-apoptotic protein. Downregulation of Bcl-2 protein can promote the cell apoptosis.

Sorafenib can induce HCC cell arrest at G0/G1 phase through inhibition of the MAPK/ERK pathway and down-regulation of cyclin D1 instead of affecting the Bcl-2 family proteins. Sorafenib-resistant HCC cells have elevated activation of Akt. ATO treatment can not only down-regulate the expression of cyclin D1, but also inhibit Akt activation, down-regulate the expression of Bcl-2 and Bcl-xL, and up-regulate the expression of Bax. The combination of ATO and

Sorafenib can synergize to result in HCC cell proliferation inhibition and apoptosis promotion (Zhai et al. 2015).

Metformin can inhibit the growth of cancer cells by down-regulating the PI3K/Akt/mTOR signaling pathway via activation of AMPK. Metformin can also down-regulate the Bcl-2 protein. Though Metformin seems to have similar effect on cells as ATO, the combination of Metformin and ATO was demonstrated to have a synergistic effect on cell growth inhibition of HCC (Yang et al. 2015) and GBM stem cells (Carmignani et al. 2014).

#### **1.1.4.1.4 Combination therapy targeting DNA damage repair suppression**

ATO treatment can induce oxidative DNA damage due to the increased generation of ROS (Kessel et al. 2002). The ATO-induced DNA damage triggers cell cycle arrest at G2/M phase; this is proposed to be a cell survival mechanism because sufficient time for the cell to repair damaged DNA is provided at the G2/M checkpoint (Luo et al. 2015). Poly(ADP ribose) polymerase-1 (PARP-1) plays an important role in DNA damage repair. Luo et al. (2015) utilized a classical PARP-1 inhibitor, 4-amino-1,8-naphthalimide (4AN), to suppress the activity of PARP-1 in HepG2 cells and found that the cells were sensitized to ATO treatment with a decreased IC<sub>50</sub> of ATO.

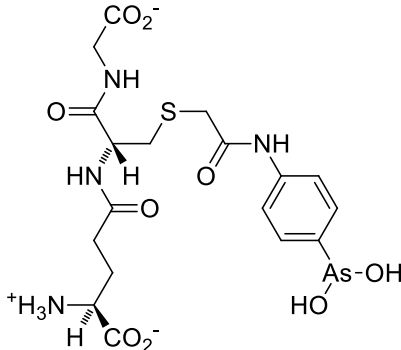
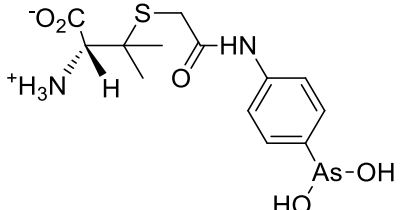
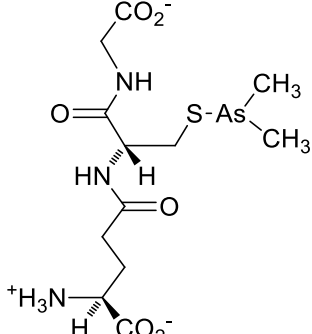
Trivalent arsenic and its methylated metabolites are known to inhibit the activity of PARP-1 at very low concentration (Hartwig et al. 2003; Walter et al. 2007) by replacing Zn with As in the zinc finger structure of PARP-1 (Ding et al. 2009; Zhou et al. 2011; Zhou et al. 2014), which further inhibits the nucleotide excision repair (SW Shen et al. 2013). It is possible that ATO treatment can sensitize the induction of apoptosis by other chemotherapeutic agents such as doxorubicin by inhibiting DNA damage repair.

#### 1.1.4.2 Novel organoarsenicals

Some organoarsenicals have been investigated in hematological malignancies and solid tumors. Dipropyl-S-glycerol arsenic (GMZ27) and S-dimethylarsino-thiosuccinic acid (MER1) are much less toxic than ATO yet have comparable or higher anti-leukemic activity (X Cheng et al. 2012; Golemovic et al. 2010). Arsenicin A, a natural adamantine-type tetra-arsenical, was recently shown to be 20 times more potent than ATO for the induction of proliferation arrest and cell death in APL cells and it can bind to dithiols (Mancini et al. 2006; Lu et al. 2012). MMA<sup>III</sup>, an intermediate metabolite of ATO, is more potent than ATO and DMA<sup>III</sup> in inducing apoptosis in MCF7 cells via induction of ER stress (YF Zhang et al. 2015).

Few organoarsenicals are currently undergoing clinical trials. Those involving dimethylarsinic acid and melarsoprol have been well reviewed by Dilda and Hogg (2007). Therefore, I focused on summarizing the recent progresses of the studies on 4-(N-glutathionylacetyl)amino phenylarsonous acid (GSAO), *P*-(N-(S-penicillaminylacetyl)amino) phenylarsonous acid (PEANO), and S-dimethylarsino-glutathione (ZIO-101, or Darinaparsin, or SGLU-1). The chemical structures of GSAO, PENAO, and ZIO-101 are shown in **Table 1.1**.

**Table 1.1. Chemical structures of GSAO, PENAO, and ZIO-101**

Arsenical	Structure
4-(N-glutathionylacetyl)amino phenylarsonous acid (GSAO)	
4-(N-(S-penicillaminylacetyl)amino) phenylarsonous acid (PENAO)	
S-dimethylarsino-glutathione (ZIO-101, Darinaparsin, SGLU-1)	

#### 1.1.4.2.1 GSAO

GSAO, a hydrophilic derivative of lethal phenylarsine oxide (PAO), was developed for clinical use. GSAO targets mitochondria and selectively perturbs angiogenic endothelial cells *in vitro* and *in vivo*. It inactivates the mitochondrial inner membrane transporter, adenine nucleotide translocase (ANT), by inducing arsenic-mediated cross-linking between the matrix facing thiols (Cys57, Cys160, Cys257) in ANT (Don et al. 2003). A follow-up study verified that the crosslinking was between Cys57 and Cys257, as the biotin-tagged GSAO could bind to wild-type

ANT and the C160A mutant protein but did not bind to the C57A or C257A ANT mutant proteins (Park et al. 2012).

The high selectivity of GSAO for proliferating endothelial cells is a consequence of the higher mitochondrial calcium levels (a several-fold increase over non-proliferating cells) in these cells. ANT is a calcium receptor that undergoes a calcium-induced conformational change. GSAO can bind to ANT when the calcium concentration is high, but binds only minimally in the absence of calcium ions (Don et al. 2003).

Interestingly, a study addressing the transportation question of GSAO through the endothelial cell membrane revealed that 4-(N-(S-cysteinylglycylacetyl)amino) phenylarsonous acid (GCAO), the metabolite of GSAO cleavage by  $\gamma$ -glutamyltranspeptidase ( $\gamma$ GT) on the cell membrane, is transported across the plasma membrane by the organic anion-transporting polypeptide family, instead of by GSAO itself (**Figure 1.2**) (Dilda et al. 2008). GCAO is further cleaved by dipeptidases in the cytosol, forming 4-(N-(S-cysteinylacetyl)amino) phenylarsonous acid (CAO). CAO reacts with its mitochondrial target, ANT, and inactivates the functions of ANT, which then increases the concentration of ROS, arrests proliferation, and induces apoptosis. GSAO is a pro-drug that is dependent on cell surface processing by  $\gamma$ GT in order to function. A phase I clinical trial indicated that daily 1-hour infusions of GSAO, across 9 dose levels (1.3–44.0 mg/m<sup>2</sup>), were tolerated well by patients with advanced solid tumors (Horsley et al. 2013).

#### **1.1.4.2.2 PENAO**

PEANO is a cysteine mimetic analogue of CAO, the cysteine-S-conjugate metabolite of GSAO. PEANO bypasses the cell membrane processing and accumulates in cells 85 times faster than GSAO, which translates to a 44-fold increase in anti-proliferative activity *in vitro* and 20-fold better antitumor efficacy *in vivo* (Dilda et al. 2009). PENAO has a similar mechanism of

mitochondrial targeted inhibition as GSAO (Park et al. 2012). PENAO is highly active in proliferation inhibition of GBM cells both *in vitro* and *in vivo* (Chung et al. 2011; H Shen et al. 2013).

To promote the mitochondrial targeted proliferation inhibition, a combination of DCA and PENAO was tested on GBM cells (Shen et al. 2015) and breast cancer cells (Gang et al. 2014). DCA can sensitize T-47D and MDA-MB-231 breast cancer cells to the treatment of PENAO, and synergize the effect of PENAO in U87, U251, DBTRG, and LN229 GBM cells. A phase I clinical trial of PENAO is being tested on patients with advanced solid tumors (ACTRN12612000908831).

#### **1.1.4.2.3 ZIO-101**

ZIO-101, a conjugate of glutathione and dimethylarsinous acid, is a more potent pro-apoptotic agent than ATO (Dilda and Hogg 2007). ZIO-101 was well-tolerated in phase I/II clinical trials with both oral and intravenous administration (Mann et al. 2009). It has lower cardiac toxicity and hepatotoxicity than ATO. A phase II multi-center trial was conducted in patients diagnosed with advanced lymphomas that had received at least one prior therapy and required additional treatment (Craig et al. 2008; Hosein et al. 2012). Among the 13 patients who received two cycles of ZIO-101 (300 mg/m<sup>2</sup> of ZIO-101 intravenously for five consecutive days every 28 days for one cycle), 1 patient diagnosed with peripheral T-cell lymphoma (PTCL) achieved a complete response (CR); 3 patients diagnosed with marginal zone transformed to diffuse large B-cell, marginal zone, and Hodgkin's nodular sclerosis, respectively, achieved partial responses (PRs); and 2 patients diagnosed with PTCL and Hodgkin's, respectively, achieved stable disease (SD). Encouraged by the positive ZIO-101 activity on PTCL, a phase II trial on PTCL patients is being planned (NCT02653976). A phase II trial of ZIO-101 in patients with advanced HCC has been conducted as well (J Wu et al. 2010). ZIO-101 was administered at 420 mg/m<sup>2</sup> intravenously twice weekly at

least 72 h apart for 3 weeks in a 4-week cycle. Although ZIO-101 was tolerated well at this dose and schedule, there were no objective responses in HCC.

The activity of ZIO-101 is probably associated with the hydrolysis of the arsenic-glutathione bond, and the reaction of the resulting dimethylarsinous acid with a protein thiol. The glutathione moiety of ZIO-101 mimics GSAO in the translocation of the arsenicals into cells (Garnier et al. 2014). The hydrolysis of ZIO-101 requires  $\gamma$ GT processing which is the same as GSAO. The difference with GSAO, which is first hydrolyzed to GCAO with the mediation of  $\gamma$ GT on the cell membrane followed with further hydrolysis by intracellular dipeptidases, is that ZIO-101 is further hydrolysed to S-dimethylarsino-cysteine (DMAC) on the cell membrane. DMAC is transported through the cysteine transporter system (Garnier et al. 2014). However, the possibility that some DMAC is also formed inside the cells cannot be excluded. The existence of the putative hydrolysis intermediate, S-(dimethylarsino)-cysteinylglutamic acid, in the cell cytosol, has yet to be verified.

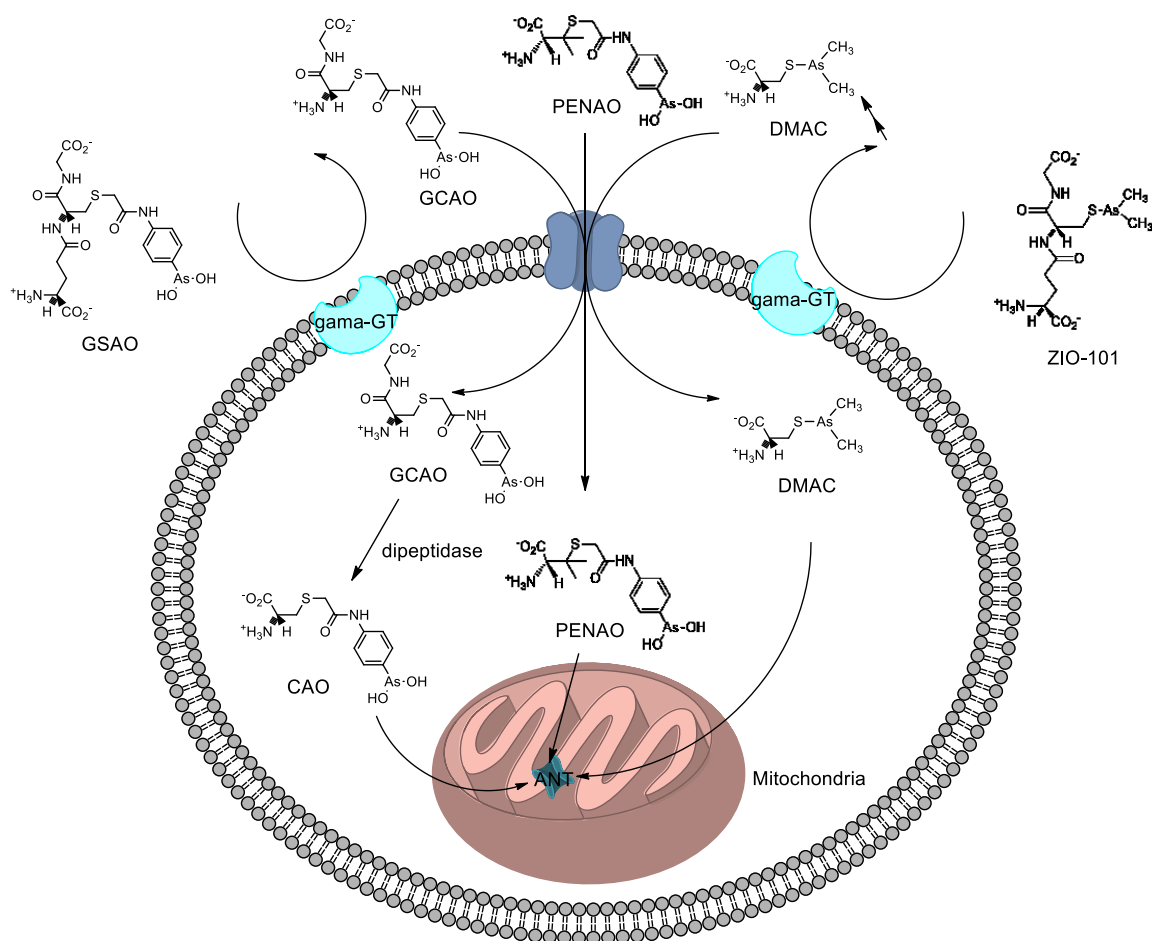


**Figure 1.2. Metabolism and transportation of GSAO, PENAO and ZIO-101 by endothelial cells.** The  $\gamma$ -glutamyl residue of GSAO and ZIO-101 is cleaved at the cell surface by  $\gamma$ -GT. The corresponding products (GCAO and DMAC) are then transported across the plasma membrane by an organic anion-transporting polypeptide or via an anionic amino acid transport system. PENAO is transported without any cleavage on the cell membrane. The target of these organoarsenicals in the cytoplasm is ANT on the inner mitochondrial membrane. GCAO may be further processed to CAO before it reacts with ANT. (Adapted from references Park et al. 2012, Horsley et al. 2013, and J Wu et al. 2010)

### 1.1.4.3 Nanoscale formulations for targeted delivery of arsenic

The clinical utility of ATO has been expanded to other types of malignancies in addition to APL, but the application of ATO is limited by either toxicity at higher doses (e.g., peripheral neuropathies, liver failure and cardiac toxicity), or by low bioavailability of the arsenic compounds for solid tumor targets at lower doses. Localized administration of ATO such as transarterial embolization may be able to largely avoid these adverse effects while simultaneously enhancing

therapeutic activity. Kim et al. (2009) evaluated the efficacy of transarterial embolization with ATO oil emulsion in a rabbit VX2 liver tumor model and demonstrated impressive anticancer effects without significant increase in hepatic and renal toxicity. However, this kind of administration method is too invasive. Nanomedicine has attracted considerable focus due to its characteristics such as targeted drug delivery and slow drug release (Venugopal et al. 2008).

As<sub>4</sub>S<sub>4</sub> has been tested to treat APL for its ease of oral administration. Several clinical trial studies demonstrated the activity of As<sub>4</sub>S<sub>4</sub> in APL treatment and its similar mode of action to ATO (Lu et al. 2002; Zhu et al. 2013). As<sub>4</sub>S<sub>4</sub> has low bioavailability (~ 4%), because of its insolubility in water (J Liu et al. 2008). Its bioavailability and cytotoxicity increased when As<sub>4</sub>S<sub>4</sub> was ground to nano sizes, typically with diameter of 100 to 200 nm (Zhao et al. 2011). An animal model study demonstrated the enhanced absorption of As<sub>4</sub>S<sub>4</sub> nanoparticles (NPs) (Wu and Ho 2006). More than 50% of orally administered arsenic in the form of As<sub>4</sub>S<sub>4</sub> NPs was recovered from urine during the first 48 hours post-administration to rats. When coarse As<sub>4</sub>S<sub>4</sub> was orally administered, less than 25% of administered As<sub>4</sub>S<sub>4</sub> was recovered from the rat urine and the majority of As<sub>4</sub>S<sub>4</sub> was recovered from the feces. As<sub>4</sub>S<sub>4</sub> NPs can also be administered transdermally (Zhao et al. 2010). The tumor tissues were found to have the highest arsenic concentration, followed by liver, kidney, lung, small intestine, and heart.

Although ATO is water soluble and has good bioavailability, the study by Dong et al. (2015) showed that ATO NPs were more potent in inducing NB4 cell apoptosis than dissolved ATO solution with enhanced down-regulation of Bcl-2 protein. The ATO NPs were prepared using the sol-gel method. SEM scanning results showed that the morphology of ATO NPs was spherical or elliptical and the diameter was smaller than 40 nm. Though the reason for the enhanced potency

of ATO NPs was not elucidated, the researchers hypothesized that it was likely due to increased ease of uptake by tumor cells and slow drug release.

Arsonolipids are analogues of phosphonolipids, which were first synthesized by Tsivgoulis et al. (1991) Fatouros et al. (2010) mixed arsonolipids with phosphonolipids and prepared arsonoliposomes. A study on cytotoxicity evaluation of arsonoliposomes showed selective inhibition of tumor cells (HL-60, C6, and GH3 cells) survival with no significant effect on normal cells (HUVEC and RAME) under the same exposure conditions (Gortzi et al. 2002). More studies on the relation between the composition of arsonoliposomes and the stability and *in vivo* distribution of arsonoliposomes, and on the anticancer and antiprotozoal activity of arsonoliposomes were conducted (Antimisiaris et al. 2005; Piperoudi et al. 2005; Piperoudi et al. 2006). The researchers found that the anticancer activity of arsonoliposomes may be linked with the reduction of the pentavalent arsenic content to its more toxic trivalent form; the reduction was enhanced in areas where increased concentrations of thiol-containing reductive compounds prevailed (Antimisiaris 2009). The surface of arsonoliposomes can also be modified with affinity ligands. Al-Shehri et al. (2015) modified the arsonoliposome surface with antibodies of transferrin receptors (Tfr), which increased the uptake of arsonoliposomes by cells expressing Tfr.

Liposomes encapsulating ATO have been prepared by mixing ATO solution with small unilamellar lipid vesicles in suspension followed by dehydration and rehydration procedures (Kallinteri et al. 2004). However, ATO-encapsulated liposomes prepared using this method had fast arsenic release. To control the release of arsenic from liposomes, O'Halloran's group developed a new strategy by "taking advantage of weak acid transport properties and the fact that arsenite forms insoluble transitional metal (e.g., Ni<sup>2+</sup>, Co<sup>2+</sup>, Cu<sup>2+</sup>, Zn<sup>2+</sup>, Mn<sup>2+</sup>, Fe<sup>2+</sup>, and Pb<sup>2+</sup>) compounds" to co-encapsulate Ni and As NPs in classic liposomes (Chen et al. 2006). This strategy

enables pH-triggered slow release by converting the solid phase arsenic to aqueous phase and overcomes the limitation of the fast arsenic release (>95% after 24 h) from liposome capsules due to the high solubility of  $\text{AsO}_2^-$  in aqueous solution. The antitumor efficacy and pharmacokinetics of (Ni, As)-encapsulated liposomes were evaluated in breast cancer models, both *in vitro* and *in vivo* (Ahn et al. 2010; Chen et al. 2009). O'Halloran's group recently developed (Pt, As)-encapsulated liposomes. (Swindell et al. 2013) The combination of two chemotherapeutic agents is expected to be more potent in tumor suppression.

Inspired by the arsenic encapsulation strategy based on the formation of a water insoluble complex between arsenic and transitional ions, Gao and co-workers loaded  $\text{NiAsO}_x$  (Zhao et al. 2014) and  $\text{MnAsO}_x$  (ZH Zhao et al. 2015) into the hollow interiors of hollow silica NPs using an ion gradient mediated loading method. The  $\text{NiAsO}_x@SiO_2$  and  $\text{MnAsO}_x@SiO_2$  nanomaterials exhibited acidic pH-triggered release. Surface modification with EGFR-affibody can realize targeted delivery of arsenic to human HCC SMMC-7721 cells and murine hepatoma H22 cells (Zhao et al. 2014). Surface modification with GSH enhanced the colloidal stability of these NPs and extended the blood circulation duration (ZH Zhao et al. 2015). In addition, in the case of  $\text{MnAsO}_x@SiO_2$  nanomaterial,  $\text{Mn}^{2+}$  is a typical longitudinal relaxation time (T1) magnetic resonance imaging (MRI) contrast agent. Upon release of arsenic,  $\text{Mn}^{2+}$  is released simultaneously and the free  $\text{Mn}^{2+}$  ions have increased efficiency of direct chemical exchange between metal centers and surrounding protons. Therefore, the T1 signal is switched on when arsenic and  $\text{Mn}^{2+}$  are released. This phenomenon can be utilized for real-time monitoring of arsenic release *in vivo*. The researchers demonstrated the real-time visualization and monitoring of arsenic release and delivery in a mouse model and improved arsenic efficacy in HCC growth inhibition without noticeable adverse effects.

Multiple drugs can also be loaded onto the same nano drug carrier. Cai et al. (2014) loaded ATO and doxorubicin onto Fe<sub>3</sub>O<sub>4</sub> magnetic NPs via mechanical absorption polymerization. Although the loading amounts of arsenic and doxorubicin were not reported, the researchers demonstrated that dual-drug loaded formulation had better Raji cell growth inhibition induction and enhanced cellular accumulation of doxorubicin than mono-drug loaded formulations and control groups. Muhammad et al. (2014) utilized mesoporous silica nanoparticles (MSNs) as the nano drug carriers, and strategically loaded a hydrophobic drug camptothecin in the porous structures of MSNs and tethered Fe<sub>3</sub>O<sub>4</sub> magnetic NPs and ATO on the functionalized MSN surface. Dual-drug nano-formulation had significantly enhanced cell growth inhibition performance compared to single drug formulation and Fe<sub>3</sub>O<sub>4</sub> magnetic NPs allowed for MRI real-time monitoring of the nano drug delivery system *in vivo*.

Other nano drug carriers such as polymeric vesicles and polymer NPs have been used to encapsulate arsenic compounds. Polymeric vesicles are assembled from amphiphilic polymers and have a similar bilayer structure as liposomes. The Huang research group loaded ATO into the hydrophilic core of the vesicle formed by diblock copolymer of poly(ethylene glycol)-*block*-poly(D, L-lactide) (PEG-*b*-PDLLA), which achieved slow arsenic release (Qian et al. 2013; Zeng et al. 2014). The surface of the PEG-*b*-PDLLA vesicle can be conjugated with affinity ligands such as anti-CD44v6 single chain variable fragment for active targeted delivery of arsenic to PANC-1 cells expressing CD44 (Qian et al. 2013). Vesicles can also be prepared from polymer mixtures, such as PEG-*b*-PDLLA and poly(ethylene glycol)-*block*-poly(L-lysine) (PEG-*b*-PLL) for co-delivery of siRNA and ATO (Zeng et al. 2014). Wang et al. (2007) encapsulated ATO into NPs formed by high molecular weight PEGylated poly(lactic-*co*-glycolic acid) (PEG<sup>1500</sup>-*b*-

PLGA<sup>15000</sup>). The arsenic loading was relatively low (1.8 wt%) while the arsenic was released slowly over 20 days. The release of ATO was based mainly on the degradation of PLGA polymers.

## **1.2 Polymeric micelles as nano drug delivery carriers**

### **1.2.1 Nanomedicine**

Chemotherapy, together with surgery, radiation, and hormonal therapies, is the major treatment for cancer. The low molecular weight of chemotherapeutic agents causes short duration of circulation in blood, large volume of bio-distribution, and less specific retention in tumor tissue, which leads to severe adverse side effects. Most chemotherapeutic agents such as doxorubicin (DOX), paclitaxel (PTX), and camptothecin (CPT), are hydrophobic. The poor water solubility of these hydrophobic agents affects their absorption and bio-distribution *in vivo*, which in turn affects their therapeutic activity and induction of adverse side effects. Nanocarriers have been invented to improve the solubility and efficacy while alleviating the side effects of chemotherapeutic agents by changing the pharmacokinetics (Venugopal et al. 2008).

Nanocarriers that are extensively studied include NPs such as silica NPs (He and Shi 2011), quantum dots (Zrazhevskiy et al. 2010), and gold NPs (Boisselier and Astruc 2009), nanocapsules with core-shell structures such as liposomes (Sercombe et al. 2015), polymeric micelles (Gothwal et al. 2016), and polymeric vesicles (Uchegbu 2006), and single macromolecules (Cheng et al. 2011). These nanocarriers share the feature of their size which ranges from 30 nm to 200 nm. Chemotherapeutic agents delivered via these nanocarriers have shown a better accumulation in solid tumor tissues than free drugs (Markman et al. 2013). This phenomenon is attributed to the enhanced permeation and retention (EPR) effect, which is closely associated with tumor angiogenesis and reduced or obstructed lymphatic drainage in tumor area (Barreto et al. 2011). The EPR effect was first observed by Maeda and Matsumura when they were evaluating the bio-

distribution and pharmacokinetics of the protein-polymer conjugate SMANCS (Matsumura and Maeda 1986). The researchers found that the conjugate had more prolonged circulation in plasma and improved drug accumulation in tumor than the free protein. The researchers related their observation to the vascular characteristics including “(a) hypervascularity, (b) enhanced vascular permeability, (c) little recovery of macromolecules via blood vessels, and (d) little recovery from the lymphatic system.” (Matsumura and Maeda 1986) The EPR effect is heterogeneous due to the heterogeneity of solid tumors (Maeda 2012). The optimum size of nanocarriers that can be accumulated in tumor areas by the EPR effect is unknown. The cut-off size of the pores in tumor vessels ranges as wide as 200 nm to 2 μm (Gothwal et al. 2016). Nanocarriers whose size ranges from 30 to 200 nm can avoid the excretion from renal system (<30 nm) and clearance by phagocytosis (>200 nm) and avoid normal tissues via the intact endothelial blood vessels while being able to enter the tumor area (Barreto et al. 2011).

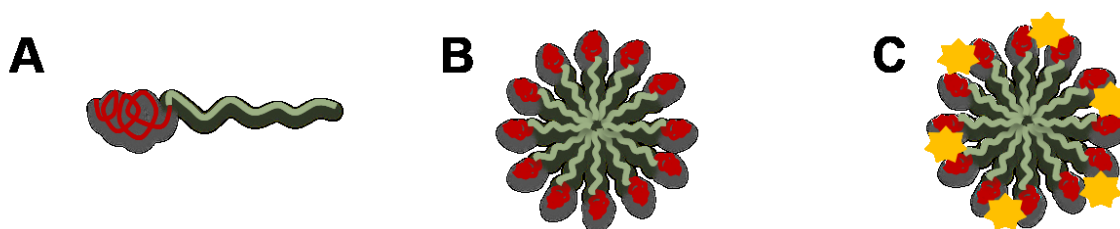


**Figure 1.3. Structure of micelles.** (A) Amphiphilic polymer chain; (B) Micelle assembled from polymer chains; (C) Micelle with surface modification of affinity ligands.

Polymeric micelles are among the most popular nanocarriers studied (Elsabagy and Wooley 2012; Gothwal et al. 2016; Tong et al. 2014; van der Meel et al. 2013). Polymeric micelles are self-assembled by amphiphilic block copolymers, with hydrophilic segments forming the micelle shell and hydrophobic segments forming the micelle core (**Figure 1.3**). The micelle surface is usually composed of poly(ethylene oxide) (PEO), which is known for its excellent biocompatibility and stealth nature in blood circulation (Otsuka et al. 2003). The micelle surface

can be modified with affinity ligands that can recognize target tumor cells or be functionalized with stimuli-responsive moieties. The micelle surface properties control the pharmacokinetics of drug-loaded micelles. Hydrophobic chemotherapeutic agents can be encapsulated inside the micelle core, as the hydrophobic micelle core environment enables better solubilisation and retention of hydrophobic drugs.

Polymer chains, especially the hydrophobic segments, are very versatile. The hydrophobic segments of the amphiphilic polymers can be polyesters, polyamides, polyethyleneimines, and polyacrylates (Elsabahy and Wooley 2012). The polymer chain can be formed from two or multiple blocks of polymers, or from randomly distributed copolymers (Bergman et al. 2014; Wyman and Liu 2013). Pendant groups with different functionalities can be grafted onto the polymer backbone. Since the property of micelle assembly is controlled by the chemical nature of each polymer chain and polymer block, the properties of micelles can be tuned to fulfill specific requirements simply through polymer modification (Tong et al. 2014). Polymer chains can also be crosslinked either at the micelle core (Rijcken et al. 2007) or at the micelle shell (Jimenez-Pardo et al. 2015) to improve the stability of the micelles and control the release of the drug. The versatility of polymer chains enables polymeric micelles as a promising nanocarrier for targeted drug delivery.

## **1.2.2 Advantages of micelles derived from the versatile polymer structures**

### **1.2.2.1 Enhanced cargo loading**

The encapsulation of drugs into polymeric micelle cores is based on hydrophobic interaction, hydrogen bonding, complexation, covalent bonding, or a mixture of two or more of the mechanisms mentioned. To increase the drug loading content and better retain the drug in polymeric micelles, a variety of strategies to promote the interactions between drug and polymer chains have been developed (Ishihara and Mizushima 2010).

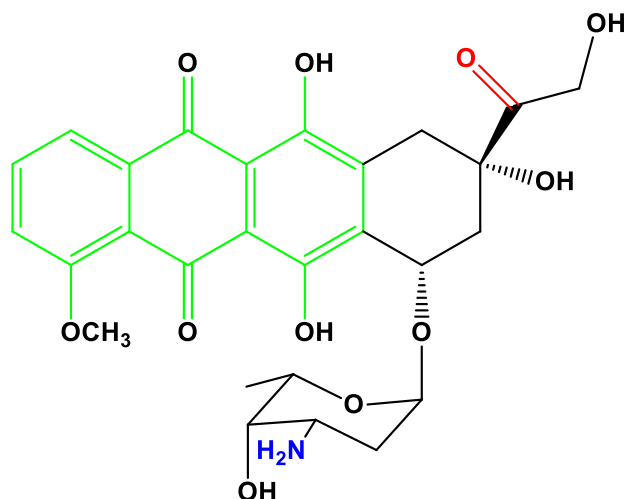


**Figure 1.4. Structure of doxorubicin (DOX).** DOX contains a tetracycline ring structure and an amino sugar daunosamine moiety. The presence of a primary amine group (blue), a carbonyl group (red), as well as a planar anthraquinone (green) structure allows for different types of interaction between DOX and polymer chains.

Taking into account the versatile nature of polymers and relatively more conserved structures of drugs, polymer chains are amenable to modifications to enhance the encapsulation of a certain drug based on its structure. DOX is a popular model drug used in drug delivery system development research. DOX (**Figure 1.4**) is an anthracycline antibiotic which has been widely used as an effective chemotherapeutic agent in different cancers, though it has severe cardiac toxicity (Chlebowski 1979). The chemical structure of DOX involves a tetracycline ring structure and an amino sugar daunosamine moiety (**Figure 1.4**). The presence of hydroxyl groups, a primary amine group, a carbonyl group, as well as a planar anthraquinone structure allows for strong interaction between DOX and polymer chains with multiple mechanisms. Zhang and coworkers incorporated phenylethyl amine in poly(amide amine)-graft-poly(ethylene glycol) (PAA-g-PEG) synthesis and prepared micelles for DOX encapsulation (Sun et al. 2010; Y Sun et al. 2013). The planar anthraquinone structure enables  $\pi$ - $\pi$  stacking and hydrophobic interaction between DOX and the phenyl groups in the micelle core, which resulted in high DOX loading content in these PAA-g-PEG micelles (Y Sun et al. 2013). The primary amine group on the daunosamine moiety

of DOX can be easily protonated. This phenomenon enables complexation between the acidified DOX and anionic polymer chains. Yousefpour et al. (2011) used the polyanionic carbohydrate dextran sulfate (DS) to form DOX-encapsulated NPs. The DOX-DS complexation could be thoroughly disturbed at ionic strengths  $>0.3$  M when the ions in solution shielded electrostatic charges of DS and DOX. DOX release was triggered upon addition of the polycationic chitosan which competed for the binding of the polyanionic DS. These results strongly suggested that electrostatic interaction played an important role in DOX-DS complexation. In this DOX-DS complexation situation, electrostatic interaction is not the unique mechanism. The addition of ethanol, which is a hydrogen bond disturbing agent, could also dissociate the DOX-DS complex, suggesting that hydrogen bonding was another mechanism for DOX-DS complexation. A more prevalent strategy in DOX encapsulation is via covalent bonding. The amine group on the daunosamine moiety can be used to form an amide bond for DOX conjugation to the polymer chain (Xiong et al. 2010a), and the carbonyl group on the 2-hydroxyl acetyl substitute can be used to form an acid-labile hydrazone bond (Kang et al. 2015; HA Li et al. 2015; Xiong et al. 2010a).

#### **1.2.2.2 Triggered release**

During tumor progression, both the extracellular and the intracellular microenvironments in tumor cells and tissues experience alterations. Fast tumor cell proliferation and chronic inflammation are accompanied by reduced pH in the extracellular matrix surrounding the tumor cells, elevated temperature in tumor area, elevated redox potential in the tumor cells, and overexpression of enzymes and signal-transduction receptors on the cell membrane and in the cytosol and specific organelles (Hanahan and Weinberg 2011). Taking advantage of these physiopathological alterations in tumor tissues, stimuli-responsive strategies can be designed to trigger the drug release from nano-carriers (**Figure 1.5**). External stimuli such as heat, ultrasound, magnetic fields, and light can also be utilized to facilitate and enhance the local release of encapsulated drugs.

Stimuli-responsive carriers for targeted drug delivery have been extensively reviewed (JZ Du et al. 2015; Li et al. 2013; Zhu and Torchilin 2013). Herein, selected popular strategies for pH-, redox-, and thermo-triggered drug release from polymeric micelles are summarized. These strategies can be easily combined in one drug delivery system to realize programmed site-specific drug delivery (Chen et al. 2013; Cheng et al. 2013; Lee et al. 2014; Salehi et al. 2015).

#### **1.2.2.2.1 pH-responsive polymeric micelle**

A typical pH-responsive micelle system is based on acid-catalyzed bond cleavage. Polymer backbones composed of polyesters and polyamides are biodegradable. The polymer backbone degradation results in the disassembly of the micelles, which facilitates the drug release (Hu et al. 2015; XF Liu et al. 2015). The majority of esters and amides are not sensitive to the mildly acidic extracellular environment of tumor tissues (~ pH 6.8) and can only respond to the more acidic lysosome environment (~ pH 4–5) (Tong et al. 2014). More sensitive acid-labile bonds such as cis-aconityl bond (Song et al. 2015) and hydrozone bond are more popular in recent research.

The hydrozone bond can be used to conjugate doxorubicin to the end of a polymer chain (Kang et al. 2015) or to the pendant groups of a polymer (Nguyen et al. 2013; Xiong et al. 2010a). The release of doxorubicin was significantly enhanced at pH 6 compared to neutral pH (Kang et al. 2015). The hydrozone bond can serve as a linker to connect the hydrophobic and the hydrophilic segments of an amphiphilic polymer (XL Zhang et al. 2015). XL Zhang et al. (2015) demonstrated that the release of paclitaxel from the PEG-hydrozone-farnesylthiosalicylate micelles was triggered at pH 6.8 while the micelles were fairly stable at pH 7.4.

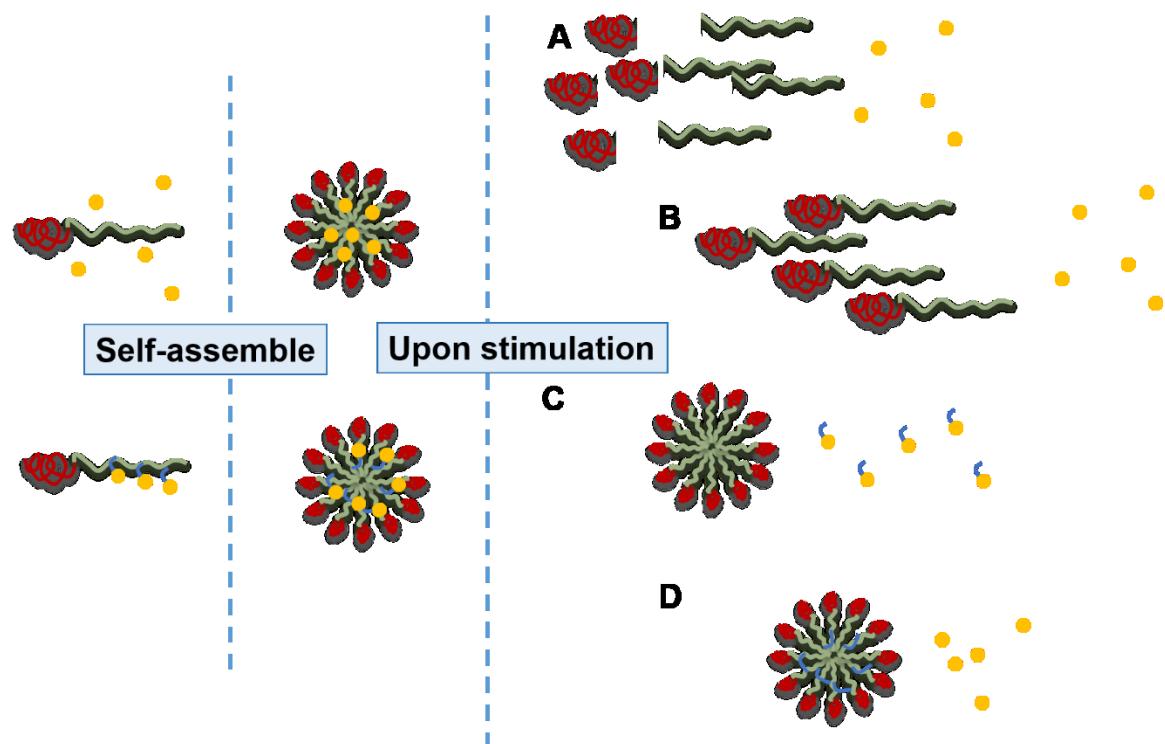


**Figure 1.5. Stimuli-triggered release.** (A) Polymer degradation upon stimulation resulting in drug release; (B) Micelle dissociation upon stimulation resulting in drug release; (C) Conjugated drug together with the linker is cleaved from the polymer backbone; (D) Conjugated drug is cleaved from the polymer backbone.

Another pH-responsive design is based on ionisable polymers at low pH that causes micelle swelling or dissociation. Polymers with imidazole rings such as poly(histidine) are hydrophobic at neutral pH, therefore can be used to form the micelle core structure (Sun et al. 2015). When the solution pH decreases, the imidazole rings are protonated and the polymer is gradually converted from hydrophobic to hydrophilic. The hydrophobic–hydrophilic transition leads to micelle dissociation, which causes burst release of encapsulated drug. The release of encapsulated doxorubicin from poly(ethylene glycol)-block-poly(glutamic acid)-graft-(N-[3-aminopropyl]-imidazole) micelles was enhanced when the pH decreased from 7.4 to 6.5 and further to 5.0 (Guan et al. 2015). Tertiary amide-containing polymers such as poly(2-ethyl-2-oxazoline) can swell at

low pH as well, and have been used to prepare pH-responsive micelles for drug delivery (Y Zhao et al. 2015).

#### **1.2.2.2.2 Redox-responsive polymeric micelle**

Redox-sensitive micelles have been designed to trigger burst release of encapsulated drugs in response to the intracellular redox potential. Reduction sensitive micelles usually contain characteristic disulfide linkages in the main chain (MT Cai et al. 2015; TJ Yin et al. 2015), at the side chain (Chen et al. 2015), or in the crosslinking segment (Han et al. 2015; Shao et al. 2014), as reviewed by HL Sun et al. (2013) When the disulfide bond is cleaved via thiol-disulfide exchange reactions by intracellular reducing molecules, such as GSH, which occurs naturally in cells at mM levels, the release of encapsulated drug will be triggered, either due to micelle collapse resulting from a broken polymer backbone or reduced micelle stability, or due to the cleaved covalent bond that conjugates the drug to the polymer chain.

For instance, Li et al. (2012) used a disulfide bond to connect the hydrophilic hyaluronic acid (HA) segment with the hydrophobic deoxycholic acid (DOCA). The HA-SS-DOCA conjugate can form micelles with a core-shell structure and can be used as the carrier for paclitaxel delivery. After entering the tumor cell via endocytosis, the conjugate would be cleaved by GSH, leading to the collapse of the micelles and triggering a burst release of encapsulated paclitaxel in the cytosol.

In contrast to the large number of studies on reduction-responsive micelles, micelles that respond to oxidative molecules in tumor cells have been studied to a less extent. Due to the elevated metabolic activity in tumor cells, the majority of tumor cells have a higher concentration of ROS in cytosol. Illuminescence methods based on peroxalate and boronic esters were developed to determine the concentration of hydrogen peroxide ( $H_2O_2$ ) in living cells (Lee et al. 2008; Lee et al. 2011; Lippert et al. 2011; Sun et al. 2012). Some of these  $H_2O_2$  detection methods were applied to

developing H<sub>2</sub>O<sub>2</sub>-responsive micelles for triggered drug release. Almutairi and coworkers synthesized two sets of polymers with 2,6-di(hydroxymethyl)benzene and adipic acid forming the polymer backbone and boronic acid pinacol ester as the pendant group (**Figure 1.6**) (Lux et al. 2012). **Polymer 1** had the boronic ester directly bound to the benzene ring, while **Polymer 2** used a benzylic ether linker to connect the boronic ester to the polymer backbone. Both polymers could form biodegradable NPs and the NPs formed from **Polymer 2** were more sensitive to biologically relevant levels of H<sub>2</sub>O<sub>2</sub> (50–100 μM). Inspired by the study of Almutairi and coworkers, Fu et al. (2015) prepared ABA-type triblock amphiphilic polycarbonates, with PEG grafted on A block and 4-methylphenylboronic acid pinacol ester grafted on B block. Micelles were prepared from these triblock polycarbonates with B blocks bearing the hydrophobic aromatic boronate forming the micelle core. Upon exposure to H<sub>2</sub>O<sub>2</sub>, boronate and 4-methylenecyclohexa-2,5-dienone were subsequently cleaved, leaving a hydrophilic polycarbonate backbone. Consequently, the micelles collapsed and the release of encapsulated drug was triggered. Polyoxalates were also used to prepare H<sub>2</sub>O<sub>2</sub>-responsive biodegradable NPs for drug delivery (Kim et al. 2010). Oxidative-responsive micelles with polyoxalate components are expected to be synthesized in the near future.

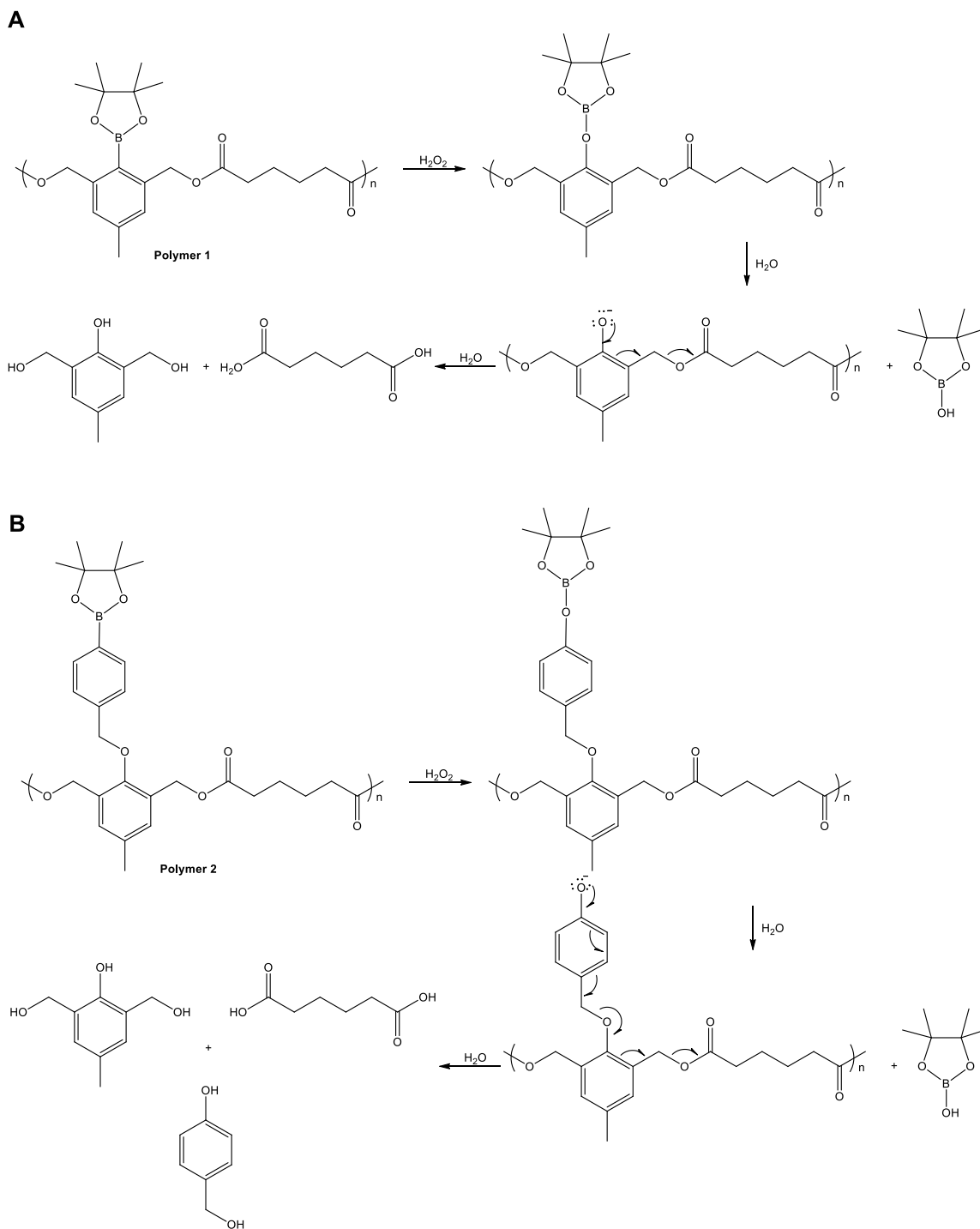


**Figure 1.6** Schema illustrating  $\text{H}_2\text{O}_2$ -triggered degradation of polymers containing boronic ester. (Adapted from reference Sun et al. 2012)

### 1.2.2.2.3 Thermo-responsive polymeric micelles

Poly(N-isopropylacrylamide) (PNIPAAm) is known for exhibiting reversible thermo-responsive phase transition in an aqueous solution at around 32 °C, termed lower critical solution temperature (LCST) (Da Silva et al. 2007). PNIPAAm adopts an extended coil conformation and is hydrophilic when the temperature is lower than LCST, while it has a globular conformation and is hydrophobic when the temperature is higher than LCST. This feature can be used to realize site-specific drug release upon local heating. An LCST at 32 °C is not desirable for further application in human body. The LCST can be increased to 37–42 °C by incorporating co-monomers with higher hydrophilicity, such as acrylamide (BR Liu et al. 2008; Yang et al. 2007), N,N-dimethylacrylamide (DMAM) (Xu et al. 2013), and N-hydroxymethylacrylamide (PHMAAm) (C Cheng et al. 2008).

Xu et al. (2013) synthesized the diblock terpolymer P(NIPAAm-*co*-DMAM)-*b*-PDLLA with an LCST at 40.0 °C to prepared micelles with PDLLA forming the micelle core and P(NIPAAm-*co*-DMAM) forming the micelle shell. When the temperature was increased from 37 °C to 45 °C, the P(NIPAAm-*co*-DMAM) polymer shrank from extended coil conformation to granular conformation with increased hydrophobicity, which resulted in deformation and collapse of the micelle structure. Therefore the loaded drug (prednisone in the study by Xu et al. 2013) was released much faster at 45 °C than at 37 °C and the cytotoxicity of prednisone-loaded micelles was substantially enhanced with the increase of incubation temperature. To further enhance the stability of micelles, Chen et al. (2008) prepared micelles from the triblock polymer PEG-*b*-P(NIPAAm-*co*-HMAAm)-*b*-PMMA with an LCST at 40.8 °C, where poly(methyl methacrylate) (PMMA) formed the hydrophobic micelle core, P(NIPAAm-*co*-HMAAm) formed the thermoresponsive stealth layer, and PEG formed the hydrophilic micelle shell. Similarly, the release of the encapsulated drug was enhanced when the temperature was increased from 37 °C to 42 °C.

Another set of thermosensitive polymers is hydroxypropyl cellulose (HPC). When the temperature increases, the hydrophobicity of HPC increases, promoting agglomeration. Bagheri et al. (2014) functionalized the pendent hydroxyl groups on HPC with PEG, cholesterol (Chol), and biotin, and prepared NPs with core-shell structure with Chol forming the core. The PEG-HPC-Chol-Biotin polymer had an LCST at around 40 °C and was able to release the encapsulated drug at a higher speed at 41 °C than at 37 °C.

#### **1.2.2.2.4 Tumor targeting**

As mentioned above, tumor tissues exhibit alterations in the extracellular matrix compared to normal tissues, including increased acidity and temperature, as well as overexpression of enzymes and signal transduction receptors on the cell membrane. Therefore, strategies responsive to these stimuli can also be applied to promote the internalization of micelles into tumor cells (**Figure 1.7**).

The strategy of using micelles with surface modification of affinity ligands that recognize receptors specifically expressed or overexpressed in tumor cells is the most common. Peptides containing the arginine-glycine-aspartic acid (RGD) motif are among the most popular ligands in proof-of-concept model studies (Gao et al. 2015; Guan et al. 2015; JJ Liu et al. 2015; Makino et al. 2015; Song et al. 2015). Many solid tumor cells and tumor vasculature endothelial cells overexpress  $\alpha_v\beta_3$  integrin, which promotes the metastatic phenotypes by supporting specific adhesive, invasive, and migratory properties of tumor cells (Felding-Habermann et al. 2002). The RGD-containing peptide is well known as a recognition motif in multiple ligands for integrins (Duggan and Hutchinson 2000). Due to the rigidity of cyclic peptides, cyclic RGD peptides are more specific and sensitive in recognizing their receptors than linear RGD peptides (Gurrath et al. 1992). Micelles with surface conjugation of cyclic RGD peptides such as c(RGDfK) (JJ Liu et al.

2015) and c(RGDyK) (Gao et al. 2015) have demonstrated enhanced accumulation of anti-tumor therapeutics in tumors and better antitumor activity than free drugs in *in vivo* studies.

Other commonly used affinity ligands include folic acid (Hu et al. 2015), antibodies (Zhou et al. 2015), functional antibody fragments (Talelli et al. 2011), and transferrin (Singh et al. 2016). In some cases, an antibody is too large to be conjugated on a micelle surface. To circumvent this challenge, pre-targeting is proposed. Considering the considerable affinity between biotin and avidin, C Cheng et al. (2008) pretreated HeLa cells with biotin-transferrin complex for 2 h before treating the cells with avidin-conjugated rhodamine B-loaded micelles. HeLa cells pretreated with biotin-transferrin showed remarkably more intense fluorescence in both the cell membrane and the cytoplasm than those without biotin-transferrin pretreatment.

In addition to the ligand-receptor interaction, a surface charge switch responsive to the mild acidic extracellular tumor cell environment can also be used to promote the micelle internalization specifically into tumor cells but not normal cells. XF Yu et al. (2014) synthesized a pH-responsive conformation switching polymer bearing multiple choline phosphate (CP) pendant groups. The CP groups can bind to the phosphatidyl choline (PC) lipids in cell membrane. At pH 7.4, the polymers collapsed hydrophobically and the CP groups were buried inside the polymer globule, which prevented the binding of the polymer to the cell membrane via CP-PC interaction. The researchers adjusted the pH sensitivity of this polymer by incorporating one or two 2-(dimethylamino)ethyl methacrylate (DMAEMA) monomers, which would be protonated at pH 6.8. The protonation of DMAEMA changes the hydrogen bonding and solubility of the polymer, and the polymer globule cannot be formed. Therefore, the CP groups were revealed at pH 6.8 and promoted the binding of the polymer to the cell membrane. In addition to the protonation of existing polymer pendant groups, an acid-labile bond cleaved at pH 6.8 can also reveal new primary amine groups that can

be protonated at pH 6.8. JM Shen et al. (2013) generated a lysine-galactose ligand to decorate the polymeric micelle surface. Galactose was conjugated with lysine via an acid-labile C=N bond (Schiff base), and lysine was covalently conjugated to the polymer via a stable amide bond. Upon exposure to the mildly acidic extracellular matrix at pH 6.8, the Schiff base was cleaved, leaving protonated lysine on the micelle surface. Similarly, a carboxydimethyl maleate (CDM) moiety is very sensitive to a mildly acidic environment, and has been used to enhance the endocytosis of micelles (Tangsangasaksri et al. 2016).

External stimuli such as heat can also be applied to promote the micelle internalization. Wu et al. (2015) prepared micelles from a polymer mixture of biotin-PEG-*b*-PCL and PNIPAAm-*b*-PCL. The micelle corona was composed of PNIPAAm and biotin-PEG blocks. At temperatures below the LCST, such as 25 °C, the PNIPAAm chains were in extended conformation and the biotin was buried between the PNIPAAm chains. Therefore, target tumor cells (HepG2 cells in this study) could not recognize these micelles. When the temperature was increased to 42 °C, which was above the LCST, the PNIPAAm chains underwent aggregation and converted to a globular conformation. In this situation, the buried biotin groups were revealed on the micelle surface, which led to enhanced cellular uptake of these micelles.

After being internalized into cells via endocytosis, micelles and encapsulated drugs have to escape from the endosome to reach target subcellular organelles to take action. Most drug release takes place in the endosome where the polymer micelles are dissociated or the polymer backbone is degraded at low pH in late endosomes (pH ~ 5.0), and the drug diffused out into the cytosol (ZZ Du et al. 2015). Amine-containing polymers can absorb protons by adopting the protonated state in late endosomes, which causes osmotic pressure build-up within endosomes and consequently leads to destabilization and rupture of endosomes (Behr 1997; Jhaveri and Torchilin 2016). With

sophisticated design of the structure of polymer forming micelles, Tangesangasaksri et al. (2016) were able to effectively deliver siRNA in cytosol with enhanced RNA interference efficacy.

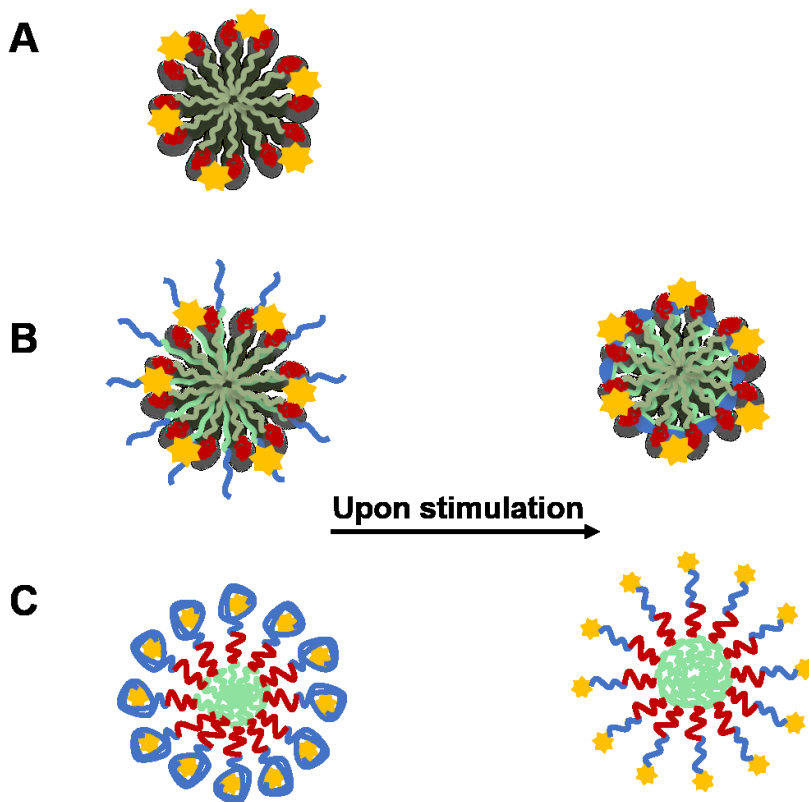


**Figure 1.7. Targeting with affinity ligands.** (A) Basic micelle with surface modification of affinity ligands; (B) Mixed micelle with affinity ligands sheathed by stimuli-responsive polymers; (C) Micelles with conjugated affinity ligands buried inside stimuli-responsive polymers. For (B) and (C), upon stimulation in the microenvironment of tumor tissues, the surface polymer will undergo conformational change, revealing affinity ligands on the micelle surface.

### 1.2.3 PEO-*b*-PCL based polymeric micelles

Poly( $\epsilon$ -caprolactone) (PCL) is an inexpensive and safe FDA-approved biomaterial with good compatibility with a variety of hydrophobic drugs, polymers, and organic solvents (Ulery et al. 2011). PCL is a highly hydrophobic polymer that can form semicrystalline structures, which results in a very slow degradation rate of PCL in aqueous environment. Capronor®, a PCL-based subdermal-implanted contraceptive device, is able to deliver levonorgestrel *in vivo* for 12 to 18 months (Darney et al. 1989). The slow biodegradation rate somehow limits the application of PCL

in drug delivery where the encapsulated drugs should be released within days or weeks (Woodruff and Hutmacher 2010). Therefore, research and application of PCL was not as popular as polyglycolide (PGA) and PDLLA during 1980s and 1990s.

The high hydrophobicity of the PCL polymer, however, helps to form PEO-*b*-PCL micelles with good thermodynamic stability and good solubilisation of hydrophobic drug in the micelle core. PEO-*b*-PCL micelles have been used to encapsulate cyclosporine A (Aliabadi et al. 2005), amiodarone (Elhasi et al. 2007), curcumin (Ma et al. 2008), and numerous other drugs with good drug retention in the micelle core. A reduction-sensitive disulfide bond can be used to conjugate the PEO segment and the PCL segment. The incorporation of S–S bond into the PEO-SS-PCL polymer backbone facilitates the triggered drug release by shedding the PEO shell and disassembling the micelle structure (Sun et al. 2009; Wang et al. 2012).

Modifications can be introduced to the  $\alpha$ -carbon of  $\epsilon$ -caprolactone, which enables the synthesis of PEO-*b*-PCL based micelles with tunable micelle stability and drug encapsulation capacity via covalent bonding. Mahmud et al. (2006) functionalized the  $\alpha$ -carbon of  $\epsilon$ -caprolactone with a benzyl carboxylate substituent by anionic activation of  $\epsilon$ -caprolactone and further treatment with benzyl chloroformate. The benzyl groups can be further removed by hydrogen reduction, leaving the carboxylic acid group as the pendant group for future functionalization. Using a similar method, Rezaei et al. (2015) were able to synthesize poly ( $\alpha$ -*tert*-butyl acetate- $\epsilon$ -caprolactone), whose *tert*-butyl acetate groups can be hydrolyzed to leave the acetic acid groups as the pendant groups for further modification. In addition to carboxylic acid groups, azide groups can also be conjugated onto the PCL backbone (Cajot et al. 2011; G Yin et al. 2015). With these functional groups on PCL polymers, drugs such as PTX (Shahin and Lavasanifar 2010) and DOX (Xiong et al. 2010a) can be covalently encapsulated inside the

micelles formed from PEO-*b*-PCL based polymers, and the polymer chains can be cross-linked to form more stable micelles (Cajot et al. 2011).

Similar to other polymeric micelles, the surface of PEO-*b*-PCL micelles can also be modified with affinity ligands for active target drug delivery. PEO with acetal-end group is usually used for peptide conjugation. RGD-containing peptides such as GRGDS (Xiong et al. 2007) and RGD4C (Xiong et al. 2010b) have been conjugated onto the PEO-*b*-PCL micelle surface. Enhanced accumulation of dye and drugs were observed in target cells. More impressively, Xiong et al. (2010b) were able to co-deliver DOX and siRNA that can down-regulate the expression of P-glycoprotein (P-gp) in a mixed PEO-*b*-PCL micelle with surface decoration of both the RGD4C peptide and the cell penetrating peptide (TAT) in MDA-MB-435/LCC6 cells which were resistant to DOX due to overexpression of the P-gp protein on the cell membrane. Improved cellular uptake, P-gp silencing, DOX cellular accumulation, DOX nuclear localization, and DOX induced cytotoxicity in MDA435/LCC6 cells were realized simultaneously with this virus-mimicking micelle delivery system.

### **1.3 Scope of this thesis**

Arsenic trioxide is an effective chemotherapeutic agent for APL while having limited activity in solid tumor treatment. Adverse side effects such as cardiac toxicity remain the main concern about arsenic therapy. Nano drug delivery systems with the capability to deliver drug into targeted tumor areas are expected to improve the therapeutic efficacy of arsenic therapy for solid tumor treatment and alleviate its adverse side effects. Nano-carriers that have been studied for arsenic encapsulation are mainly limited to liposomes, polymer vesicles, and polymer NPs, as summarized in **Section 1.1.4.3**. Polymeric micelles have not been used for arsenic delivery. Since arsenic trioxide is highly

water soluble and it is very challenging to encapsulate a small hydrophilic molecule into the hydrophobic micelle core, poor arsenic loading and fast arsenic release is expected.

The ultimate goal of my thesis research is to develop a polymeric micelle system for targeted delivery of arsenicals to specific tumor cells. To achieve this goal, the specific objectives of this thesis are (1) to develop a strategy for efficient encapsulation of arsenicals in polymeric micelles, (2) to decorate the micelle surface with affinity ligands for targeted arsenic delivery to tumor cells, and (3) to tune the micelle stability and enhance cellular uptake of arsenic via micelle endocytosis. This thesis comprises five chapters. **Chapter 1** summarizes the therapeutic application of arsenic compounds and polymeric micelles as nano drug carriers. **Chapter 2** describes a strategy development based on arsenic-sulfur chemistry for efficient arsenic encapsulation in micelles. Phenylarsine oxide, an organoarsenical, is used as a model molecule. The arsenic-encapsulated micelles were evaluated in regard of arsenic loading, *in vitro* arsenic release, and *in vitro* cytotoxicity, which demonstrated that arsenic can be successfully encapsulated into micelles by complexation between arsenic and thiol groups. **Chapter 3** evaluates mixed micelles with surface decoration of RGD peptide for targeted delivery of arsenic trioxide to MDA-MB-435 breast cancer cells. RGD peptide decoration enhances cytotoxicity and cellular uptake of encapsulated arsenic compared to control mixed micelles without the RGD peptide on the surface. However, the fast release of arsenic from mixed micelles diminishes the targeting effect of the RGD peptide. **Chapter 4** describes three terpolymeric micelles with varying polymer chain arrangements and investigates the effect of polymer chain arrangement on micelle stability and cellular uptake of encapsulated arsenic. Polymer chain arrangements influence the micelle stability and surface charge by affecting the micelle structure. **Chapter 5** summarizes the overall results, discusses the limitations and implications of this study, and suggests future perspectives.

## 1.4 References

- Ablain J, de The H. 2011. Revisiting the differentiation paradigm in acute promyelocytic leukemia. *Blood* 117:5795-5802.
- Ahn RW, Chen F, Chen HM, Stern ST, Clogston JD, Patri AK, et al. 2010. A novel nanoparticulate formulation of arsenic trioxide with enhanced therapeutic efficacy in a murine model of breast cancer. *Clinical Cancer Research* 16:3607-3617.
- Al-Shehri A, Favretto ME, Ioannou PV, Romero IA, Couraud PO, Weksler BB, et al. 2015. Permeability of pegylated immunoarsonoliposomes through in vitro blood brain barrier-medulloblastoma co-culture models for brain tumor therapy. *Pharmaceutical Research* 32:1072-1083.
- Aliabadi HM, Mahmud A, Sharifabadi AD, Lavasanifar A. 2005. Micelles of methoxy poly(ethylene oxide)-b-poly(epsilon-caprolactone) as vehicles for the solubilization and controlled delivery of cyclosporine a. *Journal of Controlled Release* 104:301-311.
- Alimoghaddam K, Sharifabrizi A, Tavangar M, Sanaat Z, Rostami S, Jahani M, et al. 2006. Anti-leukemic and anti-angiogenesis efficacy of arsenic trioxide in new cases of acute promyelocytic leukemia. *Leukemia & Lymphoma* 47:81-88.
- Antimisiaris SG, Klepetsanis P, Zachariou V, Giannopoulou E, Ioannou PV. 2005. In vivo distribution of arsenic after i.P. Injection of arsonoliposomes in balb-c mice. *International Journal of Pharmaceutics* 289:151-158.
- Antimisiaris SG. 2009. Arsonoliposomes for drug delivery applications. *Clinical Lipidology* 4:663-675.
- Arana-Trejo RM, Sanchez ER, Ignacio-Ibarra G, de la Fuente EB, Garces O, Morales EG, et al. 2002. Bcr/abl p210, p190 and p230 fusion genes in 250 mexican patients with chronic myeloid leukaemia (cml). *Clinical and Laboratory Haematology* 24:145-150.
- Bagheri M, Shateri S, Niknejad H, Entezami AA. 2014. Thermosensitive biotinylated hydroxypropyl cellulose-based polymer micelles as a nano-carrier for cancer-targeted drug delivery. *Journal of Polymer Research* 21:15.

- Bajorin DF, Halabi S, Small E. 2009. Arsenic trioxide in recurrent urothelial cancer: A cancer and leukemia group b phase ii trial (calgb 99903). *Clinical Genitourinary Cancer* 7:E66-E70.
- Barreto JA, O'Malley W, Kubeil M, Graham B, Stephan H, Spiccia L. 2011. Nanomaterials: Applications in cancer imaging and therapy. *Advanced Materials* 23:H18-H40.
- Beer TM, Tangen CM, Nichols CR, Margolin KA, Dreicer R, Stephenson WT, et al. 2006. Southwest oncology group phase ii trioxide in patients with refractory malignancies. *Cancer* 106:2624-2629.
- Behr JP. 1997. The proton sponge: A trick to enter cells the viruses did not exploit. *Chimia* 51:34-36.
- Bergman JA, Cochran EW, Heinen JM. 2014. Role of the segment distribution in the microphase separation of acrylic diblock and triblock terpolymers. *Polymer* 55:4206-4215.
- Boisselier E, Astruc D. 2009. Gold nanoparticles in nanomedicine: Preparations, imaging, diagnostics, therapies and toxicity. *Chemical Society Reviews* 38:1759-1782.
- Buchet JP, Heilier JF, Bernard A, Lison D, Jin TY, Wu XW, et al. 2003. Urinary protein excretion in humans exposed to arsenic and cadmium. *International Archives of Occupational and Environmental Health* 76:111-120.
- Burnett AK, Russell NH, Hills RK, Bowen D, Kell J, Knapper S, et al. 2015. Arsenic trioxide and all-trans retinoic acid treatment for acute promyelocytic leukaemia in all risk groups (aml17): Results of a randomised, controlled, phase 3 trial. *Lancet Oncology* 16:1295-1305.
- Byun JH, Cheong H-J, Won J-H, Park H-S, Hong YS, Kim S-J, et al. 2003. Effect of arsenic trioxide in trail (tumor necrosis factor-related apoptosis inducing ligand)-mediated apoptosis in multiple myeloma cell lines. *Cancer Research and Treatment* 35:472-477.
- Cai MT, Leng MT, Lu AJ, He L, Xie XX, Huang L, et al. 2015. Synthesis of amphiphilic copolymers containing zwitterionic sulfobetaine as ph and redox responsive drug carriers. *Colloids and Surfaces B-Biointerfaces* 126:1-9.
- Cai XH, Wang CL, Chen BA, Hua WJ, Shen F, Yu L, et al. 2014. Antitumor efficacy of dmsa modified fe<sub>3</sub>o<sub>4</sub> magnetic nanoparticles combined with arsenic trioxide and adriamycin in raji cells. *Journal of Biomedical Nanotechnology* 10:251-261.

- Cai XY, Yu K, Zhang LJ, Li YF, Li Q, Yang ZB, et al. 2015. Synergistic inhibition of colon carcinoma cell growth by hedgehog-gli1 inhibitor arsenic trioxide and phosphoinositide 3-kinase inhibitor ly294002. *Oncotargets and Therapy* 8:7.
- Cajot S, Lautram N, Passirani C, Jerome C. 2011. Design of reversibly core cross-linked micelles sensitive to reductive environment. *Journal of Controlled Release* 152:30-36.
- Carmignani M, Volpe AR, Aldea M, Soritau O, Irimie A, Florian IS, et al. 2014. Glioblastoma stem cells: A new target for metformin and arsenic trioxide. *Journal of Biological Regulators and Homeostatic Agents* 28:1-15.
- Chakraborti D, Mukherjee SC, Saha KC, Chowdhury UK, Rahman MM, Sengupta MK. 2003. Arsenic toxicity from homeopathic treatment. *Journal of Toxicology-Clinical Toxicology* 41:963-967.
- Chang JE, Voorhees PM, Kolesar JM, Ahuja HG, Sanchez FA, Rodriguez GA, et al. 2009. Phase ii study of arsenic trioxide and ascorbic acid for relapsed or refractory lymphoid malignancies: A wisconsin oncology network study. *Hematological Oncology* 27:11-16.
- Chen H, Ahn R, Van den Bossche J, Thompson DH, O'Halloran TV. 2009. Folate-mediated intracellular drug delivery increases the anticancer efficacy of nanoparticulate formulation of arsenic trioxide. *Molecular Cancer Therapeutics* 8:1955-1963.
- Chen HM, MacDonald RC, Li SY, Krett NL, Rosen ST, O'Halloran TV. 2006. Lipid encapsulation of arsenic trioxide attenuates cytotoxicity and allows for controlled anticancer drug release. *Journal of the American Chemical Society* 128:13348-13349.
- Chen HT, Kim SW, Li L, Wang SY, Park K, Cheng JX. 2008. Release of hydrophobic molecules from polymer micelles into cell membranes revealed by forster resonance energy transfer imaging. *Proceedings of the National Academy of Sciences of the United States of America* 105:6596-6601.
- Chen J, Zhang S, Li Y, Tang Z, Kong W. 2014. Hexokinase 2 overexpression promotes the proliferation and survival of laryngeal squamous cell carcinoma. *Tumor Biology* 35:3743-3753.

- Chen L, Chen F, Zhao MX, Zhu XD, Ke CH, Yu JM, et al. 2015. A redox-sensitive micelle-like nanoparticle self-assembled from amphiphilic adriamycin-human serum albumin conjugates for tumor targeted therapy. *Biomed Research International*:10.
- Chen SJ, Zhou GB, Zhang XW, Mao JH, de The H, Chen Z. 2011. From an old remedy to a magic bullet: Molecular mechanisms underlying the therapeutic effects of arsenic in fighting leukemia. *Blood* 117:6425-6437.
- Chen W, Zhong P, Meng FH, Cheng R, Deng C, Feijen J, et al. 2013. Redox and pH-responsive degradable micelles for dually activated intracellular anticancer drug release. *Journal of Controlled Release* 169:171-179.
- Cheng BH, Yang XX, Han ZW, An LX, Uu SW. 2008. Arsenic trioxide induced the apoptosis of laryngeal cancer via down-regulation of survivin mRNA. *Auris Nasus Larynx* 35:95-101.
- Cheng C, Wei H, Zhu JL, Chang C, Cheng H, Li C, et al. 2008. Functionalized thermoresponsive micelles self-assembled from biotin-peg-b-p(nipAAm-co-hMAAm)-b-PMMA for tumor cell target. *Bioconjugate Chemistry* 19:1194-1201.
- Cheng J, Wei HL, Chen J, Xie B. 2012. Antitumor effect of arsenic trioxide in human K562 and K562/ADM cells by autophagy. *Toxicology Mechanisms and Methods* 22:512-519.
- Cheng R, Meng FH, Deng C, Klok HA, Zhong ZY. 2013. Dual and multi-stimuli responsive polymeric nanoparticles for programmed site-specific drug delivery. *Biomaterials* 34:3647-3657.
- Cheng X, Quintas-Cardama A, Golemovic M, Zingaro R, Gao M-Z, Freirech EJ, et al. 2012. The organic arsenic derivative gmz27 induces pml-rar alpha-independent apoptosis in myeloid leukemia cells. *Anticancer Research* 32:2871-2880.
- Cheng YY, Zhao LB, Li YW, Xu TW. 2011. Design of biocompatible dendrimers for cancer diagnosis and therapy: Current status and future perspectives. *Chemical Society Reviews* 40:2673-2703.
- Chiche J, Brahimi-Horn MC, Pouyssegur J. 2010. Tumour hypoxia induces a metabolic shift causing acidosis: A common feature in cancer. *Journal of Cellular and Molecular Medicine* 14:771-794.

- Chiu HW, Tseng YC, Hsu YH, Lin YF, Foo NP, Guo HR, et al. 2015. Arsenic trioxide induces programmed cell death through stimulation of er stress and inhibition of the ubiquitin-proteasome system in human sarcoma cells. *Cancer Letters* 356:762-772.
- Chlebowski RT. 1979. Adriamycin (doxorubicin) cardiotoxicity - review. *Western Journal of Medicine* 131:364-368.
- Chung SA, McDonald KL, Shen H, Day BW, Stringer BW, Johns T, et al. 2011. Targeting glioblastoma metabolism with a novel arsenic-based metabolic inhibitor, penao. *Neuro-Oncology* 13:118-118.
- Coussens LM, Werb Z. 1996. Matrix metalloproteinases and the development of cancer. *Chemistry & Biology* 3:895-904.
- Craig M, Shah S, Tallman M, Patil P, Easow J, Buck J, et al. 2008. A phase ii trial of darinaparsin in advanced lymphomas: Report on safety and activity. *Blood* 112:554-554.
- Cullen WR. 2008. Is arsenic an aphrodisiac? The sociochemistry of an element. Is arsenic an aphrodisiac? The sociochemistry of an element:xvi + 412pp.-xvi + 412pp.
- Da Silva RMP, Mano JF, Reis RL. 2007. Smart thermoresponsive coatings and surfaces for tissue engineering: Switching cell-material boundaries. *Trends in Biotechnology* 25:577-583.
- Dai J, Weinberg RS, Waxman S, Jing YK. 1999. Malignant cells can be sensitized to undergo growth inhibition and apoptosis by arsenic trioxide through modulation of the glutathione redox system. *Blood* 93:268-277.
- Dang CV. 1999. C-myc target genes involved in cell growth, apoptosis, and metabolism. *Molecular and Cellular Biology* 19:1-11.
- Darney PD, Monroe SE, Klaisle CM, Alvarado A. 1989. Clinical-evaluation of the capronor contraceptive implant - preliminary-report. *American Journal of Obstetrics and Gynecology* 160:1292-1295.
- De Vita VTJ, Young RC, Canellos GP. 1975. Combination vs single agent chemo therapy a review of the basis for selection of drug treatment of cancer. *Cancer* 35:98-110.

- Decollogne S, Joshi S, Chung SA, Luk PP, Yeo RX, Nixdorf S, et al. 2015. Alterations in the mitochondrial responses to penao as a mechanism of resistance in ovarian cancer cells. *Gynecologic Oncology* 138:363-371.
- Dethe H, Chomienne C, Lanotte M, Degos L, Dejean A. 1990. The t(15-17) translocation of acute promyelocytic leukemia fuses the retinoic acid receptor-alpha gene to a novel transcribed locus. *Nature* 347:558-561.
- Dilda PJ, Hogg PJ. 2007. Arsenical-based cancer drugs. *Cancer Treatment Reviews* 33:542-564.
- Dilda PJ, Ramsay EE, Corti A, Pompella A, Hogg PJ. 2008. Metabolism of the tumor angiogenesis inhibitor 4-(n-(s-glutathionylacetyl)amino) phenylarsonous acid. *Journal of Biological Chemistry* 283:35428-35434.
- Dilda PJ, Decollogne S, Weerakoon L, Norris MD, Haber M, Allen JD, et al. 2009. Optimization of the antitumor efficacy of a synthetic mitochondrial toxin by increasing the residence time in the cytosol. *Journal of Medicinal Chemistry* 52:6209-6216.
- Ding W, Liu WL, Cooper KL, Qin XJ, Bergo PLD, Hudson LG, et al. 2009. Inhibition of poly(adp-ribose) polymerase-1 by arsenite interferes with repair of oxidative dna damage. *Journal of Biological Chemistry* 284:6809-6817.
- Dogra S, Bandi S, Viswanathan P, Gupta S. 2015. Arsenic trioxide amplifies cisplatin toxicity in human tubular cells transformed by hpv-16 e6/e7 for further therapeutic directions in renal cell carcinoma. *Cancer Letters* 356:953-961.
- Don AS, Kisker O, Dilda P, Donoghue N, Zhao XY, Decollogne S, et al. 2003. A peptide trivalent arsenical inhibits tumor angiogenesis by perturbing mitochondrial function in angiogenic endothelial cells. *Cancer Cell* 3:497-509.
- Dong XY, Ma N, Liu MM, Liu ZL. 2015. Effects of as<sub>2</sub>o<sub>3</sub> nanoparticles on cell growth and apoptosis of nb4 cells. *Experimental and Therapeutic Medicine* 10:1271-1276.
- Doyle D. 2009. Notoriety to respectability: A short history of arsenic prior to its present day use in haematology. *British Journal of Haematology* 145:309-317.
- Du JZ, Lane LA, Nie SM. 2015. Stimuli-responsive nanoparticles for targeting the tumor microenvironment. *Journal of Controlled Release* 219:205-214.

- Du ZZ, Zhang Y, Lang MD. 2015. Synthesis of functionalized pluronic-b-poly(epsilon-caprolactone) and the comparative study of their pendant groups on the cellular internalization behavior. *Journal of Materials Science-Materials in Medicine* 26:12.
- Duffy A, Le J, Sausville E, Emadi A. 2015. Autophagy modulation: A target for cancer treatment development. *Cancer Chemotherapy and Pharmacology* 75:439-447.
- Duggan ME, Hutchinson JH. 2000. Ligands to the integrin receptor alpha(v)beta(3). *Expert Opinion on Therapeutic Patents* 10:1367-1383.
- Dvorak HF. 2002. Vascular permeability factor/vascular endothelial growth factor: A critical cytokine in tumor angiogenesis and a potential target for diagnosis and therapy. *Journal of Clinical Oncology* 20:4368-4380.
- Elhasi S, Astaneh R, Lavasanifar A. 2007. Solubilization of an amphiphilic drug by poly(ethylene oxide)-block-poly(ester) micelles. *European Journal of Pharmaceutics and Biopharmaceutics* 65:406-413.
- Elmore S. 2007. Apoptosis: A review of programmed cell death. *Toxicologic Pathology* 35:495-516.
- Elsabahy M, Wooley KL. 2012. Design of polymeric nanoparticles for biomedical delivery applications. *Chemical Society Reviews* 41:2545-2561.
- Emadi A, Sadowska M, Carter-Cooper B, Bhatnagar V, van der Merwe I, Levis MJ, et al. 2015. Perturbation of cellular oxidative state induced by dichloroacetate and arsenic trioxide for treatment of acute myeloid leukemia. *Leukemia Research* 39:719-729.
- Fatouros D, Gortzi O, Klepetsanis P, Antimisiaris SG, Stuart MCA, Brisson A, et al. 2001. Preparation and properties of arsonolipid containing liposomes. *Chemistry and Physics of Lipids* 109:75-89.
- Felding-Habermann B, Fransvea E, O'Toole TE, Manzuk L, Faha B, Hensler M. 2002. Involvement of tumor cell integrin alpha v beta 3 in hematogenous metastasis of human melanoma cells. *Clinical & Experimental Metastasis* 19:427-436.
- Folkman J, Shing Y. 1992. Angiogenesis. *Journal of Biological Chemistry* 267:10931-10934.

- Fu YH, Chen CY, Chen CT. 2015. Tuning of hydrogen peroxide-responsive polymeric micelles of biodegradable triblock polycarbonates as a potential drug delivery platform with ratiometric fluorescence signaling. *Polymer Chemistry* 6:8132-8143.
- Gang BP, Dilda PJ, Hogg PJ, Blackburn AC. 2014. Targeting of two aspects of metabolism in breast cancer treatment. *Cancer Biology & Therapy* 15:1533-1541.
- Gao YJ, Zhou YX, Zhao L, Zhang C, Li YS, Li JW, et al. 2015. Enhanced antitumor efficacy by cyclic rgdyk-conjugated and paclitaxel-loaded pH-responsive polymeric micelles. *Acta Biomaterialia* 23:127-135.
- Garnier N, Redstone GGJ, Dahabieh MS, Nichol JN, del Rincon SV, Gu YX, et al. 2014. The novel arsenical darinaparsin is transported by cystine importing systems. *Molecular Pharmacology* 85:576-585.
- Gazitt Y, Akay C. 2005. Arsenic trioxide: An anti cancer missile with multiple warheads. *Hematology* 10:205-213.
- Ge HY, Han ZJ, Tian P, Sun WJ, Xue DX, Bi Y, et al. 2015. Vegfa expression is inhibited by arsenic trioxide in huvecs through the upregulation of ets-2 and mirna-126. *Plos One* 10:18.
- Golemovic M, Quintas-Cardama A, Manshouri T, Orsolich N, Duzkale H, Johansen M, et al. 2010. Mer1, a novel organic arsenic derivative, has potent pml-rar alpha- independent cytotoxic activity against leukemia cells. *Investigational New Drugs* 28:402-412.
- Gortzi O, Papadimitriou E, Kontoyannis CG, Antimisiaris SG, Ioannou PV. 2002. Arsonoliposomes, a novel class of arsenic-containing liposomes: Effect of palmitoyl-arsonolipid-containing liposomes on the viability of cancer and normal cells in culture. *Pharmaceutical Research* 19:79-86.
- Gothwal A, Khan I, Gupta U. 2016. Polymeric micelles: Recent advancements in the delivery of anticancer drugs. *Pharmaceutical Research* 33:18-39.
- Goussetis DJ, Altman JK, Glaser H, McNeer JL, Tallman MS, Platanias LC. 2010. Autophagy is a critical mechanism for the induction of the antileukemic effects of arsenic trioxide. *Journal of Biological Chemistry* 285:29989-29997.

- Goussetis DJ, Gounaris E, Wu EJ, Vakana E, Sharma B, Bogyo M, et al. 2012. Autophagic degradation of the bcr-abl oncoprotein and generation of antileukemic responses by arsenic trioxide. *Blood* 120:3555-3562.
- Guan XG, Hu XL, Li ZH, Zhang H, Xie ZG. 2015. Crgd targeted and charge conversion-controlled release micelles for doxorubicin delivery. *Rsc Advances* 5:22957-22964.
- Gurrath M, Muller G, Kessler H, Aumailley M, Timpl R. 1992. Conformation activity studies of rationally designed potent antiadhesive rgd peptides. *European Journal of Biochemistry* 210:911-921.
- Gwak HS, Park MJ, Park IC, Woo SH, Jin HO, Rhee CH, et al. 2014. Tetraarsenic oxide-induced inhibition of malignant glioma cell invasion in vitro via a decrease in matrix metalloproteinase secretion and protein kinase b phosphorylation. *Journal of Neurosurgery* 121:1483-1491.
- Han HS, Choi KY, Ko H, Jeon J, Saravanakumar G, Suh YD, et al. 2015. Bioreducible core-crosslinked hyaluronic acid micelle for targeted cancer therapy. *Journal of Controlled Release* 200:158-166.
- Han MH, Lee WS, Lu JN, Yun JW, Kim G, Jung JM, et al. 2012. Tetraarsenic hexoxide induces beclin-1-induced autophagic cell death as well as caspase-dependent apoptosis in u937 human leukemic cells. *Evidence-Based Complementary and Alternative Medicine*:11.
- Hanahan D, Weinberg RA. 2011. Hallmarks of cancer: The next generation. *Cell* 144:646-674.
- Hartwig A, Pelzer A, Asmuss M, Burkle A. 2003. Very low concentrations of arsenite suppress poly(adp-ribosyl)ation in mammalian cells. *International Journal of Cancer* 104:1-6.
- He Q, Shi J. 2011. Mesoporous silica nanoparticle based nano drug delivery systems: Synthesis, controlled drug release and delivery, pharmacokinetics and biocompatibility. *Journal of Materials Chemistry* 21:5845-5855.
- Hindmarsh JT, McCurdy RF. 1986. Clinical and environmental aspects of arsenic toxicity. *Crc Critical Reviews in Clinical Laboratory Sciences* 23:315-347.
- Hiwatashi Y, Tadokoro H, Henmi K, Arai M, Kaise T, Tanaka S, et al. 2011. Antiproliferative and anti-invasive effects of inorganic and organic arsenic compounds on human and murine melanoma cells in vitro. *Journal of Pharmacy and Pharmacology* 63:1202-1210.

- Horsley L, Cummings J, Middleton M, Ward T, Backen A, Clamp A, et al. 2013. A phase 1 trial of intravenous 4-(n-(s-glutathionylacetyl)amino) phenylarsenoxide (gsao) in patients with advanced solid tumours. *Cancer Chemotherapy and Pharmacology* 72:1343-1352.
- Hosein PJ, Craig MD, Tallman MS, Boccia RV, Hamilton BL, Lewis JJ, et al. 2012. A multicenter phase ii study of darinaparsin in relapsed or refractory hodgkin's and non-hodgkin's lymphoma. *American Journal of Hematology* 87:111-114.
- Hu J, Fang J, Dong Y, Chen SJ, Chen Z. 2005. Arsenic in cancer therapy. *Anti-Cancer Drugs* 16:119-127.
- Hu J, He JL, Cao DL, Zhang MZ, Ni PH. 2015. Core cross-linked polyphosphoester micelles with folate-targeted and acid-cleavable features for ph-triggered drug delivery. *Polymer Chemistry* 6:3205-3216.
- Ishihara T, Mizushima T. 2010. Techniques for efficient entrapment of pharmaceuticals in biodegradable solid micro/nanoparticles. *Expert Opinion on Drug Delivery* 7:565-575.
- Iwasaki K, Yabushita H, Ueno T, Wakatsuki A. 2015. Role of hypoxia-inducible factor-1 alpha, carbonic anhydrase-ix, glucose transporter-1 and vascular endothelial growth factor associated with lymph node metastasis and recurrence in patients with locally advanced cervical cancer. *Oncology Letters* 10:1970-1978.
- Jabbour E, Kantarjian H. 2016. Chronic myeloid leukemia: 2016 update on diagnosis, therapy, and monitoring. *American journal of hematology* 91:252-265.
- Jeanne M, Lallemand-Breitenbach V, Ferhi O, Koken M, Le Bras M, Duffort S, et al. 2010. Pml/rara oxidation and arsenic binding initiate the antileukemia response of as<sub>2</sub>o<sub>3</sub>. *Cancer Cell* 18:88-98.
- Jhaveri A, Torchilin V. 2016. Intracellular delivery of nanocarriers and targeting to subcellular organelles. *Expert opinion on drug delivery* 13:49-70.
- Ji H, Li Y, Jiang F, Wang XX, Zhang JP, Shen J, et al. 2014. Inhibition of transforming growth factor beta/smad signal by mir-155 is involved in arsenic trioxide-induced anti-angiogenesis in prostate cancer. *Cancer Science* 105:1541-1549.

- Jiang F, Wang XX, Liu QQ, Shen J, Li Z, Li Y, et al. 2014. Inhibition of *tgf-beta*/*smad3*/*nf-kappa b* signaling by *microrna-491* is involved in arsenic trioxide-induced anti-angiogenesis in hepatocellular carcinoma cells. *Toxicology Letters* 231:55-61.
- Jiao GJ, Ren TT, Guo W, Ren CM, Yang K. 2015. Arsenic trioxide inhibits growth of human chondrosarcoma cells through *g2/m* arrest and apoptosis as well as autophagy. *Tumor Biology* 36:3969-3977.
- Jimenez-Pardo I, Gonzalez-Pastor R, Lancelot A, Claveria-Gimeno R, Velazquez-Campoy A, Abian O, et al. 2015. Shell cross-linked polymeric micelles as camptothecin nanocarriers for anti-hcv therapy. *Macromolecular Bioscience* 15:1381-1391.
- Kallinteri P, Fatouros D, Klepetsanis P, Antimisiaris SG. 2004. Arsenic trioxide liposomes: Encapsulation efficiency and in vitro stability. *Journal of Liposome Research* 14:27-38.
- Kang Y, Zhang XM, Zhang S, Ding LS, Li BJ. 2015. Ph-responsive dendritic polyrotaxane drug-polymer conjugates forming nanoparticles as efficient drug delivery system for cancer therapy. *Polymer Chemistry* 6:2098-2107.
- Kanzawa T, Kondo Y, Ito H, Kondo S, Germano I. 2003. Induction of autophagic cell death in malignant glioma cells by arsenic trioxide. *Cancer Research* 63:2103-2108.
- Kanzawa T, Zhang L, Xiao LC, Germano IM, Kondo Y, Kondo S. 2005. Arsenic trioxide induces autophagic cell death in malignant glioma cells by upregulation of mitochondrial cell death protein *bnip3*. *Oncogene* 24:980-991.
- Kao YH, Yu CL, Chang LW, Yu HS. 2003. Low concentrations of arsenic induce vascular endothelial growth factor and nitric oxide release and stimulate angiogenesis in vitro. *Chemical Research in Toxicology* 16:460-468.
- Kessel M, Liu SX, Xu A, Santella R, Hei TK. 2002. Arsenic induces oxidative dna damage in mammalian cells. *Molecular and Cellular Biochemistry* 234:301-308.
- Khorrarnizadeh MR, Saadat F, Allahyary H, Pezeshki M, Sarrafnejad A, Mirshafiey A, et al. 2006. Arsenic trioxide compound modulates multiple myeloma phenotypes: Assessment on cell line models. *Iranian Journal of Public Health* 35:17-24.

- Kim EH, Yoon NJ, Kim SU, Kwon TK, Sohn S, Choi KS. 2008. Arsenic trioxide sensitizes human glioma cells, but not normal astrocytes, to trail-induced apoptosis via ccaat/enhancer-binding protein homologous protein-dependent dr5 up-regulation. *Cancer Research* 68:266-275.
- Kim HJ, Shin JH, Kim TH, Kim EY, Park YS, Park CS, et al. 2009. Efficacy of transarterial embolization. With arsenic trioxide oil emulsion in a rabbit vx2 liver tumor model. *Journal of Vascular and Interventional Radiology* 20:1365-1370.
- Kim KB, Bedikian AY, Camacho LH, Papadopoulos NE, McCullough C. 2005. A phase ii trial of arsenic trioxide in patients with metastatic melanoma. *Cancer* 104:1687-1692.
- Kim S, Seong K, Kim O, Seo H, Lee M, Khang G, et al. 2010. Polyoxalate nanoparticles as a biodegradable and biocompatible drug delivery vehicle. *Biomacromolecules* 11:555-560.
- Kong B, Huang S, Wang W, Ma D, Qu X, Jiang J, et al. 2005. Arsenic trioxide induces apoptosis in cisplatin-sensitive and -resistant ovarian cancer cell lines. *International Journal of Gynecological Cancer* 15:872-877.
- Kujak C, Kolesar JM. 2016. Treatment of chronic myelogenous leukemia. *American journal of health-system pharmacy : AJHP : official journal of the American Society of Health-System Pharmacists* 73:113-120.
- Lecoq. 1910. Toxicity of metalloidal arsenic. *Comptes Rendus Hebdomadaires Des Seances De L Academie Des Sciences* 150:887-888.
- Lee DW, Erigala VR, Dasari M, Yu JH, Dickson RM, Murthy N. 2008. Detection of hydrogen peroxide with chemiluminescent micelles. *International Journal of Nanomedicine* 3:471-476.
- Lee I, Hwang O, Yoo D, Khang G, Lee D. 2011. Detection of hydrogen peroxide in vitro and in vivo using peroxalate chemiluminescent micelles. *Bulletin of the Korean Chemical Society* 32:2187-2192.
- Lee SY, Lee H, In I, Park SY. 2014. Ph/redox/photo responsive polymeric micelle via boronate ester and disulfide bonds with spiropyran-based photochromic polymer for cell imaging and anticancer drug delivery. *European Polymer Journal* 57:1-10.
- Leslie EM. 2012. Arsenic-glutathione conjugate transport by the human multidrug resistance proteins (mrps/abccs). *Journal of Inorganic Biochemistry* 108:141-149.

- Li CL, Wei HL, Chen J, Wang B, Xie B, Fan LL, et al. 2014. Arsenic trioxide induces autophagy and antitumor effects in burkitt's lymphoma raji cells. *Oncology Reports* 32:1557-1563.
- Li HA, Cui YN, Sui JH, Bian SQ, Sun Y, Liang J, et al. 2015. Efficient delivery of dox to nuclei of hepatic carcinoma cells in the subcutaneous tumor model using ph-sensitive pullulan-dox conjugates. *Acs Applied Materials & Interfaces* 7:15855-15865.
- Li J, Huo MR, Wang J, Zhou JP, Mohammad JM, Zhang YL, et al. 2012. Redox-sensitive micelles self-assembled from amphiphilic hyaluronic acid-deoxycholic acid conjugates for targeted intracellular delivery of paclitaxel. *Biomaterials* 33:2310-2320.
- Li XQ, Ding XZ, Adrian TE. 2004. Arsenic trioxide causes redistribution of cell cycle, caspase activation, and gadd expression in human colonic, breast, and pancreatic cancer cells. *Cancer Investigation* 22:389-400.
- Li Y, Gao GH, Lee DS. 2013. Stimulus-sensitive polymeric nanoparticles and their applications as drug and gene carriers. *Advanced Healthcare Materials* 2:388-417.
- Li Y, Jiang F, Liu QQ, Shen J, Wang XX, Li Z, et al. 2015. Inhibition of the cancer stem cells-like properties by arsenic trioxide, involved in the attenuation of endogenous transforming growth factor beta signal. *Toxicological Sciences* 143:156-164.
- Liao WT, Chang KL, Yu CL, Chen GS, Chang LW, Yu HS. 2004. Arsenic induces human keratinocyte apoptosis by the fas/fas ligand pathway, which correlates with alterations in nuclear factor-kappa b and activator protein-1 activity. *Journal of Investigative Dermatology* 122:125-129.
- Lin C-C, Hsu C, Hsu C-H, Hsu W-L, Cheng A-L, Yang C-H. 2007. Arsenic trioxide in patients with hepatocellular carcinoma: A phase ii trial. *Investigational New Drugs* 25:77-84.
- Lippert AR, De Bittner GCV, Chang CJ. 2011. Boronate oxidation as a bioorthogonal reaction approach for studying the chemistry of hydrogen peroxide in living systems. *Accounts of Chemical Research* 44:793-804.
- Liu BR, Yang M, Li RT, Ding YT, Qian XP, Yu LX, et al. 2008. The antitumor effect of novel docetaxel-loaded thermosensitive micelles. *European Journal of Pharmaceutics and Biopharmaceutics* 69:527-534.

- Liu J, Lu YF, Wu Q, Goyer RA, Waalkes MP. 2008. Mineral arsenicals in traditional medicines: Orpiment, realgar, and arsenolite. *Journal of Pharmacology and Experimental Therapeutics* 326:363-368.
- Liu JJ, Deng HZ, Liu Q, Chu LP, Zhang YM, Yang CH, et al. 2015. Integrin-targeted pH-responsive micelles for enhanced efficiency of anticancer treatment in vitro and in vivo. *Nanoscale* 7:4451-4460.
- Liu QA, Zhang H, Smeester L, Zou F, Kesic M, Jaspers I, et al. 2010. The nrf2-mediated oxidative stress response pathway is associated with tumor cell resistance to arsenic trioxide across the nci-60 panel. *Bmc Medical Genomics* 3:12.
- Liu XF, Miller AL, Waletzki BE, Mamo TK, Yaszemski MJ, Lu LC. 2015. Hydrolysable core crosslinked particles for receptor-mediated pH-sensitive anticancer drug delivery. *New Journal of Chemistry* 39:8840-8847.
- Lu D, Coote ML, Ho J, Kilah NL, Lin C-Y, Salem G, et al. 2012. Resolution and improved synthesis of (+/-)-arsenicin a: A natural adamantane-type tetraarsenical possessing strong anti-acute promyelocytic leukemia cell line activity. *Organometallics* 31:1808-1816.
- Lu DP, Qiu JY, Jiang B, Wang Q, Liu KY, Liu YR, et al. 2002. Tetra-arsenic tetra-sulfide for the treatment of acute promyelocytic leukemia: A pilot report. *Blood* 99:3136-3143.
- Lu J, Chew EH, Holmgren A. 2007. Targeting thioredoxin reductase is a basis for cancer therapy by arsenic trioxide. *Proceedings of the National Academy of Sciences of the United States of America* 104:12288-12293.
- Luo QY, Li Y, Deng JJ, Zhang ZZ. 2015. Parp-1 inhibitor sensitizes arsenic trioxide in hepatocellular carcinoma cells via abrogation of g2/m checkpoint and suppression of dna damage repair. *Chemico-Biological Interactions* 226:12-22.
- Lux CD, Joshi-Barr S, Nguyen T, Mahmoud E, Schopf E, Fomina N, et al. 2012. Biocompatible polymeric nanoparticles degrade and release cargo in response to biologically relevant levels of hydrogen peroxide. *Journal of the American Chemical Society* 134:15758-15764.
- Ma ZB, Xu HY, Jiang M, Yang YL, Liu LX, Li YH. 2014. Arsenic trioxide induces apoptosis of human gastrointestinal cancer cells. *World Journal of Gastroenterology* 20:5505-5510.

- Ma ZS, Haddadi A, Molavi O, Lavasanifar A, Lai R, Samuel J. 2008. Micelles of poly(ethylene oxide)-b-poly(epsilon-caprolactone) as vehicles for the solubilization, stabilization, and controlled delivery of curcumin. *Journal of Biomedical Materials Research Part A* 86A:300-310.
- Maeda H. 2012. Macromolecular therapeutics in cancer treatment: The epr effect and beyond. *Journal of Controlled Release* 164:138-144.
- Mahmud A, Xiong XB, Lavasanifar A. 2006. Novel self-associating poly(ethylene oxide)-block-poly(epsilon-caprolactone) block copolymers with functional side groups on the polyester block for drug delivery. *Macromolecules* 39:9419-9428.
- Makino J, Cabral H, Miura Y, Matsumoto Y, Wang M, Kinoh H, et al. 2015. Crgd-installed polymeric micelles loading platinum anticancer drugs enable cooperative treatment against lymph node metastasis. *Journal of controlled release : official journal of the Controlled Release Society* 220:783-791.
- Mancini I, Guella G, Frostin M, Hnawia E, Laurent D, Debitus C, et al. 2006. On the first polyarsenic organic compound from nature: Arsenicin a from the new caledonian marine sponge *echinochalina bargibanti*. *Chemistry-a European Journal* 12:8989-8994.
- Mann KK, Wallner B, Lossos IS, Miller WH. 2009. Darinaparsin: A novel organic arsenical with promising anticancer activity. *Expert Opinion on Investigational Drugs* 18:1727-1734.
- Mao JH, Sun XY, Liu JX, Zhang QY, Liu P, Huang QH, et al. 2010. As4s4 targets ring-type e3 ligase c-cbl to induce degradation of bcr-abl in chronic myelogenous leukemia. *Proceedings of the National Academy of Sciences of the United States of America* 107:21683-21688.
- Markman JL, Rekechenetskiy A, Holler E, Ljubimova JY. 2013. Nanomedicine therapeutic approaches to overcome cancer drug resistance. *Advanced Drug Delivery Reviews* 65:1866-1879.
- Matsumura Y, Maeda H. 1986. A new concept for macromolecular therapeutics in cancer-chemotherapy - mechanism of tumorotropic accumulation of proteins and the antitumor agent smancs. *Cancer Research* 46:6387-6392.
- Miller DM, Thomas SD, Islam A, Muench D, Sedoris K. 2012. C-myc and cancer metabolism. *Clinical Cancer Research* 18:5546-5553.

- Muhammad F, Zhao JY, Wang N, Guo MY, Wang AF, Chen L, et al. 2014. Lethal drug combination: Arsenic loaded multiple drug mesoporous silica for theranostic applications. *Colloids and Surfaces B-Biointerfaces* 123:506-514.
- Newington JT, Rappon T, Albers S, Wong DY, Rylett RJ, Cumming RC. 2012. Overexpression of pyruvate dehydrogenase kinase 1 and lactate dehydrogenase a in nerve cells confers resistance to amyloid beta and other toxins by decreasing mitochondrial respiration and reactive oxygen species production. *Journal of Biological Chemistry* 287:37245-37258.
- Nguyen DH, Bae JW, Choi JH, Lee JS, Park KD. 2013. Bioreducible cross-linked pluronic micelles: Ph-triggered release of doxorubicin and folate-mediated cellular uptake. *Journal of Bioactive and Compatible Polymers* 28:341-354.
- Nikaido M, Pi JB, Kumagai Y, Yamauchi H, Taguchi K, Horiguchi S, et al. 2003. Decreased enzyme activity of hepatic thioredoxin reductase and glutathione reductase in rabbits by prolonged exposure to inorganic arsenate. *Environmental Toxicology* 18:306-311.
- Otsuka H, Nagasaki Y, Kataoka K. 2003. Pegylated nanoparticles for biological and pharmaceutical applications. *Advanced Drug Delivery Reviews* 55:403-419.
- Park D, Chiu J, Perrone GG, Dilda PJ, Hogg PJ. 2012. The tumour metabolism inhibitors gsao and penao react with cysteines 57 and 257 of mitochondrial adenine nucleotide translocase. *Cancer Cell International* 12:6.
- Pereira DL, Ferreira ACD, de Faria GP, Kwee JK. 2015. Autophagy interplays with apoptosis and cell cycle regulation in the growth inhibiting effect of trisenox in hep-2, a laryngeal squamous cancer. *Pathology & Oncology Research* 21:103-111.
- Piperoudi S, Ioannou PV, Frederik P, Antimisiaris SG. 2005. Arsonoliposomes: Effect of lipid composition on their stability and morphology. *Journal of Liposome Research* 15:187-197.
- Piperoudi S, Fatouros D, Ioannou PV, Frederik P, Antimisiaris SG. 2006. Incorporation of peg-lipids in arsonoliposomes results in formation of highly stable arsenic-containing vesicles. *Chemistry and Physics of Lipids* 139:96-106.
- Qian C, Wang Y, Chen Y, Zeng L, Zhang Q, Shuai X, et al. 2013. Suppression of pancreatic tumor growth by targeted arsenic delivery with anti-cd44v6 single chain antibody conjugated nanoparticles. *Biomaterials* 34:6175-6184.

- Qian WB, Liu JQ, Jin J, Ni WM, Xu WL. 2007. Arsenic trioxide induces not only apoptosis but also autophagic cell death in leukemia cell lines via up-regulation of beclin-1. *Leukemia Research* 31:329-339.
- Ravandi F, Estey EH, Cortes JE, O'Brien S, Pierce SA, Brandt M, et al. 2010. Phase ii study of all-trans retinoic acid (atra), arsenic trioxide (ato), with or without gemtuzumab ozogamicin (go) for the frontline therapy of patients with acute promyelocytic leukemia (apl). *Blood* 116:472-472.
- Ray A, Chatterjee S, Mukherjee S, Bhattacharya S. 2014. Arsenic trioxide induced indirect and direct inhibition of glutathione reductase leads to apoptosis in rat hepatocytes. *Biometals* 27:483-494.
- Rezaei SJT, Amani V, Nabid MR, Safari N, Niknejad H. 2015. Folate-decorated polymeric pt(ii) prodrug micelles for targeted intracellular delivery and cytosolic glutathione-triggered release of platinum anticancer drugs. *Polymer Chemistry* 6:2844-2853.
- Rijcken CJ, Snel CJ, Schiffelers RM, van Nostrum CF, Hennink WE. 2007. Hydrolysable core-crosslinked thermosensitive polymeric micelles: Synthesis, characterisation and in vivo studies. *Biomaterials* 28:5581-5593.
- Robles-Osorio ML, Sabath-Silva E, Sabath E. 2015. Arsenic-mediated nephrotoxicity. *Renal Failure* 37:542-547.
- Roboz GJ, Dias S, Lam G, Lane WJ, Soignet SL, Warrell RP, et al. 2000. Arsenic trioxide induces dose- and time-dependent apoptosis of endothelium and may exert an antileukemic effect via inhibition of angiogenesis. *Blood* 96:1525-1530.
- Rojewski MT, Korper S, Thiel E, Schrezenmeier H. 2004. Depolarization of mitochondria and activation of caspases are common features of arsenic(iii)-induced apoptosis in myelogenic and lymphatic cell lines. *Chemical Research in Toxicology* 17:119-128.
- Salehi R, Rasouli S, Hamishehkar H. 2015. Smart thermo/ph responsive magnetic nanogels for the simultaneous delivery of doxorubicin and methotrexate. *International Journal of Pharmaceutics* 487:274-284.
- Salesse S, Verfaillie CM. 2002. Bcr/abl: From molecular mechanisms of leukemia induction to treatment of chronic myelogenous leukemia. *Oncogene* 21:8547-8559.

- Sanchez Y, Amran D, de Blas E, Aller P. 2010. Arsenic trioxide as an anti-tumour agent: Mechanisms of action and strategies of sensitization. *Journal of Applied Biomedicine* 8:199-208.
- Sarquis M. 1979. Chem-1 supplement - arsenic and old myths. *Journal of Chemical Education* 56:815-818.
- Scholz C, Richter A, Lehmann M, Schulze-Osthoff K, Dorken B, Daniel PT. 2005. Arsenic trioxide induces regulated, death receptor-independent cell death through a bcl-2-controlled pathway. *Oncogene* 24:7031-7042.
- Sercombe L, Veerati T, Moheimani F, Wu SY, Sood AK, Hua S. 2015. Advances and challenges of liposome assisted drug delivery. *Frontiers in Pharmacology* 6.
- Shahin M, Lavasanifar A. 2010. Novel self-associating poly(ethylene oxide)-b-poly( $\epsilon$ -caprolactone) based drug conjugates and nano-containers for paclitaxel delivery. *International Journal of Pharmaceutics* 389:213-222.
- Shao Y, Shi CY, Xu GF, Guo DD, Luo JT. 2014. Photo and redox dual responsive reversibly cross-linked nanocarrier for efficient tumor-targeted drug delivery. *Acs Applied Materials & Interfaces* 6:10381-10392.
- Shen H, Luk PP, Chung SA, Decollogne S, Dilda PJ, Hogg PJ, et al. 2013. Penao, a novel mitochondria-targeted agent, has shown potent antitumor effect on glioblastoma in vitro and in vivo. *Cancer Research* 73:1701.
- Shen H, Decollogne S, Dilda PJ, Hau E, Chung SA, Luk PP, et al. 2015. Dual-targeting of aberrant glucose metabolism in glioblastoma. *Journal of Experimental & Clinical Cancer Research* 34:11.
- Shen JM, Yin T, Tian XZ, Gao FY, Xu S. 2013. Surface charge-switchable polymeric magnetic nanoparticles for the controlled release of anticancer drug. *Acs Applied Materials & Interfaces* 5:7014-7024.
- Shen S, Li X, Cullen W, Weinfeld M, Le X. 2013. Arsenic binding to proteins. *Chemical Reviews* 113:7769-7792.

- Shen SW, Wang C, Weinfeld M, Le XC. 2013. Inhibition of nucleotide excision repair by arsenic. *Chinese Science Bulletin* 58:214-221.
- Shen ZX, Chen GQ, Ni JH, Li XS, Xiong SM, Qiu QY, et al. 1997. Use of arsenic trioxide (As<sub>2</sub>O<sub>3</sub>) in the treatment of acute promyelocytic leukemia (APL). 2. Clinical efficacy and pharmacokinetics in relapsed patients. *Blood* 89:3354-3360.
- Shimobayashi M, Hall MN. 2014. Making new contacts: The mTOR network in metabolism and signalling crosstalk. *Nature Reviews Molecular Cell Biology* 15:155-162.
- Sidhu MS, Desai KP, Lynch HN, Rhomberg LR, Beck BD, Venditti FJ. 2015. Mechanisms of action for arsenic in cardiovascular toxicity and implications for risk assessment. *Toxicology* 331:78-99.
- Singh RP, Sharma G, Sonali, Agrawal P, Pandey BL, Koch B, et al. 2016. Transferrin receptor targeted PLGA micelles improved efficacy and safety in docetaxel delivery. *International journal of biological macromolecules* 83:335-344.
- Smith DM, Patel S, Raffoul F, Haller E, Mills GB, Nanjundan M. 2010. Arsenic trioxide induces a beclin-1-independent autophagic pathway via modulation of Snord expression in ovarian carcinoma cells. *Cell Death and Differentiation* 17:1867-1881.
- Smith MB, Griffiths EA, Thompson JE, Wang ES, Wetzler M, Freyer CW. 2014. High pseudotumor cerebri incidence in tretinoin and arsenic treated acute promyelocytic leukemia and the role of topiramate after acetazolamide failure. *Leukemia research reports* 3:62-66.
- Song HJ, Zhang J, Wang WW, Huang PS, Zhang YM, Liu JF, et al. 2015. Acid-responsive pegylated doxorubicin prodrug nanoparticles for neuropilin-1 receptor-mediated targeted drug delivery. *Colloids and Surfaces B-Biointerfaces* 136:365-374.
- Soucy NV, Ihnat MA, Kamat CD, Hess L, Post MJ, Klei LR, et al. 2003. Arsenic stimulates angiogenesis and tumorigenesis in vivo. *Toxicological Sciences* 76:271-279.
- Sun H, Ma L, Hu X, Zhang T. 1992. Arsenic trioxide treated 32 cases of acute promyelocytic leukemia. *Chinese Journal of Integrated Traditional and Western Medicine* 12:170-171.

- Sun H, Guo B, Cheng R, Meng F, Liu H, Zhong Z. 2009. Biodegradable micelles with sheddable poly(ethylene glycol) shells for triggered intracellular release of doxorubicin. *Biomaterials* 30:6358-6366.
- Sun HL, Meng FH, Cheng R, Deng C, Zhong ZY. 2013. Reduction-sensitive degradable micellar nanoparticles as smart and intuitive delivery systems for cancer chemotherapy. *Expert Opinion on Drug Delivery* 10:1109-1122.
- Sun RC, Board PG, Blackburn AC. 2011. Targeting metabolism with arsenic trioxide and dichloroacetate in breast cancer cells. *Molecular Cancer* 10.
- Sun W, Wu JY, Li J, Fang H, Du LP, Li MY. 2012. Boronate can be the fluorogenic switch for the detection of hydrogen peroxide. *Current Medicinal Chemistry* 19:3622-3634.
- Sun Y, Yan XL, Yuan TM, Liang J, Fan YJ, Gu ZW, et al. 2010. Disassemblable micelles based on reduction-degradable amphiphilic graft copolymers for intracellular delivery of doxorubicin. *Biomaterials* 31:7124-7131.
- Sun Y, Zou W, Bian SQ, Huang YH, Tan YF, Liang J, et al. 2013. Bioreducible paa-g-peg graft micelles with high doxorubicin loading for targeted antitumor effect against mouse breast carcinoma. *Biomaterials* 34:6818-6828.
- Sun Y, Li YP, Huang HL, Wang YZ, Sa ZP, Wang JY, et al. 2015. Ph-sensitive poly(itaconic acid)-poly(ethylene glycol)-poly (l-histidine) micelles for drug delivery. *Journal of Macromolecular Science Part a-Pure and Applied Chemistry* 52:925-933.
- Suzuki T, Ishibashi K, Yumoto A, Nishio K, Ogasawara Y. 2015. Utilization of arsenic trioxide as a treatment of cisplatin-resistant non-small cell lung cancer pc-9/cddp and pc-14/cddp cells. *Oncology Letters* 10:805-809.
- Swindell EP, Hankins PL, Chen HM, Miodragovic DU, O'Halloran TV. 2013. Anticancer activity of small-molecule and nanoparticulate arsenic(iii) complexes. *Inorganic Chemistry* 52:12292-12304.
- Szegezdi E, Cahill S, Meyer M, O'Dwyer M, Samali A. 2006. Trail sensitisation by arsenic trioxide is caspase-8 dependent and involves modulation of death receptor components and akt. *British Journal of Cancer* 94:398-406.

- Talelli M, Rijcken CJF, Oliveira S, van der Meel R, Henegouwen P, Lammers T, et al. 2011. Nanobody - shell functionalized thermosensitive core-crosslinked polymeric micelles for active drug targeting. *Journal of Controlled Release* 151:183-192.
- Tangsangasaksri M, Takemoto H, Naito M, Maeda Y, Sueyoshi D, Kim HJ, et al. 2016. SiRNA-loaded polyion complex micelle decorated with charge-conversional polymer tuned to undergo stepwise response to intra-tumoral and intra-endosomal pHs for exerting enhanced RNAi efficacy. *Biomacromolecules* 17:246-255.
- Tarhini AA, Kirkwood JM, Tawbi H, Gooding WE, Islam MF, Agarwala SS. 2008. Safety and efficacy of arsenic trioxide for patients with advanced metastatic melanoma. *Cancer* 112:1131-1138.
- Thomas DJ, Waters SB, Styblo M. 2004. Elucidating the pathway for arsenic methylation. *Toxicology and Applied Pharmacology* 198:319-326.
- Thornalley PJ, Rabbani N. 2011. Glyoxalase in tumorigenesis and multidrug resistance. *Seminars in Cell & Developmental Biology* 22:318-325.
- Tong R, Tang L, Ma L, Tu CL, Baumgartner R, Cheng JJ. 2014. Smart chemistry in polymeric nanomedicine. *Chemical Society Reviews* 43:6982-7012.
- Tsivgoulis GM, Sotiropoulos DN, Ioannou PV. 1991. Rac-1,2-diacyloxypropyl-3-arsonic acids - arsonolipid analogs of phosphonolipids. *Phosphorus Sulfur and Silicon and the Related Elements* 63:329-334.
- Uchegbu IF. 2006. Pharmaceutical nanotechnology: Polymeric vesicles for drug and gene delivery. *Expert opinion on drug delivery* 3:629-640.
- Ulery BD, Nair LS, Laurencin CT. 2011. Biomedical applications of biodegradable polymers. *Journal of Polymer Science Part B-Polymer Physics* 49:832-864.
- van der Meel R, Vehmeijer LJC, Kok RJ, Storm G, van Gaal EVB. 2013. Ligand-targeted particulate nanomedicines undergoing clinical evaluation: Current status. *Advanced Drug Delivery Reviews* 65:1284-1298.

- Venugopal J, Prabhakaran MP, Low S, Choon AT, Zhang YZ, Deepika G, et al. 2008. Nanotechnology for nanomedicine and delivery of drugs. *Current Pharmaceutical Design* 14:2184-2200.
- Vuky J, Yu R, Schwartz L, Motzer RJ. 2002. Phase ii trial of arsenic trioxide in patients with metastatic renal cell carcinoma. *Investigational New Drugs* 20:327-330.
- Walker AM, Stevens JJ, Ndebele K, Tchounwou PB. 2010. Arsenic trioxide modulates dna synthesis and apoptosis in lung carcinoma cells. *International Journal of Environmental Research and Public Health* 7:1996-2007.
- Walter I, Schwerdtle T, Thuy C, Parsons JL, Dianov GL, Hartwig A. 2007. Impact of arsenite and its methylated metabolites on parp-1 activity, parp-1 gene expression and poly(adp-ribosylation) in cultured human cells. *DNA Repair* 6:61-70.
- Wang H, Liu Y, Wang X, Liu DH, Sun ZQ, Wang C, et al. 2015. Randomized clinical control study of locoregional therapy combined with arsenic trioxide for the treatment of hepatocellular carcinoma. *Cancer* 121:2917-2925.
- Wang L, Li XL, Liu XY, Lu K, Chen N, Li PP, et al. 2015. Enhancing effects of indirubin on the arsenic disulfide-induced apoptosis of human diffuse large b-cell lymphoma cells. *Oncology Letters* 9:1940-1946.
- Wang W, Sun H, Meng F, Ma S, Liu H, Zhong Z. 2012. Precise control of intracellular drug release and anti-tumor activity of biodegradable micellar drugs via reduction-sensitive shell-shedding. *Soft Matter* 8:3949-3956.
- Wang ZQ, Liu W, Xu HB, Yang XL. 2007. Preparation and in vitro studies of stealth pegylated plga nanoparticles as carriers for arsenic trioxide. *Chinese Journal of Chemical Engineering* 15:795-801.
- Warburg O, Wind F, Negelein E. 1926. Metabolism of tumors in the body. *Klin Wochenschr* 5:829-832.
- Waxman S, Anderson KC. 2001. History of the development of arsenic derivatives in cancer therapy. *Oncologist* 6:3-10.

- Westervelt P, Brown RA, Adkins DR, Khoury H, Curtin P, Hurd D, et al. 2001. Sudden death among patients with acute promyelocytic leukemia treated with arsenic trioxide. *Blood* 98:266-271.
- Williams KJ. 2009. The introduction of 'chemotherapy' using arsphenamine - the first magic bullet. *Journal of the Royal Society of Medicine* 102:343-348.
- Woo SH, Park IC, Park MJ, An S, Lee HC, Jin HO, et al. 2004. Arsenic trioxide sensitizes cd95/fas-induced apoptosis through ros-mediated upregulation of cd95/fas by nf-kappa b activation. *International Journal of Cancer* 112:596-606.
- Woodruff MA, Hutmacher DW. 2010. The return of a forgotten polymer-polycaprolactone in the 21st century. *Progress in Polymer Science* 35:1217-1256.
- Wu J, Henderson C, Feun L, Van Veldhuizen P, Gold P, Zheng H, et al. 2010. Phase ii study of darinaparsin in patients with advanced hepatocellular carcinoma. *Investigational New Drugs* 28:670-676.
- Wu JZ, Ho PC. 2006. Evaluation of the in vitro activity and in vivo bioavailability of realgar nanoparticles prepared by cryo-grinding. *European Journal of Pharmaceutical Sciences* 29:35-44.
- Wu XS, Shi JM, Wu Y, Tao Y, Hou J, Meng XQ, et al. 2010. Arsenic trioxide-mediated growth inhibition of myeloma cells is associated with an extrinsic or intrinsic signaling pathway through activation of trail or trail receptor 2. *Cancer Biology & Therapy* 10:1202-1215.
- Wu YK, Yang CL, Lai QY, Zhang Q, Wang W, Yuan Z. 2015. Fabrication of thermo-sensitive complex micelles for reversible cell targeting. *Journal of Materials Science-Materials in Medicine* 26:13.
- Wyman IW, Liu GJ. 2013. Micellar structures of linear triblock terpolymers: Three blocks but many possibilities. *Polymer* 54:1950-1978.
- Xie SL, Yang MH, Chen K, Huang H, Zhao XW, Zang YS, et al. 2015. Efficacy of arsenic trioxide in the treatment of malignant pleural effusion caused by pleural metastasis of lung cancer. *Cell Biochemistry and Biophysics* 71:1325-1333.

- Xiong XB, Mahmud A, Uludag H, Lavasanifar A. 2007. Conjugation of arginine-glycine-aspartic acid peptides to poly(ethylene oxide)-b-poly(epsilon-caprolactone) micelles for enhanced intracellular drug delivery to metastatic tumor cells. *Biomacromolecules* 8:874-884.
- Xiong XB, Ma ZS, Lai R, Lavasanifar A. 2010a. The therapeutic response to multifunctional polymeric nano-conjugates in the targeted cellular and subcellular delivery of doxorubicin. *Biomaterials* 31:757-768.
- Xiong XB, Uludag H, Lavasanifar A. 2010b. Virus-mimetic polymeric micelles for targeted siRNA delivery. *Biomaterials* 31:5886-5893.
- Xu F, Yan TT, Luo YL. 2013. Thermosensitive poly(n-isopropyl acrylamide-co-n,n-dimethyl acrylamide)-block-poly(D,L-lactide) amphiphilic block copolymer micelles for prednisone drug release. *Journal of Bioactive and Compatible Polymers* 28:66-85.
- Yang GF, Li XH, Zhao Z, Wang WB. 2010. Arsenic trioxide up-regulates fas expression in human osteosarcoma cells. *Chinese Medical Journal* 123:1768-1773.
- Yang M, Ding YT, Zhang LY, Qian XP, Jiang XQ, Liu BR. 2007. Novel thermosensitive polymeric micelles for docetaxel delivery. *Journal of Biomedical Materials Research Part A* 81A:847-857.
- Yang XJ, Sun DG, Tian Y, Ling SB, Wang LM. 2015. Metformin sensitizes hepatocellular carcinoma to arsenic trioxide-induced apoptosis by downregulating bcl2 expression. *Tumor Biology* 36:2957-2964.
- Yang YP, Liang ZQ, Gao B, Jia YL, Qin ZH. 2008. Dynamic effects of autophagy on arsenic trioxide-induced death of human leukemia cell line HL60 cells. *Acta Pharmacologica Sinica* 29:123-134.
- Yin G, Chen G, Zhou Z, Li Q. 2015. Modification of PEG-b-PCL block copolymer with high melting temperature by the enhancement of PCL crystal and ordered phase structure. *RSC Advances* 5:33356-33363.
- Yin TJ, Wang L, Yin LF, Zhou JP, Huo MR. 2015. Co-delivery of hydrophobic paclitaxel and hydrophilic aurka specific siRNA by redox-sensitive micelles for effective treatment of breast cancer. *Biomaterials* 61:10-25.

- Yousefpour P, Atyabi F, Farahani EV, Sakhtianchi R, Dinarvand R. 2011. Polyanionic carbohydrate doxorubicin-dextran nanocomplex as a delivery system for anticancer drugs: In vitro analysis and evaluations. *International Journal of Nanomedicine* 6:1487-1496.
- Yu XF, Yang XQ, Horte S, Kizhakkedathu JN, Brooks DE. 2014. A pH and thermosensitive choline phosphate-based delivery platform targeted to the acidic tumor microenvironment. *Biomaterials* 35:278-286.
- Yu Y, Liao M, Liu R, Chen J, Feng H, Fu Z. 2014. Overexpression of lactate dehydrogenase-a in human intrahepatic cholangiocarcinoma: Its implication for treatment. *World Journal of Surgical Oncology* 12.
- Zeng LJ, Li JG, Wang Y, Qian CC, Chen YT, Zhang QB, et al. 2014. Combination of sirna-directed kras oncogene silencing and arsenic-induced apoptosis using a nanomedicine strategy for the effective treatment of pancreatic cancer. *Nanomedicine-Nanotechnology Biology and Medicine* 10:463-472.
- Zhai B, Jiang X, He CJ, Zhao DL, Ma LX, Xu LS, et al. 2015. Arsenic trioxide potentiates the anti-cancer activities of sorafenib against hepatocellular carcinoma by inhibiting akt activation. *Tumor Biology* 36:2323-2334.
- Zhang HN, Yang LN, Ling JY, Czajkowsky DM, Wang JF, Zhang XW, et al. 2015. Systematic identification of arsenic-binding proteins reveals that hexokinase-2 is inhibited by arsenic. *Proceedings of the National Academy of Sciences of the United States of America* 112:15084-15089.
- Zhang L, Kim S, Ding WP, Tong YY, Zhang XL, Pan MG, et al. 2015a. Arsenic sulfide inhibits cell migration and invasion of gastric cancer in vitro and in vivo. *Drug Design Development and Therapy* 9:5579-5590.
- Zhang L, Tian W, Kim S, Ding WP, Tong YY, Chen SY. 2015b. Arsenic sulfide, the main component of realgar, a traditional chinese medicine, induces apoptosis of gastric cancer cells in vitro and in vivo. *Drug Design Development and Therapy* 9:79-92.
- Zhang QY, Mao JH, Liu P, Huang QH, Lu J, Xie YY, et al. 2009. A systems biology understanding of the synergistic effects of arsenic sulfide and imatinib in bcr/abl-associated leukemia.

Proceedings of the National Academy of Sciences of the United States of America 106:3378-3383.

Zhang XL, Huang YX, Ghazwani M, Zhang P, Li J, Thorne SH, et al. 2015. Tunable ph-responsive polymeric micelle for cancer treatment. *Acs Macro Letters* 4:620-623.

Zhang XW, Yan XJ, Zhou ZR, Yang FF, Wu ZY, Sun HB, et al. 2010. Arsenic trioxide controls the fate of the pml-rar alpha oncoprotein by directly binding pml. *Science* 328:240-243.

Zhang XY, Yang SM, Zhang HP, Yang Y, Sun SB, Chang JP, et al. 2015. Endoplasmic reticulum stress mediates the arsenic trioxide-induced apoptosis in human hepatocellular carcinoma cells. *International Journal of Biochemistry & Cell Biology* 68:158-165.

Zhang YF, Zhang M, Huang XL, Fu YJ, Jiang YH, Bao LL, et al. 2015. The combination of arsenic and cryptotanshinone induces apoptosis through induction of endoplasmic reticulum stress-reactive oxygen species in breast cancer cells. *Metallomics* 7:165-173.

Zhao LL, Liu YF, Peng LJ, Fei AM, Cui W, Miao SC, et al. 2015. Arsenic trioxide rewires mantle cell lymphoma response to bortezomib. *Cancer Medicine* 4:1754-1766.

Zhao QH, Zhang Y, Liu Y, Wang HL, Shen YY, Yang WJ, et al. 2010. Anticancer effect of realgar nanoparticles on mouse melanoma skin cancer in vivo via transdermal drug delivery. *Medical Oncology* 27:203-212.

Zhao WZ, Lu X, Yuan Y, Liu CS, Yang BC, Hong H, et al. 2011. Effect of size and processing method on the cytotoxicity of realgar nanoparticles in cancer cell lines. *International Journal of Nanomedicine* 6:1569-1577.

Zhao Y, Zhou YX, Wang DS, Gao YJ, Li JW, Ma SJ, et al. 2015. Ph-responsive polymeric micelles based on poly(2-ethyl-2-oxazoline)-poly(D,L-lactide) for tumor-targeting and controlled delivery of doxorubicin and p-glycoprotein inhibitor. *Acta Biomaterialia* 17:182-192.

Zhao ZH, Zhang H, Chi XQ, Li H, Yin ZY, Huang DT, et al. 2014. Silica nanovehicles endow arsenic trioxide with an ability to effectively treat cancer cells and solid tumors. *Journal of Materials Chemistry B* 2:6313-6323.

Zhao ZH, Wang XM, Zhang ZJ, Zhang H, Liu HY, Zhu XL, et al. 2015. Real-time monitoring of arsenic trioxide release and delivery by activatable t-1 imaging. *Acs Nano* 9:2749-2759.

- Zhong F, Zhang S, Shao C, Yang J, Wu X. 2010. Arsenic trioxide inhibits cholangiocarcinoma cell growth and induces apoptosis. *Pathology & Oncology Research* 16:413-420.
- Zhou J, Zhang YM, Li JM, Li XX, Hou JX, Zhao YQ, et al. 2010. Single-agent arsenic trioxide in the treatment of children with newly diagnosed acute promyelocytic leukemia. *Blood* 115:1697-1702.
- Zhou XX, Sun X, Cooper KL, Wang F, Liu KJ, Hudson LG. 2011. Arsenite interacts selectively with zinc finger proteins containing c3h1 or c4 motifs. *Journal of Biological Chemistry* 286:22855-22863.
- Zhou XX, Sun X, Mobarak C, Gandolfi AJ, Burchiel SW, Hudson LG, et al. 2014. Differential binding of monomethylarsonous acid compared to arsenite and arsenic trioxide with zinc finger peptides and proteins. *Chemical Research in Toxicology* 27:690-698.
- Zhou ZL, Badkas A, Stevenson M, Lee JY, Leung YK. 2015. Herceptin conjugated plga-phis-peg ph sensitive nanoparticles for targeted and controlled drug delivery. *International Journal of Pharmaceutics* 487:81-90.
- Zhu H-H, Wu D-P, Jin J, Li J-Y, Ma J, Wang J-X, et al. 2013. Oral tetra-arsenic tetra-sulfide formula versus intravenous arsenic trioxide as first-line treatment of acute promyelocytic leukemia: A multicenter randomized controlled trial. *Journal of Clinical Oncology* 31:4215-+.
- Zhu J, Koken MHM, Quignon F, ChelbiAlix MK, Degos L, Wang ZY, et al. 1997. Arsenic-induced pml targeting onto nuclear bodies: Implications for the treatment of acute promyelocytic leukemia. *Proceedings of the National Academy of Sciences of the United States of America* 94:3978-3983.
- Zhu J, Chen Z, Lallemand-Breitenbach V, de The H. 2002. How acute promyelocytic leukaemia revived arsenic. *Nature Reviews Cancer* 2:705-713.
- Zhu JW, Zheng M. 2012. Verrucous carcinoma due to arsenic ingestion in a psoriasis patient. *Journal of Cutaneous Medicine and Surgery* 16:445-447.
- Zhu L, Torchilin VP. 2013. Stimulus-responsive nanopreparations for tumor targeting. *Integrative Biology* 5:96-107.

Zrazhevskiy P, Sena M, Gao XH. 2010. Designing multifunctional quantum dots for bioimaging, detection, and drug delivery. *Chemical Society Reviews* 39:4326-4354

## **Chapter 2. Strategy development for enhanced arsenic encapsulation and GSH-triggered arsenic release in polymeric micelles**

### **2.1 Introduction**

Previous studies have shown the encapsulation of arsenic trioxide (ATO) in liposomes (Kallinteri et al. 2004; Zagana et al. 2008), albumin nanoparticles (Yang et al. 2008), and polymer nanoparticles (Wang et al. 2007). In these reported studies, the encapsulation of ATO was mainly dependent on its dissolution in the hydrophilic domain of nano-carriers. Because of the good water solubility of ATO, encapsulated ATO experienced fast release from the carriers. The O'Halloran group took advantage of the co-precipitation of arsenic with transitional metal ions (e.g., Ni<sup>2+</sup>, Fe<sup>2+</sup>, Pt<sup>2+</sup>) and developed a strategy for efficient ATO encapsulation and pH-sensitive ATO release (Chen et al. 2009a; Chen et al. 2009b; Chen et al. 2006).

In addition to the property of co-precipitation with transitional metal ions, trivalent arsenic compounds have good affinity for thiol groups and proteins with cysteine residues (Shen et al. 2013). This property of arsenic binding to thiol groups has been widely applied in the field of analytical chemistry (reviewed by Chen et al. 2015), such as biarsenical probes (e.g., FAsH-EDT<sub>2</sub>, ReAsH-EDT<sub>2</sub>) for arsenic monitoring and imaging in living cells and arsenic affinity chromatography for purification of thiol-containing proteins.

In this study, we aimed to develop a strategy for arsenic encapsulation in polymeric micelles based on arsenic binding to thiol groups. This micelle formulation is based on methoxy poly(ethylene oxide)-*block*-poly( $\alpha$ -carboxylate- $\epsilon$ -caprolactone) (PEO-*b*-PCCL) with thiol-ended

alkyl side chains conjugated to the free carboxyl groups on the PCCL block. The backbone, poly(ethylene oxide)-*block*-poly( $\epsilon$ -caprolactone) (PEO-*b*-PCL), consists of a polyester with good structure stability (Liu et al. 2007; Shin et al. 1998). Because thiols have high affinity to trivalent arsenicals, the free pendent thiol groups on the PCL backbone increased the interaction between arsenic and polymer chains when encapsulating trivalent arsenicals, thus increasing the arsenic loading content.

During the strategy development stage, we chose to encapsulate phenylarsine oxide (PAO), a trivalent organoarsenical that has higher binding affinity for thiol groups (Shen et al. 2013) and is more toxic than the commonly used ATO (Charoensuk et al. 2009). The developed polymeric micellar formulation of PAO was hypothesized to show enhanced release of the encapsulated drug in the presence of glutathione (GSH) leading to preferential PAO release and anti-cancer activity within cancer cells.

## **2.2 Materials and methods<sup>1</sup>**

### **2.2.1 Materials and cell line information**

All the chemicals and reagents, unless specified, were purchased from Sigma-Aldrich (St. Louis, MO, USA). N,N-dimethylacetamide (DMAc) was purchased from Acros Organics (Fair Lawn, NJ, USA). Dichloromethane, tetrahydrofuran (THF), triethylamine (NEt<sub>3</sub>), and hexane were dried before use. (Armarego 2009) The multi-element ICP-MS calibration standard-2A for arsenic analysis was purchased from Agilent Technologies (Santa Clara, CA, USA). The standard reference material NIST-1640a was purchased from the National Institute of Standards and Technology, Department of Commerce, USA. RPMI 1640 cell culture media, fetal bovine serum

---

<sup>1</sup> Dr. Mohammad R. Vakili provided assistance with polymer synthesis and NMR spectrum interpretation. Dr. Vijayalakshmi Somayaj did the NMR analysis. Mr. Marc-Andre Hoyle did the FTIR analysis and the elemental analysis, and Ms. Arlene Oatway did the TEM analysis.

(FBS), and penicillin–streptomycin solution were purchased from Life Technologies (Grand Island, NY, USA).

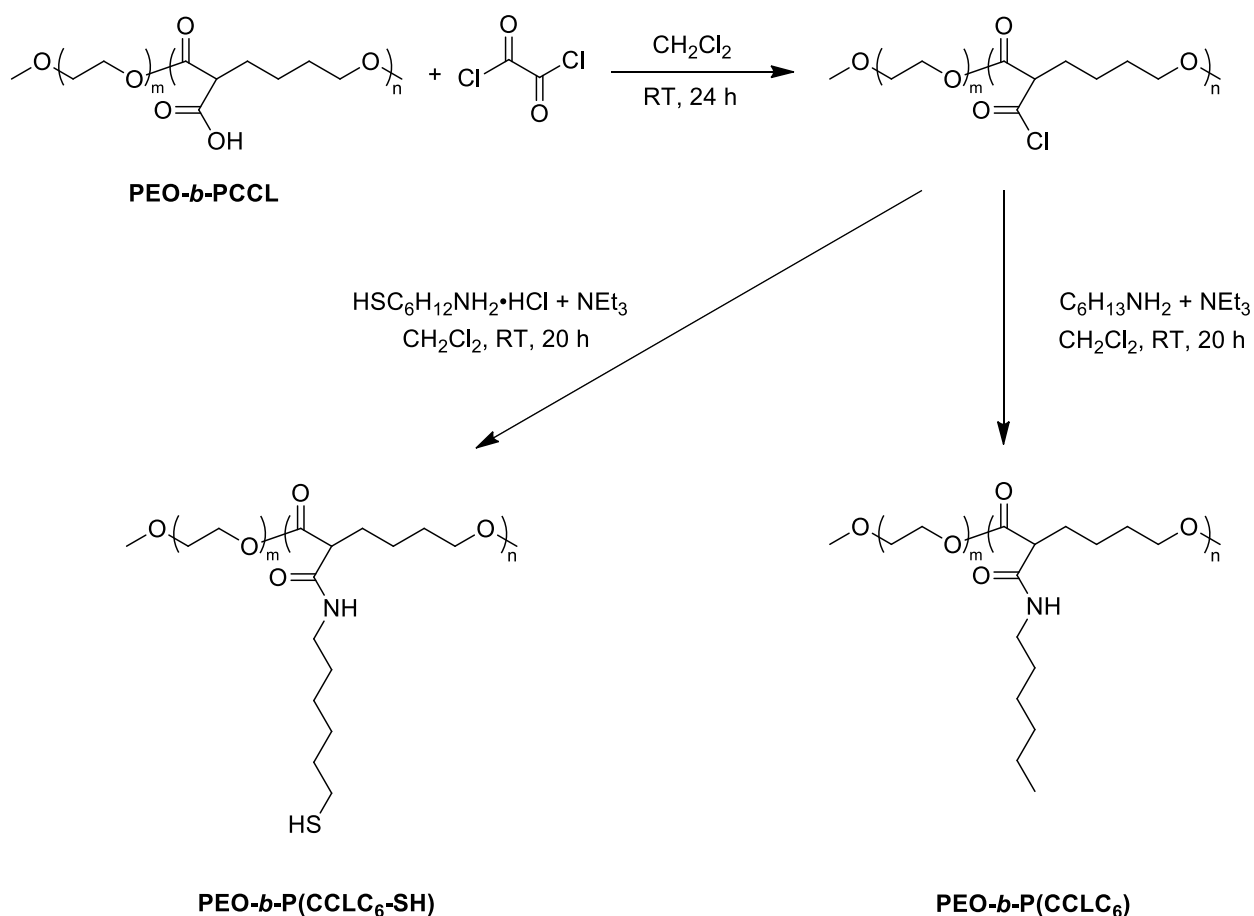
The MDA-MB-435 cancer cell line was originally received from the laboratory of Dr. R. Clarke, Georgetown University Medical School, Washington, DC, USA. The cells were cultured in RPMI 1640 medium with 10% FBS and 1% penicillin–streptomycin solution at 37 °C and 5% CO<sub>2</sub>.

### 2.2.2 Synthesis of thiol-functionalized copolymer PEO-*b*-P(CCLC<sub>6</sub>-SH)

The thiol-functionalized block copolymer, methoxy poly(ethylene oxide)-*block*-poly[ $\alpha$ -(6-mercaptopethyl amino)carboxylate- $\epsilon$ -caprolactone] [PEO-*b*-P(CCLC<sub>6</sub>-SH)], was synthesized from PEO-*b*-PCCL (**Scheme 2.1**). The methods for the synthesis of PEO-*b*-PCCL were described in previous publications (Mahmud et al. 2006; Xiong et al. 2008). The thiol-functionalized copolymer, PEO-*b*-P(CCLC<sub>6</sub>-SH), was synthesized using the following procedures. PEO<sub>114</sub>-*b*-PCCL<sub>15</sub> (100 mg, 0.20 mmol COOH) was dissolved in 10 mL freshly dried CH<sub>2</sub>Cl<sub>2</sub>. After the polymer solution was cooled down to 0 °C, oxalyl chloride (28 mg, 0.22 mmol) was added. The reaction temperature was increased from 0 °C to room temperature. After 24 h, CH<sub>2</sub>Cl<sub>2</sub> was evaporated and the unreacted oxalyl chloride was removed by washing with dry hexane. The activated polymer was re-dissolved in dry CH<sub>2</sub>Cl<sub>2</sub> and cooled down to 0 °C. Mercaptohexylamine hydrochloride (SHC<sub>6</sub>H<sub>12</sub>NH<sub>2</sub>·HCl) (34 mg, 0.20 mmol) was first dissolved in 1 mL dry CH<sub>2</sub>Cl<sub>2</sub> and neutralized by dry NEt<sub>3</sub> (61  $\mu$ L, 0.44 mmol) before being added to the polymer solution. After another 20 h, CH<sub>2</sub>Cl<sub>2</sub> was evaporated and the product was re-dissolved in toluene. After centrifugation, the collected supernatant was dialysed against DMAc and then against water. Each dialysis lasted for 24 h. The respective solvents were changed at 1, 3, 6, and 24 h. The purified PEO-*b*-P(CCLC<sub>6</sub>-SH) was lyophilized for further use.

### 2.2.3 Synthesis of alkyl substituted PEO-*b*-PCCL copolymer without thiol functional group PEO-*b*-P(CCLC<sub>6</sub>)

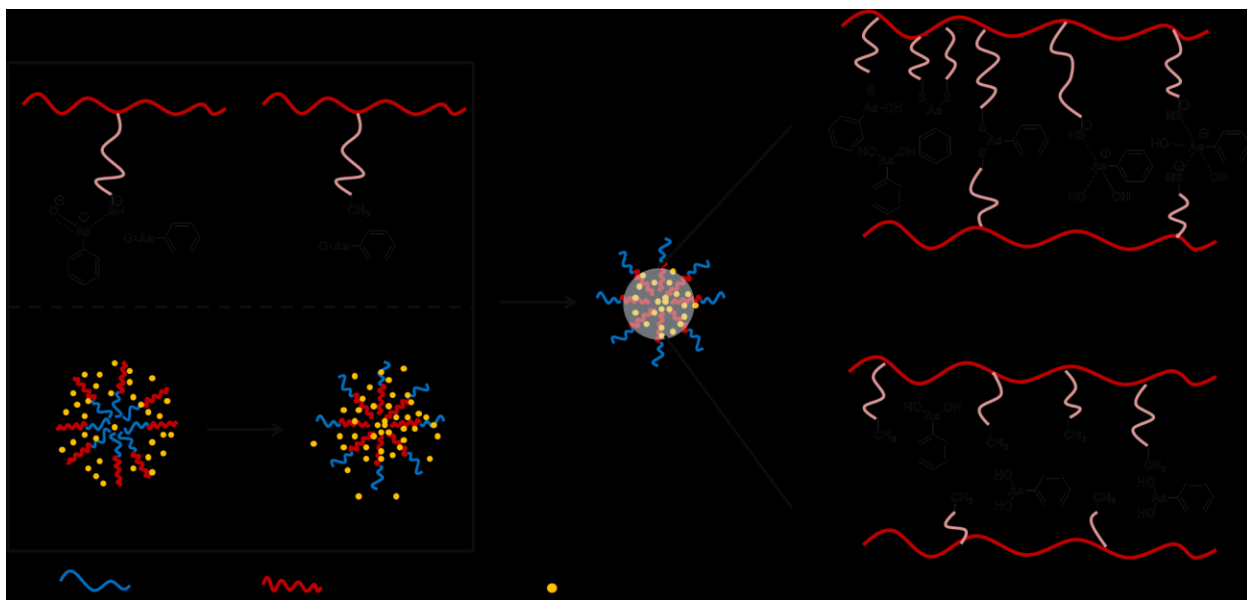
The alkyl substituted block copolymer, methoxy poly(ethylene oxide)-*block*-poly[ $\alpha$ -(hexyl amino)carboxylate- $\epsilon$ -caprolactone] [PEO-*b*-P(CCLC<sub>6</sub>)], without a thiol functional group was also synthesized from PEO-*b*-PCCL (**Scheme 2.1**). The major synthesis procedures were similar to those for PEO-*b*-P(CCLC<sub>6</sub>-SH) synthesis, except that hexylamine (C<sub>6</sub>H<sub>13</sub>NH<sub>2</sub>) was used to react with PEO-*b*-PCCL instead of SHC<sub>6</sub>H<sub>12</sub>NH<sub>2</sub>·HCl, in the presence of NEt<sub>3</sub>.



**Scheme 2.1.** Synthesis of thiol-containing polymer PEO-*b*-P(CCLC<sub>6</sub>-SH) and the control polymer without thiol groups PEO-*b*-P(CCLC<sub>6</sub>)

#### 2.2.4 Preparation of micelles loaded with phenylarsine oxide (PAO)

Freshly synthesized PEO-*b*-P(CCLC<sub>6</sub>-SH) and PEO-*b*-P(CCLC<sub>6</sub>) without any dialysis were mixed with 0.2, 1, 2, and 10 mmol of PAO per gram of PEO<sub>114</sub>-*b*-PCCL<sub>15</sub> (Scheme 2.2). The mixture was stirred for 6 h in toluene at room temperature in the dark, followed with dialysis against DMAc and water. The corresponding final products, PEO-*b*-P(CCLC<sub>6</sub>-S-PAO) and PEO-*b*-P(CCLC<sub>6</sub>-PAO), were lyophilized.



**Scheme 2.2. Encapsulation of PAO into PEO-*b*-P(CCLC<sub>6</sub>-SH) and PEO-*b*-P(CCLC<sub>6</sub>) micelles.** The unloaded PAO was removed by sequential dialysis against DMAc and water. Since toluene is a non-polar organic solvent, the polymer micelles are likely to have the hydrophilic PEO blocks in the core and the hydrophobic modified PCCL blocks in the corona. After dialysis against the polar organic solvent DMAc, the polymer micelles switch the aggregation format and have the hydrophobic PCCL groups in the core. The nature of the As-S bond under these conditions is not clear. Possible forms include one sulfur residue on one arsenic atom, or two sulfur residues on one arsenic atom and ionic interaction between thiol groups and hydrolyzed PAO. If two sulfur residues are on one arsenic atom, the sulfur residues can be on the same polymer chain or on two different polymer chains. Whereas no thiol groups exist in PEO-*b*-P(CCLC<sub>6</sub>), the encapsulation of PAO in PEO-*b*-P(CCLC<sub>6</sub>) micelles is based on hydrophobic interaction between PAO and PCCL blocks.

#### 2.2.5 Determination of arsenic loading in the micelles

Arsenic loading was determined by inductively coupled plasma mass spectrometry (ICP-MS, Agilent 7500cs Octopole Reaction System). Each polymer micelle (1 mg) was weighted and

digested in 1 mL 10% nitric acid in a 50 °C water bath overnight. The digested polymer solution was diluted 1000 times in 1% nitric acid and filtered with a 0.45 µm polyvinylidene difluoride (PVDF) filter purchased from Mandel (Guelph, ON, Canada) before ICP-MS analysis. Triplicate polymer samples were prepared. The quantification of elemental arsenic in digested polymer samples was based on arsenic external standard calibration prepared from arsenic-containing multi-element ICP-MS calibration standard-2A solutions. The method was evaluated with diluted 1640a standard, a certified reference for trace element determination in fresh water. Triplicate analyses were performed on all standard solutions and samples. The arsenic loading in polymer micelles was determined as the weight percentage of arsenic element in lyophilized micelles encapsulated with PAO.

### **2.2.6 Characterization of polymers and their self-assembled structures**

PEO-*b*-PCCL, PEO-*b*-P(CCLC<sub>6</sub>-SH), PEO-*b*-P(CCLC<sub>6</sub>), and PEO-*b*-P(CCLC<sub>6</sub>-S-PAO) were characterized using <sup>1</sup>H NMR (Bruker Advance 600 MHz NMR spectrometer), FT-IR (Thermo Scientific Nicolet 8700 Fourier transformed infrared spectrometer), and elemental analysis (Carlo Erba EA 1108 elemental analyzer). <sup>1</sup>H NMR spectra of polymers in CDCl<sub>3</sub> solution were measured at 600 MHz. The proton intensity of –CH<sub>2</sub>–O–CO– (δ = 4.35-3.95 ppm) was compared with the intensity of PEO (–CH<sub>2</sub>CH<sub>2</sub>O–, δ = 3.80-3.53 ppm) to obtain the total caprolactone unit number in PEO-*b*-PCCL, PEO-*b*-P(CCLC<sub>6</sub>-SH), PEO-*b*-P(CCLC<sub>6</sub>), and PEO-*b*-P(CCLC<sub>6</sub>-S-PAO), considering a 5000 Da molecular weight of PEO (114 units of –CH<sub>2</sub>CH<sub>2</sub>O–). The methylene proton intensity of –NH–CH<sub>2</sub>– (δ = 2.89 ppm) in PEO-*b*-P(CCLC<sub>6</sub>) was compared to the intensity of PEO to estimate the unit number of caprolactone modified with the hexylamino group. The sum of methylene proton intensity of –NH–CH<sub>2</sub>– (δ = 2.96-2.81 ppm) and –CH<sub>2</sub>–SH (δ = 2.72–2.63 ppm) was used to estimate the unit number of caprolactone modified with the mercaptohexylamino

group. The aromatic proton in PEO-*b*-P(CCLC<sub>6</sub>-S-PAO) was used to confirm the loading of PAO. The FT-IR spectrum was obtained by preparing polymer/KBr pellets. The peaks for the amide bond ( $\nu = 1640 \text{ cm}^{-1}$ ) and phenyl group ( $\nu = 741$  and  $694 \text{ cm}^{-1}$ ) were used to confirm the pendant group conjugation and arsenic encapsulation. Sulfur content was measured by elemental analysis (Carlo Erba EA 1108 elemental analyzer).

The micelle sizes of PEO-*b*-PCCL, PEO-*b*-P(CCLC<sub>6</sub>-SH), and PEO-*b*-P(CCLC<sub>6</sub>-S-PAO) were measured by the dynamic light scattering (DLS) technique (detection angle:  $173^\circ$ , temperature:  $25^\circ \text{C}$ , Malvern Nano-ZS zetasizer) and transmission electron microscopy (TEM, Philips/FEI Morgagni<sup>TM</sup> transmission electron microscope with CCD camera). To confirm the morphology of PAO particles, PAO was also measured by TEM. For the TEM measurement, a droplet of micelle solution (2 mg/mL) or PAO solution (aq.,  $200 \mu\text{M}$ ) was placed on a copper-coated grid. The grid was held horizontally for 1 min to allow the micelles to settle. The excess solution was carefully dried off by filter paper. Then, a drop of phosphotungstic acid (PAT) solution (2%) was added onto the grid for negative staining. After 30 s, the excess fluid was again removed by filter paper. The sample was then air-dried and loaded into the TEM. Pictures were taken at 80 kV with magnification of 71000. The size distribution in TEM pictures was analyzed by Nano Measurer 1.2 software (Department of Chemistry, Fudan University, China).

Critical micelle concentrations (CMC) of PEO-*b*-PCCL, PEO-*b*-P(CCLC<sub>6</sub>-SH), and PEO-*b*-P(CCLC<sub>6</sub>-S-PAO) were measured using the pyrene fluorescence method. (Ohyashiki and Mohri 1983; Wilhelm et al. 1991) The details of measurement were described in a previous publication. (Shahin and Lavasanifar 2010)

### **2.2.7 *In vitro* polymer stability study**

The stability of PEO-*b*-P(CCLC<sub>6</sub>-SH) and PEO-*b*-P(CCLC<sub>6</sub>-S-PAO) was evaluated in both the absence and presence of surfactants. Specifically, PEO-*b*-P(CCLC<sub>6</sub>-SH) and PEO-*b*-P(CCLC<sub>6</sub>-S-PAO) solution (1 mg/mL) was prepared in water and 2 mg/mL sodium dodecyl sulfate (SDS) aqueous solution by direct re-suspension. All the aqueous solutions were filtered with a 0.45 μm PVDF filter before incubation in a 37 °C water bath. The micelle size distribution at different incubation times was monitored by DLS for 15 days.

### **2.2.8 *In vitro* release of arsenic from the polymer micelles**

Two milliliters of 1 mg/mL PEO-*b*-P(CCLC<sub>6</sub>-S-PAO) were re-suspended in CH<sub>3</sub>COONH<sub>4</sub> buffer (1.45 M, pH 7.4) with different GSH concentrations (0, 1, 5, and 10 mM GSH) at 37 °C. For one experiment, GSH stock solution (100 mM) was added to the PEO-*b*-P(CCLC<sub>6</sub>-S-PAO) solution at a specific release time of 12 h, to make the final GSH concentration 1 mM. This batch of release experiment was denoted as 12 h–1 mM GSH. A 50-μL aliquot of the solution containing the micelles was used for determination of total arsenic. At various time intervals (0, 1, 3, 6, 12, 24, 36, and 48 h), a 120-μL aliquot of the solution was used to determine arsenic release from the polymer micelles. The aliquot was filtered using an Amicon Ultra-0.5 mL centrifugal filter (molecular weight cutoff: 3,000 Da), purchased from Millipore (Billerica, MA, USA), at 13500 × g for 20 min. The small molecule fraction in the filtrate was analyzed for arsenic concentration released from the micelles. The level of As in each sample was determined by ICP-MS. All the analyses were performed in triplicate.

### 2.2.9 *In vitro* cell cytotoxicity of arsenic before and after encapsulation in micelles

Neutral red assay was used to evaluate the *in vitro* cytotoxicity of PEO-*b*-P(CCLC<sub>6</sub>-SH) and PEO-*b*-P(CCLC<sub>6</sub>-S-PAO) against MDA-MB-435 cells. The cytotoxicity of encapsulated PAO was compared to that of free PAO.

MDA-MB-435 cells were seeded into a 96-well plate at a density of 8000 cells/200  $\mu$ L per well and incubated in an incubator humidified with 5% CO<sub>2</sub>. After overnight incubation, the cells were treated with PAO, PEO-*b*-P(CCLC<sub>6</sub>-SH), and PEO-*b*-P(CCLC<sub>6</sub>-S-PAO) micelles for 24 and 48 h. Mercaptohexylamine in complete RPMI 1640 medium was prepared from 1 to 2500  $\mu$ M. PEO-*b*-P(CCLC<sub>6</sub>-S-PAO) stock solutions (0.8 mg/mL) were prepared in PBS buffer. Prematurely released PAO in stock solutions was removed by centrifugal filters prior to serial dilution. PEO-*b*-P(CCLC<sub>6</sub>-SH) stock solution (4 mg/mL) was prepared in complete RPMI 1640 medium, from 0.00004 to 1 mg/mL polymer concentration. PEO-*b*-P(CCLC<sub>6</sub>-S-PAO) was prepared from 0.00004 to 0.04 mg/mL polymer concentration, with equivalent arsenic concentrations ranging from 0.001 to 10  $\mu$ M. The exact arsenic concentrations in PEO-*b*-P(CCLC<sub>6</sub>-S-PAO) solutions with PAO levels of 0.5, 1, and 10  $\mu$ M were determined by ICP-MS. PAO concentrations of more diluted PEO-*b*-P(CCLC<sub>6</sub>-S-PAO) solutions were calculated based on solutions with known concentration and the respective dilution times. Cell viability was measured according to the standard protocol for neutral red assay. Absorbance at 540 nm wavelength was detected by a multiplate reader and was subtracted from the background signal at 690 nm.

The cell survival rate was expressed as the percentage of viable cells in the treated wells compared to those in the untreated wells which served as the control. The dose effect of each compound was fitted by the *Sigmoidal Dose-Response (variable slope)* equation in GraphPad

Prism 5 software (La Jolla, CA, USA) to obtain IC<sub>50</sub> values. The IC<sub>50</sub> values were expressed as mean with 95% confidence interval (95% CI) in parentheses. Triplicate assays were conducted.

### 2.2.10 Data analysis

All results were expressed as mean  $\pm$  standard deviation (SD) unless otherwise noted. Statistical analysis was performed by two-tailed unpaired Student's t-test for two groups. A value of  $P < 0.05$  was considered statistically significant.

## 2.3 Results

### 2.3.1 Polymer synthesis and characterization

The conjugation of mercaptohexylamino side chain was based on a two-step reaction (**Scheme 2.1**). The carboxylic acid group in the starting polymer PEO-*b*-PCCL was first activated by oxalyl chloride. The freshly synthesized acyl chloride was then substituted with neutralized mercaptohexylamine. The synthesis has an overall yield of  $\sim 40\%$ .

PEO-*b*-P(CCLC<sub>6</sub>-SH) was characterized using <sup>1</sup>H NMR (

**Figure 2.1**) and Fourier transformed infrared spectroscopy (FT-IR) (**Figure 2.2**) to confirm the conjugation of the mercaptohexylamino group. In **Figure 2.1-C** the peaks at  $\delta$  of 2.8 ppm and 2.6 ppm were assigned to protons of the methylene group adjacent to the amide bond and thiol group on the pendant groups in PEO-*b*-P(CCLC<sub>6</sub>-SH), respectively. In the NMR spectrum of PEO-*b*-P(CCLC<sub>6</sub>) (

**Figure 2.1-B**), the peak of the pendent methyl group appeared at  $\delta$  0.9 ppm. Except for the proton peak of the methylene group adjacent to the amide bond ( $\delta$ , 2.8 ppm), the signals of other methylenes related to the hexylamino pendant group were mixed with backbone methylenes ( $\delta$ , 1.95–1.20 ppm). After loading PAO, peaks of protons on the aromatic ring from PAO were seen

at  $\delta$  7.31–7.41 ppm. FT-IR spectra (**Figure 2.2**) show that peaks for the amide bond ( $\nu$ , 1640  $\text{cm}^{-1}$ ) arose after side chain conjugation. New peaks for single-substituted aromatic rings ( $\nu$ , 694 and 741  $\text{cm}^{-1}$ ) appeared after loading PAO.

Peak integration from  $^1\text{H}$ -NMR spectra suggested that not all the PCCL units were substituted with mercaptohexylamino groups and that a few hydrophobic blocks were chopped off. The unit numbers of polymer blocks based on NMR data are summarized in **Table 2.1**. According to elemental analysis, sulfur accounted for  $1.6 \pm 0.4$  wt% of total PEO-*b*-P(CCLC<sub>6</sub>-SH) weight.

**Table 2.1. Molecular weight of block polymers**

Polymer name	Composition <sup>a</sup>	Theoretical Molecular Weight ( $\text{g}\cdot\text{mol}^{-1}$ )
PEO- <i>b</i> -PCCL	PEO <sub>114</sub> - <i>b</i> -PCCL <sub>15</sub>	7370
PEO- <i>b</i> -P(CCLC <sub>6</sub> )	PEO <sub>114</sub> - <i>b</i> -PCCL <sub>4.3</sub> -co-P(CCLC <sub>6</sub> ) <sub>9.3</sub>	7921
PEO- <i>b</i> -P(CCLC <sub>6</sub> -SH)	PEO <sub>114</sub> - <i>b</i> -PCCL <sub>7.3</sub> -co-P(CCLC <sub>6</sub> -SH) <sub>5.5</sub>	7655

<sup>a</sup>The unit number of each block was calculated based on  $^1\text{H}$  NMR peak integration

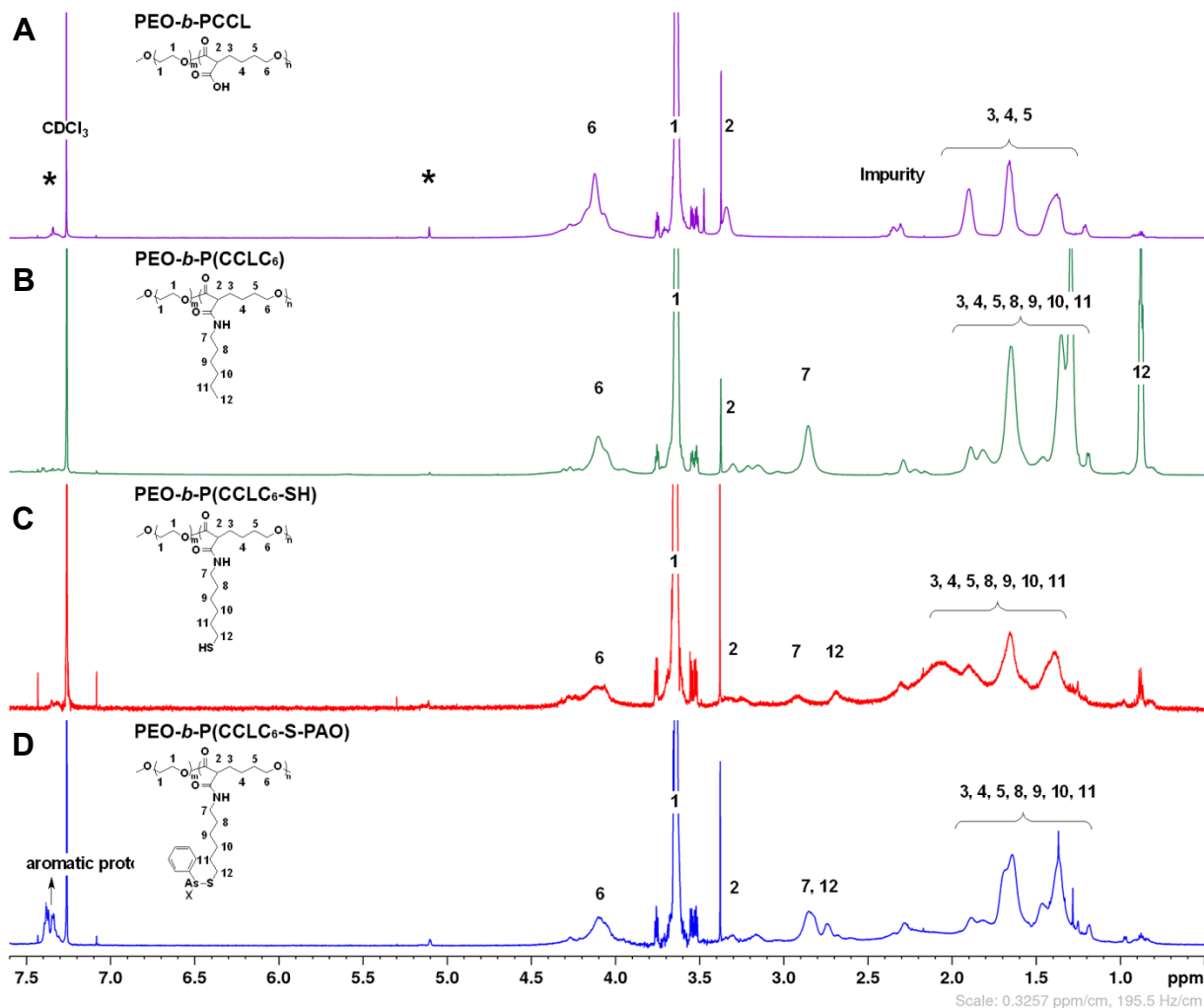


**Figure 2.1.**  $^1\text{H}$  NMR spectra of PEO-*b*-PCCL (A), PEO-*b*-P(CCLC<sub>6</sub>) (B), PEO-*b*-P(CCLC<sub>6</sub>-SH) (C), and PEO-*b*-P(CCLC<sub>6</sub>-S-PAO) (D) in CDCl<sub>3</sub>. The spectra were adjusted by setting the chemical shift of CDCl<sub>3</sub> at 7.26. \*: Peaks at 5.2 ppm and 7.4 ppm in (A) belong to the benzyl group remained from the incomplete reduction of methoxy poly(ethylene oxide)-*block*-poly(benzyl carboxylate- $\epsilon$ -caprolactone) (PEO-*b*-PBCL), and the remaining BCL groups accounted for less than 5% of total CCL units. The remaining benzyl groups could interfere with the phenyl group signal in (D). However, the substantial increase of the aromatic proton signal intensity confirmed the PAO loading.

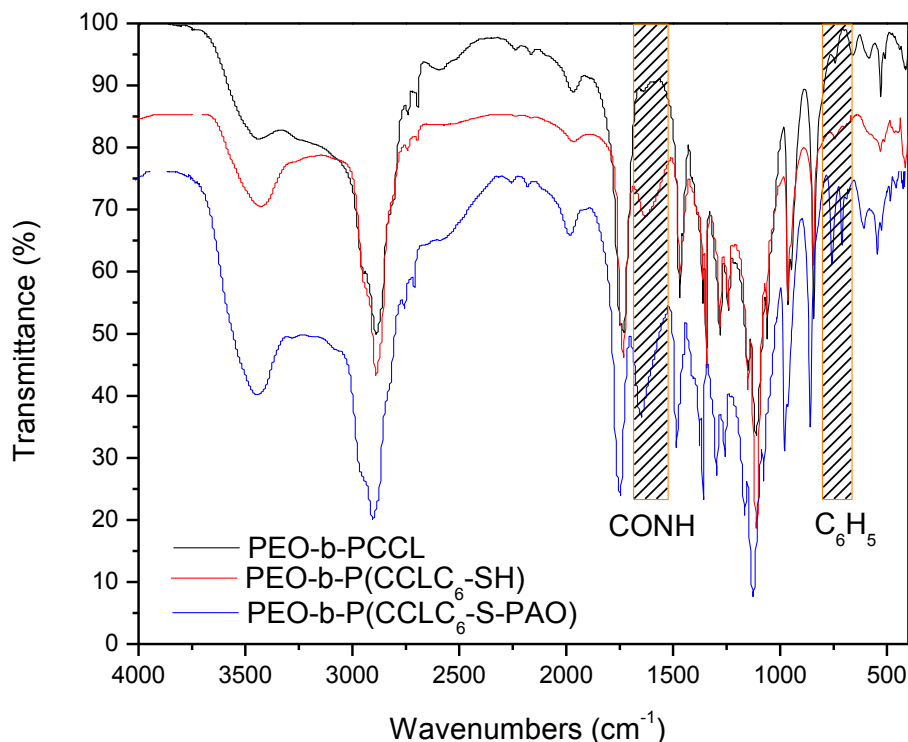


**Figure 2.2.** FT-IR spectra of PEO-*b*-PCCL, PEO-*b*-P(CCLC<sub>6</sub>-SH), and PEO-*b*-P(CCLC<sub>6</sub>-S-PAO) in KBr pellets.

### 2.3.2 Optimization of PAO loading into polymeric micelles

Different amounts of PAO were mixed with polymers in toluene and stirred for 6 h at room temperature in the dark. During the dialysis against DMAc and water, PAO was encapsulated inside the polymeric micelles (**Scheme 2.2**). Meanwhile, the extramolecular PAO was removed. To avoid the severe oxidation of thiol groups, we used the freshly synthesized PEO-*b*-P(CCLC<sub>6</sub>-SH) for PAO encapsulation. Therefore, the exact polymer weight was not obtained. The PAO amount added was based on the weight of the starting polymer, PEO-*b*-PCCL.

Physical encapsulation of PAO inside PEO-*b*-P(CCLC<sub>6</sub>) based on hydrophobic interaction was very low (**Figure 2.3**). However, by increasing the PAO amount added, the arsenic loading in PEO-*b*-P(CCLC<sub>6</sub>) could be increased. The maximum loading of PAO in PEO-*b*-P(CCLC<sub>6</sub>) was

0.17±0.03 wt%, which is not substantial. After replacing the hexylamino pendant group with the mercaptohexylamino group, the arsenic loading was increased ~15 times and reached 2.4±0.2 wt% (Figure 2.3).

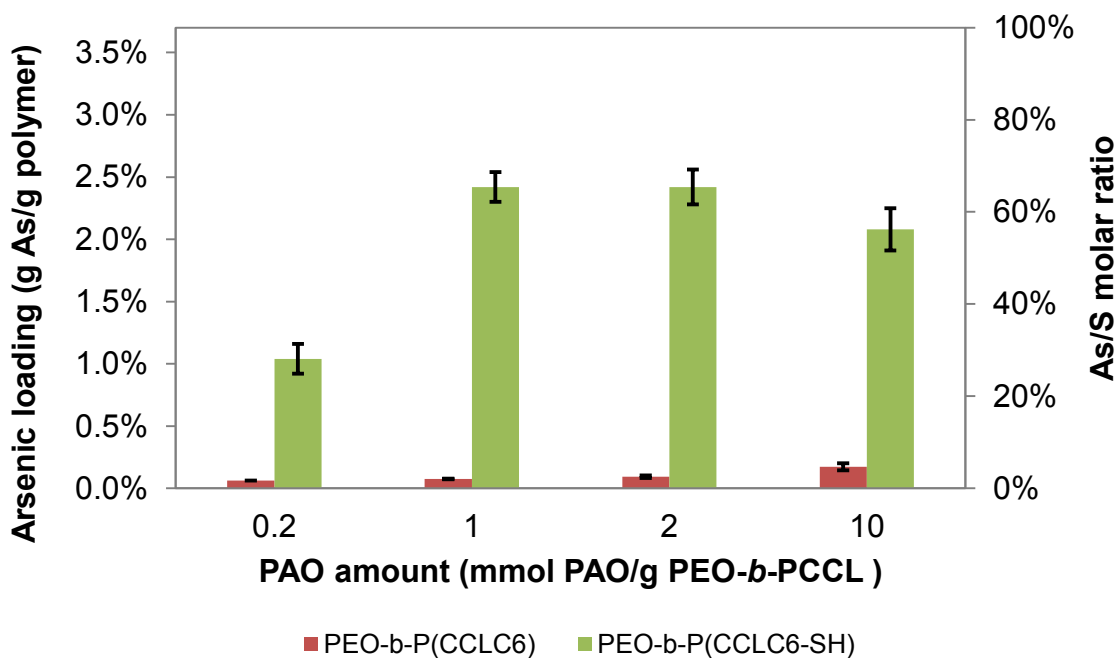


**Figure 2.3. Arsenic loading in PEO-b-P(CCLC<sub>6</sub>) and PEO-b-P(CCLC<sub>6</sub>-SH) micelles with different PAO amounts added.** The right vertical axis represent the corresponding molar ratio of arsenic to sulfur in PAO-loaded PEO-b-P(CCLC<sub>6</sub>-SH) micelles. Data are presented as mean ± SD (n = 3).

### 2.3.3 Characterization of the assembly of block polymers

Diblock polymers underwent self-assembly in each dialysis process during purification (Scheme 2.2), especially when the concentration of polymer was high. After dialysis, polymer products were lyophilized for further use. The micelles were easily regenerated by simple dissolution of the freeze-dried polymer powder in aqueous solution.

The CMC values of PEO-*b*-PCCL, PEO-*b*-P(CCLC<sub>6</sub>-SH) and PEO-*b*-P(CCLC<sub>6</sub>-S-PAO) were 89±4, 92±7, and 70±5 µg/mL, respectively (Figure 2.4). When functionalized with carboxylic acid groups, the PCCL block was less hydrophobic than the PCL block, and therefore the CMC of

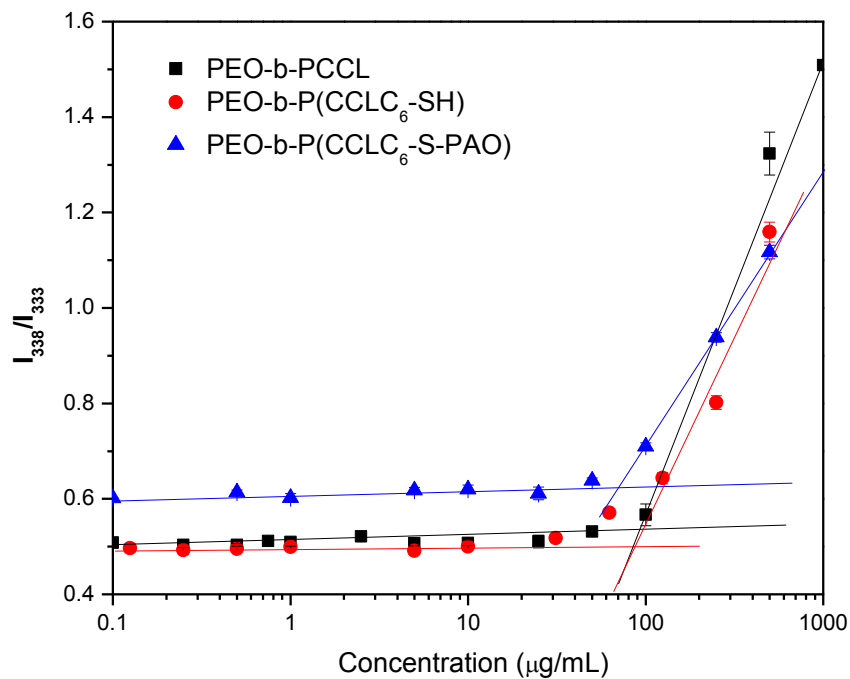
PEO-*b*-PCCL was much higher than PEO-*b*-PCL. (Mahmud et al. 2006) Mercaptohexylamino modification did not change polymer CMC value significantly ( $P=0.606$ ), which is likely due to the partial chopping off of PCCL units. However, the loading of PAO decreased the CMC value compared to PEO-*b*-PCCL ( $P=0.006$ ) and PEO-*b*-P(CCLC<sub>6</sub>-SH) ( $P=0.011$ ) with statistical significance.

The particle sizes of PEO-*b*-P(CCLC<sub>6</sub>-SH) and PEO-*b*-P(CCLC<sub>6</sub>-S-PAO) in different solvents were traced during purification. Typical size distribution profiles by DLS analysis are shown in **Figure 2.5**. The zeta-average diameter of PEO-*b*-P(CCLC<sub>6</sub>-SH) in toluene, DMAc, and water was  $35.5\pm 0.3$ ,  $54\pm 2$ , and  $136\pm 1$  nm, respectively. As for PEO-*b*-P(CCLC<sub>6</sub>-S-PAO), the diameter was  $44.27\pm 0.03$  nm in toluene,  $21.81\pm 0.03$  nm in DMAc, and  $151\pm 1$  nm in water. The micelle formation of polymers in toluene and DMAc is due to the high concentration of polymer (10 mg/mL). PEO-*b*-P(CCLC<sub>6</sub>-SH) formed two populations of assembly in both DMAc and water. The peak diameter for the smaller assembly in water was roughly 20 nm, and for the larger one  $195\pm 4$  nm. However, PEO-*b*-P(CCLC<sub>6</sub>-S-PAO) formed only one population of micelles in DMAc and water. The polydispersity index (PDI) of the size distribution estimated by DLS of PEO-*b*-P(CCLC<sub>6</sub>-SH) in water was  $0.276\pm 0.004$ , while the PDI of PEO-*b*-P(CCLC<sub>6</sub>-S-PAO) micelles in water was  $0.13\pm 0.02$ .

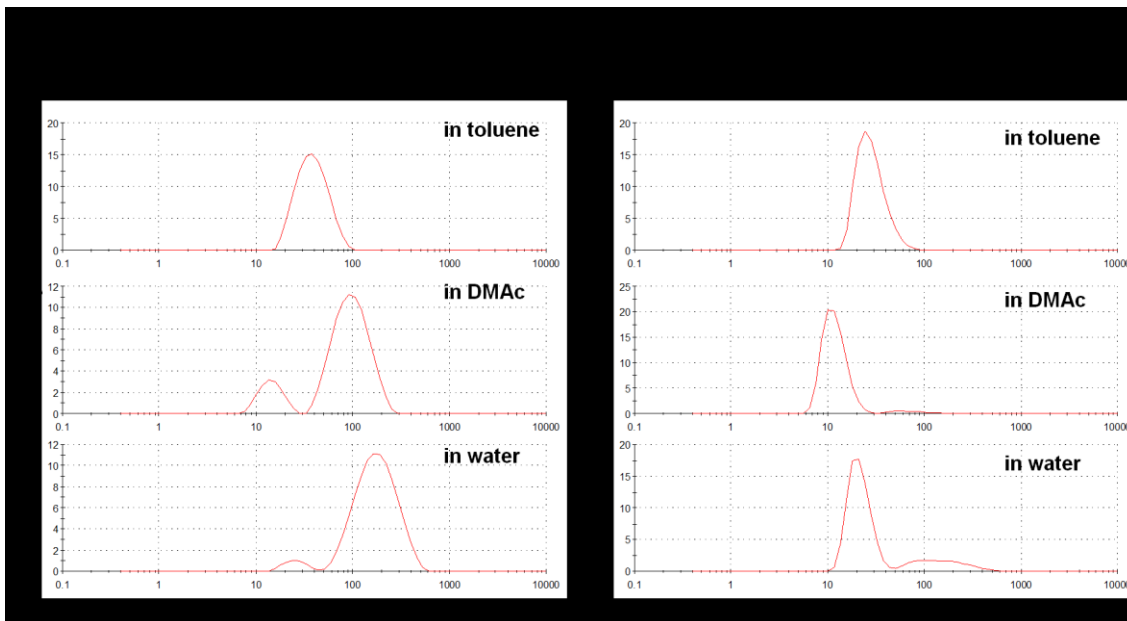
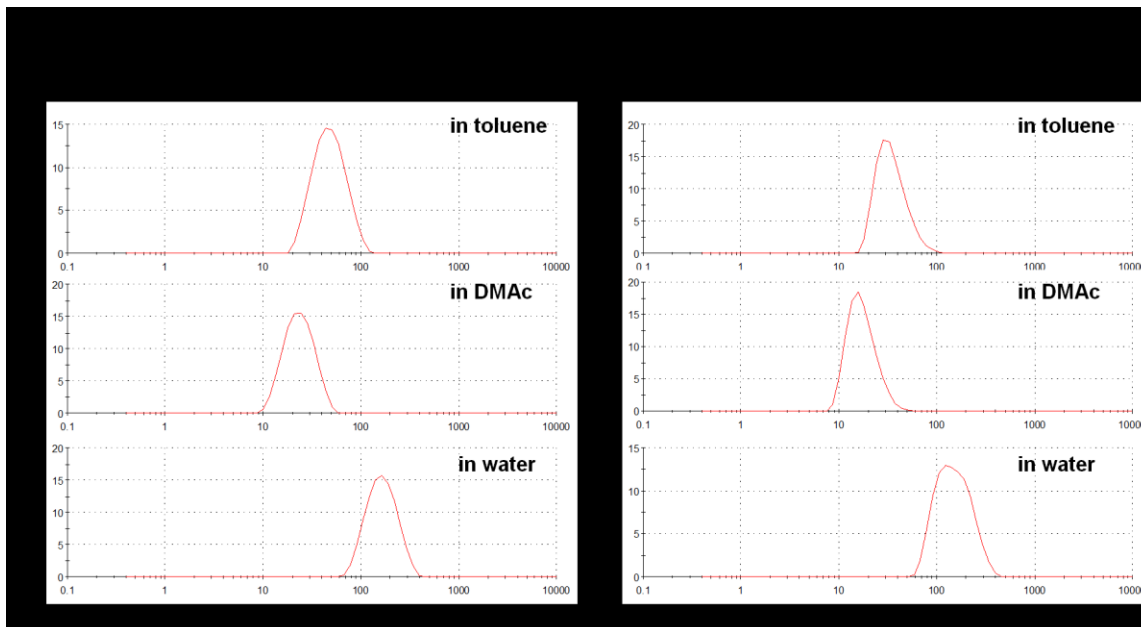
Since the intensity of scattered light is very sensitive to particle size, the same number of large micelles will show much stronger intensity than the small ones. After converting the size distribution by intensity to size distribution by volume, we found that PEO-*b*-P(CCLC<sub>6</sub>-SH) small-size micelles were the dominant population in DMAc (**Figure 2.5-A**, right panel). After dialysis against water, the percentage of PEO-*b*-P(CCLC<sub>6</sub>-SH) large-size micelles increased slightly. However, since only one size population of PEO-*b*-P(CCLC<sub>6</sub>-S-PAO) micelles existed in DMAc

and water, nothing but a slight size shift was observed after the intensity/volume conversion (**Figure 2.5-B**).

The TEM of PEO-*b*-PCCL, PEO-*b*-P(CCLC<sub>6</sub>-SH), and PEO-*b*-P(CCLC<sub>6</sub>-S-PAO) micelles were obtained (**Figure 2.6**) to visualize the size and shape of micelles in dry state. The average size of PEO-*b*-PCCL was 25±6 nm. Two populations of different size were observed in PEO-*b*-P(CCLC<sub>6</sub>-SH) micelles, which was consistent with the DLS results. The small size population had an average size of 16±3 nm, and the larger one had an average of 63±14 nm. Both PEO-*b*-PCCL and PEO-*b*-P(CCLC<sub>6</sub>-SH) were spherical. Interestingly, PEO-*b*-P(CCLC<sub>6</sub>-S-PAO) micelles showed two types of morphology, spherical (**Figure 2.6-C**) and spindle (**Figure 2.6-D**). The spherical PEO-*b*-P(CCLC<sub>6</sub>-S-PAO) micelles had an average size of 22±7 nm, which was similar to the PEO-*b*-PCCL particles or a bit larger than the small population observed for PEO-*b*-P(CCLC<sub>6</sub>-SH) micelles. Unlike the defined border of PEO-*b*-PCCL micelles, the margin of PEO-*b*-P(CCLC<sub>6</sub>-S-PAO) particles was very ambiguous. We observed branch-like antennae at the edge of some particles (**Figure 2.6-C**, red circle) and alignment of a few tiny particles (**Figure 2.6-C**, red rectangle). The spindles had an average length of 70±19 nm and width of 10±2 nm. TEM pictures of PAO (**Figure 2.7**) indicated that these spindle morphologies were related to free PAO, which was probably released during sample preparation.



**Figure 2.4. CMC determination of PEO-*b*-PCCL, PEO-*b*-P(CCLC<sub>6</sub>-SH), and PEO-*b*-P(CCLC<sub>6</sub>-S-PAO).** By fitting  $I_{338}/I_{333}$  to  $\log[\text{concentration } (\mu\text{g/mL})]$  in two concentration range, i.e., 0.1–10  $\mu\text{g/mL}$  and 100–1000  $\mu\text{g/mL}$ , two linear regression lines were drawn. The crossover point was indicated as CMC.

**A****B**

**Figure 2.5.** Size distribution of (A) PEO-*b*-P(CCLC<sub>6</sub>SH) and (B) PEO-*b*-P(CCLC<sub>6</sub>-S-PAO) (10 mg/mL) in toluene, DMAc, and water. A representative scan profile is presented here. Each sample was scanned three times. Similar results were obtained in two additional experiments.

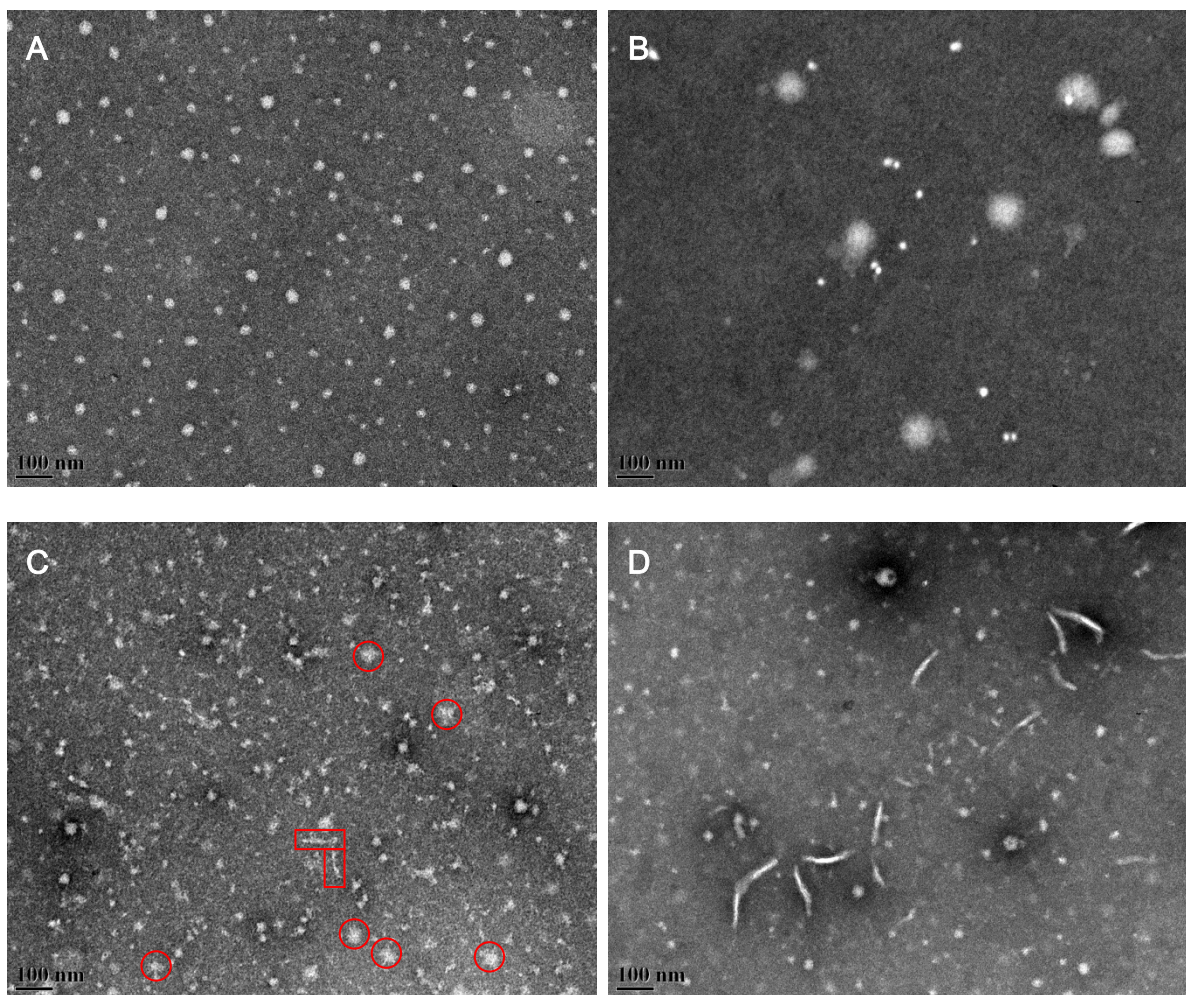


**Figure 2.6.** TEM pictures of micelles prepared from PEO-*b*-PCCL (A), PEO-*b*-P(CCLC<sub>6</sub>-SH) (B), and PEO-*b*-P(CCLC<sub>6</sub>-S-PAO) (C and D). C and D are different views of PEO-*b*-P(CCLC<sub>6</sub>-S-PAO) micelles on the same grid. Red circle: particles with branch-like antennae. Red rectangle: alignments of a few tiny particles.

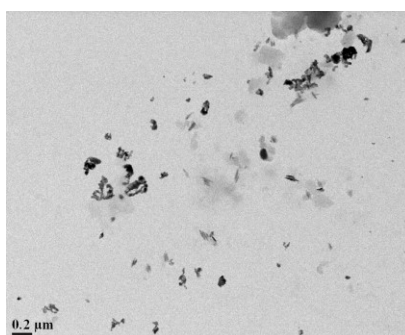


**Figure 2.7.** TEM picture of PAO. The picture was taken at 80 kV with magnification of 28000. The PAO particles with spindle shape had an average length of  $90 \pm 21$  nm, and an average width of  $17 \pm 5$  nm.

### 2.3.4 Stability study

To evaluate the stability of polymeric micelles *in vitro*, SDS was added to the micelle solution to introduce environmental perturbation. Sizes of PEO-*b*-P(CCLC<sub>6</sub>-SH) and PEO-*b*-P(CCLC<sub>6</sub>-S-PAO) solutions (1 mg/mL) in water and SDS solution (2 mg/mL) were monitored over time (**Figure 2.8**). Both solutions were incubated in a 37 °C water bath for 15 days.

The size distribution by intensity weight showed that both PEO-*b*-P(CCLC<sub>6</sub>-SH) and PEO-*b*-P(CCLC<sub>6</sub>-S-PAO) were stable in distilled water within the 19 h incubation period. No dissociation or severe aggregation was observed. However, the zeta-average diameter of PEO-*b*-P(CCLC<sub>6</sub>-SH) micelles increased gradually from 79±2 nm to 154±3 nm over 15 days of incubation. The trend of size increase was more obvious when the intensity-weighted distribution was converted to the volume-weighted distribution. The peak of PEO-*b*-P(CCLC<sub>6</sub>-SH) micelle size shifted from 27±9 nm to 174±11 nm. Nevertheless, PEO-*b*-P(CCLC<sub>6</sub>-S-PAO) micelles remained as one population with a similar size distribution profile up to 15 days of incubation.

Perturbation induced by SDS was observed in both PEO-*b*-P(CCLC<sub>6</sub>-SH) and PEO-*b*-P(CCLC<sub>6</sub>-S-PAO) solution. Although SDS is an anionic surfactant, it has high affinity for the non-ionic PEO according to early work on polymer/surfactant interaction. (Goddard 1986) The association between PEO and SDS triggers the extension of the hydrophilic PEO corona and allows the hydrophobic chains to become more exposed to water, hence turning the micelles less stable. The zeta-average diameter of PEO-*b*-P(CCLC<sub>6</sub>-SH) micelles in SDS solution was larger and the size distribution was less uniform than those of the micelles in water. Despite the zeta-average diameter of PEO-*b*-P(CCLC<sub>6</sub>-SH) micelles remaining the same statistically, the size distribution by volume (**Figure 2.8-A**, right panel) showed that the majority of PEO-*b*-P(CCLC<sub>6</sub>-SH) micelles dissociated in SDS solution after 36 h incubation. The peak of PEO-*b*-P(CCLC<sub>6</sub>-SH)

micelle size shifted from  $20\pm 6$  nm to  $3.8\pm 0.1$  nm. In contrast to what was observed in water, reassembly and aggregation of PEO-*b*-P(CCLC<sub>6</sub>-SH) micelles were not observed within 15 days of incubation in SDS solution.

PEO-*b*-P(CCLC<sub>6</sub>-S-PAO) micelles showed different behavior than PEO-*b*-P(CCLC<sub>6</sub>-SH) in SDS solution. In the presence of SDS, the size of PEO-*b*-P(CCLC<sub>6</sub>-S-PAO) micelles decreased to  $53\pm 2$  nm, which was much smaller than the size of PEO-*b*-P(CCLC<sub>6</sub>-S-PAO) in water. The peak of PEO-*b*-P(CCLC<sub>6</sub>-S-PAO) micelle size decreased from  $160\pm 9$  nm down to the PEO-*b*-P(CCLC<sub>6</sub>-SH) size peak level,  $27\pm 2$  nm according to the volume-weighted size distribution. Unlike the dissociation of PEO-*b*-P(CCLC<sub>6</sub>-SH) micelles, this PEO-*b*-P(CCLC<sub>6</sub>-S-PAO) micelle/unimer mixture slowly re-assembled during the following incubation periods. The zeta-average sizes shifted from  $53\pm 2$  nm to  $126\pm 1$  nm. Severe aggregation was observed after 15 days.

### 2.3.5 *In vitro* release study

The evaluation of PAO release from PEO-*b*-P(CCLC<sub>6</sub>-SH) was carried out in CH<sub>3</sub>COONH<sub>4</sub> buffer (1.45 M, pH 7.4) with different GSH concentrations at 37 °C. The commonly used PBS buffer was replaced with CH<sub>3</sub>COONH<sub>4</sub> buffer to avoid ion suppression in ICP-MS analysis. The As-S bond formation between PAO and thiol-ended polymer side chains is reversible. Water can slowly cleave PAO from polymer chains (**Scheme 2.3-A**). Thiol-containing compounds such as GSH can compete with the mercaptohexylamino group by forming more stable As-S bonds (**Scheme 2.3-B**), which enhances PAO cleavage from the polymer chains. We hypothesized that GSH could enhance PAO release from PEO-*b*-P(CCLC<sub>6</sub>-SH) micelles.

**Figure 2.9** describes the accumulative release of PAO from PEO-*b*-P(CCLC<sub>6</sub>-S-PAO) solutions (1 mg/mL) with different GSH concentrations in two days. The release patterns were similar when there was no GSH present or when GSH concentration was low, e.g., 1 mM. In both

situations, after a burst release within 3 h, the release turned to prolonged release. The presence of GSH increased PAO release during the burst release stage; however, it did not affect the PAO release speed or release amount during the slow release stage.

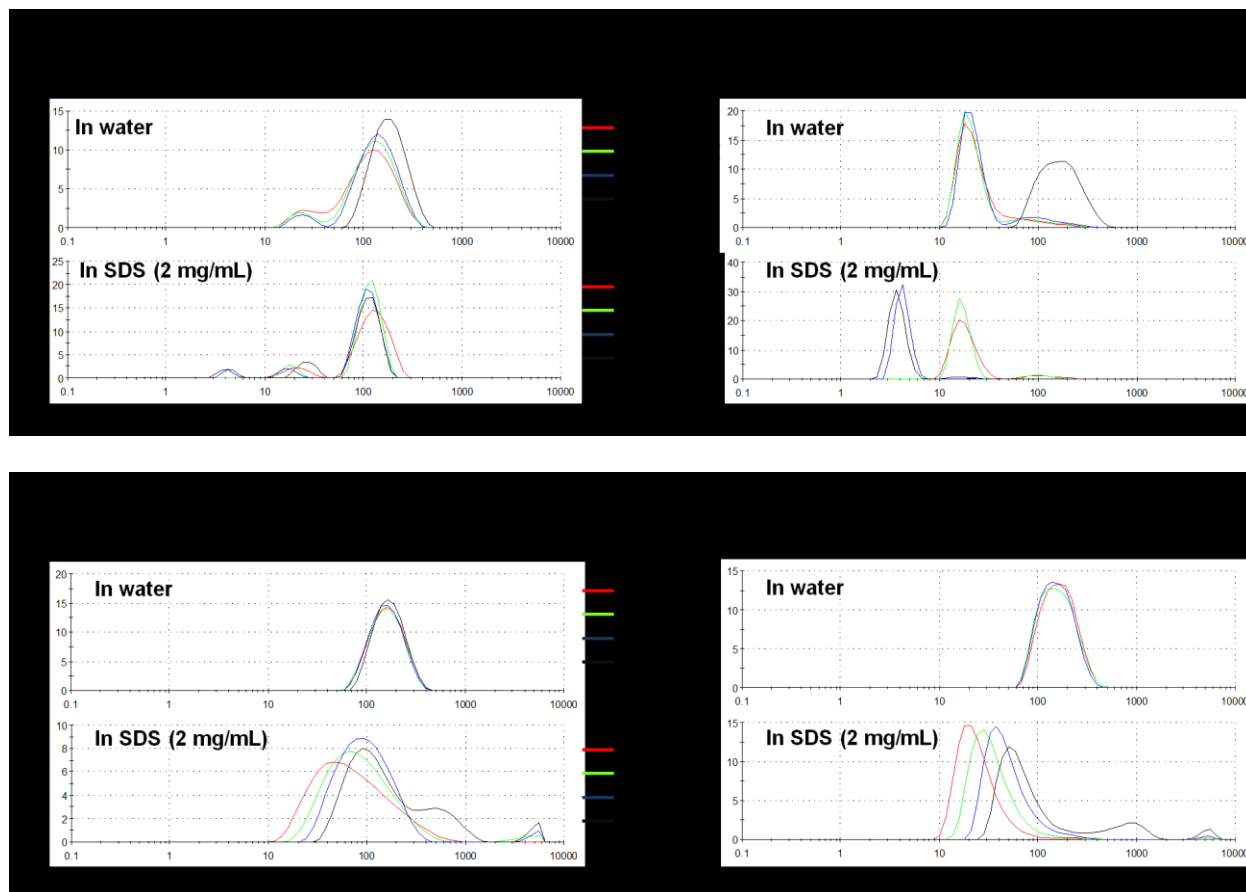
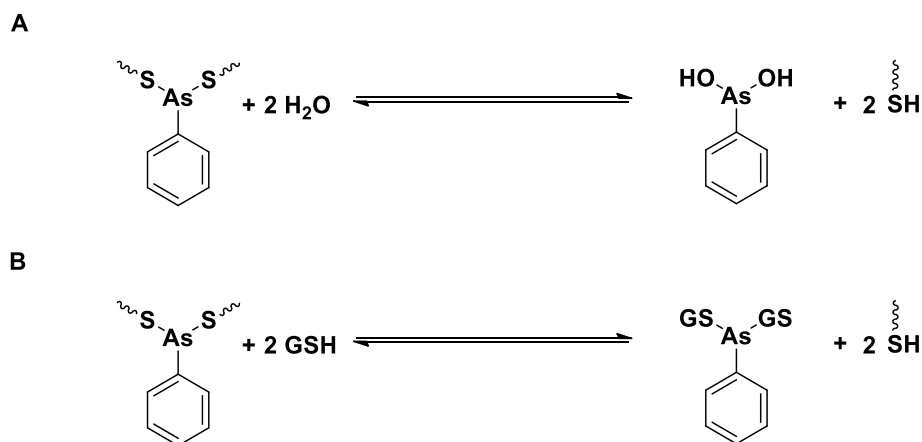


**Figure 2.8.** Size distribution of (A) PEO-*b*-P(CCLC<sub>6</sub>-SH) and (B) PEO-*b*-P(CCLC<sub>6</sub>-S-PAO) micelles (1 mg/mL) in water and SDS solution after incubation in a 37 °C water bath over time. A representative scan profile is presented here. Each sample was scanned three times.

To verify the role of GSH in enhancing PAO release, 1 mg/mL PEO-*b*-P(CCLC<sub>6</sub>-S-PAO) was first incubated without GSH for 12 h until the slow release stage was reached. GSH stock solution (100 mM) was added to the micelle solution to make the final GSH concentration 1 mM. The PAO release was measured at 1, 3, 12, 24, and 36 h post GSH addition (**Figure 2.9**, 12h-1 mM GSH). The PAO release was substantially increased within 1 h after GSH addition; then the release slowed down. The interaction between GSH and PAO was very fast. The formation of GS-PAO

complex quickly reached equilibrium. Soon after GSH formed a complex with PAO, PAO was released to the buffer from the micelles. When GSH concentration was high, e.g., 5 mM and 10 mM, ~ 85% of total encapsulated PAO was released within 1 h.



**Scheme 2.3.** The dissociation of PAO from PEO-*b*-P(CCLC<sub>6</sub>-S-PAO) (A) in buffer without GSH, and (B) the competition reaction between GSH and PEO-*b*-P(CCLC<sub>6</sub>-S-PAO).

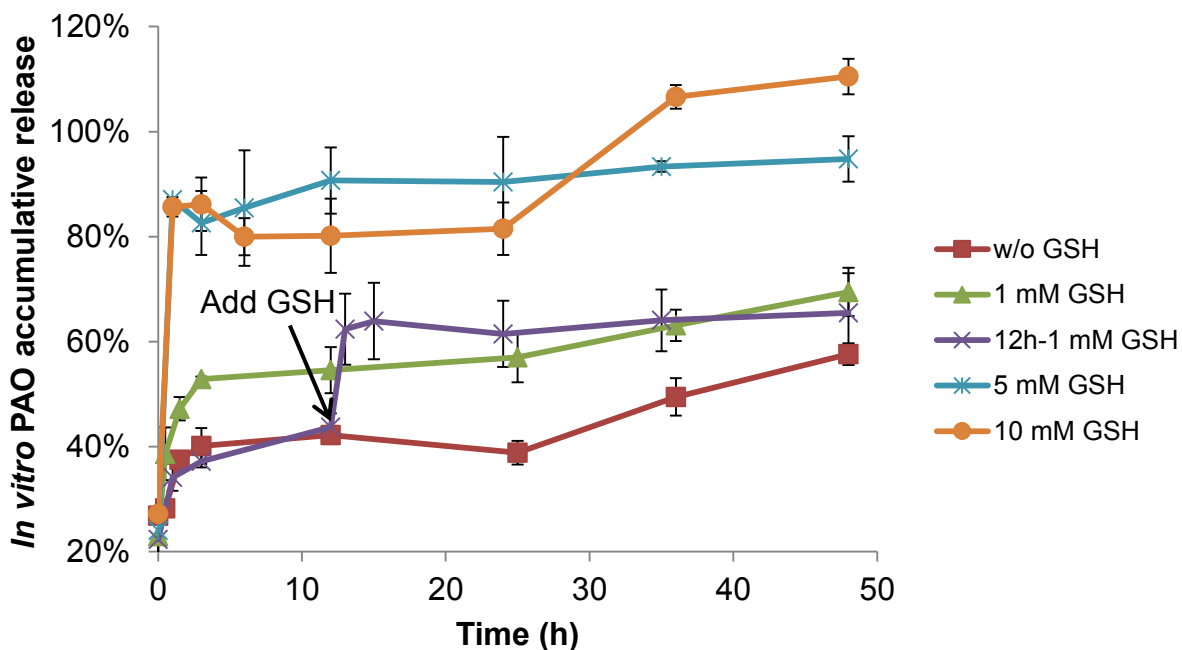


**Figure 2.9.** *In vitro* release profile of PEO-*b*-P(CCLC<sub>6</sub>-S-PAO) in CH<sub>3</sub>COONH<sub>4</sub> buffer (pH 7.4) with different GSH concentrations at 37 °C. For 12 h–1 mM GSH plot, GSH was added to PEO-*b*-P(CCLC<sub>6</sub>-S-PAO) solution after 12 h of release. Data are presented as mean ± SD (n = 3).

### 2.3.6 *In vitro* cytotoxicity study of block polymers

To evaluate the cytotoxicity of PEO-*b*-P(CCLC<sub>6</sub>-SH), the MDA-MB-435 cell line was treated with different concentrations of micelle solutions for 24 and 48 h (**Figure 2.10-A**). Cells treated with complete cell culture medium served as the negative control. The neutral red assay was used in the cytotoxicity evaluation. According to the dose–survival profile, PEO-*b*-P(CCLC<sub>6</sub>-SH) was toxic against cancer cells when its concentration was larger than 0.1 mg/mL. The toxicity of PEO-*b*-P(CCLC<sub>6</sub>-SH) for both 24 and 48 h treatment was greatly decreased when the polymer concentration was reduced to 0.02 mg/mL. The toxicity of PEO-*b*-P(CCLC<sub>6</sub>-SH) is associated with mercaptohexylamine conjugation. We conducted the cytotoxicity evaluation of mercaptohexylamine against MDA-MB-435 cells (**Figure 2.11**). The IC<sub>50</sub> of mercaptohexylamine (24 h treatment) was 272 (237–313) μM, which had the same magnitude of the equivalent mercaptohexylamine concentration in PEO-*b*-P(CCLC<sub>6</sub>-SH) solution at corresponding IC<sub>50</sub> polymer concentration.

The cytotoxicity of PEO-*b*-P(CCLC<sub>6</sub>-S-PAO) was tested with the same method. To prepare equivalent PAO concentrations of 0.01 to 10 μM, PEO-*b*-P(CCLC<sub>6</sub>-S-PAO) stock solution (0.8 mg/mL) was diluted to 0.00004–0.04 mg/mL. At this concentration range, PEO-*b*-P(CCLC<sub>6</sub>-SH) showed negligible cytotoxicity towards cells. The cytotoxicity of PEO-*b*-P(CCLC<sub>6</sub>-S-PAO) measured were mainly caused by the loaded PAO. The results are summarized in **Figure 2.10-B** and **Figure 2.10-C**. IC<sub>50</sub> values expressed as the equivalent PAO concentration of PEO-*b*-P(CCLC<sub>6</sub>-S-PAO) of 24 h and 48 h treatment were 0.149 (0.122–0.181) μM, and 0.117 (0.101–0.136) μM, respectively. IC<sub>50</sub> values of free PAO of 24 h and 48 h treatment were 0.163 (0.115–0.231) μM, and 0.103 (0.090–0.120) μM, respectively. IC<sub>50</sub> values of PEO-*b*-P(CCLC<sub>6</sub>-S-PAO) were not significantly different than those of free PAO with the same treatment time ( $P > 0.05$ ),

which indicated similar cytotoxicity of free PAO and PEO-*b*-P(CCLC<sub>6</sub>-S-PAO). The similar IC<sub>50</sub> values were attributed to the low concentration of PEO-*b*-P(CCLC<sub>6</sub>-S-PAO) micelles used in the cytotoxicity study. The concentrations of PEO-*b*-P(CCLC<sub>6</sub>-S-PAO) micelles were lower than its CMC in water. Under these conditions, the micelles may have been dissociated and most PAO may have been released from the micelles.

## 2.4 Discussion

Broadening the application of arsenic for solid tumor treatment and enhancing its therapeutic efficacy is of increasing interest. We aim to achieve this goal by applying polymeric micelles for arsenic encapsulation and delivery. Polymeric micelle encapsulated arsenic compounds are expected to have enhanced accumulation and retention in target tumor areas with less toxicity to normal organs in comparison to free arsenic. Arsenic encapsulation in PEO-PLGA polymeric micelles has been reported before. We improved the arsenic loading capacity and achieved GSH triggered arsenic release by functionalizing PEO-PCL micellar cores with pendent thiol groups which can bind arsenic. With this strategy, the arsenic element content reached  $2.4 \pm 0.2$  wt% of the total polymer. At its maximum loading, PAO occupied  $\sim 65\%$  of total sulfur in PEO-*b*-P(CCLC<sub>6</sub>-S-PAO). The arsenic loading capacity was increased 15 times.

Trivalent arsenic species have a relatively good affinity for sulfur. The binding constant between arsenic and sulfur varies from  $10^4$  to  $10^9$  M<sup>-1</sup>. The magnitude of this binding constant is influenced by the arsenic species and the property of thiol-containing compounds. (Shen et al. 2013) PAO is a very toxic organic arsenical. Phenylarsine dichloride, the PAO precursor, was used in chemical warfare during World War I and II due to its high lethality. (Haas and Krippendorf 1997; Kroening et al. 2009) Research has shown that PAO has much higher affinity for sulfur than

inorganic arsenic trioxide.(Shen et al. 2013) Hence, PAO was used as an arsenic model molecule in this micelle development study.

We synthesized the novel thiol substituted PEO-PCL block copolymer, PEO-*b*-P(CCLC<sub>6</sub>-SH), to encapsulate PAO. According to element analysis data, the weight percent of sulfur in the PEO-*b*-P(CCLC<sub>6</sub>-SH) was 1.6±0.4%, accounting for 3.8 thiol-ended PCCL among 12.8 total PCCL units per polymer chain, and the calculated CCLC<sub>6</sub>-SH unit number was comparable to the number calculated from the <sup>1</sup>H-NMR peak integral (**Table 2.1**). However, oxidation of thiol groups to disulfide bonds, sulfinic groups, and sulfuric groups before conjugation with PAO may limit the availability of free thiols for interaction with PAO. To reduce the effect of thiol oxidization on PAO loading, freshly synthesized PEO-*b*-P(CCLC<sub>6</sub>-SH) was mixed with PAO in toluene before any further purification. After incubation for 6 h, the mixture was dialyzed against DMAc and water sequentially. We purified PEO-*b*-P(CCLC<sub>6</sub>-SH) using the same procedures as for PEO-*b*-P(CCLC<sub>6</sub>-S-PAO) to make it a good reference for comparison in size distribution analysis and stability evaluation. Polymers were expected to be random chains or unimers in organic solvents such as toluene and DMAc. However, DLS results revealed that the polymers under study assembled even in organic solvents when their concentration was as high as 10 mg/mL (**Figure 2.5**). Considering the non-polarity of toluene, PEO-*b*-P(CCLC<sub>6</sub>-SH) micelles in toluene may have the structure of inverse micelles with the hydrophobic P(CCLC<sub>6</sub>-SH) blocks in the corona and the hydrophilic PEO blocks in the core. After dialysis against DMAc, a polar solvent, the polymer chains may flip over and have the hydrophobic P(CCLC<sub>6</sub>-SH) block in the core. During this process, some aggregation was noticed in PEO-*b*-P(CCLC<sub>6</sub>-SH) in DMAc. Few disulfide bonds between polymer chains may have been formed at this stage. After dialysis against water, the aggregation of PEO-*b*-P(CCLC<sub>6</sub>-SH) micelles was enhanced.

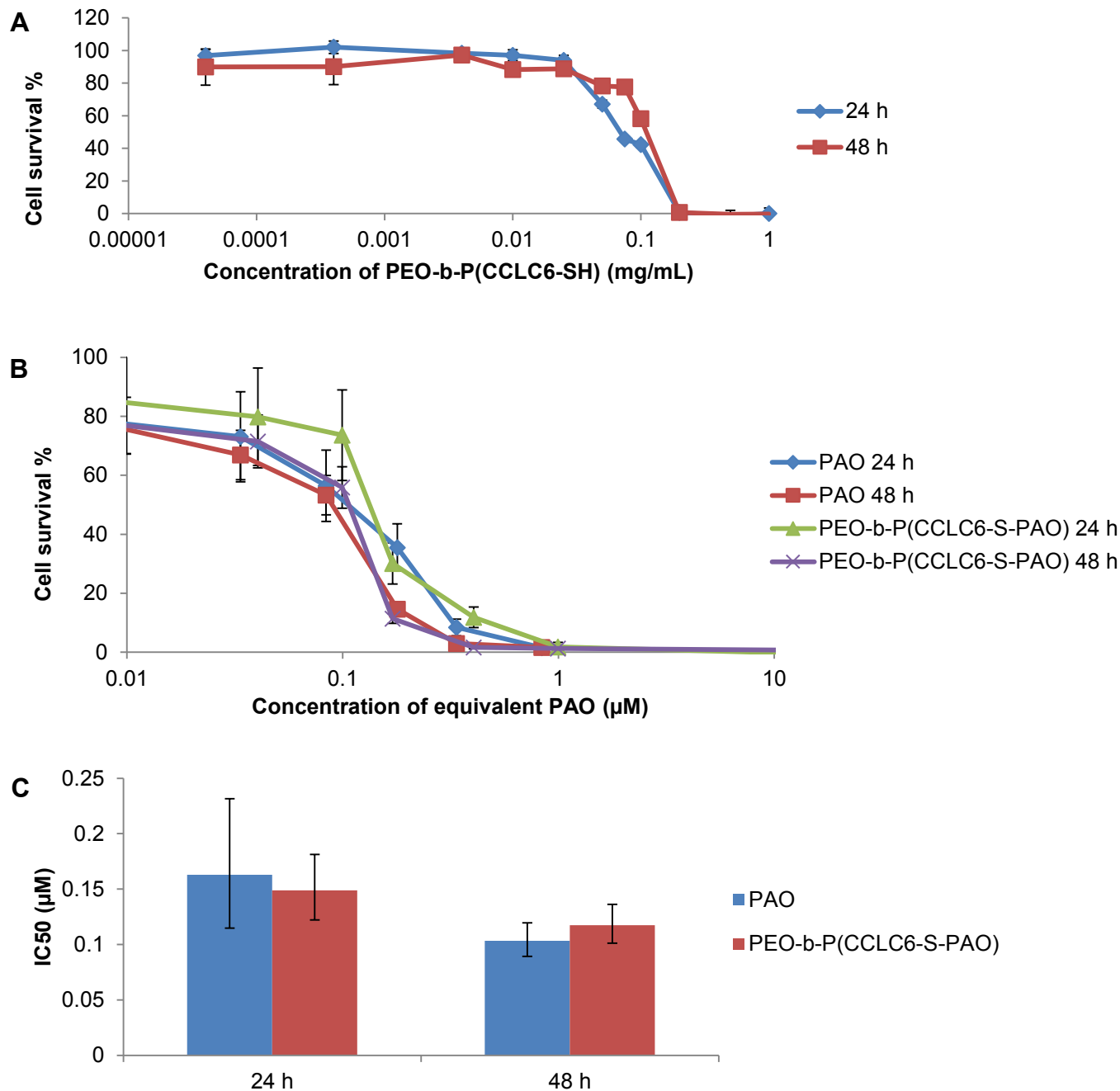
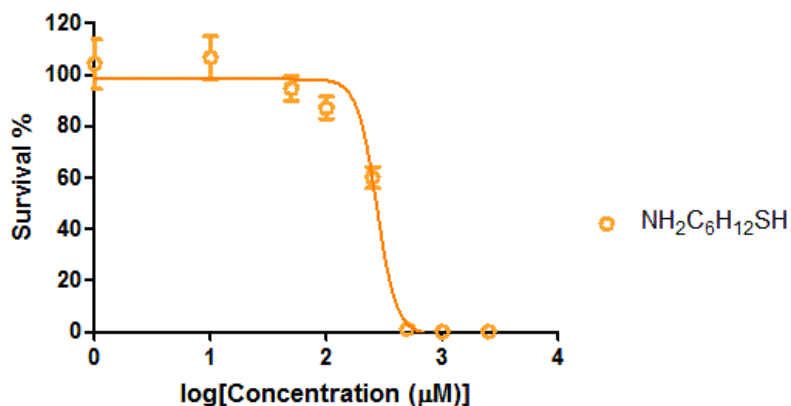


**Figure 2.10. Cytotoxicity of (A) PEO-*b*-P(CCLC<sub>6</sub>-SH) and (B) free PAO and PEO-*b*-P(CCLC<sub>6</sub>-S-PAO) to MDA-MB-435 cell line using neutral red assay. IC<sub>50</sub> values expressed as equivalent PAO concentration of free and encapsulated PAO are summarized in the chart (C). The data presented in (A) and (B) are as mean  $\pm$  SD (n = 3), and the data in (C) are mean with 95% confidence interval (n = 3). The data of a single experiment are presented here. Similar results were obtained in at least one additional experiment.**

### Cytotoxicity of mercaptohexylamine against MDA-MB-435 cell line (24 h)



	IC <sub>50</sub> (μM)	95% Confidence Interval
NH <sub>2</sub> C <sub>6</sub> H <sub>12</sub> SH	272	237–313

**Figure 2.11.** Cytotoxicity of mercaptohexylamine against MDA-MB-435 cells.

The PAO loading changed the micelle size distribution. The size of the PEO-*b*-P(CCLC<sub>6</sub>-S-PAO) micelle was substantially increased after dialysis against water and only one size population was observed. The increased hydrodynamic diameter of the PEO-*b*-P(CCLC<sub>6</sub>-S-PAO) micelle in water is likely due to As–S interaction as suggested in **Scheme 2.2**. The weak interaction between arsenic and thiol groups might exist in organic solvents when the structure of PAO remains as C<sub>6</sub>H<sub>5</sub>–As=O. But after dialysis against water, PAO was hydrolyzed and As–S interaction was favored in water. However, the exact nature of PAO interaction with polymer chains in PEO-*b*-P(CCLC<sub>6</sub>SH) micelles is not clear (**Scheme 2.2**). The interaction between thiol group and PAO can be covalent, weak ionic interaction, or a mixture of both. One PAO molecule can interact with one thiol group, or two thiol groups simultaneously. The two thiol groups can be on the same polymer chain or on two different ones. Since one PAO molecule can interact with two thiol groups on different polymer chains, PAO can act as a “cross-linking” agent in PEO-*b*-P(CCLC<sub>6</sub>-S-PAO)

micelles. The ~ 25% of total encapsulated PAO release from PEO-*b*-P(CCLC<sub>6</sub>-S-PAO) at zero time point (**Figure 2.9**) indicates the presence of PAO as free molecules between micelles or adsorbed ones on the micelle surface. The particle alignment and antenna on the particles observed in TEM pictures (**Figure 2.6-C**) may result from the enhanced association between micelles due to these free and adsorbed PAO, to which the increased hydrodynamic size of PEO-*b*-P(CCLC<sub>6</sub>-S-PAO) micelles in water can be attributed.

The loading of PAO increased the hydrophobicity of the micelle core and enhanced the interaction between polymer chains via As-S interaction. Hence, PAO encapsulation increased micelle stability. With PAO loading, the CMC of PEO-*b*-P(CCLC<sub>6</sub>-SH) decreased from 92±7 µg/mL to 70±5 µg/mL. In addition, PAO prevented micelles from undergoing dissociation in water or in the presence of SDS (**Figure 2.8**). SDS was reported to interrupt the hydrophobic interaction between block polymers and form aggregation of SDS/polymer. (Hsu et al. 2006; Kondo et al. 2007) In our study, the inducing effect of SDS on micelle dissociation was observed in the case of PEO-*b*-P(CCLC<sub>6</sub>-SH) micelles. After 36 h of incubation, most of the PEO-*b*-P(CCLC<sub>6</sub>-SH) micelles with initial diameter of 20 nm dissociated to small assemblies of 4 nm of the diameter. Since the concentration of SDS (2 mg/mL, 7 mM) was below its CMC (8.2 mM), the small assemblies are more likely free copolymer chains aggregated with SDS molecules. (Vangeyte et al. 2004) In contrast, PEO-*b*-P(CCLC<sub>6</sub>-S-PAO) micelles re-aggregated during incubation in SDS solution rather than dissociating. The PEO-*b*-P(CCLC<sub>6</sub>-S-PAO) micelle size was lower than the PEO-*b*-P(CCLC<sub>6</sub>-SH) levels when the polymer was dissolved in SDS solution. How SDS led to the re-aggregation of PEO-*b*-P(CCLC<sub>6</sub>-S-PAO) micelles rather than their dissociation is not clear.

We then conducted *in vitro* release studies on PEO-*b*-P(CCLC<sub>6</sub>-S-PAO) at concentrations above its CMC level. Dissociation of PAO from the polymer backbone was found to be the rate-

limiting step in the release of PAO from the developed nano-carrier. In the  $\text{CH}_3\text{COONH}_4$  buffer, a burst PAO release within 3 h was followed by a steady PAO release. Under these conditions, only 60% of loaded PAO was released from the carrier within 48 h. Water can slowly but steadily compete with thiol groups of  $\text{P}(\text{CCLC}_6\text{-SH})$  to chop off PAO from the polymer backbone. GSH has a higher binding affinity for PAO than  $\text{P}(\text{CCLC}_6\text{-SH})$  and  $\text{H}_2\text{O}$  (**Figure 2.9**). After GSH addition, the resulting GS-PAO complex was quickly diffused out from the micelles. The amount of PAO triggered release was dependent on GSH concentration. With 1 mM GSH, an additional 15–20% of total arsenic was released; when GSH was increased to 5 mM, PAO release was ~ 85% of total arsenic within 1 h. GSH is a well-known ubiquitous antioxidant in cells with concentration ranging from 0.5 mM to 10 mM. (Wu et al. 2004) The concentration of GSH in plasma is relatively low, typically 5–50  $\mu\text{M}$  (Griffith 1999) and a maximum of 1 mM (Richie et al. 1996). Hence, triggered release of arsenic from developed polymeric micellar formulation in cells is expected due to the increased concentration of GSH.

$\text{PEO-}b\text{-PCCL}$  was shown to have low cytotoxicity. (Shahin and Lavasanifar 2010) However, with thiol-ended pendant group conjugation,  $\text{PEO-}b\text{-P}(\text{CCLC}_6\text{-SH})$  has a relatively low  $\text{IC}_{50}$  value (0.07–0.11 mg/mL). The cytotoxicity of  $\text{PEO-}b\text{-P}(\text{CCLC}_6\text{-SH})$  is associated with mercaptohexylamine conjugation (**Figure 2.11**). No toxicity study of mercaptohexylamine has been previously reported; whereas cysteamine can induce cell death by generating  $\text{H}_2\text{O}_2$ . (Jeitner and Lawrence 2001) Considering the similar structures of mercaptohexylamine and cysteamine, these two compounds may share similar toxic effects. In the study evaluating the cytotoxicity of  $\text{PEO-}b\text{-P}(\text{CCLC}_6\text{-S-PAO})$  against MDA-MB-435 cells, the polymer concentration was below 0.04 mg/mL, so the cytotoxicity induced by  $\text{PEO-}b\text{-P}(\text{CCLC}_6\text{-SH})$  polymer was not expected to interfere with the cytotoxicity induced by PAO. However, the polymer concentration during this

study (0.00004–0.04 mg/mL) was much lower than the CMC of PEO-*b*-P(CCLC<sub>6</sub>-S-PAO) (0.07 mg/mL) and the micelles dissociated under these conditions. Furthermore, thiol-containing proteins and amino acids in cell culture medium (10% FBS in RPMI 1640 medium) can also trigger the PAO release. Therefore, PAO may be present in its free form, which resulted in similar IC<sub>50</sub> values of free PAO and PEO-*b*-P(CCLC<sub>6</sub>-S-PAO).

## 2.5 Conclusion

A thiol containing pendant group, mercaptohexylamine, was successfully conjugated to the PEO-*b*-PCCL backbone and formed PEO-*b*-P(CCLC<sub>6</sub>-SH) which was then associated to polymeric micelles. The thiol group played a crucial role in enhanced arsenic encapsulation in polymeric micelles. With As–S interaction, the arsenic encapsulation capacity of polymer was increased ~15 fold. The loading of arsenic provided additional advantages to the polymer micelle system as the PEO-*b*-P(CCLC<sub>6</sub>-S-PAO) micelles showed narrower micelle size distribution and better stability compared to PEO-*b*-P(CCLC<sub>6</sub>-SH) micelles (that did not contain PAO). The release of arsenic from micelles was triggered by adding thiol-containing competing peptides, such as GSH. Developed PEO-*b*-P(CCLC<sub>6</sub>-S-PAO) showed similar cytotoxicity to that of free PAO against MDA-MB-435 cells, reflecting the release of PAO from the micellar carrier under the study conditions. Strategies such as increasing the length of the hydrophobic block, including more hydrophobic PCL units, and inducing micelle crosslinking by forming stable disulfide bonds can be explored to further increase the stability of these micelles, which is essential for the success of micellar drug targeting *in vivo*. Nevertheless, PEO-*b*-P(CCLC<sub>6</sub>-SH) was proven to be an effective system for arsenic encapsulation. The application of PEO-*b*-P(CCLC<sub>6</sub>-SH) assembly system for encapsulation of other arsenic compounds with medical relevance, such as inorganic arsenic and monomethylarsonous acid (MMA<sup>III</sup>), is also promising.

## 2.6 References

- Armarego WLF. 2009. Purification of laboratory chemicals: Butterworth-Heinemann.
- Charoensuk V, Gati WP, Weinfeld M, Le XC. 2009. Differential cytotoxic effects of arsenic compounds in human acute promyelocytic leukemia cells. *Toxicology and Applied Pharmacology* 239:64-70.
- Chen BB, Liu QQ, Popowich A, Shen SW, Yan XW, Zhang Q, et al. 2015. Therapeutic and analytical applications of arsenic binding to proteins. *Metalomics* 7:39-55.
- Chen H, Ahn R, Van den Bossche J, Thompson DH, O'Halloran TV. 2009a. Folate-mediated intracellular drug delivery increases the anticancer efficacy of nanoparticulate formulation of arsenic trioxide. *Molecular Cancer Therapeutics* 8:1955-1963.
- Chen H, Pazicni S, Krett NL, Ahn RW, Penner-Hahn JE, Rosen ST, et al. 2009b. Coencapsulation of arsenic- and platinum-based drugs for targeted cancer treatment. *Angewandte Chemie-International Edition* 48:9295-9299.
- Chen HM, MacDonald RC, Li SY, Krett NL, Rosen ST, O'Halloran TV. 2006. Lipid encapsulation of arsenic trioxide attenuates cytotoxicity and allows for controlled anticancer drug release. *Journal of the American Chemical Society* 128:13348-13349.
- Goddard ED. 1986. Polymer surfactant interaction .1. Uncharged water-soluble polymers and charged surfactants. *Colloids and Surfaces* 19:255-300.
- Griffith OW. 1999. Biologic and pharmacologic regulation of mammalian glutathione synthesis. *Free Radical Biology and Medicine* 27:922-935.
- Haas R, Krippendorf A. 1997. Determination of chemical warfare agents in soil and material samples - gas chromatographic analysis of phenylarsenic compounds (sternutators) (1st communication). *Environmental Science and Pollution Research* 4:123-124.
- Hsu YH, Chiang WH, Chen MC, Chern CS, Chiu HC. 2006. Effects of sds on the thermo- and ph-sensitive structural changes of the poly(acrylic acid)-based copolymer containing both poly(n-isopropylacrylamide) and monomethoxy poly(ethylene glycol) grafts in water. *Langmuir* 22:6764-6770.

- Jeitner TM, Lawrence DA. 2001. Mechanisms for the cytotoxicity of cysteamine. *Toxicological Sciences* 63:57-64.
- Kallinteri P, Fatouros D, Klepetsanis P, Antimisiaris SG. 2004. Arsenic trioxide liposomes: Encapsulation efficiency and in vitro stability. *Journal of Liposome Research* 14:27-38.
- Kondo S, Mori H, Sasai Y, Kuzuya M. 2007. Conventional synthesis of amphiphilic block copolymer utilized for polymeric micelle by mechanochemical solid-state polymerization. *Chemical & Pharmaceutical Bulletin* 55:389-392.
- Kroening KK, Solivio MJV, Garcia-Lopez M, Puga A, Caruso JA. 2009. Cytotoxicity of arsenic-containing chemical warfare agent degradation products with metallomic approaches for metabolite analysis. *Metallomics* 1:59-66.
- Liu JB, Zeng FQ, Allen C. 2007. In vivo fate of unimers and micelles of a poly(ethylene glycol)-block-poly( $\epsilon$ -caprolactone) copolymer in mice following intravenous administration. *European Journal of Pharmaceutics and Biopharmaceutics* 65:309-319.
- Mahmud A, Xiong XB, Lavasanifar A. 2006. Novel self-associating poly(ethylene oxide)-block-poly( $\epsilon$ -caprolactone) block copolymers with functional side groups on the polyester block for drug delivery. *Macromolecules* 39:9419-9428.
- Ohyashiki T, Mohri T. 1983. Fluorometric analysis of the micelle formation process of surfactants in aqueous-solution .1. Utility of pyrene in determination of the critical micelle concentration. *Chemical & Pharmaceutical Bulletin* 31:1296-1300.
- Richie JP, Skowronski L, Abraham P, Leutzinger Y. 1996. Blood glutathione concentrations in a large-scale human study. *Clinical Chemistry* 42:64-70.
- Shahin M, Lavasanifar A. 2010. Novel self-associating poly(ethylene oxide)-b-poly( $\epsilon$ -caprolactone) based drug conjugates and nano-containers for paclitaxel delivery. *International Journal of Pharmaceutics* 389:213-222.
- Shen S, Li X, Cullen W, Weinfeld M, Le X. 2013. Arsenic binding to proteins. *Chemical Reviews* 113:7769-7792.

- Shin ILG, Kim SY, Lee YM, Cho CS, Sung YK. 1998. Methoxy poly(ethylene glycol) epsilon-caprolactone amphiphilic block copolymeric micelle containing indomethacin. I. Preparation and characterization. *Journal of Controlled Release* 51:1-11.
- Vangeyte P, Leyh B, Auvray L, Grandjean J, Misselyn-Bauduin AM, Jerome R. 2004. Mixed self-assembly of poly(ethylene oxide)-b-poly(epsilon-caprolactone) copolymers and sodium dodecyl sulfate in aqueous solution. *Langmuir* 20:9019-9028.
- Wang ZQ, Liu W, Xu HB, Yang XL. 2007. Preparation and in vitro studies of stealth pegylated plga nanoparticles as carriers for arsenic trioxide. *Chinese Journal of Chemical Engineering* 15:795-801.
- Wilhelm M, Zhao CL, Wang YC, Xu RL, Winnik MA, Mura JL, et al. 1991. Polymer micelle formation .3. Poly(styrene-ethylene oxide) block copolymer micelle formation in water - a fluorescence probe study. *Macromolecules* 24:1033-1040.
- Wu GY, Fang YZ, Yang S, Lupton JR, Turner ND. 2004. Glutathione metabolism and its implications for health. *Journal of Nutrition* 134:489-492.
- Xiong XB, Mahmud A, Uludag H, Lavasanifar A. 2008. Multifunctional polymeric micelles for enhanced intracellular delivery of doxorubicin to metastatic cancer cells. *Pharmaceutical Research* 25:2555-2566.
- Yang ZW, Yang MH, Peng JA. 2008. Evaluation of arsenic trioxide-loaded albumin nanoparticles as carriers: Preparation and antitumor efficacy. *Drug Development and Industrial Pharmacy* 34:834-839.
- Zagana P, Haikou M, Klepetsanis P, Giannopoulou E, Loannou PV, Antimisiaris SG. 2008. In vivo distribution of arsonoliposomes: Effect of vesicle lipid composition. *International Journal of Pharmaceutics* 347:86-92.

## Chapter 3. Mixed micelles for targeted delivery of arsenic compounds

### 3.1 Introduction

The model cell line involved in this project, MDA-MB-435 cell line, overexpresses  $\alpha_v\beta_3$  integrin on the cell membrane and is highly metastatic and invasive (Price and Zhang 1990).  $\alpha_v\beta_3$  integrin is a cell adhesion receptor recognizing mainly extracellular matrix ligands and cell-surface ligands, and plays an important role in promoting the metastatic phenotypes by supporting specific adhesive, invasive, and migratory properties of the tumor cells (Felding-Habermann et al. 2002). The arginine-glycine-aspartic acid (RGD) containing peptide is well known as a recognition motif in a number of ligands for integrins (Duggan and Hutchinson 2000). Studies using RGD peptide decoration for targeted drug delivery to integrin-overexpressing tumor cells have been reported (Liu et al. 2007; Lu et al. 2006).

The aim of this study is to demonstrate that targeted delivery of arsenic trioxide (ATO) to MDA-MB-435 cells can be achieved by decorating the PEO-*b*-PCCL micelle surface with an RGD-containing peptide. To achieve this goal, the PCCL block should be functionalized with mercaptohexylamino groups for efficient arsenic encapsulation as demonstrated in **Chapter 2**, and the distal end of the PEO block should be functionalized with RGD peptide for targeting. PEO with an acetal group on the distal end is commonly used for peptide conjugation (**Figure 3.1**) (Xiong et al. 2008). However, this peptide conjugation method is hardly compatible with acetal-PEO-*b*-P(CCLC<sub>6</sub>-S-As<sup>III</sup>), as the method includes steps at low pH and incubation over time, where the encapsulated arsenic may be released. The peptide-conjugate PEO-*b*-PCCL cannot survive in

the harsh conditions for mercaptohexylamino conjugation, which involves oxalyl chloride activation.

To circumvent the synthesis challenge in functionalization of a same block copolymer with mercaptohexylamino pendant groups on the PCCL block and RGD peptide on the distal end of the PEO block, we simply mixed two diblock copolymers, namely PCCL-*b*-PEO-GRGDS-amide and P(CCLC<sub>6</sub>-SH)-*b*-PEO, to prepare peptide-decorated mixed micelles (PMM) for ATO encapsulation. Arsenic-encapsulated control micelles without peptide decoration include control mixed micelles (CMM) prepared by monomethoxy PEO-*b*-PCCL and PEO-*b*-P(CCLC<sub>6</sub>-SH) and non-mixed micelles PEO-*b*-P(CCLC<sub>6</sub>-SH). In this study, we demonstrated the potential of targeted delivery of arsenic compounds to target tumors cells using affinity ligand decorated mixed micelles.

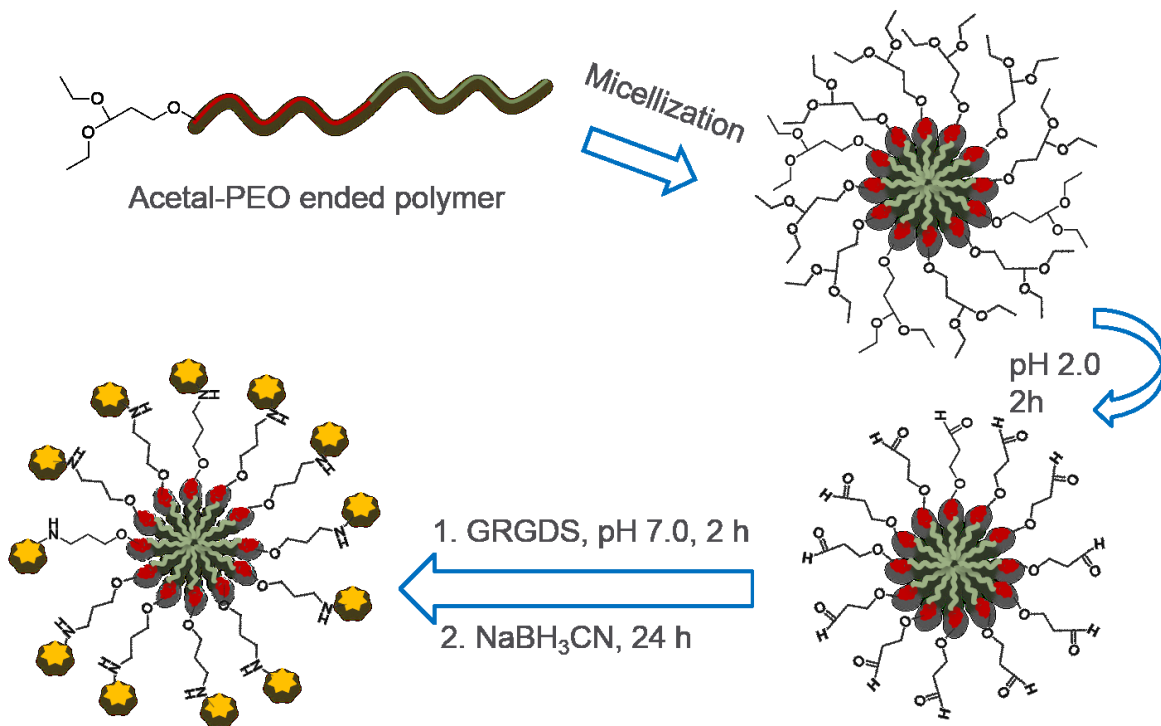


**Figure 3.1. Scheme illustrating peptide conjugation onto the distal end of PEO.** Acetal-PEO-*b*-PCCL first assembles into micelles. The micelle structure can protect the polyester segment from acid-catalyzed degradation. Acetal groups on the micelle surface are then converted into a formyl group at acid pH. The primary amine on the N-terminus of the peptide, glycine in this case, reacts with the formyl group, forming an unstable Schiff base. The Schiff base can be reduced by NaBH<sub>3</sub>CN to form a stable C–N bond.

## **3.2 GRGDS-PEO<sup>6000</sup>-b-PCCL<sub>15</sub>/PEO<sup>5000</sup>-b-PCCL<sub>15</sub> mixed micelle system for arsenic encapsulation**

### **3.2.1 Materials and Methods<sup>2</sup>**

#### **3.2.1.1 Materials and cell information**

All the chemicals and reagents, unless specified, were purchased from Sigma-Aldrich (St. Louis, MO, USA). Mercaptohexylamine hydrochloride was purchased from Annker Organics Co. Ltd. (Wuhan, Hubei, China), and  $\alpha$ -benzyl carboxylate- $\epsilon$ -caprolactone (BCL) from Alberta Research Chemicals Inc. (Edmonton, AB, Canada). GRGDS-amide was purchased from RS Synthesis LLC. (Louisville, KY, USA). GelCode™ blue stain reagent was purchased from Fisher Scientific (Ottawa, ON, Canada). RPMI-1640 cell culture media and penicillin–streptomycin solution were purchased from Life Technologies (Grand Island, NY, USA). MEBM BulletKit cell culture media were purchased from Lonza Inc. (Allendale, NJ, USA).

The MDA-MB-435 cancer cell line was originally received from the laboratory of Dr. R. Clarke, Georgetown University Medical School, Washington, DC, USA. The cells were cultured in RPMI 1640 medium with 10% fetal bovine albumin (FBA) and 1% penicillin–streptomycin solution at 37 °C and 5% CO<sub>2</sub>. MCF10A cells were originally purchased from ATCC (Manassas, VA, USA) and were cultured following the recommendations of ATCC. The MEBM medium was supplemented with 100 ng/mL Cholera Toxin to boost cell proliferation and increase the maximum passage number.

---

<sup>2</sup> Dr. Mohammad R. Vakili provided assistance with acetal-PEO synthesis. Ms. Jing Zheng did the MALDI-MS analysis.

And Ms. Jennifer Jones did the elemental analysis.

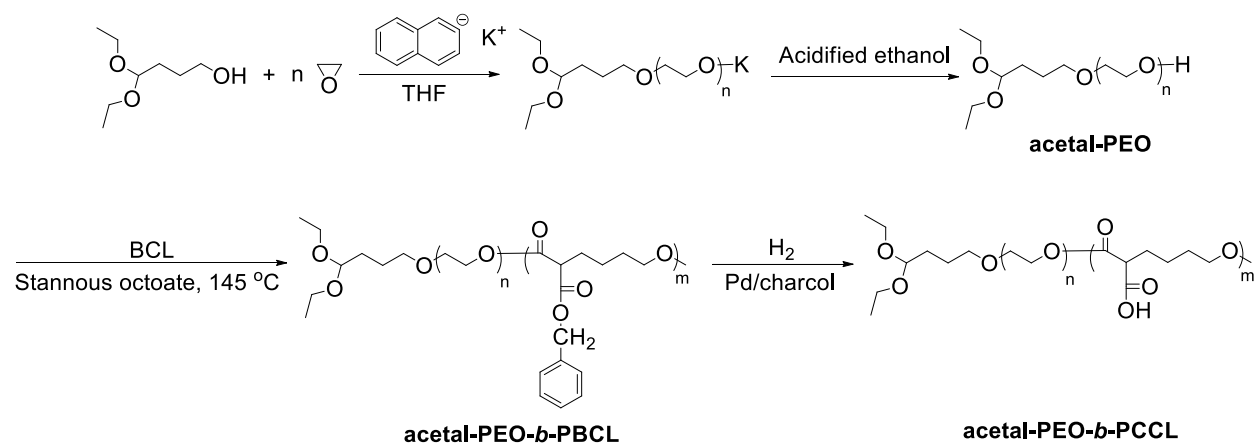
### 3.2.1.2 Synthesis of acetal-PEO<sup>6000</sup>

The synthesis of the PEO polymer with functionalization on one end group is based on anionic ring opening polymerization. We followed the method developed by Nagasaki et al. (1995) for the synthesis of acetal-PEO<sup>6000</sup> (**Scheme 3.1**). Potassium naphthalene, the catalyst, was freshly prepared before the synthesis of acetal-PEO. To prepare the catalyst, 1.65 g (12.9 mmol) naphthalene and 0.575 g (14.7 mmol) potassium was added into 50 mL anhydrous THF. The reaction was protected under dry argon (Ar) gas and kept running for 24 hours, and the catalyst in THF solution with dark green colour was obtained.

To prepare acetal-PEO, 0.3 mL (2 mmol) 3,3-diethoxy propanol, the initiator, was first added into 40 mL anhydrous THF in a three-neck round bottom flask. The flask was purged with dry Ar gas and maintained an Ar atmosphere. The catalyst solution (7 mL, ~2 mmol) was added dropwise into the reaction solution to activate the initiator. After 10 min of stirring, the flask was transferred into an ice water bath. Ethylene oxide (11.4 mL, 228 mmol) was added into the reaction solution. After 48 hours, the reaction was quenched by acidified ethanol (2 mL). Acetal-PEO was recovered by precipitation in ethyl ether. The product was purified by dissolution in THF and precipitation in ethyl ether, and was vacuum dried for further use. The composition of acetal-PEO was confirmed by <sup>1</sup>H-NMR and MALDI-MS.

To prepare samples for MALDI-MS analysis, acetal-PEO stock solution (10 mg/mL) was prepared in dichloromethane (DCM). 2[(2E)-3-(4-tert-Butylphenyl)-2-methylpropy-2-enylidene]-malononitrile (DCTB) was used as the matrix compound. Matrix solution was prepared in DCM with a concentration of 10 mg/mL. Sample/matrix solutions with different concentrations were made by mixing 2  $\mu$ L sample solution with 2, 4, 6, and 8  $\mu$ L of matrix solution. The sample/matrix solution (0.8  $\mu$ L) was mixed with 0.8  $\mu$ L of sodium chloride solution (saturated in methanol), and then spotted onto a stainless steel MALDI target. The spots with good crystallization were chosen

for MALDI-MS analysis. MALDI-MS analysis was performed on an ultraflexXtreme™ MALDI-TOF/TOF mass spectrometer (Bruker Daltonics, Billerica, MA, USA) in positive MS mode.



**Scheme 3.1. Synthesis of acetal-PEO and acetal-PEO-*b*-PCCL.**

### 3.2.1.3 Synthesis of acetal-PEO<sup>6000</sup>-*b*-PCCL<sub>17</sub>

To synthesize acetal-PEO<sup>6000</sup>-*b*-PCCL<sub>17</sub>, acetal-PEO-*b*-PBCL was first prepared through bulk ring opening polymerization, followed by hydrogen reduction catalyzed by Pd/charcoal (**Scheme 3.1**). Acetal-PEO<sup>6000</sup> (600 mg, 0.1 mmol) was reacted with BCL (500 mg, 2 mmol) under vacuum at 145 °C for 6 h. The polymerization reaction was catalyzed by stannous octoate. The degree of polymerization was determined by <sup>1</sup>H-NMR. The benzyl groups on acetal-PEO-*b*-PBCL were then removed through hydrogen reduction in anhydrous THF. The produced acetal-PEO-*b*-PCCL was recovered and purified by precipitation in hexane. The composition of acetal-PEO-*b*-PCCL was confirmed by <sup>1</sup>H-NMR.

### 3.2.1.4 Peptide conjugation on acetal-PEO<sup>6000</sup>-*b*-PCCL<sub>17</sub>

GRGDS-amide peptide was conjugated to acetal-PEO<sup>6000</sup>-*b*-PCCL<sub>17</sub> based on a method previously developed in our laboratory with minor modification. (Xiong et al. 2007) Briefly, 60 mg (7 μmol) acetal-PEO<sup>6000</sup>-*b*-PCCL<sub>17</sub> was dissolved in 3 mL THF to prepare a polymer solution with concentration of 20 mg/mL. The polymer solution was added dropwise into 30 mL double distilled

H<sub>2</sub>O (ddH<sub>2</sub>O) with stirring. Micelles of acetal-PEO<sup>6000</sup>-*b*-PCCL<sub>17</sub> (2 mg/mL) were formed after overnight evaporation of THF. The pH of the micelle solution was adjusted to 2 by adding diluted HCl. After 2 h of stirring, the acetal groups were converted to formyl groups. The micelle solution was neutralized by adding diluted NaOH solution. Phosphate buffer (300 μL, 1 M, pH 7) was added to the micelle solution to maintain a neutral pH. GRGDS-amide peptide (3.5 mg, 7 μmol) was then added into the formyl-PEO<sup>6000</sup>-*b*-PCCL<sub>17</sub> solution. A Schiff base was formed between the aldehyde group on the micelle surface and primary amine on the peptide (glycine end). After 2 h of reaction, 44 mg (0.7 mmol) sodium cyanoborohydride was added into the reaction solution to reduce the Schiff base to a stable C–N bond. The reduction reaction was kept overnight. Excess amount of NaBH<sub>3</sub>CN, non-reacted peptide, and salt in the buffer was removed through 24 h of dialysis against water. The final product, PCCL<sub>17</sub>-*b*-PEO<sup>6000</sup>-GRGDS-amide, was lyophilized. PCCL<sub>17</sub>-*b*-PEO<sup>6000</sup>-GRGDS-amide samples were prepared in D<sub>2</sub>O for <sup>1</sup>H-NMR analysis to confirm the conjugation of peptide.

Samples of formyl micelle solution, micelle solution upon peptide addition, peptide conjugated micelle solution after 24 h reduction by sodium cyanoborohydride, and peptide conjugated micelle solution after dialysis were collected for HPLC-UV analysis to quantify the peptide conjugation efficiency. Free peptide standards (12.5 μg/mL to 100 μg/mL) were analyzed to prepare the calibration curve for quantification of unreacted peptide. The amount of conjugated peptide was then calculated by subtracting the amount of unreacted peptide from the amount of initial peptide added to the reaction. The HPLC-UV analysis conditions were as follows:

Column: μBondapak C-18 analytical column (10 μm, 3.9×300 mm) (Waters, Billerica, MA);

Flow rate: 1 mL/min (model 600 pump, Waters);

Mobile phase: 0.1% TFA in H<sub>2</sub>O (solution A) and acetonitrile (solution B);

Mobile phase gradient: (1) Prerun: 100% A for 1 min; (2) a linear gradient from 100% A to 20% A in 10 min; (3) a linear gradient from 20% A to 100% A in 1 min; (4) 100% A for another 6 min;

UV detection wavelength: 214 nm; Sample injection volume: 30  $\mu$ L.

### **3.2.1.5 Encapsulation of As<sup>III</sup> in micelles**

The thiolated polymer PEO<sup>5000</sup>-*b*-P(CCLC<sub>6</sub>-SH) was synthesized according to the method developed previously for encapsulation of phenylarsine oxide (PAO). (Zhang et al. 2014) Inorganic ATO, in the form of arsenic acid (As<sup>III</sup>) when dissolved in aqueous solution, has less affinity for thiol groups compared to organic arsenicals such as PAO. (Shen et al. 2013) We tested whether increasing temperature can enhance the As-S complex formation between As<sup>III</sup> and thiol groups. Freshly synthesized PEO-*b*-P(CCLC<sub>6</sub>-SH) was used to encapsulate As<sup>III</sup> in the preliminary study. Two sets of encapsulation experiments were conducted, one set without heating and the other with 1 h incubation in a 37 °C water bath. To avoid the oxidation of thiol groups at high temperature, 10 mM tris(2-chloroethyl) phosphate (TCEP) solution was used as the aqueous phase for micelle formation to maintain a reductive environment. To maintain the solution pH at 7, ammonium acetate buffer (1.45 M, pH 7.4) was used instead of water for TCEP/As<sup>III</sup> solution preparation.

At the same time, the amount of arsenic added for arsenic loading was optimized. Sodium arsenite (NaAsO<sub>2</sub>) with different molar ratio to that of the theoretical carboxylic acid groups in the starting polymer, PEO-*b*-PCCL<sub>17</sub>, i.e., 1:2, 1:1, 2:1, and 5:1, was pre-added into the TCEP-supplemented ammonium acetate buffer. Briefly, 2.5 mg (0.02 mmol), 5 mg (0.04 mmol), 10 mg (0.08 mmol), or 25 mg (0.2 mmol) NaAsO<sub>2</sub> was dissolved into 4 mL TCEP-supplemented ammonium acetate buffer. PEO-*b*-P(CCLC<sub>6</sub>-SH), which was freshly synthesized from 20 mg

PEO-*b*-PCCL<sub>17</sub> (equivalent to 0.04 mmol COOH in the starting polymer), was dissolved in 2 mL THF. The polymer solution was added into each arsenic solution dropwise with vigorous stirring. In the non-heated set, the mixture was left in the hood with stirring to allow THF to evaporate. In the heated set, the mixture was then incubated in a 37 °C water bath for 1 h. The THF was then evaporated overnight at room temperature with stirring. The un-loaded As<sup>III</sup> and most salt in the buffer were removed by dialysis against water for 24 hours. The water was changed every hour during the first 6 hours of dialysis, and every 3 hours till the 24<sup>th</sup> hour. The final product, PEO-*b*-P(CCLC<sub>6</sub>-S-As<sup>III</sup>) was lyophilized for arsenic loading determination. The loading of arsenic was determined by ICP-MS.

### 3.2.1.6 Preparation of mixed micelles with As<sup>III</sup> encapsulation

PEO<sup>5000</sup>-*b*-PCCL<sub>17</sub> (120 mg, 0.016 mmol) was functionalized with mercaptohexylamino groups on the hydrophobic block using the method developed in **Chapter 2**. The yielded PEO<sup>5000</sup>-*b*-P(CCLC<sub>6</sub>-SH) was mixed with 40 mg of either PEO<sup>5000</sup>-*b*-PCCL<sub>17</sub> or PCCL<sub>17</sub>-*b*-PEO<sup>6000</sup>-GRGDS-amide in THF (4 mL). After stirring for 30 min, the polymer solution in THF was added dropwise into 30 mL aqueous solution containing NaAsO<sub>2</sub> (156 mg, 1.2 mmol), TCEP (10 mM), and CH<sub>3</sub>COONH<sub>4</sub> (0.15 M, pH 7) with vigorous stirring. The mixture was incubated in a 37 °C water bath for 1 h and left in a fume hood overnight with stirring, allowing evaporation of THF. Free NaAsO<sub>2</sub> and other salts were removed during 24 h of dialysis against water. The final mixed micelles encapsulated with As<sup>III</sup> were recovered by lyophilisation (**Figure 3.2**). The mixed micelles formed by PEO<sup>5000</sup>-*b*-P(CCLC<sub>6</sub>-SH) and PCCL<sub>17</sub>-*b*-PEO<sup>6000</sup>-GRGDS-amide with As<sup>III</sup> encapsulation were denoted as peptide-decorated mixed micelles (PMM). The mixed micelles formed by PEO<sup>5000</sup>-*b*-P(CCLC<sub>6</sub>-SH) and PEO<sup>5000</sup>-*b*-PCCL<sub>17</sub> with As<sup>III</sup> encapsulation were denoted as control mixed micelles (CMM). Micelles formed by PEO<sup>5000</sup>-*b*-P(CCLC<sub>6</sub>-SH) only with As<sup>III</sup>

encapsulation were named as PEO<sup>5000</sup>-*b*-P(CCLC<sub>6</sub>-S-As<sup>III</sup>). The arsenic loading in both mixed micelles and in non-mixed micelles was determined by ICP-MS.

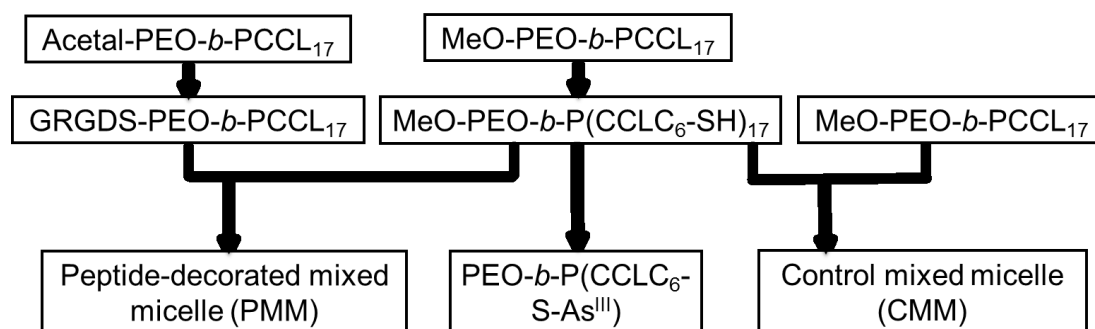


**Figure 3.2. Preparation of As<sup>III</sup>-encapsulated micelles.** Thiolated polymer was mixed with MeO-PEO-*b*-PCCL<sub>17</sub> or GRGDS-PEO-*b*-PCCL<sub>17</sub> at the weight ratio of 3:1 for mixed micelle preparation.

### 3.2.1.7 Micelle size distribution

The size distribution of As<sup>III</sup> encapsulated micelles was determined by dynamic light scattering (DLS) technology (Malvern Nano-ZS Zeta Sizer, laser wavelength: 633 nm, temperature: 25 °C). PMM, CMM, and PEO-*b*-P(CCLC<sub>6</sub>-S-As<sup>III</sup>) were dissolved in ddH<sub>2</sub>O to prepare a micelle solution with concentration of 1 mg/mL. The micelle solution was filtered sequentially through Whatman® Nuclepore Trach-Etch polycarbonate membranes with pore size of 400 μm, 200 μm, and 100 μm. The size distribution of micelle solutions before and after filtration was monitored. The arsenic concentration in each filtrate was determined by ICP-MS.

### 3.2.1.8 *In vitro* arsenic release from micelles

The arsenic release from three different micelles was evaluated in RPMI-1640 cell culture medium supplemented with 10% FBS. In each set of experiments, 1.5 mL of 1 mg/mL micelle solution was prepared by direct re-suspension. Triplicate samples were prepared for each type of micelles. The micelle solutions were incubated at 37 °C. At 0, 1, 3, 6, 12, and 24 h, a 100 μL micelle solution aliquot was collected and centrifugally filtered using an Amicon Ultra-0.5 mL centrifugal filter

(molecular weight cut-off: 3,000 Da) at  $13500 \times g$  for 30 min. The filtrate was collected for released arsenic determination using ICP-MS.

The arsenic release was expressed as the weight percentage of free arsenic at each time point compared to the total arsenic weight in the sample.

### **3.2.1.9 *In vitro* cytotoxicity of encapsulated arsenic**

Neutral red assay was used to evaluate the *in vitro* cytotoxicity of free and encapsulated As<sup>III</sup> in different micelles against MDA-MB-435 cells and MCF10A cells. MDA-MB-435 cells were seeded into a 96-well plate at a density of 8000 cells/200  $\mu$ L per well and MCF10A cells were seeded at a density of 10000 cells/200  $\mu$ L per well. The seeded cells were incubated overnight in an incubator to achieve 70–80% cell culture confluency before arsenic treatment. The cells were treated with PMM, CMM, PEO-*b*-P(CCLC<sub>6</sub>-S-As<sup>III</sup>), and free As<sup>III</sup> for 24 h with equivalent arsenic concentrations ranging from 0.1  $\mu$ M to 150  $\mu$ M. Cell viability was measured according to the standard protocol for neutral red assay. Absorbance at 540 nm wavelength was detected by the multiple-reader and was subtracted from the background signal at 690 nm.

The cell survival rate was expressed as the percentage of viable cells in the treated wells compared to those in the untreated wells which served as the control. The dose effect of each compound was fitted by *log[Dose]-Response (variable slope)* equation in GraphPad Prism 5 software (La Jolla, CA, USA) to obtain IC<sub>50</sub> values. The IC<sub>50</sub> values were expressed as mean with 95% confidence interval (95% CI) in parentheses. Triplicate assays were conducted.

### **3.2.1.10 Cellular uptake of encapsulated arsenic**

MDA-MB-435 cells and MCF10A cells ( $25 \times 10^4$  cells/mL, 2 mL per dish) were seeded into 60  $\times$  15 mm cell culture dishes. MCF10A cells were treated with PMM, CMM, PEO-*b*-P(CCLC<sub>6</sub>-S-As<sup>III</sup>), and free As<sup>III</sup> solutions with equivalent arsenic concentration of 20  $\mu$ M for 24 h. MDA-MB-

435 cells were treated free and encapsulated As<sup>III</sup> with equivalent arsenic concentration of 10 and 20  $\mu$ M for 3 and 24 h. After treatment for a certain period, the culture medium was carefully aspirated and the cells were washed with 2 mL DPBS buffer. Trypsin-EDTA solution (0.25% Trypsin/1 mM EDTA, 300  $\mu$ L) was added into each culture dish. The dissociated cells were collected and spun down at 2000 rpm for 5 min. The cell pellet was washed with 1.5 mL DPBS buffer twice. The cells were then re-suspended in 500  $\mu$ L ddH<sub>2</sub>O and lysed using freeze-thaw method.

To determine the arsenic concentration in the homogenized cell lysis, 400  $\mu$ L of the lysed cell solution was mixed with 100  $\mu$ L HNO<sub>3</sub> (Optima HPLC grade). The mixture was incubated in a 50 °C water bath overnight. The digested cell solution was diluted and filtered for ICP-MS analysis. The arsenic concentration determined was normalized to soluble protein concentration in the lysed cell solution. To determine the soluble protein concentration in cell lysis, the cell lysis was first centrifuged at 5000 rpm for 5 min. Aliquots were collected from the supernatant for protein assay. Standard Bradford assay protocol (version for 250  $\mu$ L microplate assay) was followed using a G-250 based 1 $\times$  Gelcode<sup>TM</sup> blue stain reagent.

To verify that the decoration of GRGDS-amide on the micelle surface can affect the selective delivery of encapsulated As<sup>III</sup> to target cells, competitive cellular uptake of arsenic with and without free GRGDS-amide pretreatment was evaluated. The seeded MDA-MB-435 cells and MCF10A cells were pretreated with GRGDS-amide (1 mg/mL) for 1 h before treatment of PMM, CMM, PEO-*b*-P(CCLC<sub>6</sub>-S-As<sup>III</sup>), and free As<sup>III</sup> solutions. The concentration of free GRGDS-amide was maintained over the course of arsenic formulation treatment. The cellular uptake of arsenic in the pretreatment group was compared to that in the non-pretreatment group. Since the pretreatment of free GRGDS-amide can induce detachment of MDA-MB-435 cells from the cell

culture dish, the cells suspended in the medium were collected as well for arsenic cellular uptake determination.

### 3.2.1.11 Data analysis

The results were expressed as mean  $\pm$  standard deviation (SD) (n=3). Student t-test (two-tail) and One-way ANOVA with post-test of Tukey's multiple comparison test were used to perform statistical analysis. In the cytotoxicity study, best-fitted logIC<sub>50</sub> values of free and encapsulated As<sup>III</sup> directed calculated from the log[dose]-responsive fitting were compared using extra sum-of-squares F test provided by GraphPad Prism 5 software. P<0.5 was considered as having statistical significance.

## 3.2.2 Results

### 3.2.2.1 Synthesis of polymers with acetal-ended group

The PEO polymer with acetal end group was synthesized to enable peptide conjugation on the micelle surface. The anionic ring opening polymerization method was used to synthesize acetal-PEO<sup>6000</sup>. **Figure 3.3** depicts the <sup>1</sup>H-NMR spectrum of acetal-PEO. The peak intensity of ethylene protons ( $\delta$  3.64, CH<sub>2</sub>CH<sub>2</sub>O) was compared to the peak intensity of protons on the 3,3-diethoxy propanyl end [ $\delta$  4.64, (EtO)2CHCH<sub>2</sub>CH<sub>2</sub>O;  $\delta$  1.89, (EtO)2CHCH<sub>2</sub>CH<sub>2</sub>O] to calculate the degree of polymerization (DP) of acetal-PEO. The number average molecular weight (M<sub>n</sub>) of acetal-PEO calculated from the <sup>1</sup>H-NMR spectrum was 6924 g/mol with 154 units of ethylene oxide repeating units averagely per chain.

The synthesized acetal-PEO was analyzed by MALDI-MS as well (**Figure 3.4**). The number average and weight average molecular weight of acetal-PEO and polydispersity (PD) was calculated from the MS spectrum based on the equations below. (Zhu et al. 1998)

$$M_n = \frac{\sum(n_i M_i)}{\sum n_i} \quad \text{Equation 3-1}$$

$$M_w = \frac{\sum(n_i M_i^2)}{\sum(n_i M_i)} \quad \text{Equation 3-2}$$

$$PD = M_w / M_n$$

$$\text{Equation 3-3}$$

Where  $n_i$  represents the signal intensity of polymer with  $m/z$  value of  $M_i$  ( $z=1$  in this experiment).

According to the MALDI-MS spectrum, the  $M_n$  of acetal-PEO was 5640 g/mol, the  $M_w$  was 5906 g/mol, and the PD was 1.05.

Considering the difference existing in the  $M_n$  calculation from  $^1\text{H-NMR}$  and MALDI-MS, we arbitrarily denoted the synthesized acetal-PEO as acetal-PEO<sup>6000</sup>, while the repeating unit number of ethylene oxide was presumed as 154 for DP calculation of PCCL in the synthesized acetal-PEO-*b*-PCCL polymer.

The synthesis of acetal-PEO-*b*-PCCL followed the procedures developed previously to synthesize PEO-*b*-PCCL. (Mahmud et al. 2006) The composition of acetal-PEO-*b*-PCCL was determined by  $^1\text{H-NMR}$  spectrum (Figure 3.5). The DP of PCCL was 17.

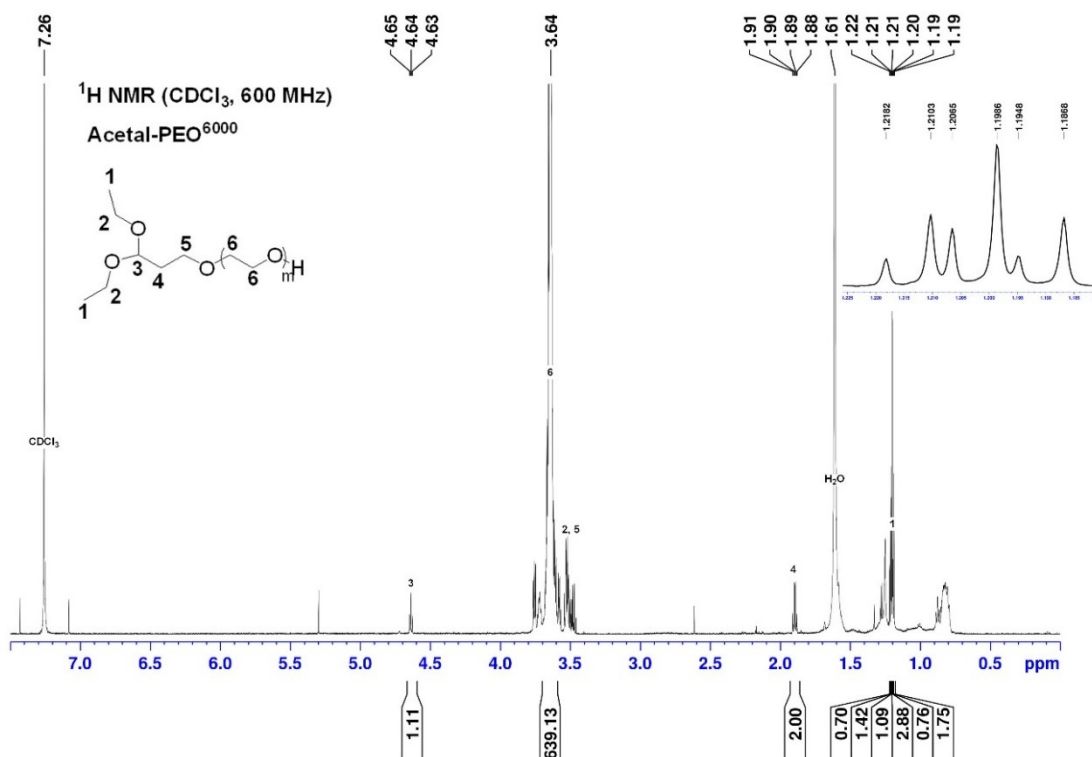


Figure 3.3.  $^1\text{H-NMR}$  spectrum of acetal-PEO<sup>6000</sup>.

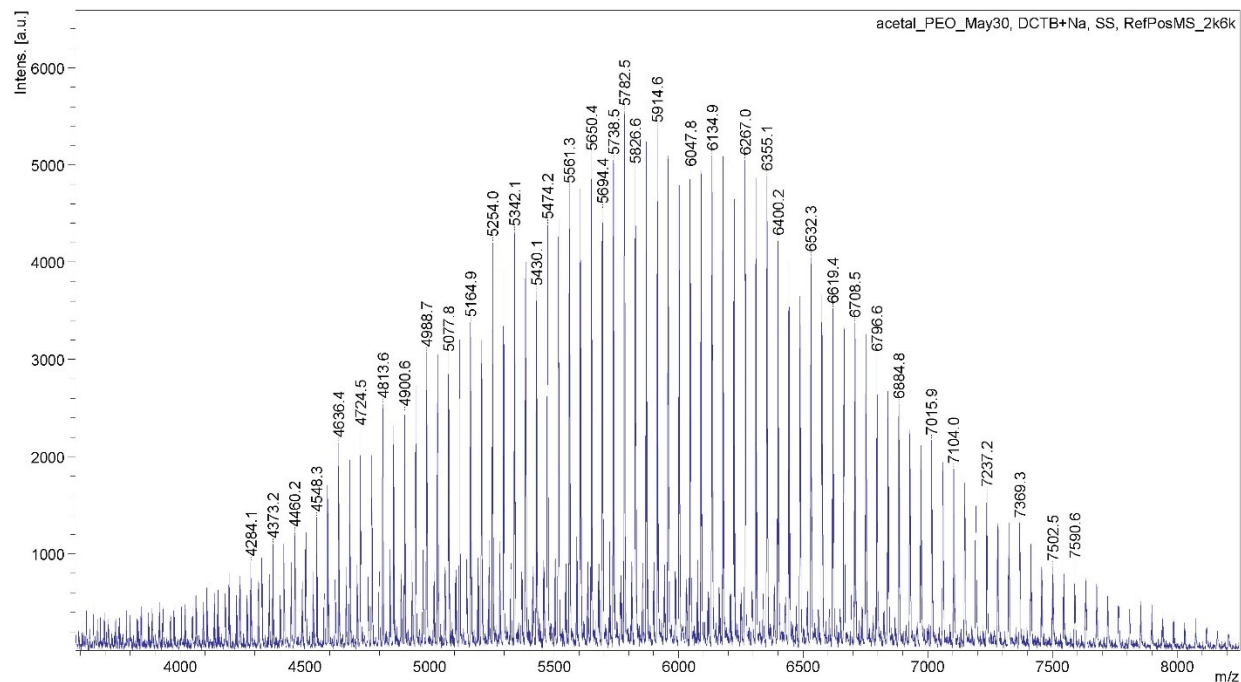


Figure 3.4. MALDI -MS spectrum of acetal-PEO<sup>6000</sup>.

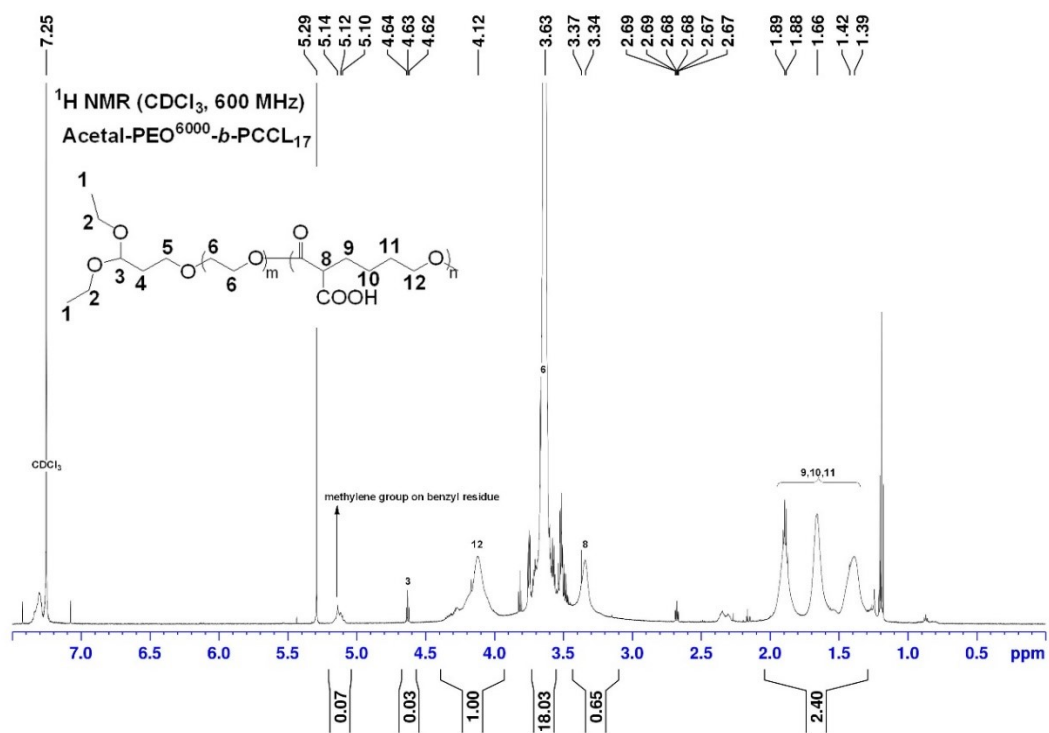


Figure 3.5. <sup>1</sup>H-NMR of acetal-PEO<sup>6000</sup>-b-PCCL<sub>17</sub>.

### 3.2.2.2 PCCL-*b*-PEO-GRGDS-amide synthesis

Conjugation of GRGDS-amide to the surface of micelles assembled from acetal-PEO-*b*-PCCL followed the procedures depicted in **Figure 3.1**. In this study, 1:1 molar ratio of free peptide and acetal-PEO-*b*-PCCL was mixed for peptide conjugation. The conjugation reaction was monitored using HPLC-UV analysis (**Figure 3.6**). The formyl-PEO-*b*-PCCL micelles generated a signal at the same retention time (3.2 min) of the free peptide. Therefore, the signal of micelle sample at retention time of 3.2 min was subtracted as a blank in the peptide concentration calculation of 0 h and 24 h samples. The calibration curve was prepared using free GRGDS-amide peptide standards (**Figure 3.7**). According to the calculation, 23% of added GRGDS-amide was conjugated to acetal-PEO-*b*-PCCL polymer. As the added GRGDS-amide peptide had equivalent mole of added acetal-PEO-*b*-PCCL polymer, 23% of the added acetal-PEO-*b*-PCCL was functionalized with GRGDS-amide at the PEO block.

The conjugation of GRGDS-amide onto acetal-PEO-*b*-PCCL was further confirmed by <sup>1</sup>H-NMR spectra of micelles before and after peptide conjugation (**Figure 3.8**). Micelle samples (1 mg/mL) of PCCL-*b*-PEO-acetal and PCCL-*b*-PEO-GRGDS-amide were prepared in D<sub>2</sub>O for <sup>1</sup>H NMR analysis. When micelles are formed, the protons on micelle surface groups will have better signal intensity. (Xiong et al. 2007) Under these conditions, proton signals for GRGDS-amide ( $\delta$  4.57, 4.34, 3.91, 3.03, and 2.64) were observed in addition to the propyloxy proton ( $\delta$  3.31) which was shown in the PCCL-*b*-PEO-acetal spectrum as well.

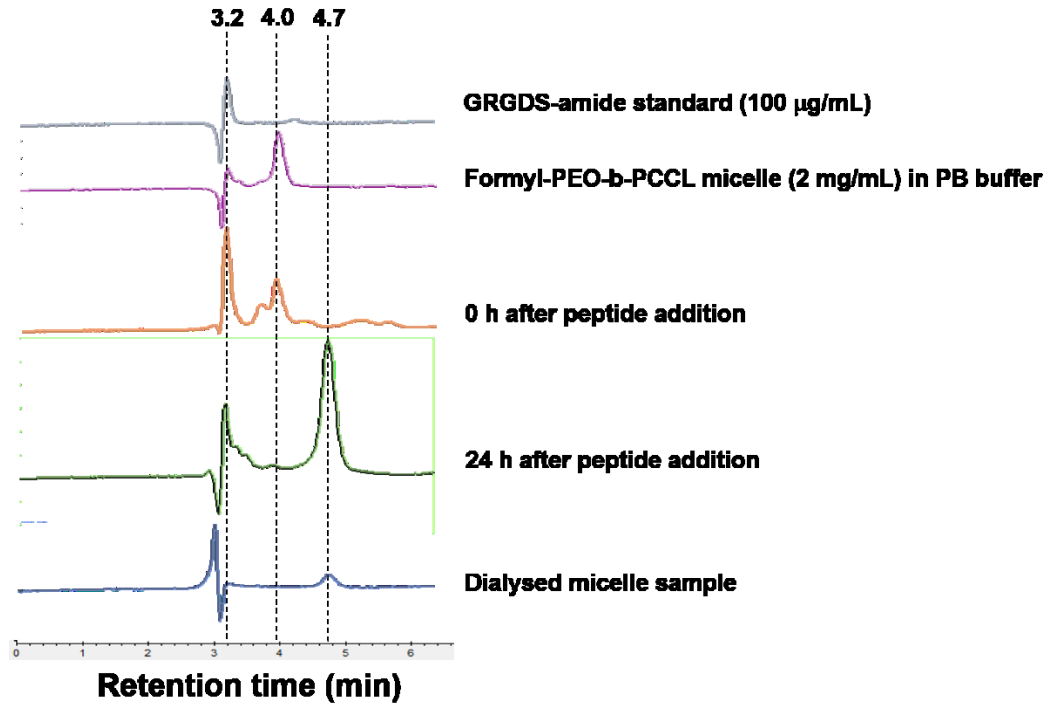


Figure 3.6. Monitoring GRGDS-amide conjugation to acetal-PEO-*b*-PCCL polymers using HPLC-UV chromatography.

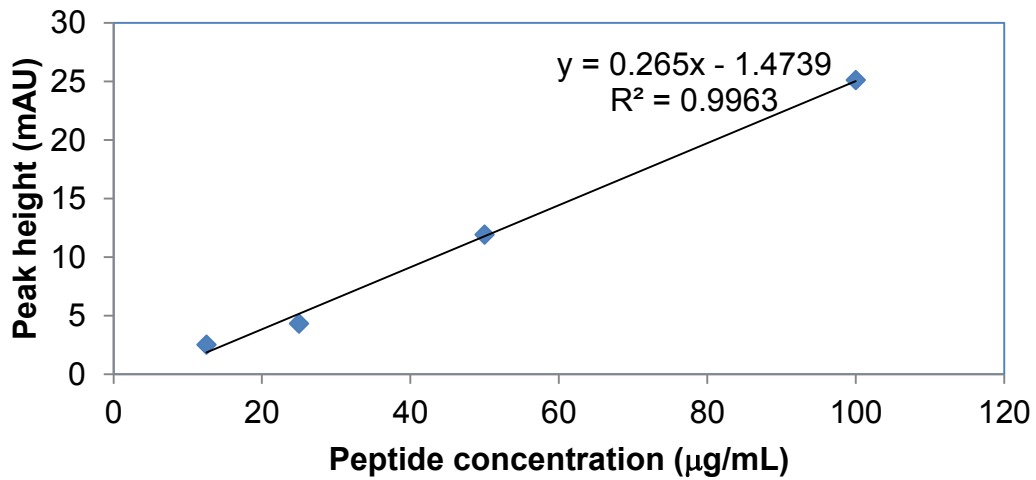


Figure 3.7. Calibration curve for free GRGDS-amide.

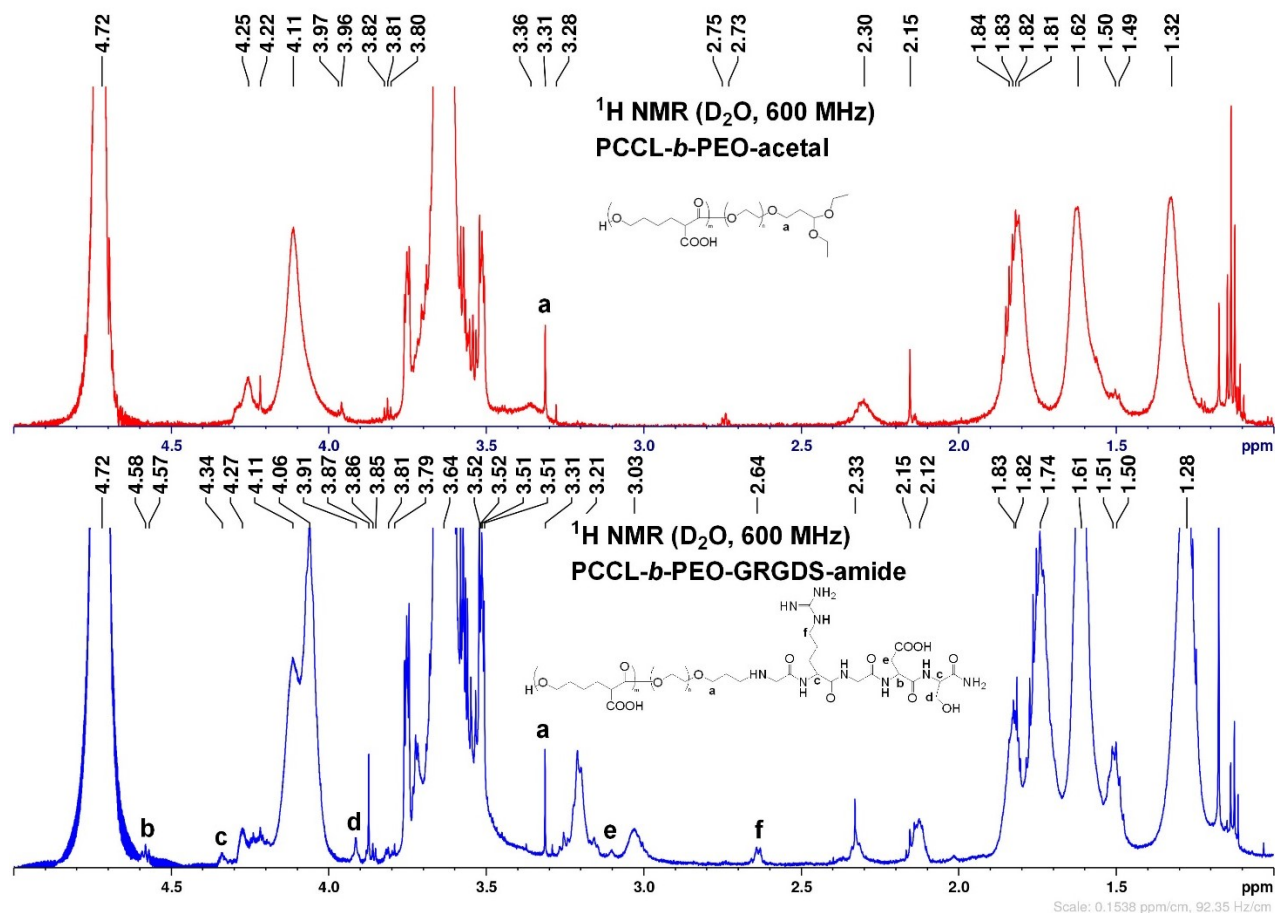


Figure 3.8.  $^1\text{H}$ -NMR spectra of micelles (1 mg/mL, prepared in  $\text{D}_2\text{O}$ ) with and without GRGDS-amide.

### 3.2.2.3 Arsenic loading in micelles

Micelles encapsulated with  $\text{As}^{\text{III}}$  were prepared by the organic solvent evaporation method. Briefly, polymer solution prepared in THF solution is added dropwise into  $\text{NaAsO}_2$ -containing aqueous solution with vigorous stirring. THF is evaporated during overnight incubation in the fume hood and micelles encapsulated with arsenic compound are self-assembled.

The amount of  $\text{NaAsO}_2$  added and the temperature for  $\text{As}^{\text{III}}$  encapsulation in PEO-*b*-P(CCLC<sub>6</sub>-SH) micelle were optimized. PEO-*b*-P(CCLC<sub>6</sub>-SH) polymer was freshly synthesized from PEO-*b*-PCCL and  $\text{NH}_2\text{C}_6\text{H}_{12}\text{SH}$  using the method developed in **Chapter 2**. According to the  $^1\text{H}$ -NMR spectrum of PEO-*b*-P(CCLC<sub>6</sub>-SH) shown in **Figure 2.1**, around 40% of total CCL

amount in the starting polymer was functionalized with thiol groups. However, the exact amount of thiol groups in the freshly synthesized PEO-*b*-P(CCLC<sub>6</sub>-SH) polymer without purification was unknown. Therefore, the addition amount of NaAsO<sub>2</sub> for arsenic encapsulation was calculated based on the CCL amount in the starting polymer. NaAsO<sub>2</sub> with different molar ratio to that of the COOH groups in PEO-*b*-PCCL<sub>17</sub>, namely, 1:2, 1:1, 2:1, and 5:1, was mixed with freshly synthesized PEO-*b*-P(CCLC<sub>6</sub>-SH). After overnight incubation at room temperature, the free NaAsO<sub>2</sub> was removed by dialysis. Arsenic loading in the micelles was determined by ICP-MS analysis. With increasing addition amount of NaAsO<sub>2</sub>, the arsenic loading was increased (**Figure 3.9-A**). However, the arsenic loading of As<sup>III</sup> was relatively low compared to PAO (~ 2.5 wt%). To further increase arsenic loading of As<sup>III</sup>-encapsulated micelles, the NaAsO<sub>2</sub>/PEO-*b*-P(CCLC<sub>6</sub>-SH) mixture solution was incubated in a 37 °C water bath for 1 h before overnight THF evaporation at room temperature in the fume hood. **Figure 3.9-B** demonstrates that the increase of temperature can enhance the arsenic loading. With 1 h-incubation at 37 °C, the arsenic loading in micelles with the added As/COOH molar ratio of 2:1 was substantially higher than that in micelles without incubation at 37 °C though with higher added As/COOH molar ratio (5:1). The optimized NaAsO<sub>2</sub> addition amount and encapsulation procedure was applied for As<sup>III</sup> encapsulation in mixed micelles. The arsenic loading in PMM and CMM was 2.1±0.3 wt% and 2.1±0.1 wt%, respectively, which was lower than the arsenic loading in non-mixed PEO-*b*-P(CCLC<sub>6</sub>-S-As<sup>III</sup>) micelles (4.0±0.3 wt%). The sulfur content of the As<sup>III</sup>-encapsulated micelles was determined by elemental analysis and the molar ratio of arsenic to sulfur was calculated. We observed that though the arsenic loading in mixed micelles and non-mixed micelles was statistically different (P<0.001, t-test), the As/S ratios of these three micelles were similar (

**Figure 3.10).** The As/S molar ratio of PMM, CMM, and PEO-*b*-P(CCLC<sub>6</sub>-S-As<sup>III</sup>) was 0.73, 0.61, and 0.67, respectively. The similar As/S molar ratio in three kinds of micelles indicates that the encapsulated arsenic amount is determined by the amount of thiol groups existing in the micelles. However, because the As/S molar ratio was calculated from average arsenic loading and average sulfur content, no standard deviation of As/S ratio was obtained and no statistical analysis on As/S molar ratio was performed.

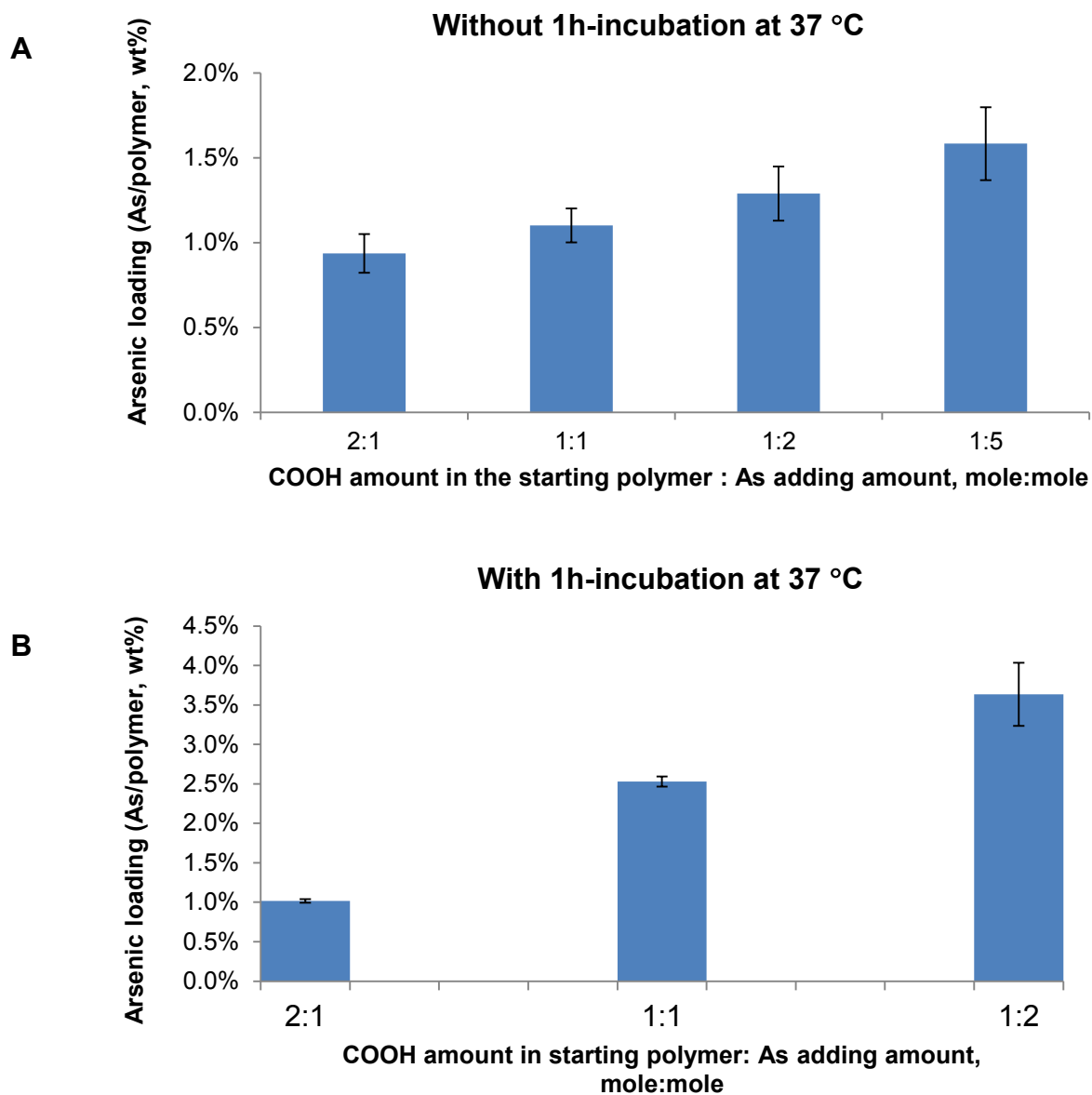


**Figure 3.9. Arsenic loading in PEO-*b*-P(CCLC<sub>6</sub>-SH) micelles without incubation at 37 °C (A) and with incubation at 37 °C (B).**

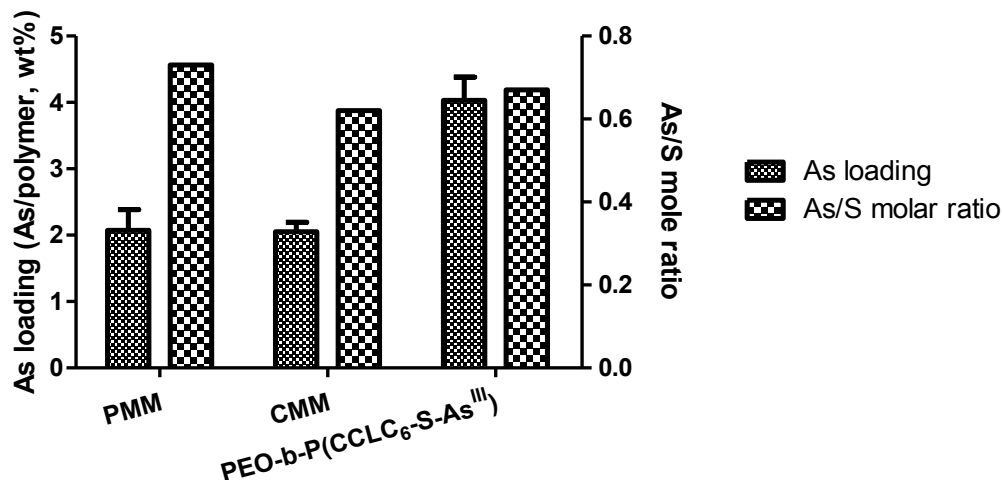


**Figure 3.10.** Arsenic loading and As/S molar ratio in PMM, CMM, and non-mixed PEO-*b*-P(CCLC<sub>6</sub>-S-As<sup>III</sup>) micelles.

#### 3.2.2.4 Size distribution of As<sup>III</sup>-encapsulated micelles

Lyophilized PMM, CMM, and PEO-*b*-P(CCLC<sub>6</sub>-S-As<sup>III</sup>) micelles were dissolved in ddH<sub>2</sub>O (1 mg/mL) for size distribution analysis using DLS. The size distribution by intensity of micelles are presented in **Figure 3.11**. Mixed micelles had broader size distribution and multiple micelle populations with different sizes compared to non-mixed micelles.

To better understand the fraction of micelles with large size, we filtered the micelle solutions through polycarbonate membrane with pore size of 400 nm, 200 nm, and 100 nm, sequentially. The arsenic concentration in each filtrate was determined and compared to corresponding samples before filtration (**Figure 3.12**). After filtration through a 400 nm membrane, the polydispersity index (PdI) of PMM decreased from 0.48 to 0.43, and the PdI of CMM decreased from 0.64 to 0.46. The quality of mixed micelle size distribution did not improve substantially. At the same time, more than 99% arsenic in micelles before filtration remained in the micelle filtrate after 400 nm membrane filtration. After further filtration through a 200 nm membrane, the PdI of PMM and CMM decreased to 0.30 and 0.31, respectively, and 96% of total arsenic was retained in the filtrate of PMM, with 88% for CMM. This observation suggests that both PMM and CMM have a small

fraction (<15%) of micelles with diameter larger than 200 nm, though CMM micelles have higher portion of large micelles compared to PMM.

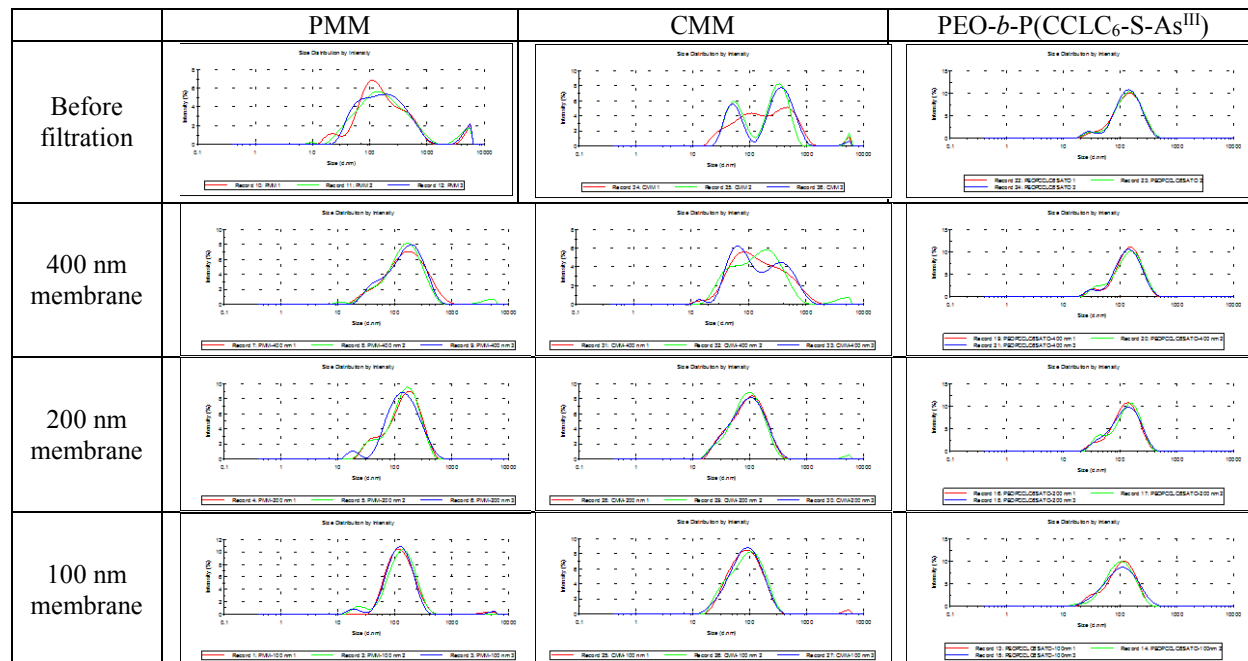


**Figure 3.11. Size distribution by intensity of micelles (1 mg/mL) before and after sequential filtration through membranes of different pore sizes.**

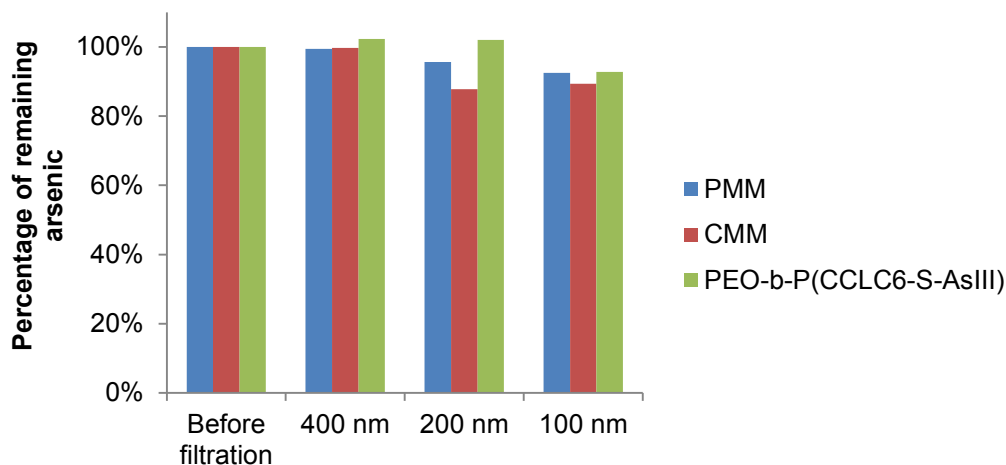


**Figure 3.12. Percentage of remaining arsenic after filtration compared to the same sample before filtration.**

### 3.2.2.5 *In vitro* arsenic release from micelles

Arsenic release from PMM, CMM, and PEO-*b*-P(CCLC<sub>6</sub>-S-As<sup>III</sup>) micelles was evaluated in cell culture medium supplemented with 10% FBS. Though the release of arsenic from micelles was slow over 24 hours, high burst release of As<sup>III</sup> was observed in all these three types of micelles, especially in the two mixed micelles (**Figure 3.13**).

According to the release study of PAO-encapsulated micelles in **Chapter 2**, the burst released arsenic is attributed to free arsenicals physically entrapped inside the micelle or adsorbed on the micelle surface. In this study, mixed micelles had double the burst released arsenic percentage of non-mixed micelles. The incorporation of PCCL<sub>17</sub>-*b*-PEO or PCCL<sub>17</sub>-*b*-PEO-GRGDS-amide polymer in mixed micelles may affect the local environment of the micelle core for stable As-S bond formation, which is likely the reason for higher burst release in mixed micelles.

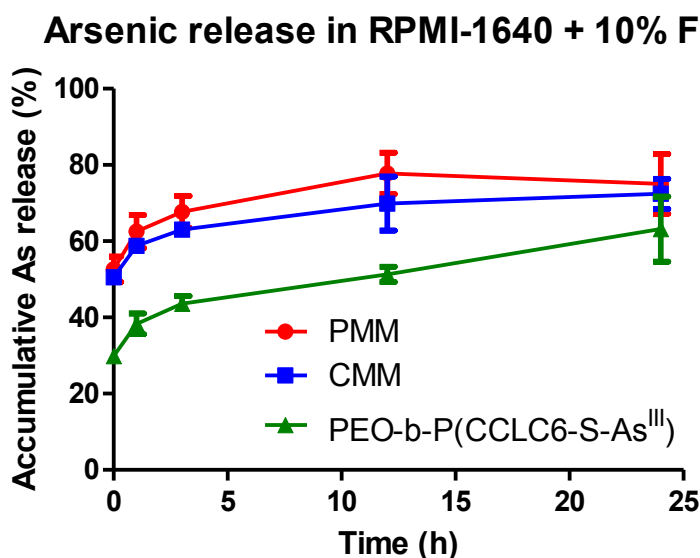


**Figure 3.13.** *In vitro* arsenic release from micelles in RPMI-1640 cell culture medium supplemented with 10% FBS at 37 °C.

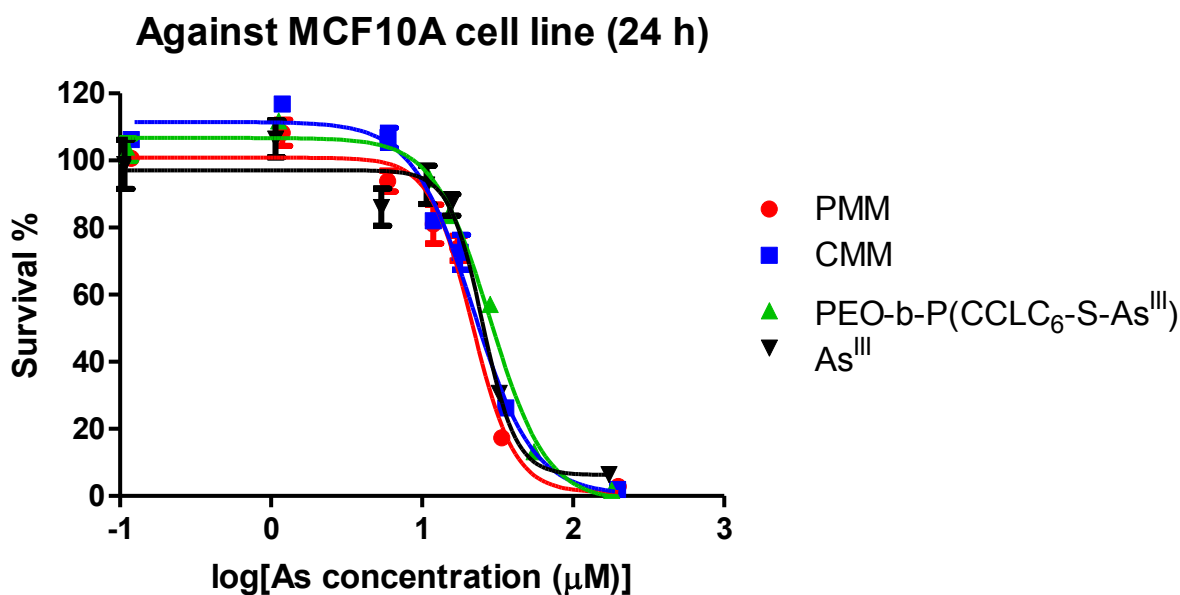
### 3.2.2.6 *In vitro* cytotoxicity of As<sup>III</sup>-encapsulated micelles

In order to test if the peptide decoration on micelle surface can realize selective delivery of arsenic to target tumor cells, two cell lines were employed to evaluate the cytotoxicity of PMM, CMM, non-mixed PEO-*b*-P(CCLC<sub>6</sub>-S-As<sup>III</sup>), and free As<sup>III</sup>. MCF10A is a non-tumorigenic epithelial cell line derived from the breast tissue of a female patient with fibrocystic disease. MCF10A cells do not overexpress  $\alpha_v\beta_3$  integrin, which is the receptor for GRGDS-amide peptide. MDA-MB-435 is a metastatic breast cancer cell line and overexpresses  $\alpha_v\beta_3$  integrin on the cell membrane. In this study, MCF10A cells serve as a control cell line and MDA-MB-435 cells serve as a target cell line.

When treated on the control cell line (**Figure 3.14**), the logIC<sub>50</sub> values of PMM and CMM were not significantly different from each other (P=0.9530) and the logIC<sub>50</sub> values of mixed micelles were not significantly different from that of free As<sup>III</sup> (P=0.2608). Though logIC<sub>50</sub> of As<sup>III</sup> encapsulated in non-mixed micelles was similar to that of free As<sup>III</sup> (P=0.2628), it was larger than As<sup>III</sup> encapsulated in PMM and CMM (P=0.0036). Generally, the decoration of GRGDS-amide on the micelle surface did not induce observable change in the cytotoxicity of As<sup>III</sup> encapsulated in mixed micelles. However, As<sup>III</sup> encapsulated in non-mixed micelles were less cytotoxic than As<sup>III</sup> encapsulated in mixed micelles.

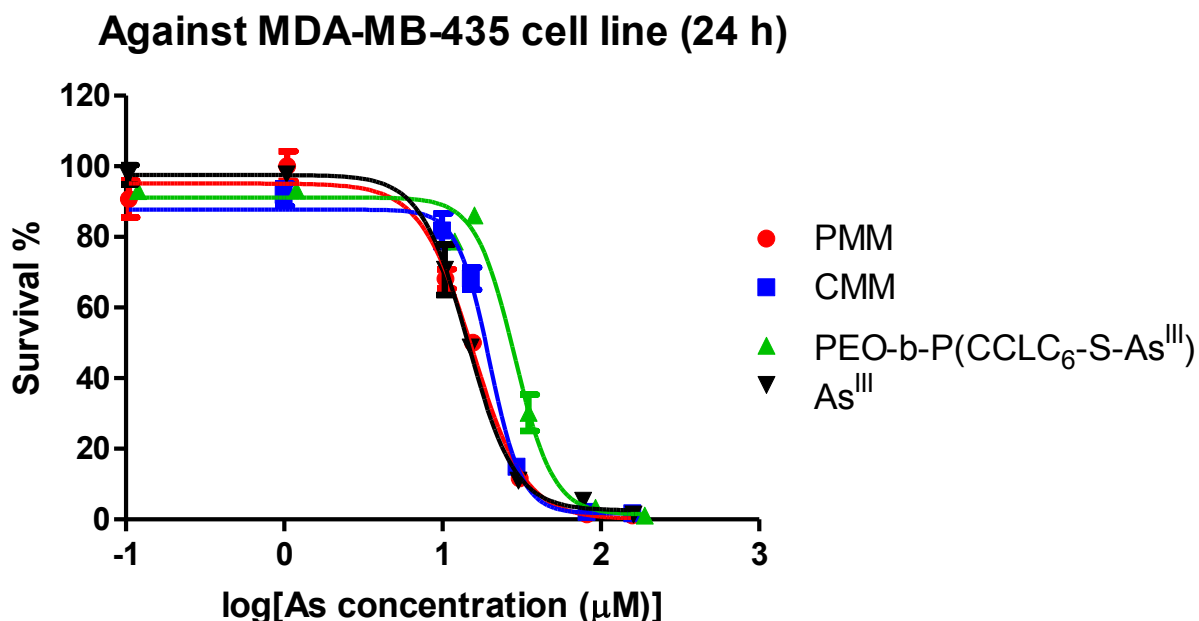
When treated on the target cell line (**Figure 3.15**), the encapsulated As<sup>III</sup> formulations demonstrated more selectivity compared to the results from the control cell line. After encapsulation inside PEO-*b*-P(CCLC<sub>6</sub>-SH) micelles, As<sup>III</sup> became less cytotoxic than the free form (P<0.0001). The encapsulation may change the bioavailability of As<sup>III</sup> and affect the activity of As<sup>III</sup> in cell apoptosis induction. However, As<sup>III</sup> encapsulated in CMM was more cytotoxic than As<sup>III</sup> encapsulated in non-mixed micelles (P<0.0001). The high burst release of As<sup>III</sup> from the mixed micelle may be the reason for the enhanced cytotoxicity, as more arsenic in CMM solution

was in the free form. However, PMM and CMM had similar burst release and overall release profile, the decoration of GRGDS-amide on PMM micelle surface further enhanced the cytotoxicity in comparison of CMM ( $P=0.0008$ ). And the  $\log IC_{50}$  value of PMM was similar to free  $As^{III}$  ( $P=0.2868$ ).



	PMM	CMM	PEO- <i>b</i> -P(CCLC <sub>6</sub> -S-As <sup>III</sup> )	As <sup>III</sup>
$IC_{50}$	21.6	21.7	28.3	25.2
95% CI	18.7 – 24.9	19.0 – 24.8	25.4 – 31.6	20.8 – 30.4

**Figure 3.14.** *In vitro* cytotoxicity of free and encapsulated  $As^{III}$  against the control cell line, MCF10A cells.



	PMM	CMM	PEO-b-P(CCLC <sub>6</sub> -S-As <sup>III</sup> )	As <sup>III</sup>
IC <sub>50</sub>	15.5	19.9	28.5	14.5
95% CI	13.9 – 17.3	18.2 – 21.7	25.6 – 31.8	13.2 – 15.8

**Figure 3.15.** *In vitro* cytotoxicity of free and encapsulated As<sup>III</sup> against the target cell line, MDA-MB-435 cells.

### 3.2.2.7 *In vitro* uptake of As<sup>III</sup>-encapsulated micelles

To verify that GRGDS-amide decoration on micelle surface can realize selective delivery of arsenic to target tumor cells, cellular uptake of arsenic by MDA-MB-435 and MCF10A cells with and without pretreatment of free GRGDS-amide peptide was evaluated.

MCF10A cells had similar As uptake when treated by either free or encapsulated As<sup>III</sup> at equivalent arsenic concentration of 20 μM (P=0.0595, One-way ANOVA) (**Figure 3.16**). The arsenic uptake by cells with and without 1 h pretreatment of GRGDS-amide (1 mg/mL) were analyzed using t-test. There was no significant difference in arsenic uptake in each type of arsenic formulation. The uptake result confirmed that similar amounts of As<sup>III</sup>, in free form or in

encapsulation form, in non-mixed micelles or mixed micelles, with or without GRGDS-amide decoration on the micelle surface, are taken up by MCF10A cells.

Since the  $IC_{50}$  values of PMM, CMM, PEO-*b*-P(CCLC<sub>6</sub>-S-As<sup>III</sup>), and free As<sup>III</sup> against MDA-MB-435 cells were different and ranged from 15  $\mu$ M to 30  $\mu$ M, cellular uptake of free and encapsulated As<sup>III</sup> with two sets of equivalent arsenic treatment concentrations, i.e., 10  $\mu$ M and 20  $\mu$ M, were evaluated. Elevated arsenic treatment concentration increased arsenic cellular uptake. However, the increase in arsenic uptake was not proportional to the increase of treated arsenic concentration. The arsenic uptake in cells treated with PMM and free As<sup>III</sup> of 20  $\mu$ M was increased to ~5 times of the arsenic uptake when treated at 10  $\mu$ M. The arsenic uptake in cells treated with CMM was increased to 3 times and in cells treated with PEO-*b*-P(CCLC<sub>6</sub>-S-As<sup>III</sup>) was increased to 1.5 times. At 10  $\mu$ M treatment level, the non-mixed micelle formulation had highest arsenic uptake among the As<sup>III</sup>-encapsulated micelles, while at 20  $\mu$ M treatment level PMM had highest arsenic uptake.

The difference in the arsenic uptake increment is most probably related to the cell biology, as the conditions of cells changed when the arsenic treatment concentration increased from 10  $\mu$ M to 20  $\mu$ M.

At the 10  $\mu$ M treatment level, the arsenic treatment concentration was smaller than the  $IC_{50}$  values of all four types of arsenic formulation. The majority of cells remained viable after 24 h treatment of arsenic. The soluble protein concentrations in the lysates of cells treated with arsenic were not significantly different from each other ( $P=0.0196$ , One-way ANOVA), and the protein concentration was ~ 90% the protein concentration in lysates of cells with no arsenic treatment, which was the negative control. Non-mixed micelles had the highest arsenic concentration in the cell lysate, which was 3 times of the arsenic concentration in the cell lysate of the free As<sup>III</sup> group.

PMM and CMM had slightly higher arsenic concentration in the cell lysate, ~ 1.3 times of the free As<sup>III</sup> group. Encapsulation of As<sup>III</sup> enhanced arsenic cellular uptake when the treated arsenic did not induce massive cell apoptosis. The high burst release in mixed micelles may be the reason for minor enhancement of arsenic cellular uptake.

When the cells were treated with arsenic formulations at the 20  $\mu$ M level, which reached the IC<sub>50</sub> concentration of CMM and was higher than IC<sub>50</sub> of PMM and free As<sup>III</sup>, around half of the seeded cells were dead after 24 h treatment. The lysate of cells treated with PMM, CMM, and free As<sup>III</sup> had similar protein concentrations (P = 0.2386, One-way ANOVA), which was ~55% of the protein concentration in the negative control samples. The IC<sub>50</sub> concentration of PEO-*b*-P(CCLC<sub>6</sub>-S-As<sup>III</sup>) was higher than 20  $\mu$ M. The lysate protein concentration in the group of non-mixed micelles was 83% of the negative control. Therefore, the cell conditions were different when cells were treated with different arsenic formulation though with same equivalent arsenic concentration.

Arsenic cellular uptake by MDA-MB-435 cells at shorter arsenic treatment duration, i.e., 3h, was evaluated as well (**Figure 3.18**). The arsenic treatment level was 10  $\mu$ M. Arsenic uptake in encapsulated As<sup>III</sup> groups was slower than free As<sup>III</sup> at the early stage of incubation. Free As<sup>III</sup> had highest arsenic uptake after 3 h of incubation, followed by PMM and CMM, and PEO-*b*-P(CCLC<sub>6</sub>-S-As<sup>III</sup>) has lowest arsenic uptake. However, considering non-mixed micelles had highest cellular uptake after 24 h, we anticipate that the majority of the arsenic uptake at shorter incubation duration is attributed to free As<sup>III</sup> released from micelles and the majority of arsenic uptake at longer incubation duration is attributed to encapsulated As<sup>III</sup>.

The pretreatment of GRGDS-amide can saturate the  $\alpha_v\beta_3$  integrin overexpressed on the membrane of MDA-MB-435 cells. We observed cell detachment from the cell culture dish after 1 hour of pretreatment of 1 mg/mL GRGDS-amide. The free peptide pretreatment was expected to

decrease the arsenic uptake in the group of PMM but to have no effect on the arsenic uptake in the free As<sup>III</sup> group and encapsulated As<sup>III</sup> groups without peptide decoration on the micelle surface. However, no significant difference of arsenic cellular uptake was observed in cells with or without pretreatment of free peptide (**Figure 3.19**). Possible reasons include but are not limited to (a) cell detachment caused by peptide pretreatment and (b) high arsenic burst release in mixed micelles. The cell detachment in pretreated groups increased loss of cells during cell harvest procedures, which introduced large standard deviation to the quantification of arsenic concentration. Meanwhile, the cell detachment may affect arsenic/micelle uptake pathway. The high arsenic burst release in mixed micelles means that a large portion of As<sup>III</sup> in mixed micelle solutions was in the free form. The uptake of free As<sup>III</sup> is a facilitated diffusion process, which occurs mainly through aquaporin-9 and aquaporin-7. (Leslie 2012) However, the uptake of encapsulated As<sup>III</sup> occurs through endocytosis of the micelles. When As<sup>III</sup> is prematurely released from the micelles before the micelles enters into cells, the peptide decoration on the micelle surface will not control the uptake of pre-released As<sup>III</sup>.

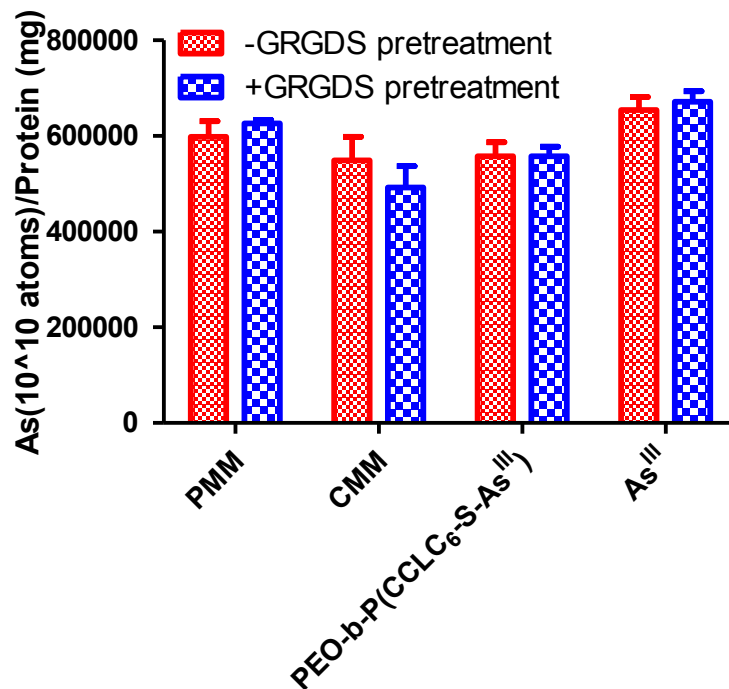


Figure 3.16. Cellular uptake of free and encapsulated As<sup>III</sup> by control cell line MCF10A cells, with and without 1 h pretreatment of free GRGDS-amide (1 mg/mL).

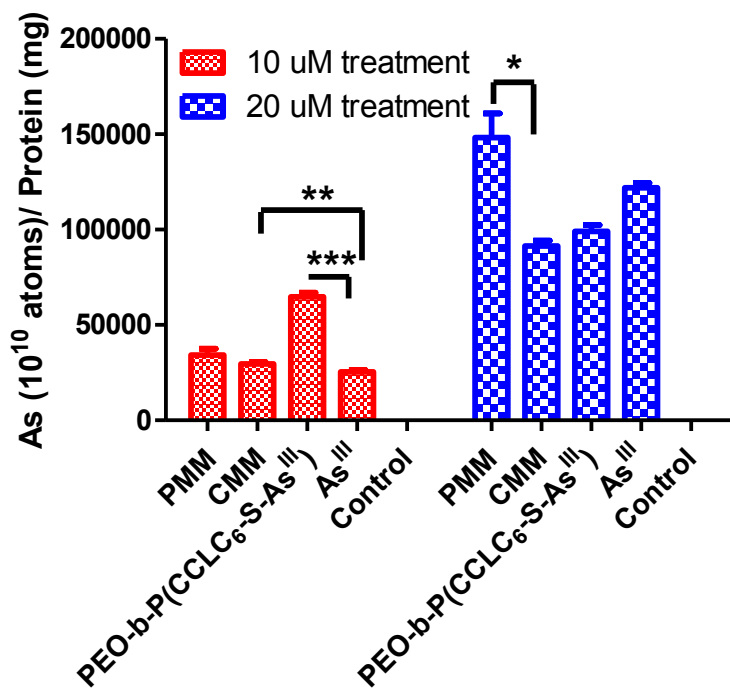


Figure 3.17. Cellular uptake of free and encapsulated As<sup>III</sup> by target cell line MDA-MB-435 cells at 24 h treatment. (\*: P<0.05, \*\*: P<0.01, \*\*\*: P <0.001, t-test)

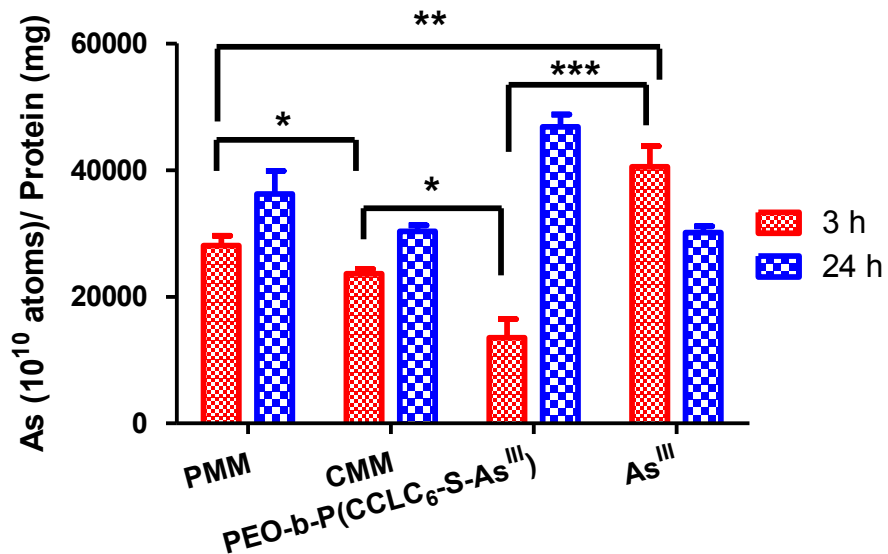


Figure 3.18. Cellular uptake of free and encapsulated As<sup>III</sup> (10  $\mu$ M) by MDA-MB-435 cells at different treatment concentration and treatment duration.

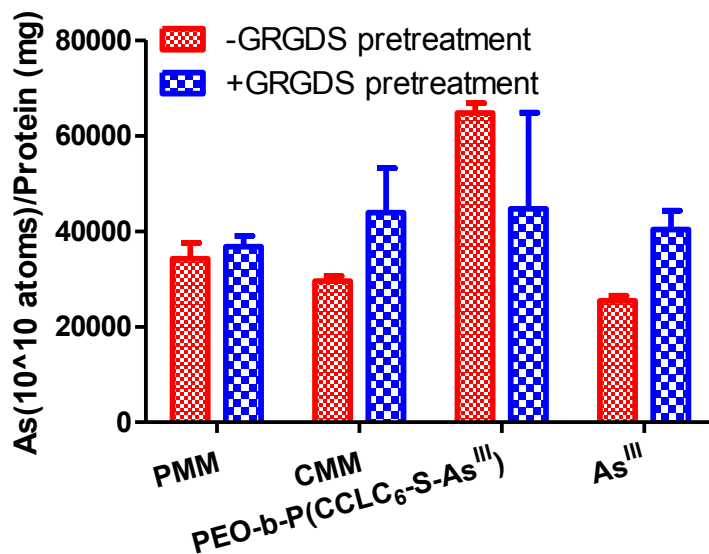


Figure 3.19. Cellular uptake of free and encapsulated As<sup>III</sup> (10  $\mu$ M) by MDA-MB-435 cells with or without 1 h pretreatment of free GRGDS-amide (1 mg/mL) after 24 h arsenic treatment duration.

### 3.3 Different mixed micelles for arsenic encapsulation

The arsenic encapsulated micelles formed by mixing PEO-*b*-PCCL<sub>17</sub> and PEO-*b*-P(CCLC<sub>6</sub>-SH)<sub>17</sub> showed high burst release of arsenic. The high arsenic burst release caused a severe pre-mature arsenic release problem, which weakened the selective delivery of arsenic to target cells. To solve this problem, different mixed micelles formed by mixing PEO-*b*-P(CCLC<sub>6</sub>-SH) with PEO-*b*-PBCL, PEO-*b*-PCL, PEO-*b*-P(D,L-LA), and PEO-*b*-PCCL with shorter hydrophobic block length were tested for arsenic encapsulation. *In vitro* release of arsenic from these mixed micelles was evaluated thoroughly.

#### 3.3.1 Methods

##### 3.3.1.1 Synthesis of block copolymers

PEO-*b*-PCL, PEO-*b*-PBCL, and PEO-*b*-P(D,L-LA) was synthesized by ring opening polymerization. Briefly, monomethoxy PEO<sup>5000</sup> (200 mg, 0.04 mmol) was reacted with CL (46 mg, 0.4 mmol; or 23 mg, 0.2 mmol), or BCL (99 mg, 0.4 mmol), or meso-lactide (30 mg, 0.2 mmol; or 15 mg, 0.1 mmol) at 140 °C under vacuum for 4 h. The reaction was catalyzed by stannous octoate. The block copolymer products were purified by dissolution in CH<sub>2</sub>Cl<sub>2</sub> and precipitation in diethyl ether. PEO<sup>5000</sup>-*b*-PCCL<sub>10</sub> was synthesized using the same method described in **Section 3.2.1.3**. The composition of block copolymers was confirmed by <sup>1</sup>H-NMR spectrometry.

##### 3.3.1.2 Preparation and *in vitro* release analysis of mixed micelles encapsulated with As<sup>III</sup>

The mixed micelles encapsulated with As<sup>III</sup> were prepared using the same method described in **Section 3.2.1.6**. Briefly, PEO<sup>5000</sup>-*b*-PCCL<sub>17</sub> (50 mg, 6.78 μmol) was first conjugated with mercaptohexylamino groups. The freshly synthesized PEO-*b*-P(CCLC<sub>6</sub>-SH) was then mixed with another block copolymer with no thiol functionality at a molar ratio of 3:1 in THF. The mixed polymer solution was then added dropwise into CH<sub>3</sub>COONH<sub>4</sub> buffer containing NaAsO<sub>2</sub> and

TCEP for As<sup>III</sup> encapsulation. The micelles were purified by dialysis against water and lyophilized for further use.

The arsenic loading was determined by ICP-MS and the sulfur content in micelles was determined by elemental analysis. *In vitro* release of arsenic from these mixed micelles was evaluated using same method described in **Section 3.2.1.8**.

### 3.3.2 Results

#### 3.3.2.1 Synthesis of PEO-*b*-PCL, PEO-*b*-PBCL, PEO-*b*-PDLLA, and PEO-*b*-PCCL

Monomethoxy PEO<sup>5000</sup> was used as the macro-initiator to synthesize block copolymers, i.e., PEO-*b*-PCL, PEO-*b*-PBCL, PEO-*b*-P(D,L-LA), and PEO-*b*-PCCL. The composition of block copolymers were confirmed with <sup>1</sup>H-NMR spectra (**Figure 3.20** to **Figure 3.25**).

A typical <sup>1</sup>H-NMR spectrum of PEO-*b*-PCL showed proton peaks at  $\delta$  (ppm) 4.05 (t, 2H per CL unit), 3.64 (m, 4H per ethylene oxide unit), 3.37 (s, 3H), 2.30 (t, 2H per CL unit), and 1.64–1.36 (m, 6 H per CL unit). The integral of the area under the peak at  $\delta$  4.05 and that under the peak at  $\delta$  3.64 were used to calculate the DP of PCL block. In this study, two sets of PEO-*b*-PCL with different DP of CL were synthesized, namely PEO<sup>5000</sup>-*b*-PCL<sub>10</sub> and PEO<sup>5000</sup>-*b*-PCL<sub>6</sub>.

A typical <sup>1</sup>H-NMR spectrum of PEO-*b*-PBCL showed proton peaks at  $\delta$  (ppm) 7.32 (m, 5H per BCL unit), 5.15 (m, 2H per BCL unit), 4.03 (m, 2H per BCL unit), 3.64 (m, 4H per ethylene oxide unit), 3.38 (s, 3H), 3.30 (m, 1H per BCL unit), and 1.88–1.27 (m, 6 H per BCL unit). The integral of the area under the peak at  $\delta$  4.03 and that under the peak at  $\delta$  3.64 were used to calculate the DP of PBCL block. In this study, PEO<sup>5000</sup>-*b*-PBCL<sub>6</sub> was synthesized.

A typical <sup>1</sup>H-NMR spectrum of PEO-*b*-P(D,L-LA) showed proton peaks at  $\delta$  (ppm) 5.18 (m, 1H per LA unit), 3.64 (m, 4H per ethylene oxide unit), and 1.54 (m, 3 H per LA unit). The integral of the area under the peak at  $\delta$  5.18 and that under the peak at  $\delta$  3.64 were used to calculate the DP

of P(D,L-LA) block. In this study, two sets of PEO-*b*-P(D,L-LA) with different DP of LA were synthesized, namely PEO<sup>5000</sup>-*b*-P(D,L-LA)<sub>8</sub> and PEO<sup>5000</sup>-*b*-P(D,L-LA)<sub>4</sub>.

A typical <sup>1</sup>H-NMR spectrum of PEO-*b*-PCCL showed proton peaks at δ (ppm) 4.13 (m, 2H per CCL and BCL unit), 3.64 (m, 4H per ethylene oxide unit), 3.37 (s, 3H), 3.36 (m, 1H per CCL unit), and 1.91–1.42 (m, 6 H per CCL unit). Peaks at δ 7.31 and 5.14 belonged to residual benzyl groups from incomplete reduction of PEO-*b*-PBCL. The integral of area under the peak at δ 4.13 and that under the peak at δ 3.64 were used to calculate the DP of PCCL block. The integral of area under the peak at δ 5.14 (m, 2H per BCL unit) and that under the peak at δ 4.13 was used to calculate the percentage of non-reduced BCL blocks in PEO-*b*-PCCL. Here in this experiment, the final PEO<sup>5000</sup>-*b*-PCCL<sub>10</sub> contained 8% residual BCL blocks and the quality of PEO-*b*-PCCL was satisfactory.

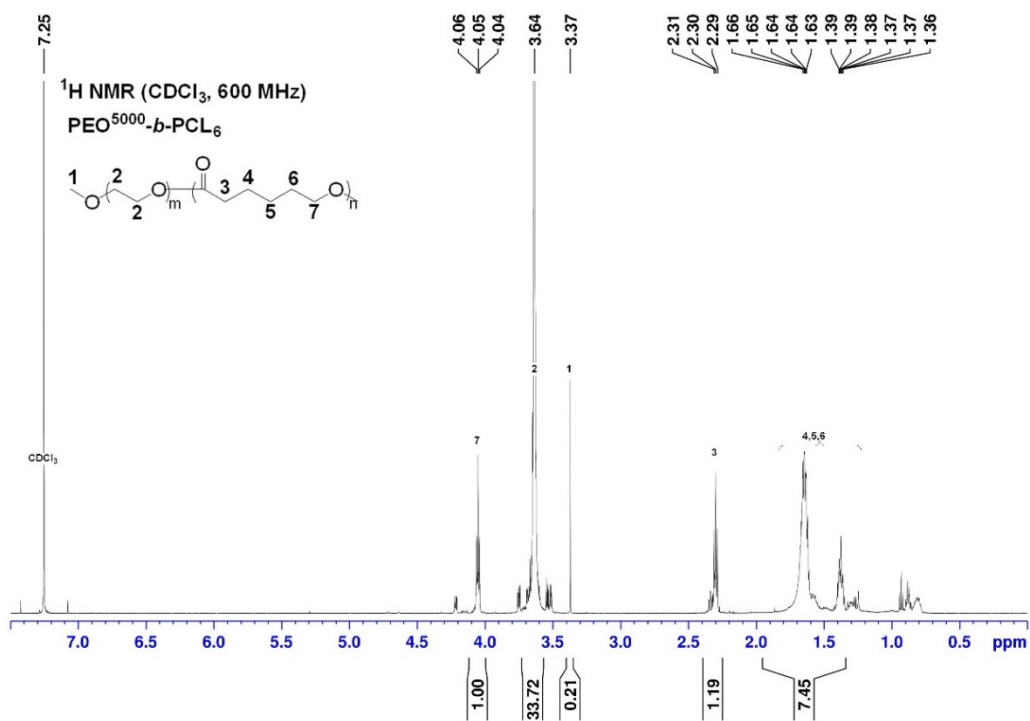


**Figure 3.20.** <sup>1</sup>H-NMR of PEO<sup>5000</sup>-*b*-PCL<sub>6</sub> in CDCl<sub>3</sub>.

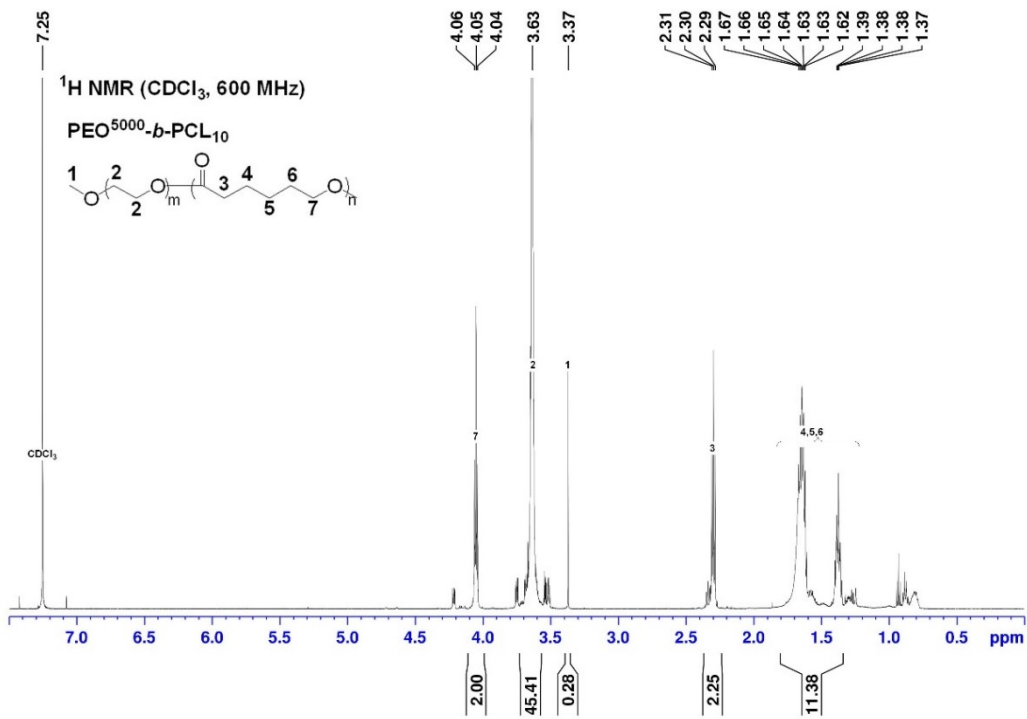


Figure 3.21. <sup>1</sup>H-NMR of PEO<sup>5000</sup>-*b*-PCL<sub>10</sub> in CDCl<sub>3</sub>.

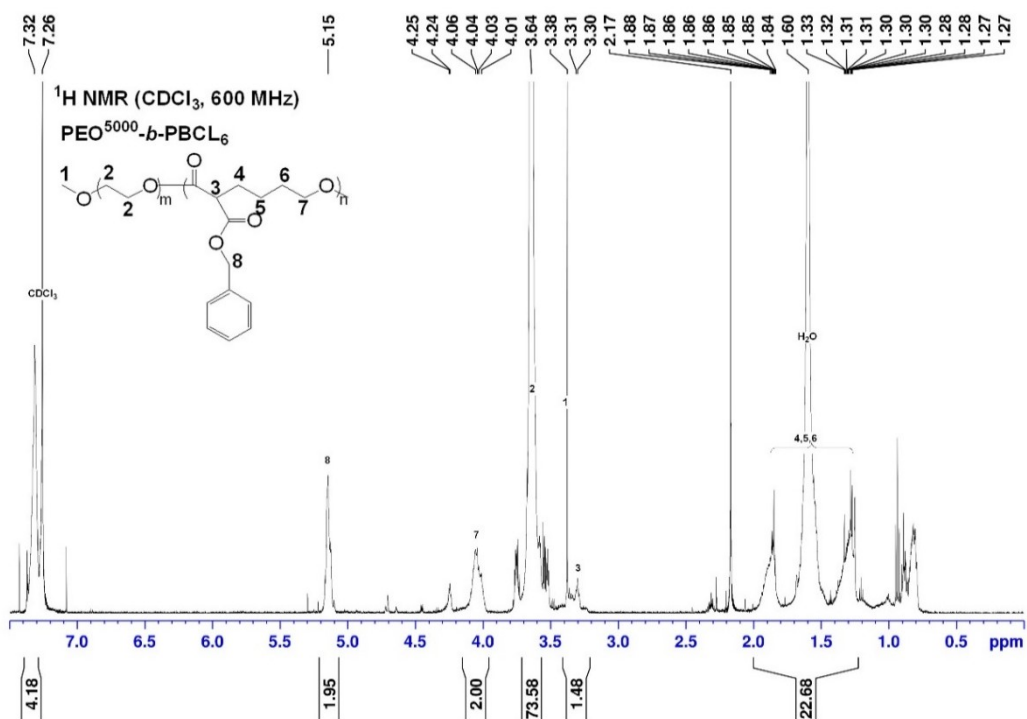


Figure 3.22. <sup>1</sup>H-NMR of PEO<sup>5000</sup>-*b*-PBCL<sub>6</sub> in CDCl<sub>3</sub>.

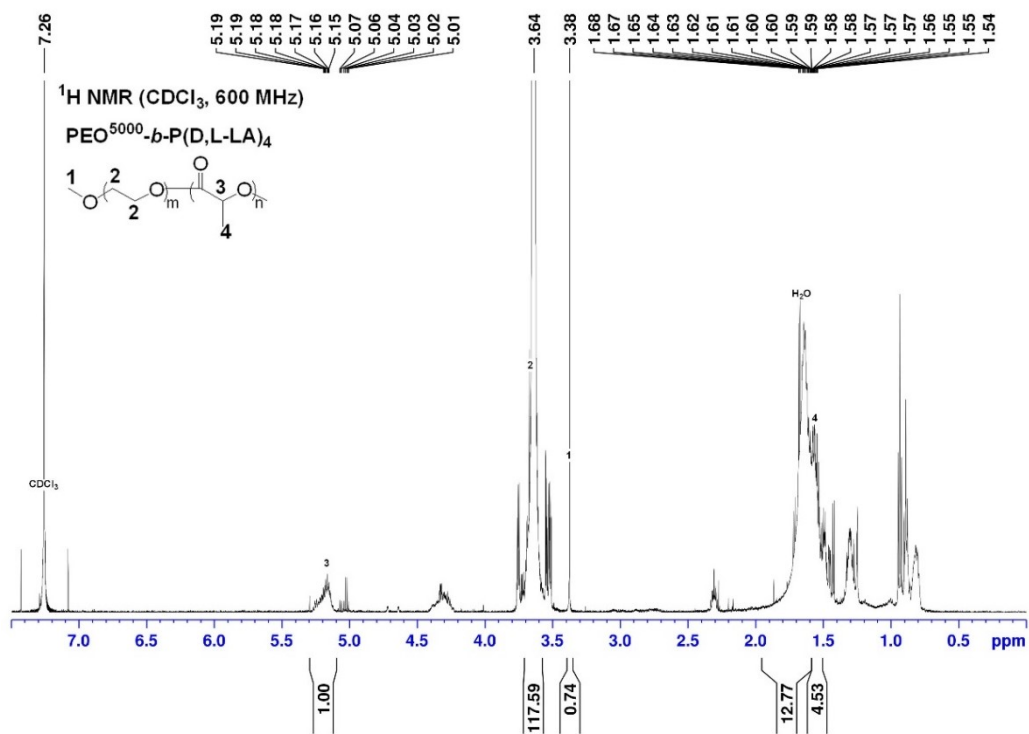


Figure 3.23. <sup>1</sup>H-NMR of PEO<sup>5000</sup>-*b*-P(D,L-LA)<sub>4</sub> in CDCl<sub>3</sub>.

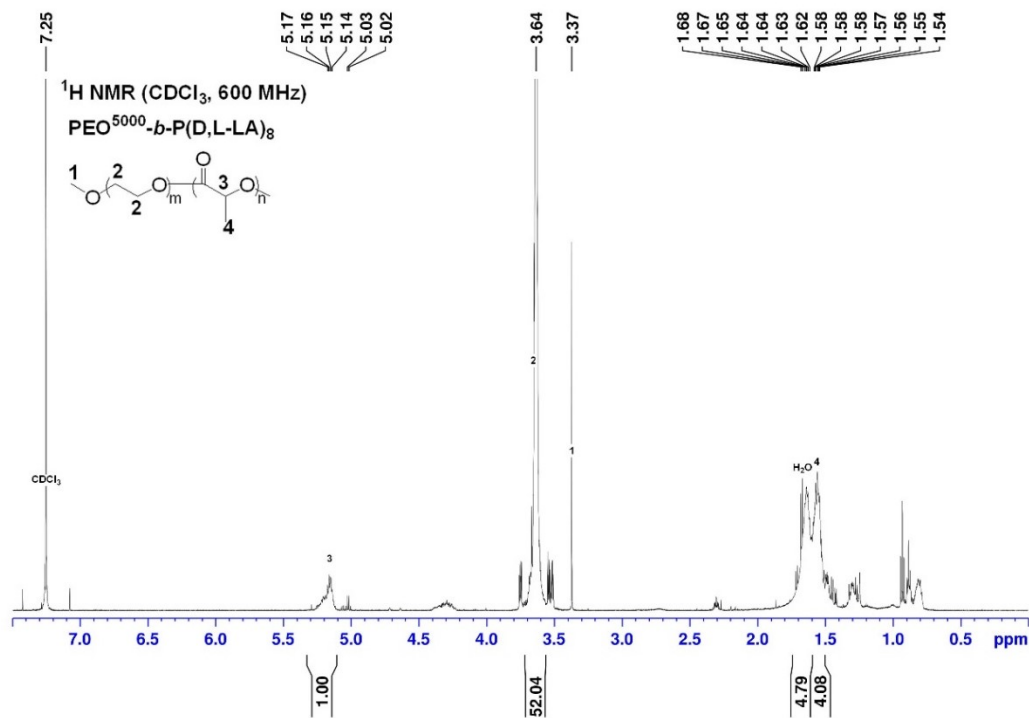
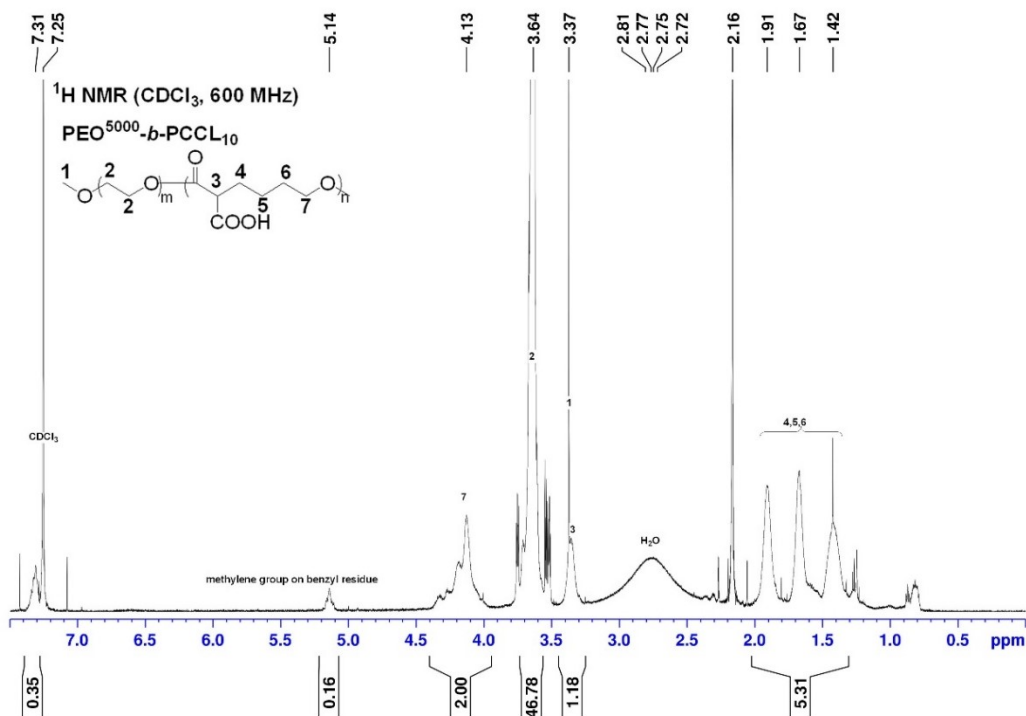


Figure 3.24. <sup>1</sup>H-NMR of PEO<sup>5000</sup>-*b*-P(D,L-LA)<sub>8</sub> in CDCl<sub>3</sub>.



**Figure 3.25.** <sup>1</sup>H-NMR of PEO<sup>5000</sup>-*b*-PCCL<sub>10</sub> in CDCl<sub>3</sub>.

### 3.3.2.2 Arsenic loading in mixed micelles

Thiol-functionalized polymer PEO-*b*-P(CCLC<sub>6</sub>-SH)<sub>17</sub> was mixed with diblock polymers without thiol-functionality at a molar ratio or 3:1 for As<sup>III</sup> encapsulation. The arsenic loading in these mixed micelles was determined by ICP-MS analysis (**Figure 3.26**) and the sulfur content was determined by elemental analysis (**Figure 3.27**). The arsenic loading in different mixed micelles was compared and there was no difference with statistical significance ( $P=0.1462$ , one-way ANOVA). No difference was observed in the sulfur content of different mixed micelles ( $P=0.9043$ , one-way ANOVA). However, the arsenic loading in mixed micelles was significantly lower than that in the non-mixed micelle PEO-*b*-P(CCLC<sub>6</sub>-S-As<sup>III</sup>) ( $P<0.001$ , One-way ANOVA). The As/S molar ratio of mixed micelles varied from 0.30 to 0.49, which was smaller than the As/S ratio of the non-mixed micelle ( $\sim 0.67$ ).

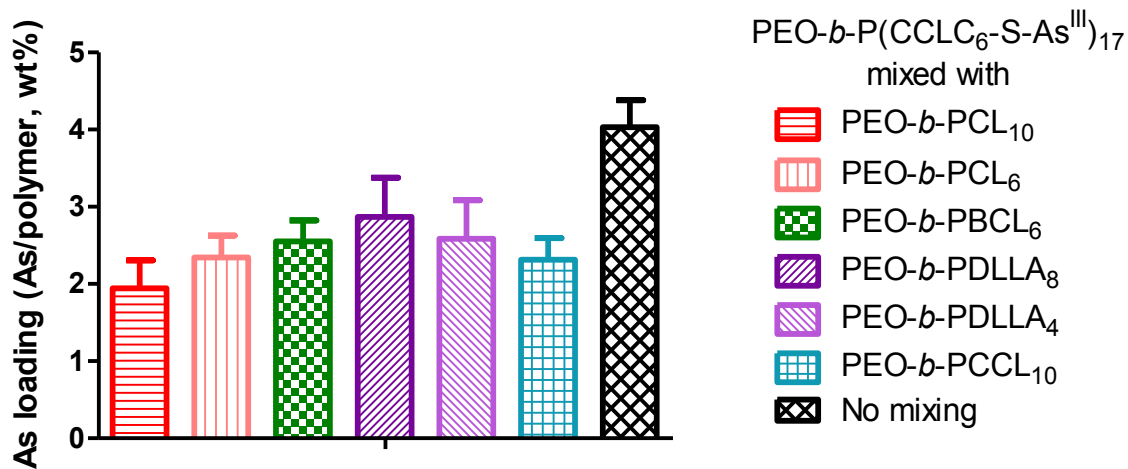


Figure 3.26. Arsenic loading in different mixed micelles.

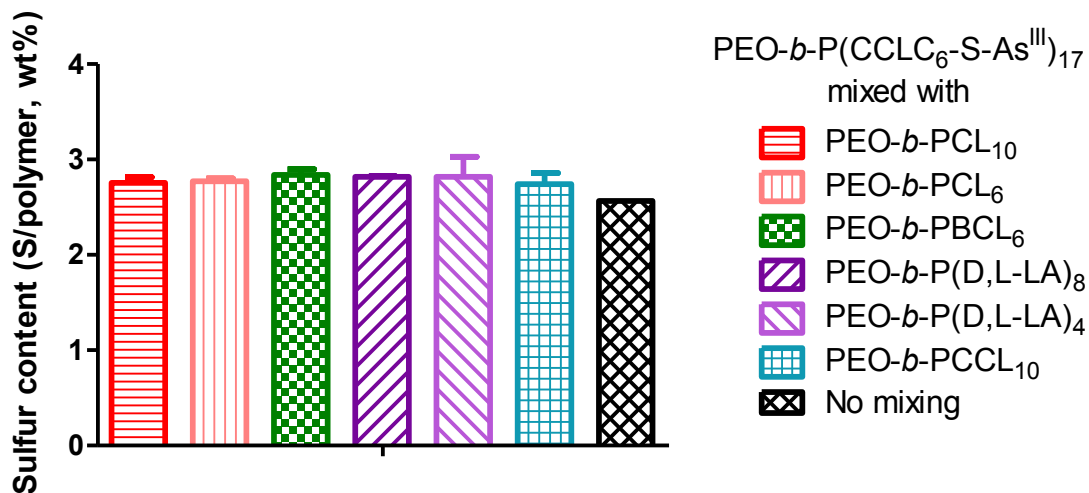


Figure 3.27. Sulfur content of different mixed micelles.

### 3.3.2.3 *In vitro* release of As<sup>III</sup> from mixed micelles

*In vitro* As<sup>III</sup> release from mixed micelles was carried out in RPMI-1640 cell culture medium supplemented with 10% FBS at 37 °C. The release profile of the mixed micelle system was compared to the non-mixed micelle system.

PEO-*b*-PCCL<sub>10</sub>, which had a shorter PCCL block than the PEO-*b*-PCCL<sub>17</sub> used in **Section 3.2.1.6** for CMM preparation, was mixed with PEO-*b*-P(CCLC<sub>6</sub>-SH) for As<sup>III</sup> encapsulation. As

shown in **Figure 3.28**, the mixing with PEO-*b*-PCCL<sub>10</sub> reduced burst As<sup>III</sup> release compared to the mixing with PEO-*b*-PCCL<sub>17</sub>, and the burst As<sup>III</sup> release of PEO-*b*-PCCL<sub>10</sub>/PEO-*b*-P(CCLC<sub>6</sub>-S-As<sup>III</sup>) was the same as the non-mixed micelle. The shorter hydrophobic chain may have less influence on the micelle core local environment for As-S bond formation. However, the release speed of mixed micelles was faster than that of non-mixed micelles during the first 3 h incubation.

PEO-*b*-P(D,L-LA) (**Figure 3.29**) and PEO-*b*-PCL (**Figure 3.30**) polymers with different DP of the hydrophobic block were used to prepared mixed micelles for As<sup>III</sup> encapsulation. Micelles mixed with either PEO-*b*-P(D,L-LA)<sub>8</sub> or PEO-*b*-P(D,L-LA)<sub>4</sub> had similar As<sup>III</sup> release profile, and the burst release was similar to non-mixed micelles. However, the As<sup>III</sup> release from these two types of mixed micelles was faster than that of non-mixed micelles. Micelles mixed with either PEO-*b*-PCL<sub>10</sub> or PEO-*b*-PCL<sub>7</sub> has similar release profiles as well and shared the properties of low burst release and fast release rate. The accumulative As<sup>III</sup> release from mixed micelles was higher than that of non-mixed micelles after 3 hours of incubation. However, the micelles mixed with PEO-*b*-PCL has less burst release than micelles mixed with PEO-*b*-P(D,L-LA).

*In vitro* release from micelles mixed with PEO-*b*-PBCL<sub>6</sub> was evaluated as well. PEO-*b*-PBCL<sub>6</sub>/PEO-*b*-P(CCLC<sub>6</sub>-S-As<sup>III</sup>) had lowest burst release among 7 types of mixed micelles tested in this study. Though the release rate was faster from mixed micelles than non-mixed micelles, accumulative As<sup>III</sup> release from PEO-*b*-PBCL<sub>6</sub>/PEO-*b*-P(CCLC<sub>6</sub>-S-As<sup>III</sup>) was similar to non-mixed micelles over 12 h of incubation.

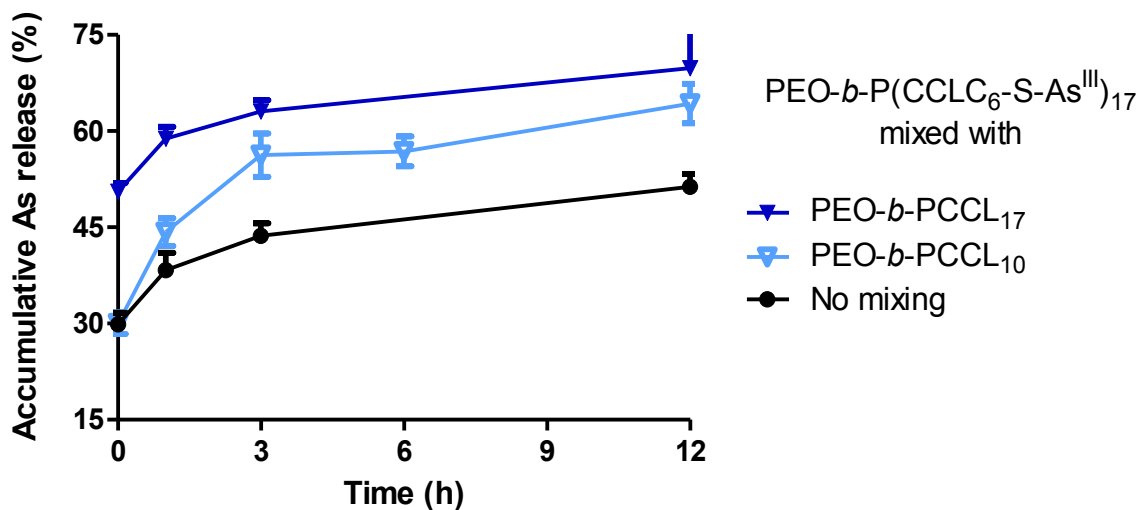


Figure 3.28. *In vitro* arsenic release from PEO-*b*-PCCL/PEO-*b*-P(CCLC<sub>6</sub>-S-As<sup>III</sup>) mixed micelle.

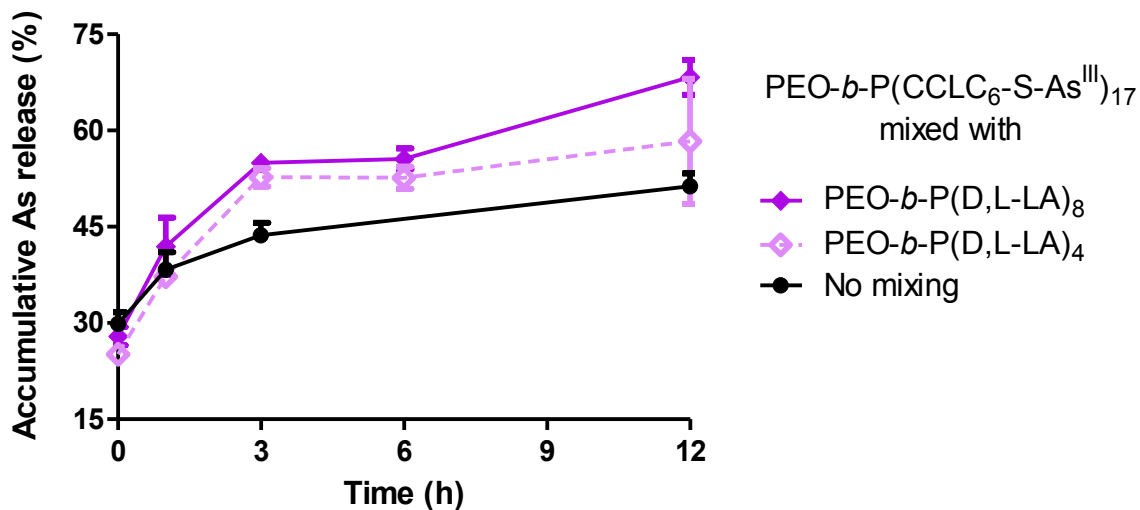


Figure 3.29. *In vitro* arsenic release from PEO-*b*-P(D,L-LA)/PEO-*b*-(CCLC<sub>6</sub>-S-As<sup>III</sup>) mixed micelles with different DP of P(D,L-LA).

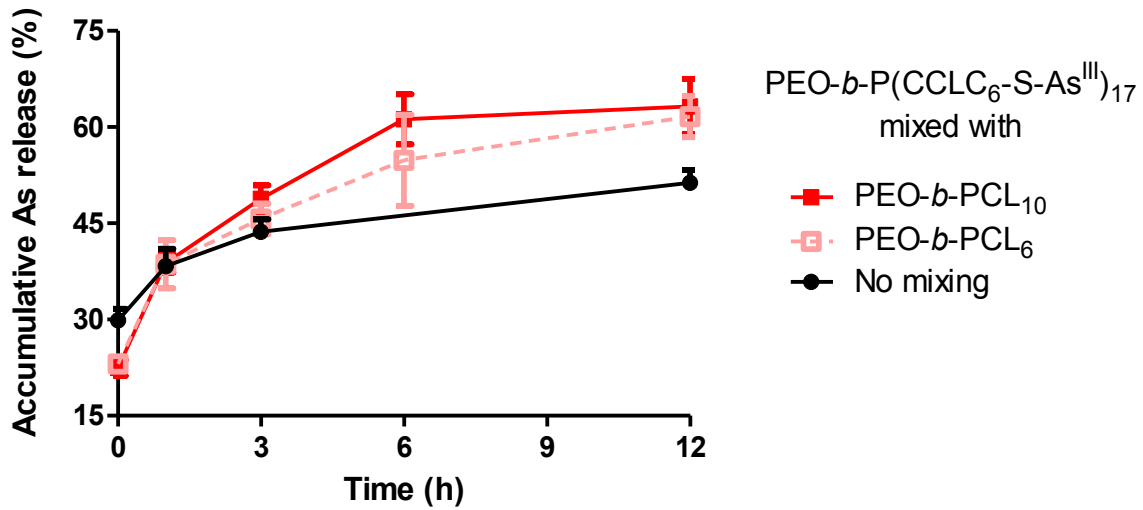


Figure 3.30. *In vitro* arsenic release from PEO-*b*-PCL/PEO-*b*-P(CCLC<sub>6</sub>-S-As<sup>III</sup>)<sub>17</sub> mixed micelles with different DP of PCL.

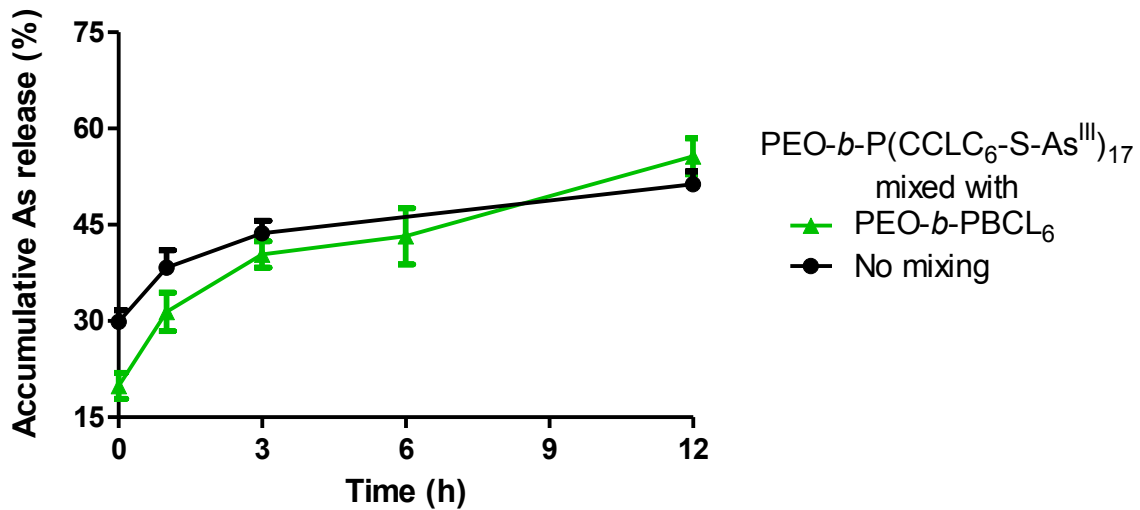


Figure 3.31. *In vitro* arsenic release from PEO-*b*-PBL<sub>6</sub>/PEO-*b*-P(CCLC<sub>6</sub>-S-As<sup>III</sup>)<sub>17</sub> mixed micelle.

### 3.4 Discussion

The aim of this study is to selectively deliver arsenic compounds to target cells by decorating the micelle surface with affinity ligands. To circumvent the challenge in modifying the block copolymer backbone with both thiol and peptide functionalities on the same polymer chain, we mixed two batches of PEO-*b*-PCCL<sub>17</sub> polymers, one batch with mercaptohexylamino pendant groups on PCCL block (PEO-*b*-P(CCLC<sub>6</sub>-SH)), and the other batch bearing GRGDS-amide groups on the end of PEO block (PCCL-*b*-PEO-GRGDS-amide), to prepare mixed micelles for As<sup>III</sup> encapsulation.

The arsenic loading in mixed micelles was less than those in non-mixed micelles. The mixing of PEO-*b*-P(CCLC<sub>6</sub>-SH) with another block copolymer without thiol functionality on the PCCL block reduces the total sulfur content in the micelles as formed. Because encapsulation of arsenic into micelles depends on the interaction between arsenical and thiol groups existing in the micelle core, reduced sulfur content in the micelles decreases the arsenic loading. We calculated the As/S molar ratio based on the arsenic loading and sulfur content in the micelles and found that mixed micelles and non-mixed micelles had similar As/S molar ratios.

In order to demonstrate that the peptide decoration on micelle surface can achieve selective arsenic delivery to the target cell line MDA-MB-435 instead of the control cell line MCF10A, we evaluated *in vitro* cytotoxicity and cellular uptake of PMM, CMM, PEO-*b*-P(CCLC<sub>6</sub>-S-As<sup>III</sup>) and free As<sup>III</sup> in these two cell lines. MDA-MB-435 cells were more sensitive to the treatment of As<sup>III</sup>. MCF10A cells can take up more arsenic than MDA-MB-435 cells when treated at the same arsenic concentration, and the IC<sub>50</sub> value of free As<sup>III</sup> against MCF10A cells was larger than that against MDA-MB-435 cells.

When treating MCF10A cells, the encapsulated As<sup>III</sup> formulations had IC<sub>50</sub> values and cellular arsenic uptake amount with no statistical difference compared to free As<sup>III</sup>. When MDA-MB-435 cells were treated, however, encapsulated As<sup>III</sup> was generally less cytotoxic than free As<sup>III</sup>, especially the formulation of the non-mixed micelle PEO-*b*-P(CCLC<sub>6</sub>-S-As<sup>III</sup>). The peptide decoration on the micelle can enhance the cytotoxicity of encapsulated As<sup>III</sup>. The IC<sub>50</sub> value of PMM had no statistical difference compared to free As<sup>III</sup>. One may argue the enhanced cytotoxicity of PMM compared to PEO-*b*-P(CCLC<sub>6</sub>-S-As<sup>III</sup>) is due to high arsenic burst release from the mixed micelles, thus cytotoxicity is induced by pre-released As<sup>III</sup> in the free form. PMM and CMM did have high burst release (~50% of total encapsulated As<sup>III</sup>) compared to the non-mixed PEO-*b*-P(CCLC<sub>6</sub>-S-As<sup>III</sup>) (~30% of total encapsulated As<sup>III</sup>). However, although PMM and CMM had similar burst release percentage and overall accumulative arsenic release over 24 hours, the IC<sub>50</sub> of PMM was lower than that of CMM with statistical significance (P=0.0008). The difference in the IC<sub>50</sub> values of PMM and CMM with similar release profiles suggests that GRGDS-amide decoration on micelle surface is playing a role in the delivery of As<sup>III</sup> and cytotoxicity induction.

High arsenic burst release from the mixed micelles influences cellular uptake of arsenic by MDA-MB-435 cells. The arsenic cellular uptake in the group of PEO-*b*-P(CCLC<sub>6</sub>-S-As<sup>III</sup>) was ~2.5 times of the group of free As<sup>III</sup> when MDA-MB-435 cells were treated with equivalent arsenic concentration of 10 μM for 24 h. While PMM and CMM had minor enhanced arsenic cellular uptake compare to free As<sup>III</sup> (134%, P=0.0503; 116%, P=0.0097, respectively), the pre-released arsenic in PMM and CMM treatment solution contributed a major part of the arsenic taken up by MDA-MB-435 cells. A shorter arsenic treatment duration of 3 h was tested in the arsenic cellular uptake evaluation study (As treatment concentration: 10 μM). Interestingly we observed lower arsenic cellular uptake in encapsulated As<sup>III</sup> groups compared to free As<sup>III</sup> (PMM: 69%, P=0.0199;

CMM: 58%,  $P=0.0128$ ; PEO-*b*-P(CCLC<sub>6</sub>-S-As<sup>III</sup>): 33%,  $P=0.0004$ ). The observation that encapsulated As<sup>III</sup> had lower cellular uptake at shorter treatment duration while it had higher cellular uptake at longer treatment duration suggests that the uptake of free As<sup>III</sup> is faster than that of encapsulated As<sup>III</sup> and reaches uptake plateau more quickly than encapsulated As<sup>III</sup>. Regardless of high arsenic burst release from mixed micelles, PMM tends to have higher arsenic cellular uptake than CMM (3 h: 119%,  $P=0.0199$ ; 24 h: 116%,  $P=0.1512$ ), confirming that the GRGDS-amide decoration on micelle surface influences cellular uptake of As<sup>III</sup> by MDA-MB-435 cells.

To further verify that the peptide decoration on the micelle enhances delivery of As<sup>III</sup> to the target tumor cells, a competitive cellular uptake study was carried out. The arsenic cellular uptake by MDA-MB-435 cells with or without 1 h pretreatment of 1 mg/mL free GRGDS-amide were compared. A reduced cellular uptake of PMM by cells pretreated with free peptide was expected as the pretreated free peptide saturated  $\alpha_v\beta_3$  integrin overexpressed on the cell membrane. However, no difference in the cellular uptake after 24 h treatment of encapsulated or free As<sup>III</sup> with equivalent arsenic concentration of 10  $\mu\text{M}$  was observed. The high arsenic burst release from mixed micelles may weaken the role of conjugated GRGDS-amide in targeted delivery of encapsulated As<sup>III</sup>.

To reduce the burst release of arsenic from mixed micelles, other block copolymers with shorter hydrophobic block and more hydrophobic backbone were tested to form mixed micelles with PEO-*b*-P(CCLC<sub>6</sub>-SH) for As<sup>III</sup> encapsulation. The micelle mixed with PEO-*b*-PCCL<sub>10</sub>, which had a shorter PCCL block than PEO-*b*-PCCL<sub>17</sub>, had substantially reduced burst release ( $\sim 30\%$  of total encapsulated arsenic) compared to the micelle mixed with PEO-*b*-PCCL<sub>17</sub> ( $\sim 50\%$  of total encapsulated arsenic). The shorter hydrophobic chain may cause less interference to the local environment of thiol groups inside the micelle core for arsenic binding. When the DP of the

hydrophobic block was shorter than 10, the reduction in the length of the hydrophobic block did not further reduce the burst release. Micelles mixed with PEO-*b*-P(D,L-LA)<sub>8</sub> or PEO-*b*-P(D,L-LA)<sub>4</sub> had similar burst release and overall accumulative arsenic release profile. The same observation was made with micelles mixed with PEO-*b*-PCL<sub>10</sub> or PEO-*b*-PCL<sub>6</sub>. Micelles mixed with PEO-*b*-PBCL<sub>6</sub> had the lowest burst release and slowest arsenic release among all mixed micelles tested over 12 h incubation in RPMI-1640 cell culture medium supplemented with 10% FBS at 37 °C.

### 3.5 Conclusion

Mixed micelles formed by PEO-*b*-P(CCLC<sub>6</sub>-SH) and PCCL<sub>17</sub>-*b*-PEO-GRGDS-amide polymers were prepared for selective arsenic delivery to the target cell line MDA-MB-435. The mixed micelles with peptide decoration on the surface showed higher cytotoxicity and enhanced cellular arsenic uptake compared to mixed micelles without peptide decoration on the surface. However, burst release of arsenic from these types of mixed micelles was substantially higher than that in non-mixed micelles. The fast burst release weakens the function of decorated peptide in targeted delivery of encapsulated arsenic to target cells. Different block copolymers with shorter hydrophobic chain and more hydrophobic backbone design were tested to form arsenic encapsulated micelles. Micelles mixed with PEO-*b*-PBCL<sub>6</sub> showed the lowest burst release and the slowest accumulative arsenic release over 12 h, which was comparable to non-mixed micelles. Peptide decorated mixed micelles formed by PEO-*b*-P(CCLC<sub>6</sub>-SH) and PBCL<sub>6</sub>-*b*-PEO-GRGDS-amide may be a better drug carrier candidate for targeted delivery of arsenic to the target cells.

### 3.6 References

- Duggan ME, Hutchinson JH. 2000. Ligands to the integrin receptor alpha(v)beta(3). *Expert Opinion on Therapeutic Patents* 10:1367-1383.
- Felding-Habermann B, Fransvea E, O'Toole TE, Manzuk L, Faha B, Hensler M. 2002. Involvement of tumor cell integrin alpha v beta 3 in hematogenous metastasis of human melanoma cells. *Clinical & Experimental Metastasis* 19:427-436.
- Leslie EM. 2012. Arsenic-glutathione conjugate transport by the human multidrug resistance proteins (mrps/abccs). *Journal of Inorganic Biochemistry* 108:141-149.
- Liu Z, Cai WB, He LN, Nakayama N, Chen K, Sun XM, et al. 2007. In vivo biodistribution and highly efficient tumour targeting of carbon nanotubes in mice. *Nature Nanotechnology* 2:47-52.
- Lu X, Lu D, Scully MF, Kakkar VV. 2006. Integrins in drug targeting-rgd templates in toxins. *Current Pharmaceutical Design* 12:2749-2769.
- Mahmud A, Xiong XB, Lavasanifar A. 2006. Novel self-associating poly(ethylene oxide)-block-poly(epsilon-caprolactone) block copolymers with functional side groups on the polyester block for drug delivery. *Macromolecules* 39:9419-9428.
- Nagasaki Y, Kutsuna T, Iijima M, Kato M, Kataoka K, Kitano S, et al. 1995. Formyl-ended heterobifunctional poly(ethylene oxide) - synthesis of poly(ethylene oxide) with a formyl group at one end and a hydroxyl group at the other end. *Bioconjugate Chemistry* 6:231-233.
- Price JE, Zhang RD. 1990. Studies of human breast-cancer metastasis using nude-mice. *Cancer and Metastasis Reviews* 8:285-297.
- Shen S, Li X, Cullen W, Weinfeld M, Le X. 2013. Arsenic binding to proteins. *Chemical Reviews* 113:7769-7792.
- Xiong XB, Mahmud A, Uludag H, Lavasanifar A. 2007. Conjugation of arginine-glycine-aspartic acid peptides to poly(ethylene oxide)-b-poly(epsilon-caprolactone) micelles for enhanced intracellular drug delivery to metastatic tumor cells. *Biomacromolecules* 8:874-884.

- Xiong XB, Mahmud A, Uludag H, Lavasanifar A. 2008. Multifunctional polymeric micelles for enhanced intracellular delivery of doxorubicin to metastatic cancer cells. *Pharmaceutical Research* 25:2555-2566.
- Zhang Q, Vakili MR, Li XF, Lavasanifar A, Le XC. 2014. Polymeric micelles for gsh-triggered delivery of arsenic species to cancer cells. *Biomaterials* 35:7088-7100.
- Zhu HH, Yalcin T, Li L. 1998. Analysis of the accuracy of determining average molecular weights of narrow polydispersity polymers by matrix-assisted laser desorption ionization time-of-flight mass spectrometry. *Journal of the American Society for Mass Spectrometry* 9:275-281.

## Chapter 4. Terpolymeric micelles for arsenic delivery with enhanced micelle stability and increased arsenic cellular uptake<sup>3</sup>

### 4.1 Introduction

As demonstrated in **Chapter 2** and **Chapter 3**, we modified the core-forming block of methoxy poly(ethylene oxide)-block-poly( $\alpha$ -carboxylic acid- $\epsilon$ -caprolactone) (PEO-*b*-PCCL) with a thiol-containing pendant group, mercaptohexylamine (NH<sub>2</sub>C<sub>6</sub>H<sub>12</sub>SH), and achieved high arsenic loading and triggered arsenic release. Though carboxylic acid (COOH) groups in PEO-*b*-PCCL provide a post-polymerization modification site in the block copolymer structure, the presence of COOH groups on the poly( $\epsilon$ -caprolactone) (PCL) backbone was shown to decrease the thermodynamic stability of micelles, perhaps because of a decrease in the hydrophobicity of the core-forming block (Aliabadi et al. 2005; Mahmud et al. 2006; Zhang et al. 2014).

Micelle stability is an important factor in successful delivery of the cargo to solid tumor targets *in vivo*, as it can affect the biodistribution, toxicity, and anti-tumor efficacy of the cargo (Wei et al. 2012). In this study, in order to mitigate the negative impact of carboxylic acid groups on micellar stability, we introduced unmodified caprolactone segments to the poly(ester) segment of the micelle-forming block copolymer. We hypothesized that the introduction of an unmodified caprolactone with higher hydrophobicity to the poly(ester) segment can compensate for the negative impact of the COOH group on micellar stability and result in the design of efficient terpolymer micelles for targeted delivery of As<sup>III</sup> to solid tumors.

---

<sup>3</sup> A manuscript was synthesized from the content in this chapter together with Section 3.2.1.5 and 3.2.2.3 in Chapter 3 and was submitted for publication.

In order to determine the micellar structures capable of targeted As<sup>III</sup> delivery, we investigated the influence of the block sequence of PEO/PCCL/PCL terpolymers on micellar stability, surface charge, and cellular As<sup>III</sup> uptake. Previous studies on the effect of block sequence and/or random versus block structure in triblock terpolymers on the characteristics of resulting micelles are limited (Cajot et al. 2011; Wyman and Liu 2013). To this end, we prepared three terpolymers with varied distribution of the unmodified caprolactone versus COOH-modified caprolactone in the PCL/PCCL segment. This included a block orientation in the poly(ester) segment, i.e., PEO-*b*-PCL-*b*-PCCL or PEO-*b*-PCCL-*b*-PCL block copolymers (shown as **ACB** and **ABC** polymers, respectively), and a random distribution, i.e., PEO-*b*-P(CL-*co*-CCL)<sub>ran</sub> (shown as **A(B/C)<sub>ran</sub>** polymers). We modified these three starting polymers with mercaptohexylamine and loaded As<sup>III</sup> into the terpolymeric micelles; then, we investigated the effect of terpolymer structure on micellar properties for As<sup>III</sup> delivery.

## 4.2 Materials and methods<sup>4</sup>

### 4.2.1 Materials and cell information

All the chemicals and reagents, unless specified, were purchased from Sigma-Aldrich (St. Louis, MO, USA). Caprolactone (CL) was purchased from Alfa Aesar (Heysham, Lancashire, UK) and  $\alpha$ -benzyl carboxylate- $\epsilon$ -caprolactone (BCL) from Alberta Research Chemicals Inc. (Edmonton, AB, Canada). Mercaptohexylamine hydrochloride was purchased from Annker Organics Co. Ltd. (Wuhan, Hubei, China).

---

<sup>4</sup> Dr. Mohammad R. Vakili and Dr. Afsaneh Lavasanifar provided insights in NMR spectrum interpretation. Ms. Arlene Oatway did the TEM analysis.

RPMI-1640 cell culture media and penicillin–streptomycin solution were purchased from Life Technologies (Grand Island, NY, USA). The MDA-MB-435 cancer cell line was originally received from the laboratory of Dr. R. Clarke, Georgetown University Medical School, Washington, DC, USA. The cells were cultured in RPMI 1640 medium with 10% fetal bovine albumin (FBA) and 1% penicillin–streptomycin solution at 37 °C and 5% CO<sub>2</sub>.

#### 4.2.2 Terpolymer synthesis and thiol functionalization

The terpolymers with block sequence of **ABC** and **ACB** were synthesized through a two-step sequential ring opening polymerization reaction, and the polymer with **A(B/C)<sub>ran</sub>** chain orientation was synthesized in a one-step bulk polymerization (**Scheme 4.1**). (Mahmud et al. 2006) Briefly, for the synthesis of PEO-*b*-PCCL-*b*-PCL (the **ABC** sequence), the macro-initiator methoxy PEO<sub>5000</sub> (0.5 g, 0.1 mmol) was exposed to  $\alpha$ -benzyl carboxylate- $\epsilon$ -caprolactone (BCL) (0.5 g, 2.0 mmol) and stannous octoate (4 drops) under vacuum at 145 °C for 4 to 6 h. The PEO-*b*-PBCL produced was then purified by solubilization in CH<sub>2</sub>Cl<sub>2</sub> and precipitation in cold ethyl ether. The purified PEO-*b*-PBCL was dried under vacuum and sent for NMR analysis. PEO-*b*-PBCL was then used as the macro-initiator, reacting with caprolactone (CL) (0.14 g, 1.2 mmol) and stannous octoate (2 drops) under vacuum at 145 °C for 2 to 4 h, yielding the triblock PEO-*b*-PBCL-*b*-PCL. Purified and vacuum-dried PEO-*b*-PBCL-*b*-PCL was sent for NMR analysis. The BCL units were then converted to  $\alpha$ -carboxylic acid- $\epsilon$ -caprolactone (CCL) via hydrogen reduction catalyzed by 10% Pd on charcoal (20 wt% of the added polymer) in anhydrous THF. For the synthesis of PEO-*b*-PCL-*b*-PCCL (the **ACB** sequence), PEO<sub>5000</sub> (0.5 g, 0.1 mmol) was first reacted with CL (0.5 g, 2.0 mmol) and then reacted with BCL (0.5 g, 2.0 mmol) in the presence of stannous octoate, and the PEO-*b*-PCL-*b*-PBCL produced underwent hydrogen reduction, following the same procedure for the synthesis of PEO-*b*-PCCL-*b*-PCL. For the synthesis of PEO-*b*-P(CL-*co*-CCL)<sub>ran</sub> (the

random **A(B/C)<sub>ran</sub>** sequence), PEO<sub>5000</sub> (0.5 g, 0.1 mmol) was reacted with a mixture of CL (0.14 g, 1.2 mmol) and BCL (0.5 g, 2.0 mmol) in the presence of stannous octoate (6 drops). This was followed by the hydrogenation of the BCL units as explained previously in **Chapter 2** and **Chapter 3**.

The composition of polymer products was confirmed by <sup>1</sup>H-NMR (Bruker Advance 600 MHz NMR spectrometer, Billerica, MA, USA) using CDCl<sub>3</sub> as solvent. The degree of polymerization (DP) of each block was calculated based on the <sup>1</sup>H-NMR spectra of terpolymers, comparing the area under the peak for PEO<sup>5000</sup> (4H, CH<sub>2</sub>-CH<sub>2</sub>-O; δ 3.5-3.8) to the methylene hydrogens of the benzyl group on the BCL units of PBCL (2H, C<sub>6</sub>H<sub>5</sub>-CH<sub>2</sub>-O-CO δ 5.2), and to that of the α-methylene group on the CL units of PCL (2H, CO-CH<sub>2</sub>(CH<sub>2</sub>)<sub>3</sub>CH<sub>2</sub>-O, δ 2.2-2.4) or the ε-methylene groups on either CL, BCL, or CCL units on PCL, PBCL, or PCCL, respectively (2H, CO-CH(R)(CH<sub>2</sub>)<sub>3</sub>CH<sub>2</sub>-O, δ 3.9-4.2). PEO-*b*-PCL-*b*-PCCL (**ACB** orientation) is denoted as polymer **1**, PEO-*b*-P(CCL-*co*-CL)<sub>ran</sub> (**A(B/C)<sub>ran</sub>** orientation) as polymer **2**, and PEO-*b*-PCCL-*b*-PCL (**ABC** orientation) as polymer **3** (

**Table 4.1).**

The conjugation of mercaptohexylamine to the polymer backbone was accomplished using the method developed in **Chapter 2**. Briefly, the COOH groups on a terpolymer were activated by oxalyl chloride (oxalyl chloride:COOH = 1.1:1, m/m) in chilled anhydrous CH<sub>2</sub>Cl<sub>2</sub>. The activation reaction ran for 24 h. The solvent was removed under vacuum and the chlorinated polymer was briefly washed with anhydrous hexane to remove un-reacted oxalyl chloride. The chlorinated polymer was then dissolved in anhydrous CH<sub>2</sub>Cl<sub>2</sub> and reacted with SHC<sub>6</sub>H<sub>12</sub>NH<sub>2</sub>·HCl (SH:COOH = 1:1, m/m), which was pre-neutralized with anhydrous NEt<sub>3</sub> (NEt<sub>3</sub>:SH = 2.2:1, m/m). The reaction was carried out in the dark for 20 h at room temperature. The solvent was again evaporated under vacuum and the thiolated terpolymer product was dissolved in toluene. Salts such as NEt<sub>3</sub>·HCl could not be dissolved in toluene, which was removed by centrifugation. The thiolated terpolymers were then precipitated out in cold hexane. The polymers were further purified by dialysis against water to remove un-reacted mercaptohexylamine. <sup>1</sup>H-NMR analysis confirmed the conjugation of thiol-containing pendant groups, as two peaks at δ 2.86 ppm (2H, CONH-CH2-(CH<sub>2</sub>)<sub>4</sub>-CH<sub>2</sub>-SH) and δ 2.68 ppm (2H, CONHCH<sub>2</sub>-(CH<sub>2</sub>)<sub>4</sub>-CH2-SH) appeared. The thiolated terpolymers of the **ACB**, **A(B/C)<sub>ran</sub>**, and **ABC** orientation are denoted as polymers **1a**, **2a**, and **3a**, respectively (**Scheme 4.1**).



### 4.2.3 Encapsulation of As<sup>III</sup>

The procedures described in **Section 3.2.1.5** were followed to encapsulate As<sup>III</sup> into terpolymeric micelles. Briefly, freshly synthesized thiol-functionalized polymers were first dissolved in THF (10 mg/mL). The polymer solution was added dropwise into arsenic solution prepared in CH<sub>3</sub>COONH<sub>4</sub> buffer (pH 7.4) supplemented with 10 mM tris(2-carboxyethyl)phosphine (TCEP) with vigorous stirring. The mixture was then incubated in a 37 °C water bath for 1 hour. The THF was then evaporated during overnight stirring at room temperature. The un-loaded As<sup>III</sup> and most salts in the buffer were removed by dialysis against water for 24 hour. The As<sup>III</sup> loaded micelle solution was lyophilized for further characterization and application. The As<sup>III</sup> encapsulated micelles are denoted as **1b**, **2b**, and **3b**. The loading of arsenic was determined by inductively coupled plasma mass spectrometry (ICP-MS) using an Agilent 7500cs Octopole Reaction System ICP Mass Spectrometer. The loading of arsenic was expressed as weight percent of arsenic element in As<sup>III</sup>-encapsulated polymeric micelle powder. The arsenic encapsulated polymers were sent for elemental analysis using a Carlo Erba EA 1108 elemental analyzer to determine the sulfur content. The molar ratio of As to S in each polymer sample was then calculated to evaluate the arsenic encapsulation efficiency.

### 4.2.4 Characterization of micelles

The micelles formed by starting terpolymers and thiol-functionalized terpolymers, and micelles with As<sup>III</sup> encapsulation were characterized for their critical micelle concentration (CMC), surface charge, size distribution, and micelle morphology. The CMC of polymers **1**, **2**, and **3** were measured using the pyrene probe method as reported previously. (Shahin and Lavasanifar 2010) The zeta potential of micelles (1 mg/mL) prepared from polymer **1**, **2**, **3**, **1a**, **2a**, **3a**, **1b**, **2b** and **3b** at different pH were measured using a Malvern Nano-ZS Zeta Sizer (Worcestershire, UK) (laser

wavelength: 633 nm, temperature: 25 °C). The buffers for pH 4.5 and 5.0 were based on CH<sub>3</sub>COOK (0.1 M) and the buffers for pH 6.0, 7.0, and 10.5 were based on KH<sub>2</sub>PO<sub>4</sub> (0.1 M). NaOH (1 M) solution was used to adjust the pH of buffers. Each micelle sample was vortexed, filtered through 0.45 μm PVDF filters, and stabilized in a 4 °C fridge for 3 h before zeta-potential measurement. The size distribution and zeta-average diameter of As<sup>III</sup>-encapsulated micelles (0.1 mg/mL) in different solvents (water and PBS) was measured using the same Malvern Nano-ZS Zeta Sizer (detecting light angle: 173°, temperature: 25 °C) as well. The morphology of As<sup>III</sup>-encapsulated micelles was analyzed by transmission electron microscopy (TEM) (Philips/FEI Morgagni™ TEM with Gatan Digital Camera, Hillsboro, OR, USA). The samples were stained with phosphotungstic acid (PTA). The size distribution of micelles in TEM pictures was analyzed by Nano Measurer 1.2 software (Department of Chemistry, Fudan University, China).

#### **4.2.5 Micelle <sup>1</sup>H-NMR in D<sub>2</sub>O**

To evaluate the exposure of hydrophobic groups on the terpolymers to water, the micelle solutions (1 mg/mL) of polymers **1**, **2**, **3**, **1a**, **2a**, and **3a** were prepared in D<sub>2</sub>O and CDCl<sub>3</sub> for <sup>1</sup>H-NMR analysis. In our study, the area under the peak of typical signals related to the hydrophobic groups (i.e., δ 2.4–2.2 for CL, 2H per unit; δ 4.2–3.9 for both CL and CCL, 2H per unit; δ 2.96–2.78 and δ 2.75–2.58 for CCL-C<sub>6</sub>-SH, 4H per unit) were measured and divided by the area under the peak of PEO<sub>5000</sub> (δ 3.8–3.5, 4H per unit and 114 units in total). The ratios of areas under the peaks from the <sup>1</sup>H-NMR spectra in D<sub>2</sub>O were compared to the same ratios from <sup>1</sup>H-NMR spectra of polymer samples in CDCl<sub>3</sub>.

#### **4.2.6 *In vitro* arsenic release from the micelles**

The As<sup>III</sup> release from three different micelles was evaluated in ddH<sub>2</sub>O, RPMI-1640 cell culture medium, and cell culture medium supplemented with 10% FBS. In each set of experiments, 1.5

mL of 1 mg/mL micelle solution was prepared by direct re-suspension. Triplicate samples were prepared for each type of micelle. The micelle solutions were incubated at 37 °C. At 0, 1, 3, 6, 12, 24, 30, and 48 h, a 100 µL micelle solution aliquot was collected and centrifugally filtered using an Amicon Ultra-0.5 mL centrifugal filter (molecular weight cut-off: 3,000 Da) at 13500 × g for 40 min. The filtrate was collected for released arsenic determination using ICP-MS. Free As<sup>III</sup>, instead of micelle encapsulated As<sup>III</sup>, dissolved in water and in the buffers was used as control.

The arsenic release was expressed as the weight percentage of free arsenic at each time point compared to the total arsenic weight in the sample.

#### **4.2.7 Cellular uptake of As<sup>III</sup>-encapsulated micelles**

To study the cellular uptake of encapsulated As<sup>III</sup> by MDA-MB-435 cells, two parallel sets of experiments were conducted at the same time. One set measured the arsenic concentration in homogenized cells, and the other measured the arsenic concentration in the separated cell lysate and cell debris fractions. Both sets included three cell culture dishes for each arsenic formulation and a control treated with arsenic-free media. MDA-MB-435 cells ( $25 \times 10^4$  cells/mL, 2 mL) were seeded into each 60 × 15 mm cell culture dish. The cells were treated with **1b**, **2b**, **3b**, and free As<sup>III</sup> solutions within 1/3 to 1/2 of their corresponding IC<sub>50</sub> values. The IC<sub>50</sub> values were determined using the neutral red assay as described in **Chapter 2**. The exact arsenic concentration in the treatment medium was determined by ICP-MS. After 24 h treatment, the cells were washed with 3 mL Dulbecco's PBS (DPBS) three times. Double distilled water (ddH<sub>2</sub>O) (500 µL) was added into each culture dish. The cells were then scraped off from the dish and collected. The cells were lysed using the freeze-thaw method. To determine the soluble protein concentration in the lysed cell solution, the lysed cell solution was first centrifuged at 5000 rpm for 2 min, and a 20 µL aliquot was collected from the supernatant for protein concentration determination following the

standard Bradford assay protocol (the version for 250  $\mu\text{L}$  microplate assay). To determine the arsenic concentration in the homogenized cells, 400  $\mu\text{L}$  of the lysed cell solution was mixed with 100  $\mu\text{L}$   $\text{HNO}_3$  (Optima HPLC grade). The mixture was incubated in a 50  $^\circ\text{C}$  water bath overnight. The digested cell solution was diluted and filtered for ICP-MS analysis. To determine the arsenic concentration in cell lysate and cell debris, the lysed cell solution was first centrifuged at 5000 rpm for 2 min to separate the cell debris and lysate (supernatant). The cell debris was re-suspended in 500  $\mu\text{L}$  ddH<sub>2</sub>O for arsenic concentration determination. The measured arsenic concentration was normalized to soluble protein concentration in the lysed cell solution. The arsenic uptake was expressed as arsenic atoms per gram of soluble protein in cells.

#### **4.2.8 Data analysis**

The results were expressed as mean  $\pm$  standard deviation (SD). Unpaired two tail Student's t-test, One-way ANOVA with post-test of Tukey's multiple comparison or Two-way ANOVA were used to perform statistical analysis as noted for each experiment in the results section. The software used was GraphPad Prism5 software (La Jolla, CA, USA). A value of  $P < 0.05$  was considered as statistically significant.

### **4.3 Results**

#### **4.3.1 Synthesis, thiol-functionalization, and As<sup>III</sup> encapsulation**

The synthesis of polymers **1**, **2**, and **3** started from the initiator methoxy PEO and BCL and/or CL monomers. The composition of the polymer product in each step was monitored using <sup>1</sup>H-NMR spectrometry (**Figure 4.1**, **Figure 4.3** and **Figure 4.5**). On average, polymer **1** was composed of 114 units of ethyl oxide (EO), 9 units of CL, and 19 units of CCL; polymer **2** was composed of 114 units of EO, 10 units of CL, and 15 units of CCL; polymer **3** was composed of 114 units of EO, 11 units of CL, and 17 units of CCL (

**Table 4.1).**  $^1\text{H-NMR}$  spectra of the intermediate products during the synthesis of polymer, **1**, **2**, and **3** are not presented here.

$^1\text{H-NMR}$  spectra (**Figure 4.2**, **Figure 4.4** and **Figure 4.6**) also confirmed the successful conjugation of mercaptohexylamine, yielding the thiol-functionalized terpolymers **1a**, **2a** and **3a**, respectively. On average, based on our calculations from the  $^1\text{H-NMR}$  spectra of these polymers, 7.7 units from 19 units of CCL in polymer **1a**, 6.7 units from 15 units of CCL in polymer **2a**, and 6.0 units from 17 units of CCL in polymer **3a** were conjugated to mercaptohexylamine. This corresponds to 41%, 45%, and 35% of the total CCL units modified with thiol functionality in terpolymers **1a**, **2a**, and **3a**, respectively.

The arsenic content in **1b**, **2b**, and **3b** was determined using ICP-MS and the sulfur content was determined by elemental analysis. The arsenic loading in **1b**, **2b**, and **3b** was  $3.8 \pm 0.3$ ,  $3.3 \pm 0.1$ , and  $3.1 \pm 0.1$  wt%, respectively (**Figure 4.7**). In other words, the bound arsenic occupied  $57 \pm 5\%$ ,  $59 \pm 3\%$ , and  $50 \pm 2\%$  of total thiol groups in **1b**, **2b**, and **3b**, respectively. There was significant difference in arsenic loading ( $P < 0.05$ , One-way ANOVA, Tukey's multiple comparison post-test) and As/S molar ratio ( $P < 0.05$ , One-way ANOVA, Tukey's multiple comparison post-test) between the three polymer orientations. In general, arsenic loading and the As/S ratio in polymer **3b** was significantly lower than in the other polymers studied. This may be attributed to higher accessibility of thiol groups in polymers **1b** and **2b** for arsenic binding than those in polymer **3b**.

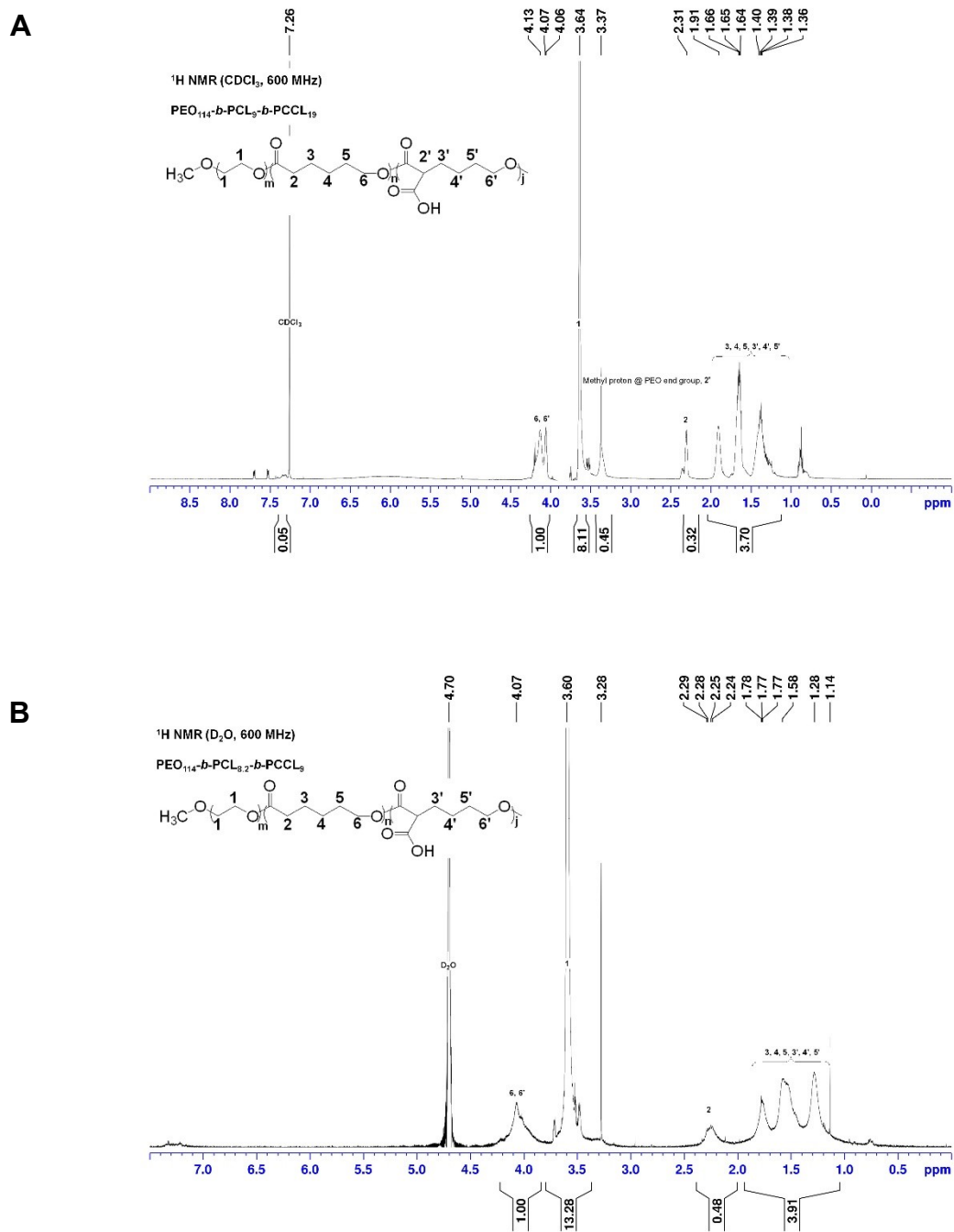


Figure 4.1. <sup>1</sup>H-NMR spectrum of PEO-*b*-PCL-*b*-PCCL in CDCl<sub>3</sub> (A) and D<sub>2</sub>O (B).

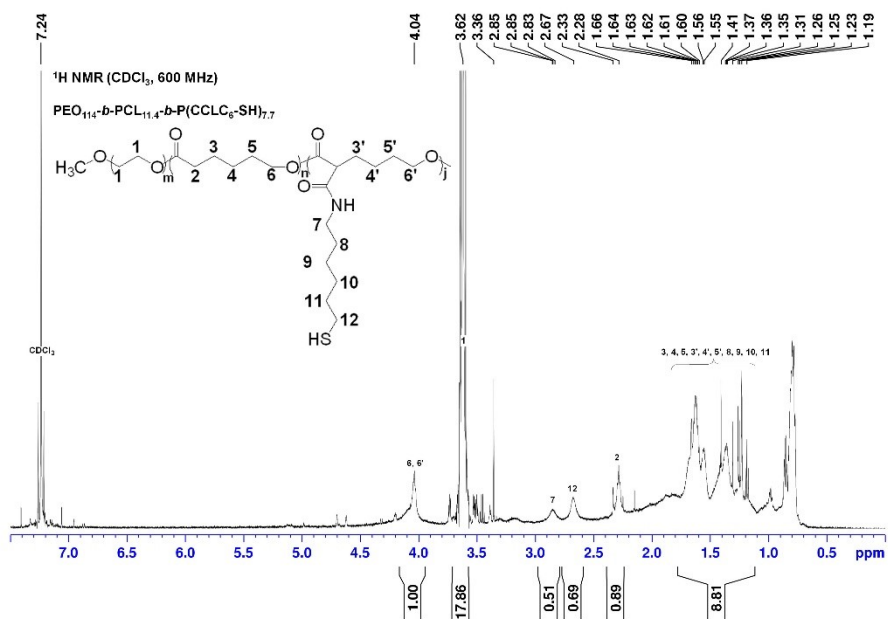
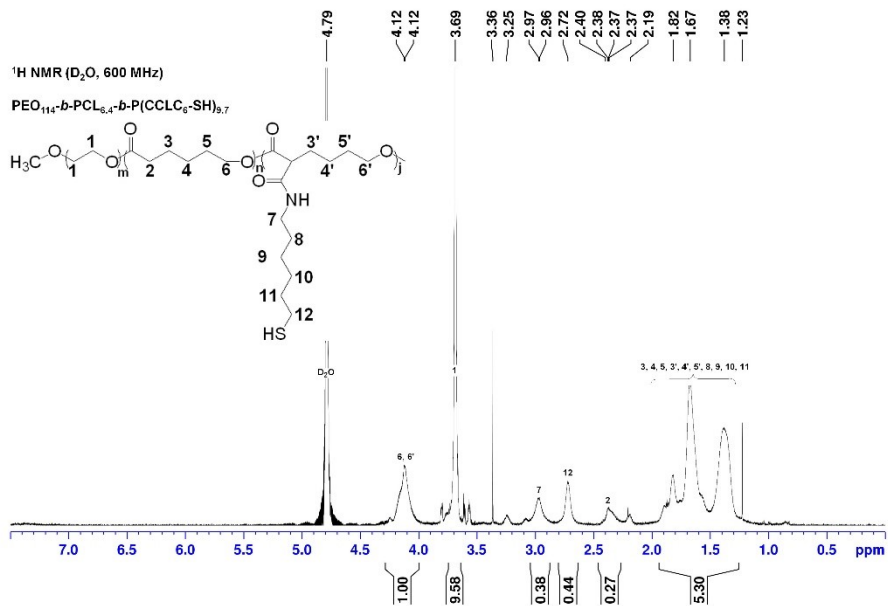
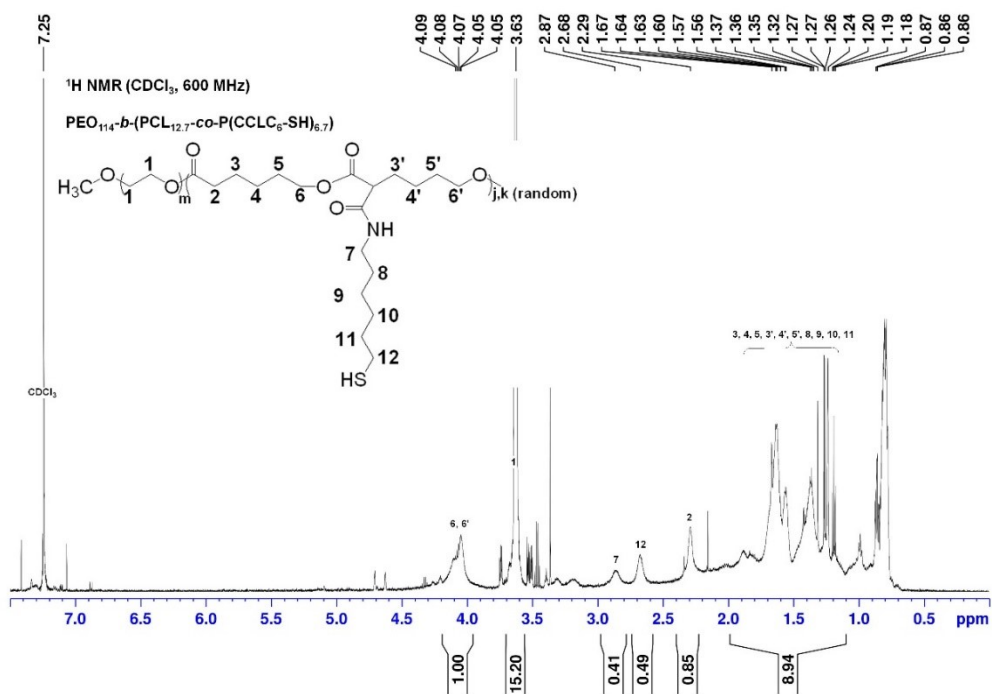
**A****B**

Figure 4.2. <sup>1</sup>H-NMR spectrum of PEO-*b*-PCL-*b*-P(CCLC<sub>6</sub>-SH) in CDCl<sub>3</sub> (A) and D<sub>2</sub>O (B).



**A**



**B**

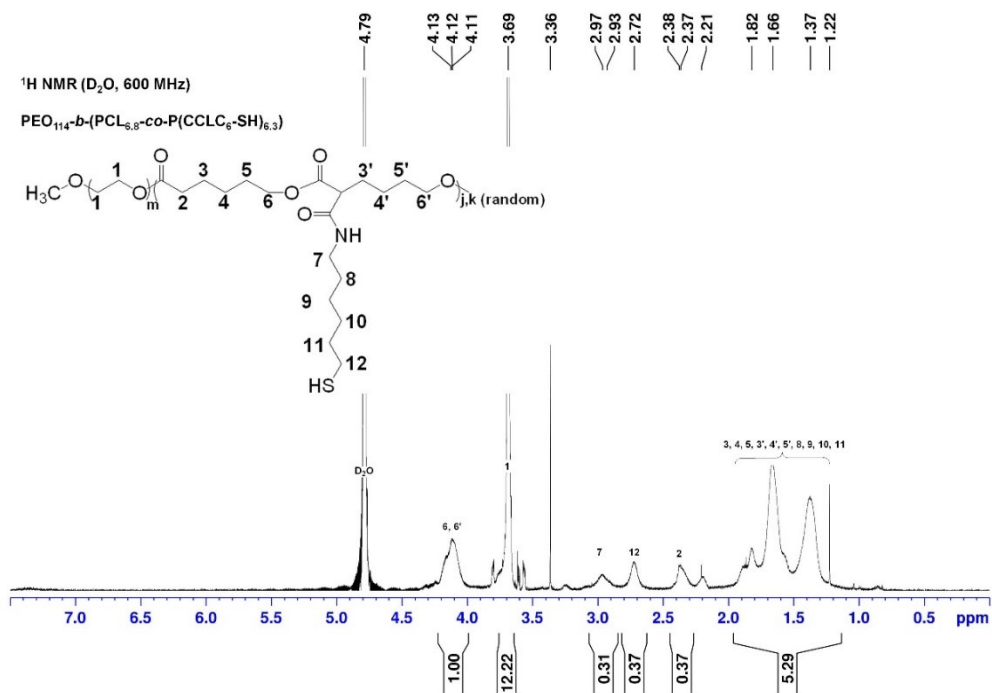


Figure 4.4. <sup>1</sup>H-NMR spectrum of PEO-*b*-(PCL-*co*-P(CCLC<sub>6</sub>-SH)) in CDCl<sub>3</sub> (A) and D<sub>2</sub>O (B).

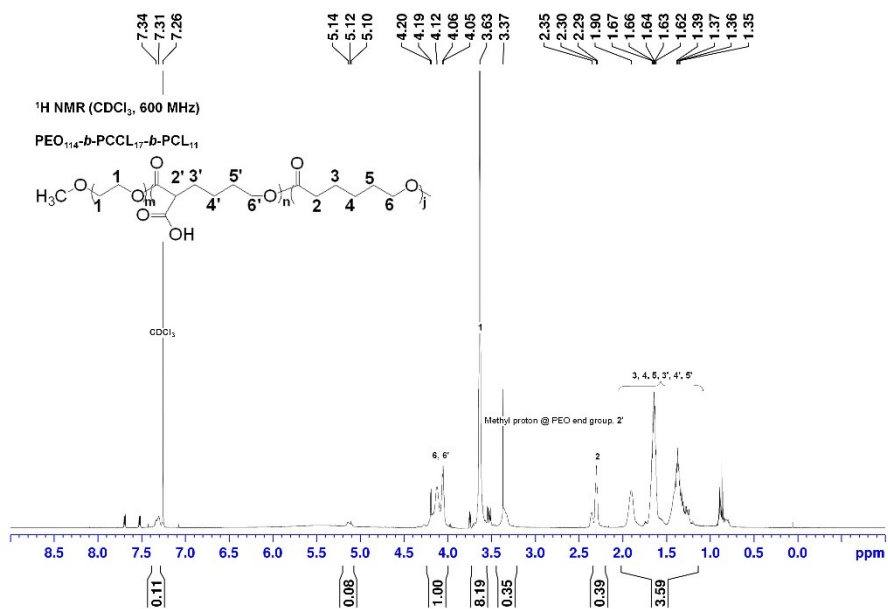
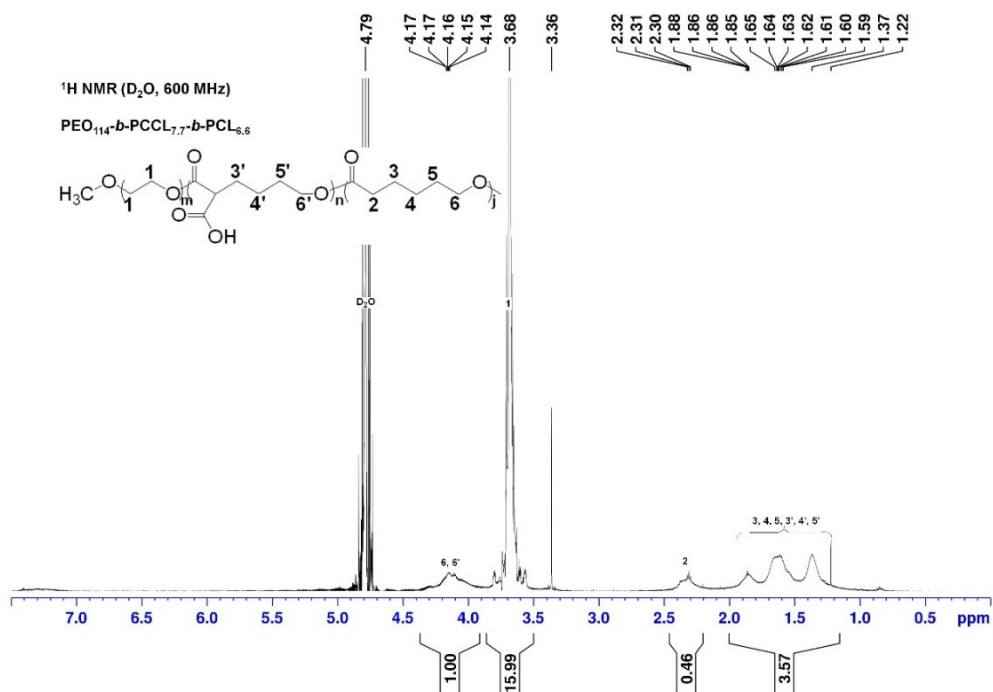
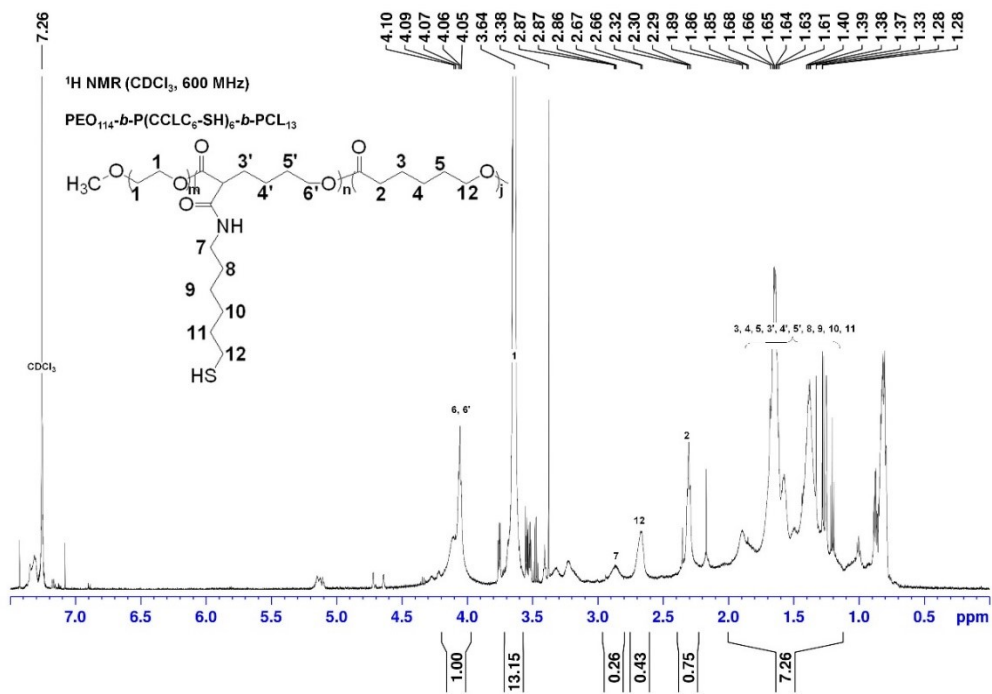
**A****B**

Figure 4.5. <sup>1</sup>H-NMR spectrum of PEO-*b*-PCCL-*b*-PCL in CDCl<sub>3</sub> (A) and D<sub>2</sub>O (B).

**A**



**B**

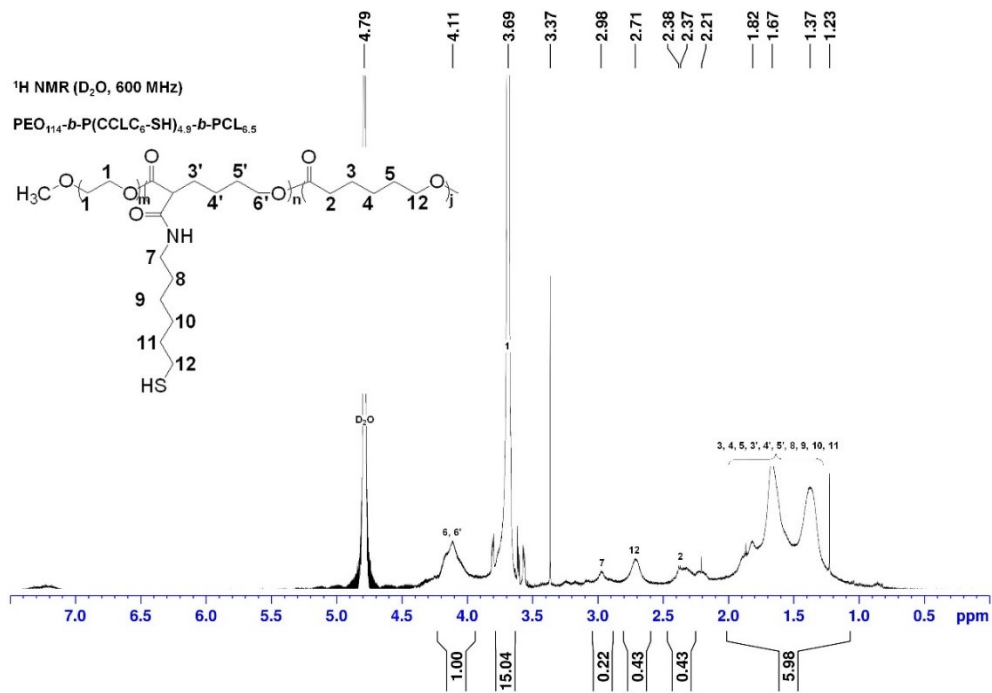
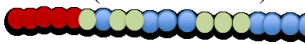


Figure 4.6. <sup>1</sup>H-NMR spectrum of PEO-*b*-P(CCLC<sub>6</sub>-SH)-*b*-PCL in CDCl<sub>3</sub> (A) and D<sub>2</sub>O (B).

**Table 4.1. Molecular weight, composition, critical micelle concentration (CMC) and size of block polymers**

Denotation	Polymer name and illustration <sup>a</sup>	Composition	Theo. Mol. Weight (g/mol)	CMC ± SD (µg/mL)	Zeta-average diameter ± SD (nm) <sup>c</sup>		
					Micelles from starting polymers	Micelles from thiolated polymers	Arsenic-encapsulated micelles
1	PEO- <i>b</i> -PCL- <i>b</i> -PCCL 	PEO <sub>114</sub> - <i>b</i> -PCL <sub>9</sub> - <i>b</i> -PCCL <sub>19</sub>	9028	36±3	61±1	141±1	124±1
2	PEO- <i>b</i> -(PCL- <i>co</i> -PCCL) 	PEO <sub>114</sub> - <i>b</i> -(PCL <sub>10</sub> - <i>co</i> -PCCL <sub>15</sub> )	8510	36±2	72±1	130±1	121±4
3	PEO- <i>b</i> -PCCL- <i>b</i> -PCL 	PEO <sub>114</sub> - <i>b</i> -PCCL <sub>17</sub> - <i>b</i> -PCL <sub>11</sub>	8940	11±1	72±1	317±7 (Two peaks Peak 1: 60-90 nm Peak 2: 450-650 nm )	107±2

<sup>a</sup>. : ethylene oxide (EO) unit; : carboxyl-caprolactone (CCL) unit; : caprolactone (CL) unit.

<sup>b</sup>. The degree of polymerization of each block is represented as subscripts and was calculated based on <sup>1</sup>H-NMR spectra for each polymer

<sup>c</sup>. The Zeta-average diameter of micelles were measured by DLS.

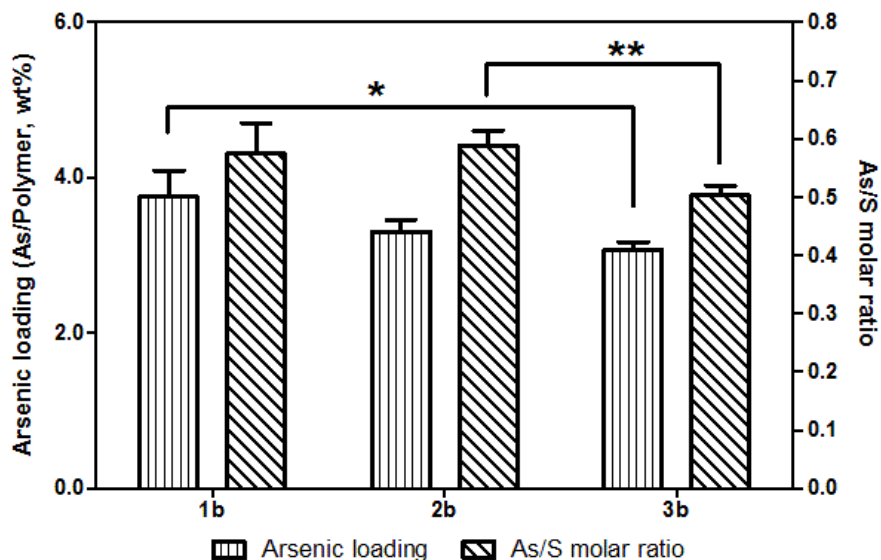


**Figure 4.7. Arsenic loading and As/S molar ratio in thiol-functionalized terpolymeric micelles encapsulated with As<sup>III</sup>.** The data were expressed as mean  $\pm$  SD (N = 3). One-way ANOVA with post-test of Tukey's multiple comparison test was performed among three types of arsenic-encapsulated micelles. (\*: P<0.05; \*\*: P<0.01)

#### 4.3.2 The effect of terpolymer structure on micellar stability

We evaluated the thermodynamic stability of micelles by measuring their CMC. The effect of terpolymer structure and orientation on the dissociation of micelles was then investigated measuring micellar tendency for dissociation in different solvents.

In comparison to diblock copolymer PEO-*b*-PCCL (CMC: 89 $\pm$ 4  $\mu$ g/mL), the introduction of PCL into the polymer backbone decreased the polymer CMC and enhanced the micelle stability as expected (**Figure 4.8**). This is due to the higher hydrophobicity of PCL than the carboxylic acid group containing PCCL. The CMCs of polymers **1**, **2**, and **3** were 36 $\pm$ 3, 36 $\pm$ 2, and 11 $\pm$ 1  $\mu$ g/mL, respectively. Among the three terpolymers, polymer **3** has the lowest CMC (P<0.0001, One-way ANOVA), indicating that the micelles formed by polymers with **ABC** chain orientation has the highest thermodynamic stability.

The As<sup>III</sup>-loaded micelles **1b**, **2b** and **3b** were dissolved in water or PBS for DLS size distribution analysis at room temperature. All three types of micelles had a unimodal size distribution by intensity in water, though aggregates were observed in the **2b** sample (**Figure 4.9**). The polydispersity index (PDI) of **1b**, **2b**, and **3b** in water was 0.2, 0.4, and 0.2, respectively. When the dispersion solution was changed from water to PBS, a broader size distribution of **1b** and **2b** was observed with an increased PDI of 0.4 and 0.5, respectively. The size distribution by volume indicated that the majority of **1b** and **2b** micelles dissociated and re-assembled into micelles of smaller sizes (5–30 nm) in PBS. In contrast, **3b** micelles remained in a narrow size distribution (average PDI: 0.2) with no observable change in micelle size. The dissociation and re-assembly of micelles **1b** and **2b** in PBS is likely due to the facilitated interaction between ions and the polymer chains in these micelles. The salt effect on micellization and micelle size is usually observed in micelles assembled from ionic surfactants. (Kamenka et al. 1992; Varade et al. 2005) Overall, our observations indicated micelle **1b** with the **ACB** orientation and **2b** with **A(B/C)<sub>ran</sub>** orientation are less stable than micelle **3b** with the **ABC** orientation, particularly in the presence of electrolytes.

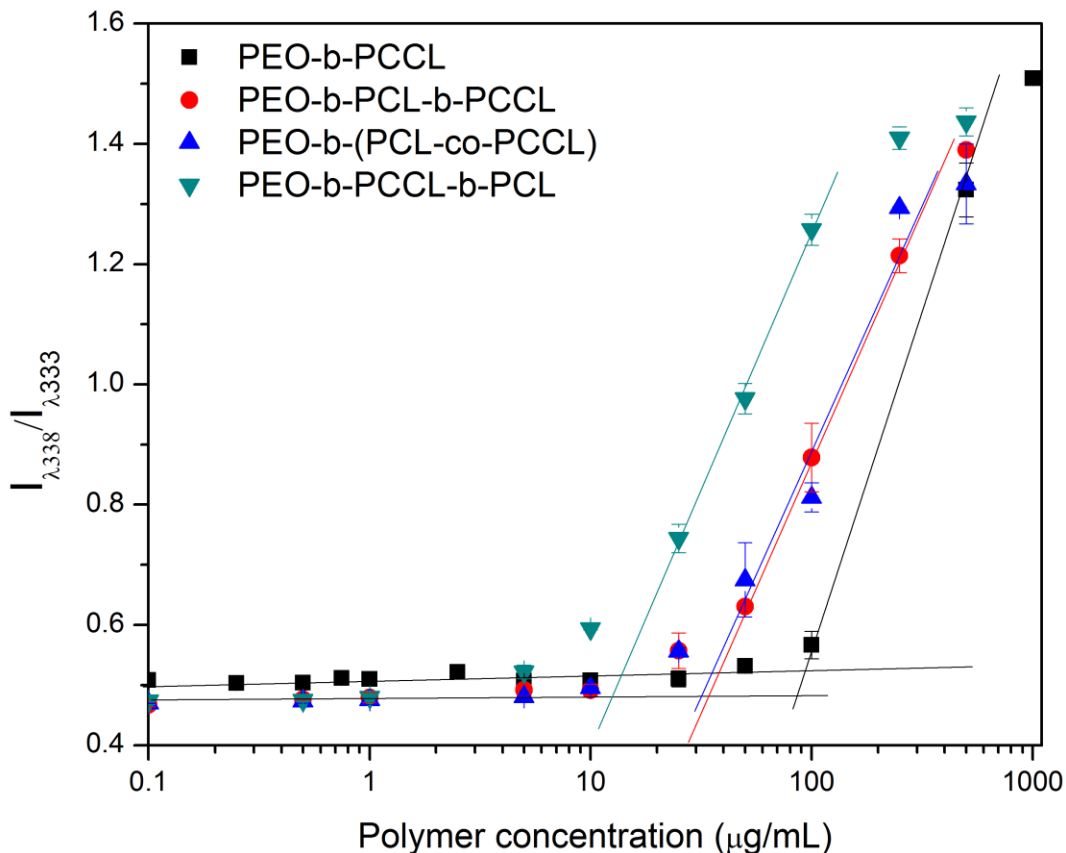


**Figure 4.8. CMC of polymer 1, polymer 2, polymer 3, and PEO-*b*-PCCL<sub>17</sub>.** The CMC measurement was conducted three times and representative data is presented here. The CMC was  $36 \pm 3$   $\mu\text{g/mL}$ ,  $36 \pm 2$   $\mu\text{g/mL}$ , and  $11 \pm 1$   $\mu\text{g/mL}$  for polymers **1**, **2**, and **3**, respectively. The CMC measurement of PEO-*b*-PCCL<sub>17</sub> was from **Chapter 2**. One-way ANOVA with post-test was performed on the CMC values of terpolymer and dipolymer. The CMC values ranked as polymer **3** < polymer **2**, polymer **1** < PEO-*b*-PCCL<sub>17</sub>.

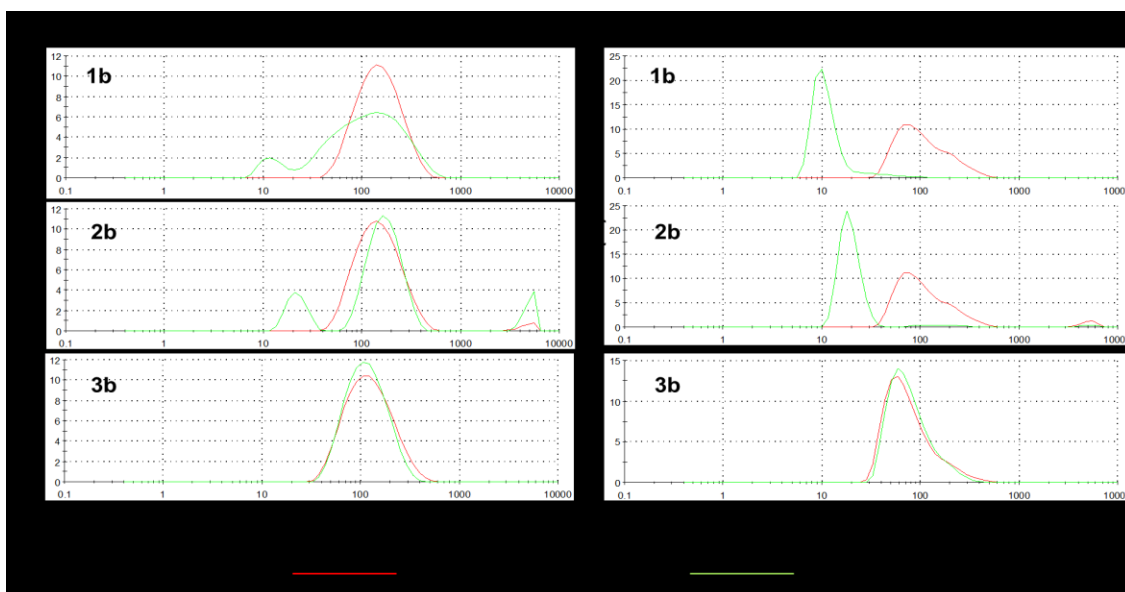


**Figure 4.9. Size distribution of arsenic-loaded micelles (0.1 mg/mL) in water and PBS using DLS technology.** Each sample was scanned three times. Representative results are presented here. Micelle **3b** had narrow size distribution in water and PBS. Dissociation of **1b** and **2b** micelles was observed in PBS.

#### 4.3.3 The effect of terpolymer structure on micelle surface charge at different pH

The surface charge of micelles plays an important role in the interaction between micelles and biological membranes and can influence the cellular uptake of micelles. (Honary and Zahir 2013; Ma et al. 2013) The zeta-potential measurement of micelles assembled from starting polymers (polymers **1**, **2** and **3**), thiol-functionalized polymers (polymers **1a**, **2a** and **3a**), and the As<sup>III</sup>-loaded micelles (polymers **1b**, **2b** and **3b**) showed a negative surface charge for all micelles studied in buffers with pH ranging from 4.5 to 10.5 (**Figure 4.10**). Because of the presence of methoxy PEO on the micellar shell, we expected relatively neutral micelles with no change on the surface charge as a function of the solution pH value. Contrary to our expectation, we found that the micelle surface to become more negative as a function of an increase in pH. This may be attributed to the ionisable COOH and SH groups in the hydrophobic segments of terpolymers, that become deprotonated at pH larger than pKa of carboxyl or SH groups (pKa of ~ 5 and 8, respectively).

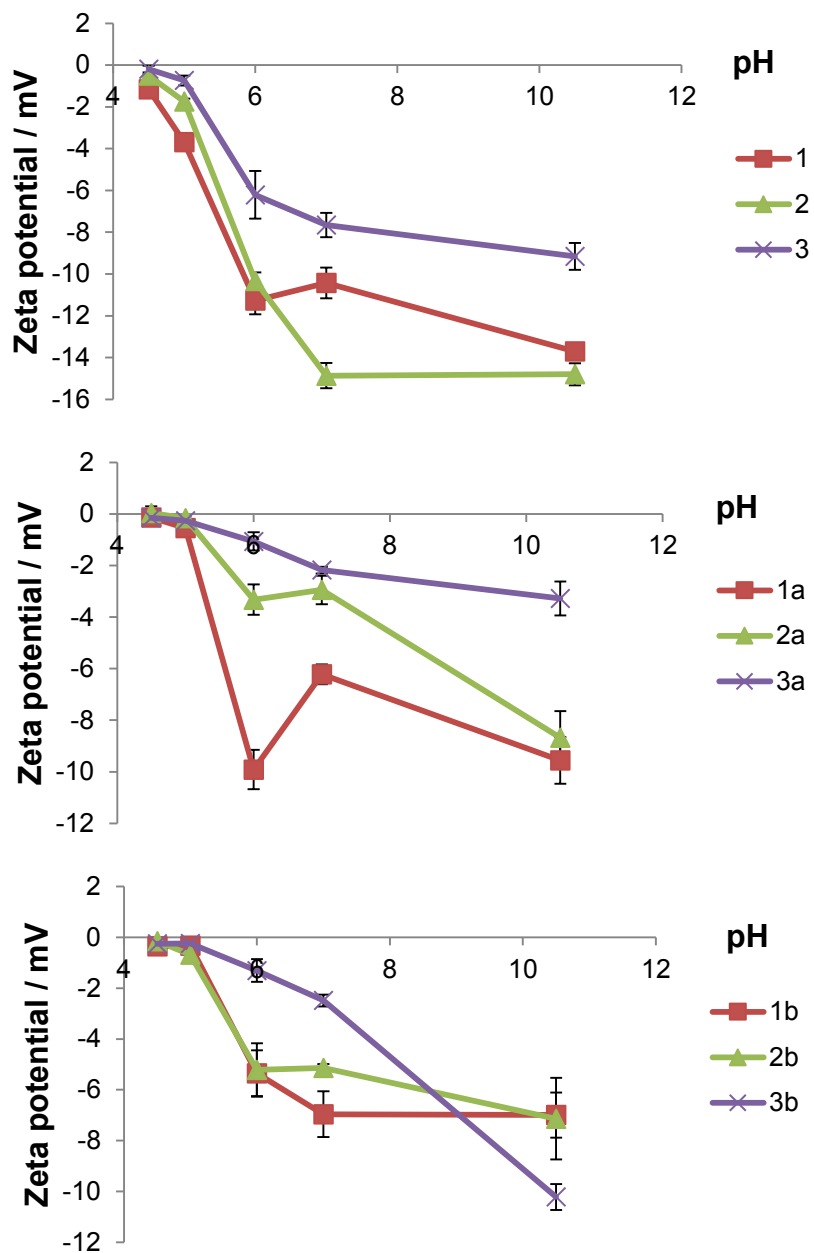


**Figure 4.10. Zeta potential of micelles prepared from 1 mg/mL starting polymers (A), thiol-containing polymers (B), and As<sup>III</sup>-loaded polymers (C) at different pH values. Data are presented as average  $\pm$  SD (n=3).**

Comparing the zeta potential of micelles at pH 7.0 (Figure 4.11) indicated that the partial thiolation (~ 40%) reduced the negative charge on the micelle surface for all three different terpolymer structures ( $P < 0.0001$ , Two-way ANOVA). The reduced zeta-potential of micelles with

thiol functionality is perhaps due to the higher pKa of thiol groups (~ 8) than that of carboxyl groups (~ 5). At pH 7.0, less than 10% of the total thiol groups on the thiolated terpolymers are deprotonated, while more than 90% of the total carboxylic acid groups are deprotonated. This fact accounts for the less negatively charged surface of thiolated micelles compared to micelles with 100% carboxyl functionalization. Arsenic incorporation in thiolated micelles did not impact the zeta potential of micelles except for micelles formed from polymer **2a**, which showed slight increase in zeta potential upon arsenic incorporation. The pKa<sub>1</sub> of arsenous acid is 9.2 and the second pKa of arsenous acid is higher than 10. Loading of As<sup>III</sup> in the thiolated micelles can lead to the formation of either –S–As(OH)<sub>2</sub>, or –S–As(OH)–S–, or even weak interaction between As(OH)<sub>3</sub> and thiol group, which will remain majorly in an unionized form at pH 7.0. The net charge of thiolated and As<sup>III</sup>-incorporated micelles is mostly attributed to the ionization of remaining COOH rather than SH groups in terpolymer structure at pH 7.0.

Our results indicated that the polymer sequence arrangement can affect the micelle surface charge (P<0.0001, Two-way ANOVA). Micelles of the **ABC** orientation (from polymers **3**, **3a**, and **3b**) displayed lower negative surface charge compared to their **ACB** counterparts (from polymers **1**, **1a**, and **1b**).

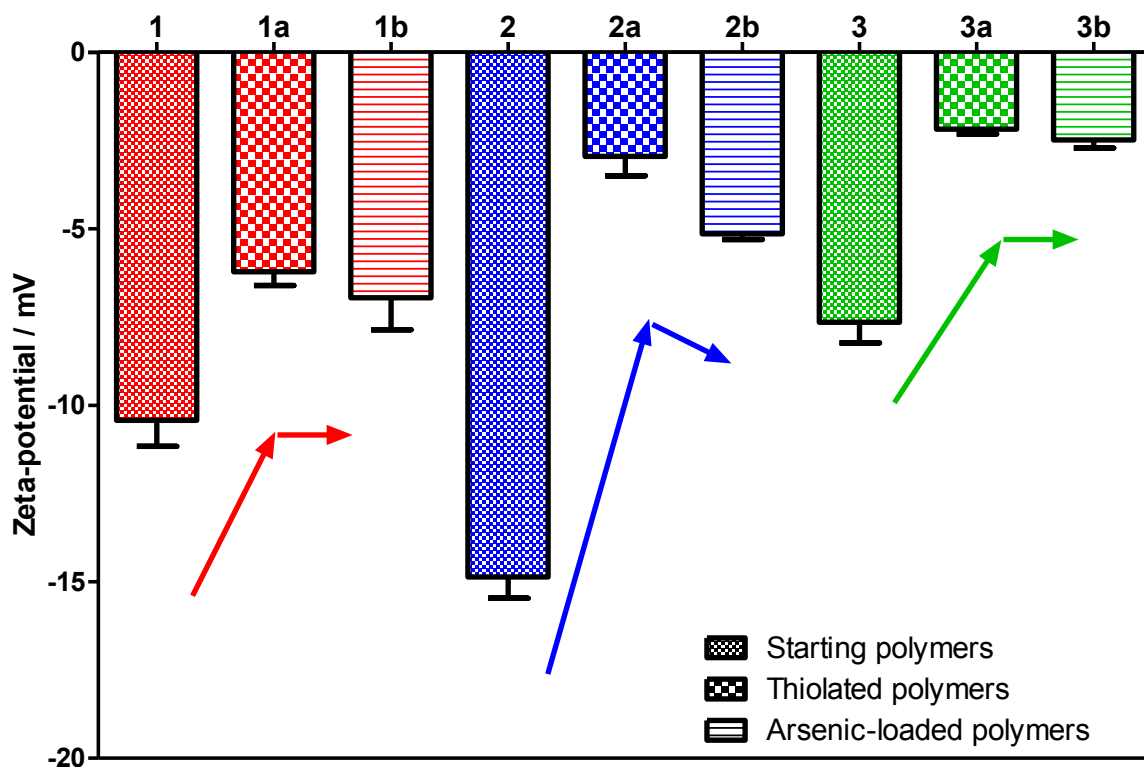


**Figure 4.11. Zeta-potential of micelles (1 mg/mL) in phosphate buffer (0.1 M, pH 7).** The patterns with red color refer to polymer 1 series with ACB orientation, the blue color to polymer 2 series with A(B/C)<sub>ran</sub> orientation, and the green color to polymer 3 series with ABC orientation. The zeta-potential data were expressed as mean  $\pm$  SD (N = 3) of three scans of each sample.

#### 4.3.4 Investigations on the block arrangement in the micellar structure by <sup>1</sup>H-NMR

In an aqueous environment, the hydrophobic blocks are expected to reside in the core of the micelle or the core/shell interface, while the hydrophilic blocks on the micelle corona. In D<sub>2</sub>O, the exposure of hydrophobic blocks to media is expected to be reduced. As a result, the NMR signals associated with substituent groups on these blocks, is expected to decrease. This is in comparison to the intensity of the same peaks for polymer in CDCl<sub>3</sub>. (Xiong et al. 2007) Therefore, a comparison of normalized peak intensity between two NMR spectra, one obtained from CDCl<sub>3</sub> (a good solvent for hydrophilic and hydrophobic blocks) and the other from D<sub>2</sub>O (a non-solvent for

hydrophobic blocks), can serve as an indirect indicator of the extent of hydrophobic block (and their substituents) exposure to water in a micellar structure. In this study, groups associated with the hydrophobic block of the polymers under study, i.e., CL, CCL, CCL-C<sub>6</sub>-SH, were anticipated to be buried inside the micelle core and have less exposure to D<sub>2</sub>O. This would have been reflected by the lower intensity of proton peaks that belong to CL, CCL, and CCL-C<sub>6</sub>-SH in their <sup>1</sup>H-NMR spectra in D<sub>2</sub>O compared to those in CDCl<sub>3</sub>. As the micelle corona was composed of PEO blocks and both CDCl<sub>3</sub> and D<sub>2</sub>O are good solvents for PEO, we normalized the proton signals of groups attached to hydrophobic segments to that of PEO. Specifically we calculated the ratios of the area under the peak for the protons of CL and CCL groups in non-thiolated terpolymers and that of CL and CCL-C<sub>6</sub>-SH groups in the thiolated terpolymers, to that for PEO methylene proton peaks as described in the **experimental section 4.2.5**. These normalized area under the peak for protons associated with CL and CCL backbone was then divided by the correspondent normalized peak areas from the NMR spectra of the polymer in CDCl<sub>3</sub> to calculate D<sub>2</sub>O/CDCl<sub>3</sub> specific ratios (**Table 4.2**). A ratio around 1 was considered to be a reflection of similar exposure of the protons of a certain chemical structure to water and chloroform. A ratio < 1 indicates less exposure of the chemical structure to water compared to chloroform, suggesting the group is buried inside the micelle core in aqueous media. A ratio > 1 means better exposure of a certain chemical structure to water compared to chloroform, suggesting a translocation of the chemical groups to the micelle surface in water.

For polymers **1**, **2**, and **3**, the  $CL_{D_2O}/CL_{CDCl_3}$  <sup>1</sup>H-NMR peaks ratios were 0.91, 1.00, and 0.60, respectively. This reflects the exposure of the CL groups in **C** block to water in the **ACB** and **A(B/C)<sub>ran</sub>** micelles but its localization in the more rigid environment of micellar core in the **ABC** micelles (green section in micelle **1** versus micelle **3**, **Scheme 4.2**). In thiolated micelles, the

$CL_{D2O}/CL_{CDCl3}$  ratio was 0.56, 0.53, and 0.50 for terpolymers **1a**, **2a**, and **3a**, respectively. This indicates similar environment of PCL block in terms of water exposure in micelles from polymer **3a** compared to other two structures (green section in micelle **1a**, **2a** and **3a**, **Scheme 4.2**), and might be a reflection of formation of loose micelles in all three types of terpolymer micelles.

Micelle from polymers **1**, **2**, and **3** showed  $CCL_{D2O}/CCL_{CDCl3}$   $^1H$ -NMR peak ratios of 0.47, 0.65 and 0.45, respectively. Although the PCCL block was located at the hydrophobic end of the **ACB** chain, it showed similar ratio to that of **ABC** micelles indicating similar exposure to water in these two polymer structures (blue segment in micelle **1** and **3**, **Scheme 4.2**). This may be attributed to the folding of the **ACB** chain leading to the localization of the **B** block in the micellar core/shell interface and/or formation of loose micelles that allow partial water exposure to PCCL core. The  $CCL-C_6-SH_{D2O}/CCL-C_6-SH_{CDCl3}$  ratios in polymers **1a**, **2a**, and **3a** were 1.26, 0.93, and 0.82, respectively. The higher than 1 ratio observed for polymer **1a** suggests a translocation of block **B** (P(CCL/CCL- $C_6$ -SH)) to the micelle surface for this structure (blue segment in micelles **1a**, **Scheme 4.2**). This observation is in line with the proposed structure of three different types of micelles in terms of terpolymer orientation demonstrated in **Scheme 4.2**.

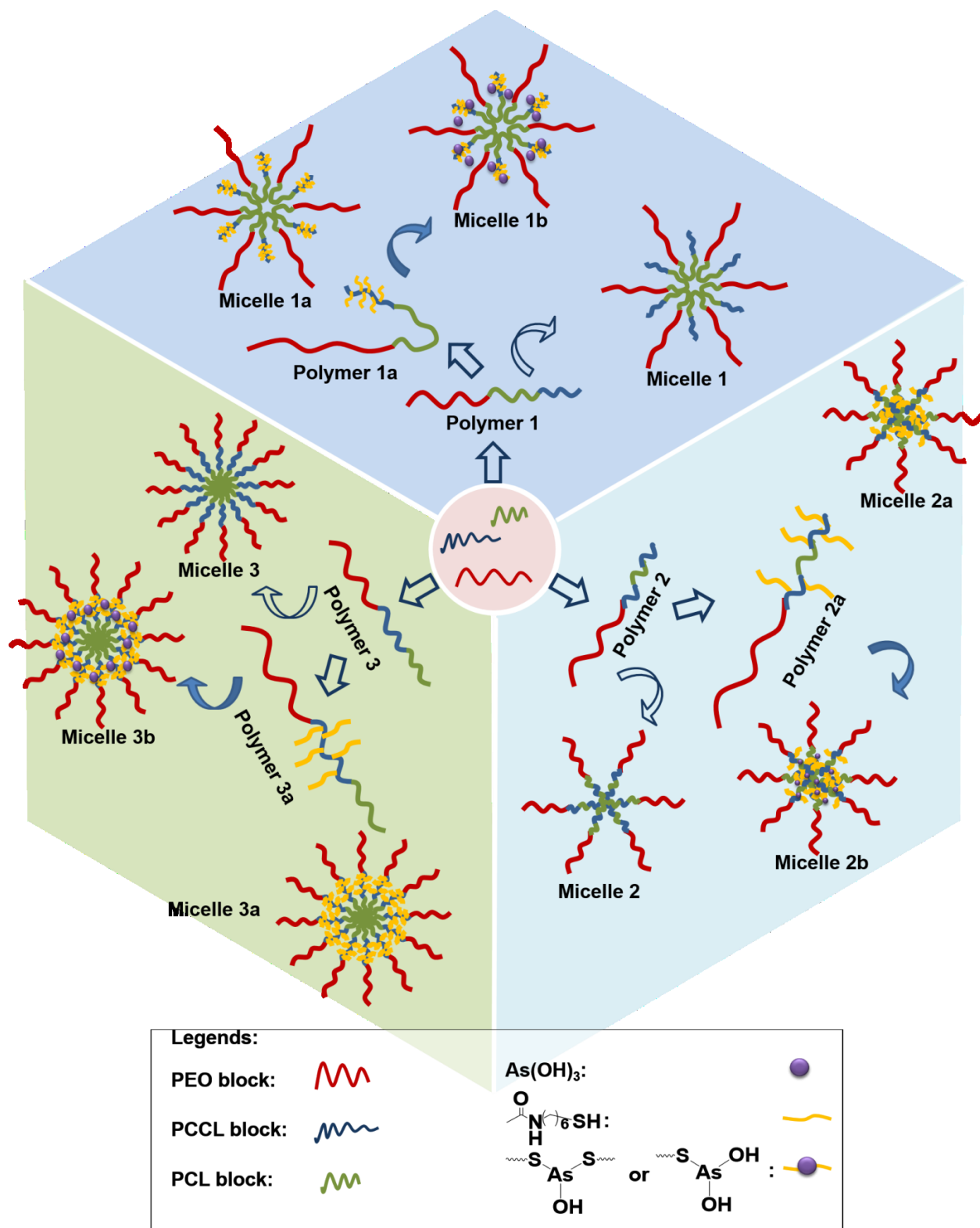
These proposed structures in **Scheme 4.2** implicated by  $^1H$ -NMR spectroscopy, can explain some of our observations on the zeta potential and size of prepared micelles. For instance, our NMR data implies formation of loose micelles from thiolated polymers and/or micelles with thiol groups hanging out of the micellar core, which are prone to formation of aggregates. In either case, a large size will be expected; a phenomenon observed in measurement of size for micelles 1a, 2a and 3a (

**Table 4.1).** Moreover, the average size of micelles **1b**, **2b**, and **3b** in water (As<sup>III</sup> loaded micelles) was 124±1 nm, 121±4 nm, and 107±2 nm, respectively. Micelles **1b** and **2b** had similar size and micelle **3b** was the smallest (P<0.0001, One-way ANOVA). This implies a more compact micellar structure from polymer **3b** which had linear PCL block (with no ionisable side group) at the hydrophobic end of the polymer chain. The same category of micelles (**3**, **3a**, and **3b**) have shown the minimum zeta potential compared to their polymer **1** and **2** micellar counterparts, which again might be attributed to a more compact structure restricting water access COOH groups thereby limiting their ionization.

**Table 4.2. Ratio of CL, CCL, and CCL-C6-SH components in terpolymers calculated from <sup>1</sup>H-NMR spectra obtained in CDCl<sub>3</sub> and D<sub>2</sub>O.**

	Area under proton peaks of hydrophobic segments normalized to that of PEO segment*				Ratio of the normalized area under proton peaks of hydrophobic segments in D <sub>2</sub> O to that in CDCl <sub>3</sub>	
	in CDCl <sub>3</sub>		in D <sub>2</sub> O		CL <sub>D2O</sub> /CL <sub>CDCl3</sub>	CCL <sub>D2O</sub> /CCL <sub>CDCl3</sub>
	CL	CCL	CL	CCL		
1	0.039	0.0833	0.036	0.039	0.9	0.47
2	0.0044	0.066	0.044	0.043	1	0.65
3	0.048	0.075	0.029	0.034	0.6	0.45
	in CDCl <sub>3</sub>		in D <sub>2</sub> O		CL <sub>D2O</sub> /CL <sub>CDCl3</sub>	CCL-C <sub>6</sub> -SH <sub>D2O</sub> /CCL-C <sub>6</sub> -SH <sub>CDCl3</sub>
	CL	CCL-C <sub>6</sub> -SH	CL	CCL-C <sub>6</sub> -SH		
	1a	0.050	0.068	0.028	0.085	0.56
2a	0.056	0.059	0.030	0.055	0.53	0.93
3a	0.057	0.053	0.029	0.043	0.50	0.82

\* The peak area related to CL, CCL, and CCL-C<sub>6</sub>-SH components were calculated from the integral of peaks at δ 2.40 – 2.22 (2H, CL), δ 4.20 – 3.95 (2H, CL and CCL), δ 2.96 – 2.78 and δ 2.75 – 2.58 (4H, CCL-C<sub>6</sub>-SH), respectively. These proton peak areas were normalized against the proton peak area of PEO, which was calculated from the integral of peak δ 3.76 – 3.57 (114 × 4H, PEO).



**Scheme 4.2. Proposed structures of micelles.** Micelles are assembled from starting polymers (polymer 1, 2, 3) and thiol-functionalized polymers (polymer 1a, 2a, 3a), and arsenous acid loaded micelles (micelle 1b, 2b, 3b).

#### 4.3.5 Morphology of As<sup>III</sup>-loaded micelles.

The morphology of As<sup>III</sup>-loaded micelles was determined by TEM with PTA negative staining ( **Figure 4.12**). Micelles **1b** and **3b** had similar size at dry state. Their diameter ranged from 9 to 27 nm. Micelles from **2b** were relatively larger and their diameters ranged from 12 to 40 nm. Micelles from **1b** polymers showed noticeable aggregate formation (**Figure 4.13A**). This is probably because of the exposure of the thiol groups to the micelle surface in micelle **1b** facilitating micellar interactions. Packs of micelle **3b** can also be observed (**Figure 4.13B**), however, the micelles still maintain clear boundary from each other.

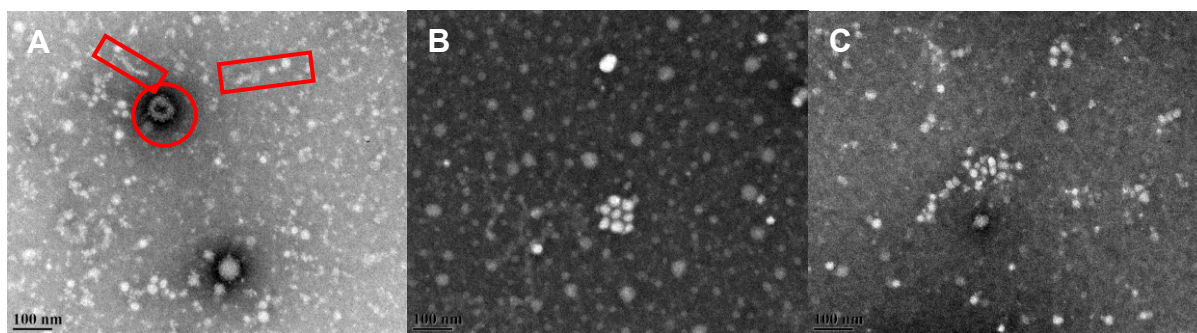


**Figure 4.12. TEM of arsenic-loaded micelles.** (A) Micelle **1b**, (B) micelle **2b**, and (C) micelle **3b** (taken at 80 kV with magnification of 110,000). All the micelles had spherical morphology. Micelle **1b** and **3b** had similar size at dry state, and their diameter ranged from 9 nm to 27 nm with an average of 16 nm. Micelle **2b** was relatively bigger with diameter ranging from 12 nm to 40 nm with an average of 22 nm. Necklace (red circle) and chains (rectangle) of micelle **1b** were observed. The width of micelle necklace was about 16 nm, the same as the micelle diameter.

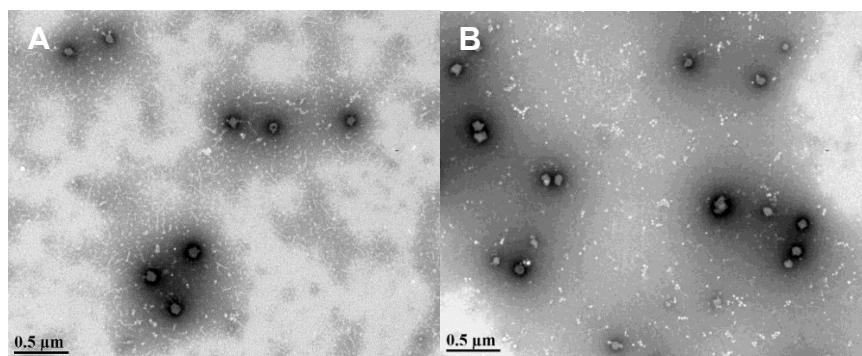


**Figure 4.13. TEM of micelle 1b (A) and micelle 3b (B) taken at 80 kV with magnification of 28,000.** Aggregates of micelles **1b** and **3b** were observed. The aggregates of micelle **3b** had an average diameter of 89 nm. The aggregates of micelle **1b** had two kinds of morphology. Most of them were spherical with an average diameter of 60 nm, few of which were of necklace shape. Micelle **1b** tends to line up and merge at one dimension.

#### 4.3.6 *In vitro* arsenic release from micelles

The rate of arsenic release from the three types of micelles during the first 12 hours of incubation was not statistically different ( $P > 0.05$ , One-way ANOVA). The release patterns of these three micelle types in H<sub>2</sub>O, or in RPMI-1640 medium, or in FBS-supplemented medium were similar (Figure 4.14).

The initial burst release of arsenic from **1b** (or **2b**, **3b**) micelle did not significantly increase when the release medium was changed from water to RMPI-1640 compared to water, but the presence of 10% FBS enhanced the initial arsenic burst release significantly ( $P < 0.05$ , One-way ANOVA). The initial arsenic release is mainly from the arsenic compound that is physically adsorbed to the micelle surface or is loosely attached to the micelle due to electrostatic interaction. According to our previous study, (Zhang et al. 2014) thiol-containing compounds such as glutathione can compete with mercaptohexylamino pendant group on the polymer chain for the binding of arsenic and trigger the arsenic release. The competition reaction can quickly reach the equilibrium and the arsenic bound to the thiol-containing small molecules can easily diffuse out from the micelle. Higher thiol content from proteins in FBS may be the reason for the initial arsenic release elevation.

A comparison between different terpolymer orientations in micelles revealed higher initial release of arsenic from micelles of **1b** polymers compared to **2b** and **3b**, either in water or in cell culture media ( $P < 0.0001$ , One-way ANOVA). This observation resonates with the micelle structure discussion in **Section 4.3.4**. The P(CCL/CCL-C<sub>6</sub>-SH) block in micelle **1b** which has binding sites for arsenic compound was better exposed to solvent than that in micelles **2b** or **3b**. The better accessibility to P(CCL/CCL-C<sub>6</sub>-SH) block in micelle **1b** results in relatively higher arsenic loading amount (**Figure 4.7**) and higher initial arsenic release (**Figure 4.14D**).

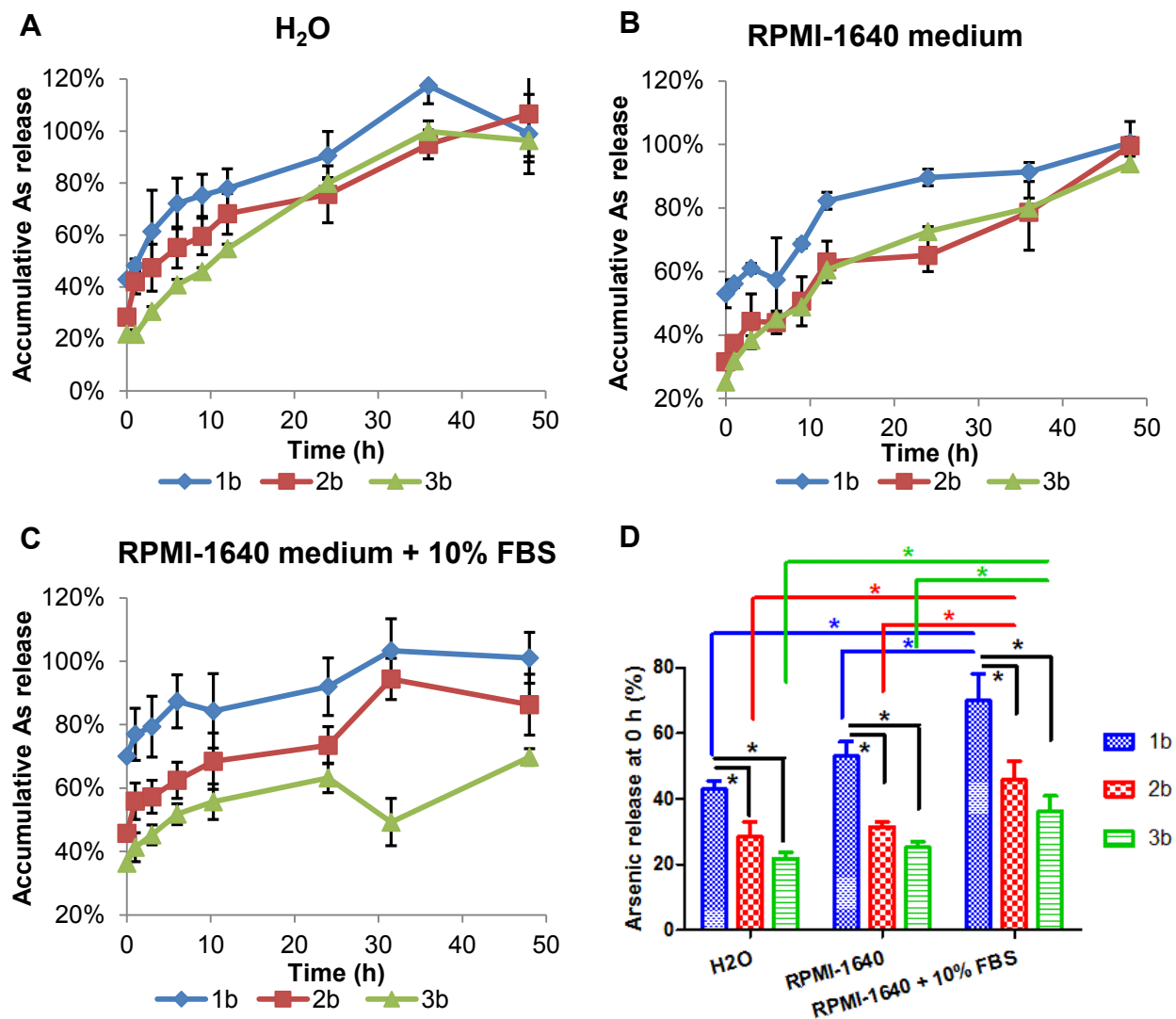


**Figure 4.14.** *In vitro* As<sup>III</sup> release from micelles at 37 °C in (A) water, (B) RPMI-1640 cell culture medium, and (C) RPMI-1640 medium supplemented with 10% FBS. Data are presented as mean ± SD (n = 3) of triplicate samples. The arsenic release from the micelles at 0 h was re-organized into a bar graph (D). One-way ANOVA with post-test of Tukey's multiple comparison test was performed among three types of arsenic-encapsulated micelles in a same solvent and among micelle solutions prepared in three different solvents. Micelle **1b** had significantly higher initial release than **2b** or **3b** (\*: P<0.05) in H<sub>2</sub>O, RPMI-1640, and RPMI-1640 supplemented with 10% FBS. And micelles prepared in RPMI-1640 supplemented with 10% FBS had significantly higher initial release than the correspondic micelles prepared in H<sub>2</sub>O or in RPMI-1640 (\*: P<0.05).

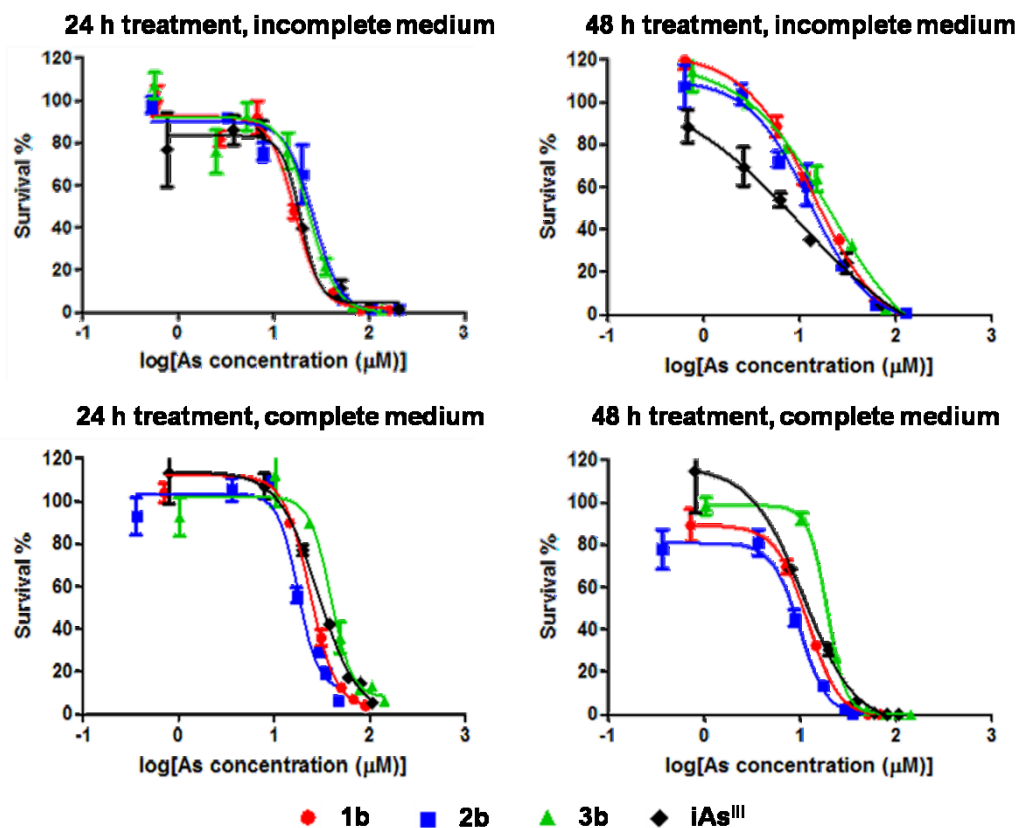
#### 4.3.7 Cellular uptake of encapsulated As<sup>III</sup>

To evaluate the cellular uptake of encapsulated As<sup>III</sup>, we treated MDA-MB-435 cells with free and encapsulated As<sup>III</sup> formulations with equivalent arsenic concentration within the range of 1/3 to 1/2 of corresponding IC<sub>50</sub> values for 24 h. The IC<sub>50</sub> values of free and encapsulated As<sup>III</sup> were determined using the neutral red assay (**Figure 4.15**). The arsenic concentration in homogenized cells, cell lysate, and cell debris were measured using ICP-MS. The cellular uptake of arsenic was calculated as the arsenic atom number per gram of soluble protein in cells. To level the effect of different arsenic treatment concentration, the relative arsenic cellular uptake was calculated by dividing the arsenic cellular uptake by the treated arsenic concentration. The results are presented in **Figure 4.16**.

According to **Figure 4.16**, the sum of arsenic amount in cell lysate and in cell debris equaled the total arsenic amount in the whole digested cells. This observation indicated that the analysis method was robust. Comparing the amount of arsenic in the whole cells treated with different As<sup>III</sup> formulations, we found with micelle encapsulation the arsenic uptake was increased substantially compared to free As<sup>III</sup> ( $p < 0.0001$ , One-way ANOVA). The relative arsenic cellular uptake by cells treated with **1b** and **2b** was ~ 3 times that of when the cells were treated with free As<sup>III</sup>, and cells treated with **3b** had ~ 7 times more relative arsenic uptake than the cells treated with As<sup>III</sup>. The relative cellular uptake ranked as **3b** > **1b**, **2b** > free As<sup>III</sup>.

We also noticed that the amount of arsenic in the cell debris fraction in the cells treated with **3b** was much larger than that in the cells treated with **1b** and **2b** ( $P < 0.0001$ , One-way ANOVA). The cell debris is mainly composed of the cell membrane. The increased arsenic cellular uptake with micelle encapsulation is likely due to the enhanced interaction between micelles and cells. Micelle **3b** which had the least negative charges on the surface had highest attachment to the cell

membrane and cellular uptake. The amount of arsenic attached to the cell membrane in the cells treated with micelles **1b** and **2b** were of no statistical difference ( $P=0.238$ , t-test), leading to similar arsenic concentrations in the cell lysate ( $P=0.058$ , t-test) and in the homogenized cells ( $P=0.059$ , t-test). This observation is in accordance with similar zeta-potential of micelles **1b** and **2b** ( $P=0.075$ , t-test). The cellular uptake of encapsulated arsenic is closely related to the surface charge of the micelles.



	Incomplete medium				Complete medium			
	24 h treatment		48 h treatment		24 h treatment		48 h treatment	
	IC <sub>50</sub>	95% CI	IC <sub>50</sub>	95% CI	IC <sub>50</sub>	95% CI	IC <sub>50</sub>	95% CI
<b>1b</b>	23.0	20.5 – 25.8	13.9	11.2 – 17.4	23.7	20.8 – 27.1	11.9	10.5 – 13.4
<b>2b</b>	27.5	24.4 – 31.1	12.7	8.7 – 18.5	17.9	15.1 – 21.3	9.8	8.2 – 11.4
<b>3b</b>	33.1	28.8 – 38.1	20.8	12.4 – 34.9	39.4	31.1 – 49.8	18.9	17.7 – 20.1
<b>As<sup>III</sup></b>	25.4	21.0 – 30.6	10.0	3.5 – 28.5	29.0	22.1 – 39.1	10.6	7.4 – 15.2

Note: The IC<sub>50</sub> and 95% CI values were expressed as the equivalent arsenic concentration (μM).

**Figure 4.15. *In vitro* cytotoxicity of free and encapsulated arsenic formulations against MDA-MB-435 cells.** Arsenic formulations were prepared in either incomplete RPMI-1640 medium or complete RPMI-1640 medium supplemented with 10% FBS. The cytotoxicity of different treatment duration, i.e., 24 h and 48 h, were evaluated. The IC<sub>50</sub> and 95% confidence interval (95% CI) were expressed as the equivalent arsenic concentration in each formulation solution. The data in the dose-responsive plots are presented as average ± SD (n = 3). The experiment of 24 h treatment of arsenic formulations in incomplete medium was repeated for three times and similar results were obtained. A representative result is presented here. One batch of the other three experiments was attempted.

### Relative cellular uptake of arsenic

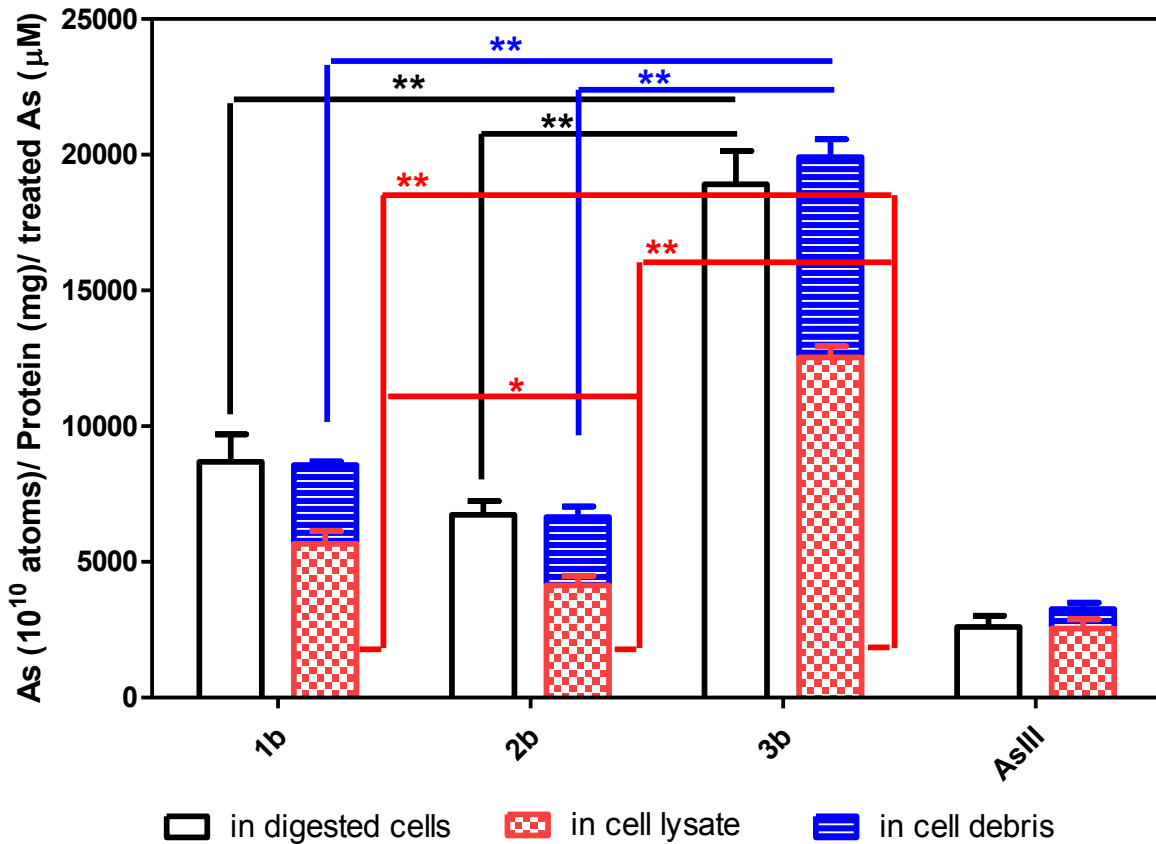


**Figure 4.16. *In vitro* cellular uptake of arsenic by MDA-MB-435 cells after 24 h treatment of free and encapsulated arsenic formulations.** The arsenic formulations were prepared in RPMI-1640 medium. Equivalent arsenic concentration in **1b**, **2b**, **3b**, and  $As^{III}$  treatment solution was 7, 9, 15, and 8  $\mu M$ , respectively, which was in the range of 1/3 to 1/2 of their respective  $IC_{50}$  Values. To mask the influence of arsenic treatment concentration variation on the cellular uptake, the relative cellular arsenic uptake is reported here, that is, the arsenic concentration in the cells (number of arsenic atoms/mg of soluble protein in cell lysate) is normalized by the arsenic treatment concentration ( $\mu M$ ). The data are presented as mean  $\pm$  SD ( $n = 3$ ). One-way ANOVA with post-test of Tukey's multiple comparison test was performed among arsenic uptake in digested cells, in cell debris, and in cell lysate of cells treated with encapsulated arsenic formulations and free  $As^{III}$ . All encapsulated arsenic formulation had significantly higher relative cellular arsenic uptake than free  $As^{III}$ , either in digested cells, cell lysate or cell debris ( $P < 0.01$ , asterisk sign not shown in the figure). Micelle **3b** had significantly higher relative cellular arsenic uptake than **1b** and **2b** (\*\*:  $P < 0.01$ ). Micelle **1b** and **2b** had similar relative cellular arsenic uptake in digested cell samples and in cell debris samples, while micelle **2b** had significantly higher relative cellular arsenic uptake in cell lysate samples than **1b** (\*:  $P < 0.05$ ). The relative arsenic cellular uptake ranks as: **3b** > **1b**, **2b** >  $As^{III}$  in digested cells; **3b** > **1b** > **2b** >  $As^{III}$  in cell lysate; and **3b** > **1b**, **2b** >  $As^{III}$  in cell debris. The uptake experiment was repeated twice. Similar results with same ranking were obtained.

#### 4.4 Discussion

Our long term objective is to design an optimum nanoparticle formulation for effective delivery of arsenic to solid tumors. We have developed thiolated polymeric micelles based on PEO-*b*-PCCL capable of PAO incorporation through As<sup>III</sup>-thiol interaction before. In this study, we tried to optimize this delivery system for the delivery of arsenous acid by mitigating the negative impact of carboxylic acid groups on the PCCL backbone on the stability of micelles. Towards this goal, unmodified caprolactone units were introduced to the polymer structure to increase the hydrophobicity of the poly(ester) segment. The effect of caprolactone unit placement in the structure of developed terpolymers on the stability, drug release and cellular uptake of arsenic-incorporated micelles was then evaluated.

Three terpolymers composed of PEO (as the hydrophilic part), PCL and PCCL (as the hydrophobic part) with varying placement of CCL units in the poly(ester) segment were synthesized (Polymers **1**, **2**, and **3** in

**Table 4.1).** Our assessments showed differences between characteristics of micelles formed from these three structures. In general, micelles formed from polymer **3** were particularly found to be superior in terms of micellar stability, arsenic release and cell uptake, although they have shown lower As<sup>III</sup> loading compared to the other structures under study.

Irrespective of the CCL placement, the introduction of CL units was found to substantially decrease the CMC of polymers, indicating increased thermodynamic stability of micelles formed by CL-containing terpolymers. This finding is in coherence with reports of Yang *et al.* (Yang *et al.* 2010) who introduced ethyl carbonate (EC) units into p(ethylene glycol)-*block*-poly(acid carbonate) (PEG-*b*-PAC) block copolymers and synthesized two blocked terpolymers of PEG-*b*-PEC-*b*-PAC and PEG-*b*-PAC-*b*-PEC, and one randomly distributed terpolymer PEG-*b*-PEAC. In that study, addition of more hydrophobic EC units resulted in a decreased CMC values of terpolymers compared to PEG-*b*-PAC diblock polymer, regardless of the distribution of EC units in the terpolymers.

The terpolymers with different chain arrangement showed different performance in terms of micellar thermodynamic stability. Polymers **1** and **2** had similar CMC values, both of which were larger than that of polymer **3**. One may argue that the lower CMC of polymer **3** compared to polymer **1** might be due to lower CCL/CL unit number ratio in polymer **3**. However, polymer **3** had similar CCL/CL unit number ratio as polymer **2**, but still showed lower CMC. This observation suggest that polymer **3** with the **ABC** orientation are more stable than polymers with **ACB** and **A(B/C)<sub>ran</sub>** orientations.

We then assessed the stability of micelles in terms of tendency for dissociation. Dissociation of micelles **1b** and **2b** was observed when the solvent was changed from water to PBS, while micelle **3b** maintained their integrity and remained at unimodal size distribution (**Figure 4.9**),

suggesting that micelle **3b** was more resistant to the salt effect and kinetically more stable than micelles **1b** and **2b**.

Yang *et al.* evaluated the stability of micelles with different chain arrangement as well.(Yang *et al.* 2010) In contrast to our observation, PEG-*b*-PEC-*b*-PAC micelles with the most hydrophobic block in the shell/core interface were more stable than PEG-*b*-PAC-*b*-PEC micelles. In that study, the randomly distributed PEG-*b*-PEAC micelles remained the least stable one among the three types of terpolymeric micelles. The difference between our results and that of Yang *et al.* could be due to the more bulky structure of PEC in polymers of Yang *et al.* (with weak inter polymer interaction within the micellar core) compared to PCL in our polymers.

Micelles formed from polymer **3** series were also found to bear less negative charge on their surface compared to micelles from polymer **1** and **2** series. Consequently, micelles from polymer **3** provided higher uptake of incorporated arsenic in cancer cells compared to free arsenic and micelles from polymers **1** and **2**. The cellular uptake of As<sup>III</sup> is via facilitated diffusion. Transporters involved in As<sup>III</sup> uptake include aquaglyceroporins,(Rosen 2002) such as AQP9 and AQP7, and glucose transporters,(Leslie 2012) such as GLUT1 and GLUT2. Therefore, the cellular uptake of As<sup>III</sup> is dependent on the expression of these transporters as well as the As<sup>III</sup> concentration gradient. After encapsulation of As<sup>III</sup> inside the micelles, the cellular uptake of the encapsulated As<sup>III</sup> is dependent on the properties of micelles.(Sahay *et al.* 2010) As observed in our study, the micelle encapsulation substantially enhanced the cellular uptake of As<sup>III</sup> compared to free As<sup>III</sup>. More importantly, micelle **3b** with the least negative zeta-potential had the highest cellular uptake of As<sup>III</sup> among the three types of micelles. This is attributed to the negative charge of phospholipids in the cell membrane that can repel nanoparticles of similar charge (e.g., micelles from polymers **1** and **2**).(Ma *et al.* 2013) We noticed that the arsenic content in the cell debris of cells treated with

micelle **3b** was substantially higher than those treated with micelles **1b** and **2b** (**Figure 4.11**). These results suggest micelle **3b** to have better interaction with MDA-MB-435 cell membrane than micelles **1b** and **2b**, leading to high cellular uptake of arsenic.

To explain our observations, we gained further insights into the structural differences between micelles from polymer **3** and those from polymers **1** and **2** using  $^1\text{H-NMR}$  spectroscopy in  $\text{D}_2\text{O}$  versus  $\text{CDCl}_3$  (**Table 4.2**). Our NMR investigations implied the following: In **ABC** micelles, the PCL block locates at the hydrophobic end and perhaps forms a compact micelle core, while in **ACB** and **A(B/C)<sub>ran</sub>** micelles the core is occupied by bulky PCCL or P(CCL/CCL- $\text{C}_6\text{-SH}$ ) blocks. In general, our results implied the burial of PCL segment in the core of **ABC** micelles and polymer folding and/or formation of loose micelles leading to the exposure of PCCL or P(CCL/CCL- $\text{C}_6\text{-SH}$ ) to water in **ACB** and **A(B/C)<sub>ran</sub>** micelles (**Scheme 4.2**). This hypothetical scheme (**Scheme 4.2**) is in line with other observations in this manuscript. For instance, the thiol group is more accessible in **ACB** and **A(B/C)<sub>ran</sub>** micelles for arsenic interaction leading to better As/S ratios in **ACB** and **A(B/C)<sub>ran</sub>** (**1b** and **2b**, respectively) versus **ABC** (**3b**) micelles (**Figure 4.7**). Moreover, the compact core of the **ABC** micelles affords micelles which can resist perturbation by the solvent and electrolytes; whereas the **ACB** and **A(B/C)<sub>ran</sub>** micelles have loose cores that are more vulnerable and accessible to the solvent (**Figure 4.9**). In addition, **ACB** micelles and **A(B/C)<sub>ran</sub>** from the polymer **1** and **2** series (that had presumably loose micelle core) are more accessible to water than the **ABC** micelles from the polymer **3** series. This might have led to better deprotonation of the  $\text{COOH}$  group and a higher negative zeta-potential on the **ACB** micelle surface (**Figure 4.11**) leading to their lower cellular uptake.

Our report confirms that the use of terpolymeric micelles to enable fine tuning of micelle characteristics and additional micelle functions compared to diblock copolymer micelles, although

the effect of block sequence arrangement on micelle characteristics can vary in different terpolymer systems.(Wyman and Liu 2013) Terpolymeric micelles may also prove to be advantageous to diblock copolymer micelles for multidrug co-encapsulation,(Endres et al. 2011; Gaspar et al. 2014) stimuli responsive design,(Bian et al. 2013; Liu et al. 2012) and multicompartment structure preparation,(Fustin et al. 2005; Sun et al. 2011) and there are increasing drug delivery studies using terpolymeric micelles. Considering the unpredictable effect of block sequence arrangement on micelle characteristics, more attention to the polymer chain design when triblock polymers are involved is warranted.

#### 4.5 Conclusions

In this study, we focused on the evaluation of three block sequence isomers of PEO/PCL/PCCL terpolymers with regards to micelle stability, surface charge, arsenic loading, release, and cellular uptake. Our results show the block sequence arrangement to have great influence on the above characteristics. In particular, the results showed the **ABC** terpolymer **3b** with PCL block at the terminal end to display maximum micelle stability, least negative surface, lowest arsenic burst release, and highest arsenic cellular uptake compared to other structures under study. Therefore, terpolymer micelles of ABC orientation are considered for further studies on As<sup>III</sup> delivery.

#### 4.6 References

- Aliabadi HM, Mahmud A, Sharifabadi AD, Lavasanifar A. 2005. Micelles of methoxy poly(ethylene oxide)-b-poly(epsilon-caprolactone) as vehicles for the solubilization and controlled delivery of cyclosporine a. *Journal of Controlled Release* 104:301-311.
- Bian QQ, Xiao Y, Zhou C, Lang MD. 2013. Synthesis, self-assembly, and pH-responsive behavior of (photo-crosslinked) star amphiphilic triblock copolymer. *Journal of Colloid and Interface Science* 392:141-150.

- Cajot S, Lautram N, Passirani C, Jerome C. 2011. Design of reversibly core cross-linked micelles sensitive to reductive environment. *Journal of Controlled Release* 152:30-36.
- Endres TK, Beck-Broichsitter M, Samsonova O, Renette T, Kissel TH. 2011. Self-assembled biodegradable amphiphilic peg-pcl-lpei triblock copolymers at the borderline between micelles and nanoparticles designed for drug and gene delivery. *Biomaterials* 32:7721-7731.
- Fustin CA, Abetz V, Gohy JF. 2005. Triblock terpolymer micelles: A personal outlook. *European Physical Journal E* 16:291-302.
- Gaspar VM, Goncalves C, de Melo-Diogo D, Costa EC, Queiroz JA, Pichon C, et al. 2014. Poly(2-ethyl-2-oxazoline)-pla-g-pei amphiphilic triblock micelles for co-delivery of minicircle dna and chemotherapeutics. *Journal of Controlled Release* 189:90-104.
- Honary S, Zahir F. 2013. Effect of zeta potential on the properties of nano-drug delivery systems - a review (part 1). *Tropical Journal of Pharmaceutical Research* 12:255-264.
- Kamenka N, Chorro M, Talmon Y, Zana R. 1992. Study of mixed aggregates in aqueous-solutions of sodium dodecyl-sulfate and dodecyltrimethylammonium bromide. *Colloids and Surfaces* 67:213-222.
- Leslie EM. 2012. Arsenic-glutathione conjugate transport by the human multidrug resistance proteins (mrps/abccs). *Journal of Inorganic Biochemistry* 108:141-149.
- Liu R, He B, Li D, Lai YS, Tang JZ, Gu ZW. 2012. Stabilization of ph-sensitive mpeg-ph-pla nanoparticles by stereocomplexation between enantiomeric polylactides. *Macromolecular Rapid Communications* 33:1061-1066.
- Ma N, Ma C, Li C, Wang T, Tang Y, Wang H, et al. 2013. Influence of nanoparticle shape, size, and surface functionalization on cellular uptake. *Journal of Nanoscience and Nanotechnology* 13:6485-6498.
- Mahmud A, Xiong XB, Lavasanifar A. 2006. Novel self-associating poly(ethylene oxide)-block-poly(epsilon-caprolactone) block copolymers with functional side groups on the polyester block for drug delivery. *Macromolecules* 39:9419-9428.
- Rosen BP. 2002. Biochemistry of arsenic detoxification. *Febs Letters* 529:86-92.

- Sahay G, Alakhova DY, Kabanov AV. 2010. Endocytosis of nanomedicines. *Journal of Controlled Release* 145:182-195.
- Shahin M, Lavasanifar A. 2010. Novel self-associating poly(ethylene oxide)-b-poly( $\epsilon$ -caprolactone) based drug conjugates and nano-containers for paclitaxel delivery. *International Journal of Pharmaceutics* 389:213-222.
- Sun GR, Cui HG, Lin LY, Lee NS, Yang C, Neumann WL, et al. 2011. Multicompartment polymer nanostructures with ratiometric dual-emission pH-sensitivity. *Journal of the American Chemical Society* 133:8534-8543.
- Varade D, Joshi T, Aswal VK, Goyal PS, Hassan PA, Bahadur P. 2005. Effect of salt on the micelles of cetyl pyridinium chloride. *Colloids and Surfaces a-Physicochemical and Engineering Aspects* 259:95-101.
- Wei XL, Wang YG, Zeng WF, Huang F, Qin L, Zhang CL, et al. 2012. Stability influences the biodistribution, toxicity, and anti-tumor activity of doxorubicin encapsulated in peg-pe micelles in mice. *Pharmaceutical Research* 29:1977-1989.
- Wyman IW, Liu GJ. 2013. Micellar structures of linear triblock terpolymers: Three blocks but many possibilities. *Polymer* 54:1950-1978.
- Xiong XB, Mahmud A, Uludag H, Lavasanifar A. 2007. Conjugation of arginine-glycine-aspartic acid peptides to poly(ethylene oxide)-b-poly( $\epsilon$ -caprolactone) micelles for enhanced intracellular drug delivery to metastatic tumor cells. *Biomacromolecules* 8:874-884.
- Yang CA, Tan JPK, Cheng W, Attia ABE, Ting CTY, Nelson A, et al. 2010. Supramolecular nanostructures designed for high cargo loading capacity and kinetic stability. *Nano Today* 5:515-523.
- Zhang Q, Vakili MR, Li X-F, Lavasanifar A, Le XC. 2014. Polymeric micelles for gsh-triggered delivery of arsenic species to cancer cells. *Biomaterials* 35:7088-7100.

## Chapter 5. General discussion and conclusions

### 5.1 General discussion

The ultimate goal of nano-arsenic-chemotherapy is to achieve enhanced therapeutic efficacy in solid tumors and alleviated adverse side effects in healthy tissues by targeted delivery of trivalent arsenic compounds to tumor areas. I selected PEO-*b*-PCL-based polymeric micelles as the nano-carrier for ATO delivery, because these micelles are biodegradable and biocompatible with tunable properties.

The challenge of arsenic encapsulation in polymeric micelles lies in the good water solubility of ATO, which results in low arsenic retention in micelles and fast arsenic release. Liposomes have been applied for ATO encapsulation, where dissolved ATO resides in the hydrophilic compartment of liposomes. (Kallinteri et al. 2004) Although the arsenic loading amount in liposomes could be achieved at levels as high as 0.5 mol As per mole of lipids, more than 70% of the initially loaded ATO was released within 24 hours, which is far less than satisfactory.

The core of polymeric micelles is hydrophobic, which is an additional challenge in encapsulating hydrophilic arsenic compounds. To increase the arsenic loading content and slow down arsenic release in micelles, the PEO-*b*-PCCL polymer was functionalized with a thiol-containing pendant group to form PEO-*b*-P(CCLC<sub>6</sub>-SH) micelles, which have high affinity for trivalent arsenic compounds (**Scheme 2.1**). The thiol-containing polymeric micelles were tested for encapsulation of an organoarsenical, phenylarsine oxide (PAO), in **Chapter 2**. With thiol groups in the micelle core, the loading of PAO was enhanced from 0.17 wt% to 2.4 wt%, which corresponded to 0.65 mol As per mol of thiol groups (**Figure 2.3**). Although a burst release around 20% of the initially encapsulated PAO was observed, the accumulative PAO release was ~ 40% within 24 hours in ammonium acetate buffer (1.45 M, pH 7) at 37 °C (**Figure 2.9**). The burst

release was attributed to arsenic compound that was physically adsorbed in micelles or merely had ionic interaction with thiol groups. The slow release during incubation in the buffer was due to the slow hydrolysis of bonded PAO in the form of S-As(phenyl)-S. The release of PAO could be triggered by the addition of glutathione (GSH) (**Figure 2.9**). An additional 15–20% of the initially encapsulated PAO was released up addition of 1 mM GSH. The thiol on the cysteine residue of GSH can compete with the polymer chain for arsenic binding. This competition reaction can reach equilibrium within 1 hour and instantly enhance PAO release. As GSH naturally exists in the cell cytosol at high concentration (0.5–10 mM) but at low concentration in plasma (5–50  $\mu$ M), the micelle encapsulated PAO is expected to have prolonged release in the circulation system and have a triggered release inside cells.

This arsenic encapsulation strategy involving As–S binding was then applied to ATO encapsulation in micelles (**Chapter 3**). The loading of ATO in PEO-*b*-P(CCLC<sub>6</sub>-SH) achieved 4.0 wt%, which corresponded to 0.67 mol As per mol of thiol groups (**Figure 3.8**). The accumulative ATO release within 24 hours was ~ 60%, however the burst release of ATO was relatively high (~ 30 %) (**Figure 3.11**).

To facilitate the targeted delivery of encapsulated arsenic compounds, I modified the micelle surface with an affinity ligand, GRGDS peptide, which has high affinity for the  $\alpha$ v $\beta$ 3 integrin overexpressed on the cell membrane of MDA-MB-435 breast cancer cells (**Section 3.2**). The peptide was conjugated onto the distal end of acetal-PEO (**Figure 3.1**). To circumvent the chemical modification challenge in conjugating both the peptide and the mercaptohexylamino group on the same polymer chain, I synthesized the peptide-conjugated polymer and thiol-functionalized polymer separately and prepared mixed micelles with GRGDS peptide on the micelle surface and thiol groups in the micelle core for ATO encapsulation using these two sets of polymers. Control

mixed micelles without surface decoration of GRGDS peptide but with thiol groups in the core were prepared for ATO encapsulation as well. The arsenic loading content was dependent on the amount of thiols in the micelles. Although the weight percentage of arsenic element in mixed micelles was lower than that in non-mixed micelles, the As/S molar ratio was maintained  $\sim 0.65$  (**Figure 3.9**). Nevertheless, the arsenic burst release from mixed micelle ( $\sim 50\%$  of initially encapsulated ATO) was substantially higher than non-mixed micelles (**Figure 3.13**).

The GRGDS peptide decoration on the mixed micelle surface enhanced the cellular uptake of arsenic and the cytotoxicity of arsenic in MDA-MB-435 cells compared to the control mixed micelles without GRGDS peptide decoration (**Figure 3.15** and **Figure 3.17**). However, the high arsenic burst release from these mixed micelles diminished the targeting effect of GRGDS peptide. The pretreatment of free GRGDS peptide in MDA-MB-435 cells did not affect the cellular uptake of arsenic encapsulated in GRGDS-decorated micelles (**Figure 3.19**). Because the majority of encapsulated ATO was released from mixed micelles upon dissolution in the cell culture medium, the arsenic taken up by cells was mainly via facilitated diffusion (Leslie 2012) instead of cell endocytosis. The surface properties of micelles would not control the cellular uptake of arsenic compound if the arsenic compound is in free form.

To reduce the burst release of ATO from mixed micelles, different block copolymers such as PEO-*b*-PCL, PEO-*b*-PDLLA, and PEO-*b*-PBCL were tested to form mixed micelles with PEO-*b*-P(CCLC<sub>6</sub>-SH) for ATO encapsulation (**Section 3.3**). PEO-*b*-P(CCLC<sub>6</sub>-SH) mixed with PEO-*b*-PBCL was found to have the lowest burst release ( $\sim 20\%$ ). How the polymer mixing system affects the arsenic release remains to be clarified. There are two possible reasons for this observation. The hydrophobic polymer chains without thiol groups in the micelle core may interfere with the stable As-S bond formation. The polymer chains with higher hydrophobicity may keep the micelle core

less accessible to water, which reduces arsenic release. Experiments to elucidate the effect of polymer mixing system on arsenic burst release are under way.

The stability of micelles is very important in successful targeted delivery of drugs *in vivo*, as it can affect the biodistribution, toxicity, and anti-tumor efficacy of the cargo (Wei et al. 2012). To improve the micelle stability, a non-modified PCL polymer was incorporated into the PEO-*b*-PCCL polymer backbone. Three PEO/PCCL/PCL terpolymers were synthesized with varying chain arrangements in the polyester segment, namely PEO-*b*-PCL-*b*-PCCL with **ACB** arrangement, PEO-*b*-P(CCL-*co*-PCL) with **A(B/C)<sub>random</sub>** arrangement, and PEO-*b*-PCCL-*b*-PCL with **ABC** arrangement. The incorporation of non-modified  $\epsilon$ -caprolactone units into the PEO-*b*-PCCL polymer decreased the critical micellar concentration (CMC) (**Table 4.1**), indicating these terpolymeric micelles were more thermodynamically stable than PEO-*b*-PCCL micelles. The polymer chain arrangement can affect the micelle stability. **ABC** micelles were more stable than **ACB** micelles and **A(B/C)<sub>random</sub>** micelles with lowest CMC value. These terpolymers were functionalized with thiol groups for ATO encapsulation. Arsenic-encapsulated **ABC** micelles maintained uniform size distribution in ionic PBS, while partial dissociation of arsenic-encapsulated **ACB** and **A(B/C)<sub>random</sub>** micelles were observed (**Figure 4.9**). The arsenic burst release from **ABC** micelles was substantially lower than **ACB** micelles either in water or in cell culture medium (**Figure 4.14**).

In addition to micelle stability, the polymer chain arrangement influenced the micelle surface charge as well. All types of terpolymeric micelles had negative charge on the surface due to the deprotonation of carboxylic acid groups in PCCL units. The zeta potential of **ACB** micelles was more negative than that of **ABC** micelles (**Figure 4.11**), which contradicted the assumption that the deprotonated CCL units (block **B**) located in the core of **ACB** micelle would result in lower

potential on the micelle surface. A polymer chain translocation in **ACB** micelle was hypothesized. A close look into the  $^1\text{H-NMR}$  spectra of micelles formed from terpolymers with or without thiol-functionality in  $\text{D}_2\text{O}$  revealed that the block **B** was translocated from the micelle core to the micelle stealth layer after thiol functionalization of **ACB** polymer (**Table 4.2**). Before thiol functionalization, the **ACB** polymers self-assembled into micelles with the block **B** forming a loose core and the block **C** in stealth layer well exposed to  $\text{D}_2\text{O}$ , while the **ABC** polymers assembled into micelles with the block **C** forming a compact core and the block **B** in stealth layer less exposed to  $\text{D}_2\text{O}$ . After thiol functionalization, the cores of the **ACB** micelles and the **ABC** micelles were both formed by the block **C**, and the block **B** in **ACB** micelles was better exposed to  $\text{D}_2\text{O}$  than the block **B** in **ABC** micelles. The translocation of the block **B** in **ACB** micelles from micelle core to micelle stealth layer after thiol functionalization is probably driven by both the stronger hydrophobicity of PCL block (block **C**) and the bulky structure of thiol-functionalized  $\text{P}(\text{CCLC}_6\text{-SH})$ . The compact core formed by PCL block in **ABC** micelles contributed to the better stability of **ABC** micelles. The less negatively charged **ABC** micelles resulted in a higher arsenic cellular uptake by MDA-MB-435 cells.

## 5.2 Conclusions

A strategy based on As-S chemistry is successfully developed for effective arsenic encapsulation in polymeric micelles. This strategy involves the thiol functionalization of polymer chains. The arsenic release from the micelles can be triggered by GSH, which exists naturally in the cell cytosol. Controlled arsenic release and good micelle stability are essential to successful targeted delivery of arsenic therapy using these nano-carriers. The arsenic burst release from micelles can be reduced by optimizing the mixed micelle system and polymer chain arrangement. The polymer chain

arrangement of terpolymers influences the micelle stability and surface charge by affecting the micelle structure, which can further affect the cellular internalization of the encapsulated drugs.

### 5.3 Future work and perspectives

In this study, I focused on the PEO-*b*-PCL-based polymers for arsenic encapsulation. Basic parameters such as arsenic loading and in vitro arsenic release, micelle stability, size distribution, and surface charge, as well as in vitro cytotoxicity and cellular uptake of encapsulated arsenic were evaluated. More extensive in vivo studies such as mouse model studies are necessary to demonstrate the biodistribution, anti-tumor efficacy, and toxicity of micelle encapsulated arsenic formulations.

Micelle encapsulation can enhance the cellular uptake of arsenic compounds as shown in **Figure 4.15**. However the enhanced accumulation of encapsulated arsenic in cells did not result in enhanced cytotoxicity (**Figure 4.14**). The targets of arsenic are located in the cytoplasm, mitochondria, and nucleus. Encapsulated arsenic needs several steps to reach its active targets, including breaking through the endosomes after endocytosis and releasing from the micelles. (Sahay et al. 2010) Encapsulated arsenic may encounter unexpected hurdles to reach its targets in specific sub-cellular organelles. Therefore, it is important to understand the sub-cellular trafficking of encapsulated arsenic. Fluorophore biarsenical probes such as FAsH-EDT<sub>2</sub> and ReAsH-EDT<sub>2</sub> could be expressed in specific organelles to monitor the distribution of arsenic compounds in living cells (Adams and Tsien 2008; Chen et al. 2015). With better understanding of the intracellular distribution of encapsulated arsenic, micelles can be designed with enhanced endosome-escaping and sub-cellular targeting functionalities to modulate the cytotoxicity of encapsulated arsenic.

The As-S based arsenic encapsulation strategy developed in this thesis can be applied to arsenic encapsulation in different nano-carrier systems, such as liposome and polymeric vesicles.

Since several transitional metal and metal ions (e.g., Au, Pt<sup>2+</sup>, Ag<sup>+</sup>) have high affinity for thiol groups, co-delivery of arsenic and these transitional metals is possible with thiol-functionalized nano-carriers. ATO has been reported to amplify the cisplatin toxicity against HPV-transformed human tubular cells (Dogra et al. 2015) and to have a synergistic effect with cisplatin in inhibiting the growth of ovarian cancer cells (Zhang et al. 2009). Co-delivery of ATO and cisplatin using thiol-functionalized micelles may have better anti-tumor efficacy.

#### 5.4 References

- Adams SR, Tsien RY. 2008. Preparation of the membrane-permeant biarsenicals flash-edt2 and reash-edt2 for fluorescent labeling of tetracysteine-tagged proteins. *Nature Protocols* 3:1527-1534.
- Chen BB, Liu QQ, Popowich A, Shen SW, Yan XW, Zhang Q, et al. 2015. Therapeutic and analytical applications of arsenic binding to proteins. *Metallomics* 7:39-55.
- Dogra S, Bandi S, Viswanathan P, Gupta S. 2015. Arsenic trioxide amplifies cisplatin toxicity in human tubular cells transformed by hpv-16 e6/e7 for further therapeutic directions in renal cell carcinoma. *Cancer Letters* 356:953-961.
- Kallinteri P, Fatouros D, Klepetsanis P, Antimisariis SG. 2004. Arsenic trioxide liposomes: Encapsulation efficiency and in vitro stability. *Journal of Liposome Research* 14:27-38.
- Leslie EM. 2012. Arsenic-glutathione conjugate transport by the human multidrug resistance proteins (mrps/abccs). *Journal of Inorganic Biochemistry* 108:141-149.
- Sahay G, Alakhova DY, Kabanov AV. 2010. Endocytosis of nanomedicines. *Journal of Controlled Release* 145:182-195.
- Wei XL, Wang YG, Zeng WF, Huang F, Qin L, Zhang CL, et al. 2012. Stability influences the biodistribution, toxicity, and anti-tumor activity of doxorubicin encapsulated in peg-pe micelles in mice. *Pharmaceutical Research* 29:1977-1989.

Zhang N, Wu Z-M, McGowan E, Shi J, Hong Z-B, Ding C-W, et al. 2009. Arsenic trioxide and cisplatin synergism increase cytotoxicity in human ovarian cancer cells: Therapeutic potential for ovarian cancer. *Cancer Science* 100:2459-2464.

## Bibliography

- Ablain J, de The H. 2011. Revisiting the differentiation paradigm in acute promyelocytic leukemia. *Blood* 117:5795-5802.
- Adams SR, Tsien RY. 2008. Preparation of the membrane-permeant biarsenicals flash-edt2 and reash-edt2 for fluorescent labeling of tetracysteine-tagged proteins. *Nature Protocols* 3:1527-1534.
- Ahn RW, Chen F, Chen HM, Stern ST, Clogston JD, Patri AK, et al. 2010. A novel nanoparticulate formulation of arsenic trioxide with enhanced therapeutic efficacy in a murine model of breast cancer. *Clinical Cancer Research* 16:3607-3617.
- Aliabadi HM, Mahmud A, Sharifabadi AD, Lavasanifar A. 2005. Micelles of methoxy poly(ethylene oxide)-b-poly(epsilon-caprolactone) as vehicles for the solubilization and controlled delivery of cyclosporine a. *Journal of Controlled Release* 104:301-311.
- Alimoghaddam K, Sharifabrizi A, Tavangar M, Sanaat Z, Rostami S, Jahani M, et al. 2006. Anti-leukemic and anti-angiogenesis efficacy of arsenic trioxide in new cases of acute promyelocytic leukemia. *Leukemia & Lymphoma* 47:81-88.
- Al-Shehri A, Favretto ME, Ioannou PV, Romero IA, Couraud PO, Weksler BB, et al. 2015. Permeability of pegylated immunoarsonoliposomes through in vitro blood brain barrier-medulloblastoma co-culture models for brain tumor therapy. *Pharmaceutical Research* 32:1072-1083.
- Antimisiaris SG, Klepetsanis P, Zachariou V, Giannopoulou E, Ioannou PV. 2005. In vivo distribution of arsenic after i.P. Injection of arsonoliposomes in balb-c mice. *International Journal of Pharmaceutics* 289:151-158.
- Antimisiaris SG. 2009. Arsonoliposomes for drug delivery applications. *Clinical Lipidology* 4:663-675.
- Arana-Trejo RM, Sanchez ER, Ignacio-Ibarra G, de la Fuente EB, Garces O, Morales EG, et al. 2002. Bcr/abl p210, p190 and p230 fusion genes in 250 mexican patients with chronic myeloid leukaemia (cml). *Clinical and Laboratory Haematology* 24:145-150.
- Armarego WLF. 2009. Purification of laboratory chemicals: Butterworth-Heinemann.

- Bagheri M, Shateri S, Niknejad H, Entezami AA. 2014. Thermosensitive biotinylated hydroxypropyl cellulose-based polymer micelles as a nano-carrier for cancer-targeted drug delivery. *Journal of Polymer Research* 21:15.
- Bajorin DF, Halabi S, Small E. 2009. Arsenic trioxide in recurrent urothelial cancer: A cancer and leukemia group b phase II trial (calgb 99903). *Clinical Genitourinary Cancer* 7:E66-E70.
- Barreto JA, O'Malley W, Kubeil M, Graham B, Stephan H, Spiccia L. 2011. Nanomaterials: Applications in cancer imaging and therapy. *Advanced Materials* 23:H18-H40.
- Beer TM, Tangen CM, Nichols CR, Margolin KA, Dreicer R, Stephenson WT, et al. 2006. Southwest oncology group phase II trioxide in patients with refractory malignancies. *Cancer* 106:2624-2629.
- Behr JP. 1997. The proton sponge: A trick to enter cells the viruses did not exploit. *Chimia* 51:34-36.
- Bergman JA, Cochran EW, Heinen JM. 2014. Role of the segment distribution in the microphase separation of acrylic diblock and triblock terpolymers. *Polymer* 55:4206-4215.
- Bian QQ, Xiao Y, Zhou C, Lang MD. 2013. Synthesis, self-assembly, and ph-responsive behavior of (photo-crosslinked) star amphiphilic triblock copolymer. *Journal of Colloid and Interface Science* 392:141-150.
- Boisselier E, Astruc D. 2009. Gold nanoparticles in nanomedicine: Preparations, imaging, diagnostics, therapies and toxicity. *Chemical Society Reviews* 38:1759-1782.
- Buchet JP, Heilier JF, Bernard A, Lison D, Jin TY, Wu XW, et al. 2003. Urinary protein excretion in humans exposed to arsenic and cadmium. *International Archives of Occupational and Environmental Health* 76:111-120.
- Burnett AK, Russell NH, Hills RK, Bowen D, Kell J, Knapper S, et al. 2015. Arsenic trioxide and all-trans retinoic acid treatment for acute promyelocytic leukaemia in all risk groups (aml17): Results of a randomised, controlled, phase 3 trial. *Lancet Oncology* 16:1295-1305.
- Byun JH, Cheong H-J, Won J-H, Park H-S, Hong YS, Kim S-J, et al. 2003. Effect of arsenic trioxide in trail (tumor necrosis factor-related apoptosis inducing ligand)-mediated apoptosis in multiple myeloma cell lines. *Cancer Research and Treatment* 35:472-477.

- Cai MT, Leng MT, Lu AJ, He L, Xie XX, Huang L, et al. 2015. Synthesis of amphiphilic copolymers containing zwitterionic sulfobetaine as pH and redox responsive drug carriers. *Colloids and Surfaces B-Biointerfaces* 126:1-9.
- Cai XH, Wang CL, Chen BA, Hua WJ, Shen F, Yu L, et al. 2014. Antitumor efficacy of dmsa modified fe<sub>3</sub>o<sub>4</sub> magnetic nanoparticles combined with arsenic trioxide and adriamycin in raji cells. *Journal of Biomedical Nanotechnology* 10:251-261.
- Cai XY, Yu K, Zhang LJ, Li YF, Li Q, Yang ZB, et al. 2015. Synergistic inhibition of colon carcinoma cell growth by hedgehog-gli1 inhibitor arsenic trioxide and phosphoinositide 3-kinase inhibitor ly294002. *Oncotargets and Therapy* 8:7.
- Cajot S, Lautram N, Passirani C, Jerome C. 2011. Design of reversibly core cross-linked micelles sensitive to reductive environment. *Journal of Controlled Release* 152:30-36.
- Carmignani M, Volpe AR, Aldea M, Soritau O, Irimie A, Florian IS, et al. 2014. Glioblastoma stem cells: A new target for metformin and arsenic trioxide. *Journal of Biological Regulators and Homeostatic Agents* 28:1-15.
- Chakraborti D, Mukherjee SC, Saha KC, Chowdhury UK, Rahman MM, Sengupta MK. 2003. Arsenic toxicity from homeopathic treatment. *Journal of Toxicology-Clinical Toxicology* 41:963-967.
- Chang JE, Voorhees PM, Kolesar JM, Ahuja HG, Sanchez FA, Rodriguez GA, et al. 2009. Phase ii study of arsenic trioxide and ascorbic acid for relapsed or refractory lymphoid malignancies: A wisconsin oncology network study. *Hematological Oncology* 27:11-16.
- Charoensuk V, Gati WP, Weinfeld M, Le XC. 2009. Differential cytotoxic effects of arsenic compounds in human acute promyelocytic leukemia cells. *Toxicology and Applied Pharmacology* 239:64-70.
- Chen BB, Liu QQ, Popowich A, Shen SW, Yan XW, Zhang Q, et al. 2015. Therapeutic and analytical applications of arsenic binding to proteins. *Metallomics* 7:39-55.
- Chen H, Ahn R, Van den Bossche J, Thompson DH, O'Halloran TV. 2009a. Folate-mediated intracellular drug delivery increases the anticancer efficacy of nanoparticulate formulation of arsenic trioxide. *Molecular Cancer Therapeutics* 8:1955-1963.

- Chen H, Pazicni S, Krett NL, Ahn RW, Penner-Hahn JE, Rosen ST, et al. 2009b. Coencapsulation of arsenic- and platinum-based drugs for targeted cancer treatment. *Angewandte Chemie-International Edition* 48:9295-9299.
- Chen HM, MacDonald RC, Li SY, Krett NL, Rosen ST, O'Halloran TV. 2006. Lipid encapsulation of arsenic trioxide attenuates cytotoxicity and allows for controlled anticancer drug release. *Journal of the American Chemical Society* 128:13348-13349.
- Chen HT, Kim SW, Li L, Wang SY, Park K, Cheng JX. 2008. Release of hydrophobic molecules from polymer micelles into cell membranes revealed by forster resonance energy transfer imaging. *Proceedings of the National Academy of Sciences of the United States of America* 105:6596-6601.
- Chen J, Zhang S, Li Y, Tang Z, Kong W. 2014. Hexokinase 2 overexpression promotes the proliferation and survival of laryngeal squamous cell carcinoma. *Tumor Biology* 35:3743-3753.
- Chen L, Chen F, Zhao MX, Zhu XD, Ke CH, Yu JM, et al. 2015. A redox-sensitive micelle-like nanoparticle self-assembled from amphiphilic adriamycin-human serum albumin conjugates for tumor targeted therapy. *Biomed Research International*:10.
- Chen SJ, Zhou GB, Zhang XW, Mao JH, de The H, Chen Z. 2011. From an old remedy to a magic bullet: Molecular mechanisms underlying the therapeutic effects of arsenic in fighting leukemia. *Blood* 117:6425-6437.
- Chen W, Zhong P, Meng FH, Cheng R, Deng C, Feijen J, et al. 2013. Redox and ph-responsive degradable micelles for dually activated intracellular anticancer drug release. *Journal of Controlled Release* 169:171-179.
- Cheng BH, Yang XX, Han ZW, An LX, Uu SW. 2008. Arsenic trioxide induced the apoptosis of laryngeal cancer via down-regulation of survivin mrna. *Auris Nasus Larynx* 35:95-101.
- Cheng C, Wei H, Zhu JL, Chang C, Cheng H, Li C, et al. 2008. Functionalized thermoresponsive micelles self-assembled from biotin-peg-b-p(nipaam-co-hmaam)-b-pmma for tumor cell target. *Bioconjugate Chemistry* 19:1194-1201.
- Cheng J, Wei HL, Chen J, Xie B. 2012. Antitumor effect of arsenic trioxide in human k562 and k562/adm cells by autophagy. *Toxicology Mechanisms and Methods* 22:512-519.

- Cheng R, Meng FH, Deng C, Klok HA, Zhong ZY. 2013. Dual and multi-stimuli responsive polymeric nanoparticles for programmed site-specific drug delivery. *Biomaterials* 34:3647-3657.
- Cheng X, Quintas-Cardama A, Golemovic M, Zingaro R, Gao M-Z, Freirech EJ, et al. 2012. The organic arsenic derivative gmz27 induces pml-rar alpha-independent apoptosis in myeloid leukemia cells. *Anticancer Research* 32:2871-2880.
- Cheng YY, Zhao LB, Li YW, Xu TW. 2011. Design of biocompatible dendrimers for cancer diagnosis and therapy: Current status and future perspectives. *Chemical Society Reviews* 40:2673-2703.
- Chiche J, Brahim-Horn MC, Pouyssegur J. 2010. Tumour hypoxia induces a metabolic shift causing acidosis: A common feature in cancer. *Journal of Cellular and Molecular Medicine* 14:771-794.
- Chiu HW, Tseng YC, Hsu YH, Lin YF, Foo NP, Guo HR, et al. 2015. Arsenic trioxide induces programmed cell death through stimulation of er stress and inhibition of the ubiquitin-proteasome system in human sarcoma cells. *Cancer Letters* 356:762-772.
- Chlebowski RT. 1979. Adriamycin (doxorubicin) cardiotoxicity - review. *Western Journal of Medicine* 131:364-368.
- Chung SA, McDonald KL, Shen H, Day BW, Stringer BW, Johns T, et al. 2011. Targeting glioblastoma metabolism with a novel arsenic-based metabolic inhibitor, penao. *Neuro-Oncology* 13:118-118.
- Coussens LM, Werb Z. 1996. Matrix metalloproteinases and the development of cancer. *Chemistry & Biology* 3:895-904.
- Craig M, Shah S, Tallman M, Patil P, Easow J, Buck J, et al. 2008. A phase ii trial of darinaparsin in advanced lymphomas: Report on safety and activity. *Blood* 112:554-554.
- Cullen WR. 2008. Is arsenic an aphrodisiac? The sociochemistry of an element. Is arsenic an aphrodisiac? The sociochemistry of an element:xvi + 412pp.-xvi + 412pp.
- Da Silva RMP, Mano JF, Reis RL. 2007. Smart thermoresponsive coatings and surfaces for tissue engineering: Switching cell-material boundaries. *Trends in Biotechnology* 25:577-583.

- Dai J, Weinberg RS, Waxman S, Jing YK. 1999. Malignant cells can be sensitized to undergo growth inhibition and apoptosis by arsenic trioxide through modulation of the glutathione redox system. *Blood* 93:268-277.
- Dang CV. 1999. C-myc target genes involved in cell growth, apoptosis, and metabolism. *Molecular and Cellular Biology* 19:1-11.
- Darney PD, Monroe SE, Klaisle CM, Alvarado A. 1989. Clinical-evaluation of the capronor contraceptive implant - preliminary-report. *American Journal of Obstetrics and Gynecology* 160:1292-1295.
- De Vita VTJ, Young RC, Canellos GP. 1975. Combination vs single agent chemo therapy a review of the basis for selection of drug treatment of cancer. *Cancer* 35:98-110.
- Decollogne S, Joshi S, Chung SA, Luk PP, Yeo RX, Nixdorf S, et al. 2015. Alterations in the mitochondrial responses to penao as a mechanism of resistance in ovarian cancer cells. *Gynecologic Oncology* 138:363-371.
- Dethe H, Chomienne C, Lanotte M, Degos L, Dejean A. 1990. The t(15-17) translocation of acute promyelocytic leukemia fuses the retinoic acid receptor-alpha gene to a novel transcribed locus. *Nature* 347:558-561.
- Dilda PJ, Decollogne S, Weerakoon L, Norris MD, Haber M, Allen JD, et al. 2009. Optimization of the antitumor efficacy of a synthetic mitochondrial toxin by increasing the residence time in the cytosol. *Journal of Medicinal Chemistry* 52:6209-6216.
- Dilda PJ, Hogg PJ. 2007. Arsenical-based cancer drugs. *Cancer Treatment Reviews* 33:542-564.
- Dilda PJ, Ramsay EE, Corti A, Pompella A, Hogg PJ. 2008. Metabolism of the tumor angiogenesis inhibitor 4-(n-(s-glutathionylacetyl)amino) phenylarsonous acid. *Journal of Biological Chemistry* 283:35428-35434.
- Ding W, Liu WL, Cooper KL, Qin XJ, Bergo PLD, Hudson LG, et al. 2009. Inhibition of poly(adp-ribose) polymerase-1 by arsenite interferes with repair of oxidative dna damage. *Journal of Biological Chemistry* 284:6809-6817.

- Dogra S, Bandi S, Viswanathan P, Gupta S. 2015. Arsenic trioxide amplifies cisplatin toxicity in human tubular cells transformed by hpv-16 e6/e7 for further therapeutic directions in renal cell carcinoma. *Cancer Letters* 356:953-961.
- Don AS, Kisker O, Dilda P, Donoghue N, Zhao XY, Decollogne S, et al. 2003. A peptide trivalent arsenical inhibits tumor angiogenesis by perturbing mitochondrial function in angiogenic endothelial cells. *Cancer Cell* 3:497-509.
- Dong XY, Ma N, Liu MM, Liu ZL. 2015. Effects of as<sub>2</sub>o<sub>3</sub> nanoparticles on cell growth and apoptosis of nb4 cells. *Experimental and Therapeutic Medicine* 10:1271-1276.
- Doyle D. 2009. Notoriety to respectability: A short history of arsenic prior to its present day use in haematology. *British Journal of Haematology* 145:309-317.
- Du JZ, Lane LA, Nie SM. 2015. Stimuli-responsive nanoparticles for targeting the tumor microenvironment. *Journal of Controlled Release* 219:205-214.
- Du ZZ, Zhang Y, Lang MD. 2015. Synthesis of functionalized pluronic-b-poly(epsilon-caprolactone) and the comparative study of their pendant groups on the cellular internalization behavior. *Journal of Materials Science-Materials in Medicine* 26:12.
- Duffy A, Le J, Sausville E, Emadi A. 2015. Autophagy modulation: A target for cancer treatment development. *Cancer Chemotherapy and Pharmacology* 75:439-447.
- Duggan ME, Hutchinson JH. 2000. Ligands to the integrin receptor alpha(v)beta(3). *Expert Opinion on Therapeutic Patents* 10:1367-1383.
- Dvorak HF. 2002. Vascular permeability factor/vascular endothelial growth factor: A critical cytokine in tumor angiogenesis and a potential target for diagnosis and therapy. *Journal of Clinical Oncology* 20:4368-4380.
- Elhasi S, Astaneh R, Lavasanifar A. 2007. Solubilization of an amphiphilic drug by poly(ethylene oxide)-block-poly(ester) micelles. *European Journal of Pharmaceutics and Biopharmaceutics* 65:406-413.
- Elmore S. 2007. Apoptosis: A review of programmed cell death. *Toxicologic Pathology* 35:495-516.

- Elsabahy M, Wooley KL. 2012. Design of polymeric nanoparticles for biomedical delivery applications. *Chemical Society Reviews* 41:2545-2561.
- Emadi A, Sadowska M, Carter-Cooper B, Bhatnagar V, van der Merwe I, Levis MJ, et al. 2015. Perturbation of cellular oxidative state induced by dichloroacetate and arsenic trioxide for treatment of acute myeloid leukemia. *Leukemia Research* 39:719-729.
- Endres TK, Beck-Broichsitter M, Samsonova O, Renette T, Kissel TH. 2011. Self-assembled biodegradable amphiphilic peg-pcl-lpei triblock copolymers at the borderline between micelles and nanoparticles designed for drug and gene delivery. *Biomaterials* 32:7721-7731.
- Fatouros D, Gortzi O, Klepetsanis P, Antimisiaris SG, Stuart MCA, Brisson A, et al. 2001. Preparation and properties of arsonolipid containing liposomes. *Chemistry and Physics of Lipids* 109:75-89.
- Felding-Habermann B, Fransvea E, O'Toole TE, Manzuk L, Faha B, Hensler M. 2002. Involvement of tumor cell integrin alpha v beta 3 in hematogenous metastasis of human melanoma cells. *Clinical & Experimental Metastasis* 19:427-436.
- Folkman J, Shing Y. 1992. Angiogenesis. *Journal of Biological Chemistry* 267:10931-10934.
- Fu YH, Chen CY, Chen CT. 2015. Tuning of hydrogen peroxide-responsive polymeric micelles of biodegradable triblock polycarbonates as a potential drug delivery platform with ratiometric fluorescence signaling. *Polymer Chemistry* 6:8132-8143.
- Fustin CA, Abetz V, Gohy JF. 2005. Triblock terpolymer micelles: A personal outlook. *European Physical Journal E* 16:291-302.
- Gang BP, Dilda PJ, Hogg PJ, Blackburn AC. 2014. Targeting of two aspects of metabolism in breast cancer treatment. *Cancer Biology & Therapy* 15:1533-1541.
- Gao YJ, Zhou YX, Zhao L, Zhang C, Li YS, Li JW, et al. 2015. Enhanced antitumor efficacy by cyclic rgdyk-conjugated and paclitaxel-loaded pH-responsive polymeric micelles. *Acta Biomaterialia* 23:127-135.
- Garnier N, Redstone GGJ, Dahabieh MS, Nichol JN, del Rincon SV, Gu YX, et al. 2014. The novel arsenical darinaparsin is transported by cystine importing systems. *Molecular Pharmacology* 85:576-585.

- Gaspar VM, Goncalves C, de Melo-Diogo D, Costa EC, Queiroz JA, Pichon C, et al. 2014. Poly(2-ethyl-2-oxazoline)-*pl*-*g*-*pe*i amphiphilic triblock micelles for co-delivery of minicircle dna and chemotherapeutics. *Journal of Controlled Release* 189:90-104.
- Gazitt Y, Akay C. 2005. Arsenic trioxide: An anti cancer missile with multiple warheads. *Hematology* 10:205-213.
- Ge HY, Han ZJ, Tian P, Sun WJ, Xue DX, Bi Y, et al. 2015. Vegfa expression is inhibited by arsenic trioxide in huvecs through the upregulation of ets-2 and mirna-126. *Plos One* 10:18.
- Goddard ED. 1986. Polymer surfactant interaction .1. Uncharged water-soluble polymers and charged surfactants. *Colloids and Surfaces* 19:255-300.
- Golemovic M, Quintas-Cardama A, Manshoury T, Orsolich N, Duzkale H, Johansen M, et al. 2010. Mer1, a novel organic arsenic derivative, has potent pml-rar alpha- independent cytotoxic activity against leukemia cells. *Investigational New Drugs* 28:402-412.
- Gortzi O, Papadimitriou E, Kontoyannis CG, Antimisiaris SG, Ioannou PV. 2002. Arsonoliposomes, a novel class of arsenic-containing liposomes: Effect of palmitoyl- arsonolipid-containing liposomes on the viability of cancer and normal cells in culture. *Pharmaceutical Research* 19:79-86.
- Gothwal A, Khan I, Gupta U. 2016. Polymeric micelles: Recent advancements in the delivery of anticancer drugs. *Pharmaceutical Research* 33:18-39.
- Goussetis DJ, Altman JK, Glaser H, McNeer JL, Tallman MS, Platanius LC. 2010. Autophagy is a critical mechanism for the induction of the antileukemic effects of arsenic trioxide. *Journal of Biological Chemistry* 285:29989-29997.
- Goussetis DJ, Gounaris E, Wu EJ, Vakana E, Sharma B, Bogyo M, et al. 2012. Autophagic degradation of the bcr-abl oncoprotein and generation of antileukemic responses by arsenic trioxide. *Blood* 120:3555-3562.
- Griffith OW. 1999. Biologic and pharmacologic regulation of mammalian glutathione synthesis. *Free Radical Biology and Medicine* 27:922-935.
- Guan XG, Hu XL, Li ZH, Zhang H, Xie ZG. 2015. Crgd targeted and charge conversion-controlled release micelles for doxorubicin delivery. *Rsc Advances* 5:22957-22964.

- Gurrath M, Muller G, Kessler H, Aumailley M, Timpl R. 1992. Conformation activity studies of rationally designed potent antiadhesive rgd peptides. *European Journal of Biochemistry* 210:911-921.
- Gwak HS, Park MJ, Park IC, Woo SH, Jin HO, Rhee CH, et al. 2014. Tetraarsenic oxide-induced inhibition of malignant glioma cell invasion in vitro via a decrease in matrix metalloproteinase secretion and protein kinase b phosphorylation. *Journal of Neurosurgery* 121:1483-1491.
- Haas R, Krippendorf A. 1997. Determination of chemical warfare agents in soil and material samples - gas chromatographic analysis of phenylarsenic compounds (sternutators) (1st communication). *Environmental Science and Pollution Research* 4:123-124.
- Han HS, Choi KY, Ko H, Jeon J, Saravanakumar G, Suh YD, et al. 2015. Bioreducible core-crosslinked hyaluronic acid micelle for targeted cancer therapy. *Journal of Controlled Release* 200:158-166.
- Han MH, Lee WS, Lu JN, Yun JW, Kim G, Jung JM, et al. 2012. Tetraarsenic hexoxide induces beclin-1-induced autophagic cell death as well as caspase-dependent apoptosis in u937 human leukemic cells. *Evidence-Based Complementary and Alternative Medicine*:11.
- Hanahan D, Weinberg RA. 2011. Hallmarks of cancer: The next generation. *Cell* 144:646-674.
- Hartwig A, Pelzer A, Asmuss M, Burkle A. 2003. Very low concentrations of arsenite suppress poly(adp-ribosylation) in mammalian cells. *International Journal of Cancer* 104:1-6.
- He Q, Shi J. 2011. Mesoporous silica nanoparticle based nano drug delivery systems: Synthesis, controlled drug release and delivery, pharmacokinetics and biocompatibility. *Journal of Materials Chemistry* 21:5845-5855.
- Hindmarsh JT, McCurdy RF. 1986. Clinical and environmental aspects of arsenic toxicity. *Crc Critical Reviews in Clinical Laboratory Sciences* 23:315-347.
- Hiwatashi Y, Tadokoro H, Henmi K, Arai M, Kaise T, Tanaka S, et al. 2011. Antiproliferative and anti-invasive effects of inorganic and organic arsenic compounds on human and murine melanoma cells in vitro. *Journal of Pharmacy and Pharmacology* 63:1202-1210.
- Honary S, Zahir F. 2013. Effect of zeta potential on the properties of nano-drug delivery systems - a review (part 1). *Tropical Journal of Pharmaceutical Research* 12:255-264.

- Horsley L, Cummings J, Middleton M, Ward T, Backen A, Clamp A, et al. 2013. A phase 1 trial of intravenous 4-(n-(s-glutathionylacetyl)amino) phenylarsenoxide (gsao) in patients with advanced solid tumours. *Cancer Chemotherapy and Pharmacology* 72:1343-1352.
- Hosein PJ, Craig MD, Tallman MS, Boccia RV, Hamilton BL, Lewis JJ, et al. 2012. A multicenter phase ii study of darinaparsin in relapsed or refractory hodgkin's and non-hodgkin's lymphoma. *American Journal of Hematology* 87:111-114.
- Hsu YH, Chiang WH, Chen MC, Chern CS, Chiu HC. 2006. Effects of sds on the thermo- and ph-sensitive structural changes of the poly(acrylic acid)-based copolymer containing both poly(n-isopropylacrylamide) and monomethoxy poly(ethylene glycol) grafts in water. *Langmuir* 22:6764-6770.
- Hu J, Fang J, Dong Y, Chen SJ, Chen Z. 2005. Arsenic in cancer therapy. *Anti-Cancer Drugs* 16:119-127.
- Hu J, He JL, Cao DL, Zhang MZ, Ni PH. 2015. Core cross-linked polyphosphoester micelles with folate-targeted and acid-cleavable features for ph-triggered drug delivery. *Polymer Chemistry* 6:3205-3216.
- Ishihara T, Mizushima T. 2010. Techniques for efficient entrapment of pharmaceuticals in biodegradable solid micro/nanoparticles. *Expert Opinion on Drug Delivery* 7:565-575.
- Iwasaki K, Yabushita H, Ueno T, Wakatsuki A. 2015. Role of hypoxia-inducible factor-1 alpha, carbonic anhydrase-ix, glucose transporter-1 and vascular endothelial growth factor associated with lymph node metastasis and recurrence in patients with locally advanced cervical cancer. *Oncology Letters* 10:1970-1978.
- Jabbour E, Kantarjian H. 2016. Chronic myeloid leukemia: 2016 update on diagnosis, therapy, and monitoring. *American journal of hematology* 91:252-265.
- Jeanne M, Lallemand-Breitenbach V, Ferhi O, Koken M, Le Bras M, Duffort S, et al. 2010. Pml/rara oxidation and arsenic binding initiate the antileukemia response of as<sub>2</sub>o<sub>3</sub>. *Cancer Cell* 18:88-98.
- Jeitner TM, Lawrence DA. 2001. Mechanisms for the cytotoxicity of cysteamine. *Toxicological Sciences* 63:57-64.

- Jhaveri A, Torchilin V. 2016. Intracellular delivery of nanocarriers and targeting to subcellular organelles. *Expert opinion on drug delivery* 13:49-70.
- Ji H, Li Y, Jiang F, Wang XX, Zhang JP, Shen J, et al. 2014. Inhibition of transforming growth factor beta/smad signal by mir-155 is involved in arsenic trioxide-induced anti-angiogenesis in prostate cancer. *Cancer Science* 105:1541-1549.
- Jiang F, Wang XX, Liu QQ, Shen J, Li Z, Li Y, et al. 2014. Inhibition of tgf-beta/smad3/nf-kappa b signaling by microrna-491 is involved in arsenic trioxide-induced anti-angiogenesis in hepatocellular carcinoma cells. *Toxicology Letters* 231:55-61.
- Jiao GJ, Ren TT, Guo W, Ren CM, Yang K. 2015. Arsenic trioxide inhibits growth of human chondrosarcoma cells through g2/m arrest and apoptosis as well as autophagy. *Tumor Biology* 36:3969-3977.
- Jimenez-Pardo I, Gonzalez-Pastor R, Lancelot A, Claveria-Gimeno R, Velazquez-Campoy A, Abian O, et al. 2015. Shell cross-linked polymeric micelles as camptothecin nanocarriers for anti-hev therapy. *Macromolecular Bioscience* 15:1381-1391.
- Kallinteri P, Fatouros D, Klepetsanis P, Antimisiaris SG. 2004. Arsenic trioxide liposomes: Encapsulation efficiency and in vitro stability. *Journal of Liposome Research* 14:27-38.
- Kallinteri P, Fatouros D, Klepetsanis P, Antimisiaris SG. 2004. Arsenic trioxide liposomes: Encapsulation efficiency and in vitro stability. *Journal of Liposome Research* 14:27-38.
- Kamenka N, Chorro M, Talmon Y, Zana R. 1992. Study of mixed aggregates in aqueous-solutions of sodium dodecyl-sulfate and dodecyltrimethylammonium bromide. *Colloids and Surfaces* 67:213-222.
- Kang Y, Zhang XM, Zhang S, Ding LS, Li BJ. 2015. Ph-responsive dendritic polyrotaxane drug-polymer conjugates forming nanoparticles as efficient drug delivery system for cancer therapy. *Polymer Chemistry* 6:2098-2107.
- Kanzawa T, Kondo Y, Ito H, Kondo S, Germano I. 2003. Induction of autophagic cell death in malignant glioma cells by arsenic trioxide. *Cancer Research* 63:2103-2108.

- Kanzawa T, Zhang L, Xiao LC, Germano IM, Kondo Y, Kondo S. 2005. Arsenic trioxide induces autophagic cell death in malignant glioma cells by upregulation of mitochondrial cell death protein bnip3. *Oncogene* 24:980-991.
- Kao YH, Yu CL, Chang LW, Yu HS. 2003. Low concentrations of arsenic induce vascular endothelial growth factor and nitric oxide release and stimulate angiogenesis in vitro. *Chemical Research in Toxicology* 16:460-468.
- Kessel M, Liu SX, Xu A, Santella R, Hei TK. 2002. Arsenic induces oxidative dna damage in mammalian cells. *Molecular and Cellular Biochemistry* 234:301-308.
- Khorramizadeh MR, Saadat F, Allahyary H, Pezeshki M, Sarrafnejad A, Mirshafiey A, et al. 2006. Arsenic trioxide compound modulates multiple myeloma phenotypes: Assessment on cell line models. *Iranian Journal of Public Health* 35:17-24.
- Kim EH, Yoon NJ, Kim SU, Kwon TK, Sohn S, Choi KS. 2008. Arsenic trioxide sensitizes human glioma cells, but not normal astrocytes, to trail-induced apoptosis via ccaat/enhancer-binding protein homologous protein-dependent dr5 up-regulation. *Cancer Research* 68:266-275.
- Kim HJ, Shin JH, Kim TH, Kim EY, Park YS, Park CS, et al. 2009. Efficacy of transarterial embolization. With arsenic trioxide oil emulsion in a rabbit vx2 liver tumor model. *Journal of Vascular and Interventional Radiology* 20:1365-1370.
- Kim KB, Bedikian AY, Camacho LH, Papadopoulos NE, McCullough C. 2005. A phase ii trial of arsenic trioxide in patients with metastatic melanoma. *Cancer* 104:1687-1692.
- Kim S, Seong K, Kim O, Seo H, Lee M, Khang G, et al. 2010. Polyoxalate nanoparticles as a biodegradable and biocompatible drug delivery vehicle. *Biomacromolecules* 11:555-560.
- Kondo S, Mori H, Sasai Y, Kuzuya M. 2007. Conventional synthesis of amphiphilic block copolymer utilized for polymeric micelle by mechanochemical solid-state polymerization. *Chemical & Pharmaceutical Bulletin* 55:389-392.
- Kong B, Huang S, Wang W, Ma D, Qu X, Jiang J, et al. 2005. Arsenic trioxide induces apoptosis in cisplatin-sensitive and -resistant ovarian cancer cell lines. *International Journal of Gynecological Cancer* 15:872-877.

- Kroening KK, Solivio MJV, Garcia-Lopez M, Puga A, Caruso JA. 2009. Cytotoxicity of arsenic-containing chemical warfare agent degradation products with metallomic approaches for metabolite analysis. *Metallomics* 1:59-66.
- Kujak C, Kolesar JM. 2016. Treatment of chronic myelogenous leukemia. *American journal of health-system pharmacy : AJHP : official journal of the American Society of Health-System Pharmacists* 73:113-120.
- Lecoq. 1910. Toxicity of metalloidalic arsenic. *Comptes Rendus Hebdomadaires Des Seances De L Academie Des Sciences* 150:887-888.
- Lee DW, Erigala VR, Dasari M, Yu JH, Dickson RM, Murthy N. 2008. Detection of hydrogen peroxide with chemiluminescent micelles. *International Journal of Nanomedicine* 3:471-476.
- Lee I, Hwang O, Yoo D, Khang G, Lee D. 2011. Detection of hydrogen peroxide in vitro and in vivo using peroxalate chemiluminescent micelles. *Bulletin of the Korean Chemical Society* 32:2187-2192.
- Lee SY, Lee H, In I, Park SY. 2014. Ph/redox/photo responsive polymeric micelle via boronate ester and disulfide bonds with spiropyran-based photochromic polymer for cell imaging and anticancer drug delivery. *European Polymer Journal* 57:1-10.
- Leslie EM. 2012. Arsenic-glutathione conjugate transport by the human multidrug resistance proteins (mrps/abccs). *Journal of Inorganic Biochemistry* 108:141-149.
- Li CL, Wei HL, Chen J, Wang B, Xie B, Fan LL, et al. 2014. Arsenic trioxide induces autophagy and antitumor effects in burkitt's lymphoma raji cells. *Oncology Reports* 32:1557-1563.
- Li HA, Cui YN, Sui JH, Bian SQ, Sun Y, Liang J, et al. 2015. Efficient delivery of dox to nuclei of hepatic carcinoma cells in the subcutaneous tumor model using ph-sensitive pullulan-dox conjugates. *Acs Applied Materials & Interfaces* 7:15855-15865.
- Li J, Huo MR, Wang J, Zhou JP, Mohammad JM, Zhang YL, et al. 2012. Redox-sensitive micelles self-assembled from amphiphilic hyaluronic acid-deoxycholic acid conjugates for targeted intracellular delivery of paclitaxel. *Biomaterials* 33:2310-2320.

- Li XQ, Ding XZ, Adrian TE. 2004. Arsenic trioxide causes redistribution of cell cycle, caspase activation, and gadd expression in human colonic, breast, and pancreatic cancer cells. *Cancer Investigation* 22:389-400.
- Li Y, Gao GH, Lee DS. 2013. Stimulus-sensitive polymeric nanoparticles and their applications as drug and gene carriers. *Advanced Healthcare Materials* 2:388-417.
- Li Y, Jiang F, Liu QQ, Shen J, Wang XX, Li Z, et al. 2015. Inhibition of the cancer stem cells-like properties by arsenic trioxide, involved in the attenuation of endogenous transforming growth factor beta signal. *Toxicological Sciences* 143:156-164.
- Liao WT, Chang KL, Yu CL, Chen GS, Chang LW, Yu HS. 2004. Arsenic induces human keratinocyte apoptosis by the fas/fas ligand pathway, which correlates with alterations in nuclear factor-kappa b and activator protein-1 activity. *Journal of Investigative Dermatology* 122:125-129.
- Lin C-C, Hsu C, Hsu C-H, Hsu W-L, Cheng A-L, Yang C-H. 2007. Arsenic trioxide in patients with hepatocellular carcinoma: A phase ii trial. *Investigational New Drugs* 25:77-84.
- Lippert AR, De Bittner GCV, Chang CJ. 2011. Boronate oxidation as a bioorthogonal reaction approach for studying the chemistry of hydrogen peroxide in living systems. *Accounts of Chemical Research* 44:793-804.
- Liu BR, Yang M, Li RT, Ding YT, Qian XP, Yu LX, et al. 2008. The antitumor effect of novel docetaxel-loaded thermosensitive micelles. *European Journal of Pharmaceutics and Biopharmaceutics* 69:527-534.
- Liu J, Lu YF, Wu Q, Goyer RA, Waalkes MP. 2008. Mineral arsenicals in traditional medicines: Orpiment, realgar, and arsenolite. *Journal of Pharmacology and Experimental Therapeutics* 326:363-368.
- Liu JB, Zeng FQ, Allen C. 2007. In vivo fate of unimers and micelles of a poly(ethylene glycol)-block-poly(caprolactone) copolymer in mice following intravenous administration. *European Journal of Pharmaceutics and Biopharmaceutics* 65:309-319.
- Liu JJ, Deng HZ, Liu Q, Chu LP, Zhang YM, Yang CH, et al. 2015. Integrin-targeted pH-responsive micelles for enhanced efficiency of anticancer treatment in vitro and in vivo. *Nanoscale* 7:4451-4460.

- Liu QA, Zhang H, Smeester L, Zou F, Kesic M, Jaspers I, et al. 2010. The nrf2-mediated oxidative stress response pathway is associated with tumor cell resistance to arsenic trioxide across the nci-60 panel. *Bmc Medical Genomics* 3:12.
- Liu R, He B, Li D, Lai YS, Tang JZ, Gu ZW. 2012. Stabilization of ph-sensitive mpeg-ph-pla nanoparticles by stereocomplexation between enantiomeric polylactides. *Macromolecular Rapid Communications* 33:1061-1066.
- Liu XF, Miller AL, Waletzki BE, Mamo TK, Yaszemski MJ, Lu LC. 2015. Hydrolysable core crosslinked particles for receptor-mediated ph-sensitive anticancer drug delivery. *New Journal of Chemistry* 39:8840-8847.
- Liu Z, Cai WB, He LN, Nakayama N, Chen K, Sun XM, et al. 2007. In vivo biodistribution and highly efficient tumour targeting of carbon nanotubes in mice. *Nature Nanotechnology* 2:47-52.
- Lu D, Coote ML, Ho J, Kilah NL, Lin C-Y, Salem G, et al. 2012. Resolution and improved synthesis of (+/-)-arsenicin a: A natural adamantane-type tetraarsenical possessing strong anti-acute promyelocytic leukemia cell line activity. *Organometallics* 31:1808-1816.
- Lu DP, Qiu JY, Jiang B, Wang Q, Liu KY, Liu YR, et al. 2002. Tetra-arsenic tetra-sulfide for the treatment of acute promyelocytic leukemia: A pilot report. *Blood* 99:3136-3143.
- Lu J, Chew EH, Holmgren A. 2007. Targeting thioredoxin reductase is a basis for cancer therapy by arsenic trioxide. *Proceedings of the National Academy of Sciences of the United States of America* 104:12288-12293.
- Lu X, Lu D, Scully MF, Kakkar VV. 2006. Integrins in drug targeting-rgd templates in toxins. *Current Pharmaceutical Design* 12:2749-2769.
- Luo QY, Li Y, Deng JJ, Zhang ZZ. 2015. Parp-1 inhibitor sensitizes arsenic trioxide in hepatocellular carcinoma cells via abrogation of g2/m checkpoint and suppression of dna damage repair. *Chemico-Biological Interactions* 226:12-22.
- Lux CD, Joshi-Barr S, Nguyen T, Mahmoud E, Schopf E, Fomina N, et al. 2012. Biocompatible polymeric nanoparticles degrade and release cargo in response to biologically relevant levels of hydrogen peroxide. *Journal of the American Chemical Society* 134:15758-15764.

- Ma N, Ma C, Li C, Wang T, Tang Y, Wang H, et al. 2013. Influence of nanoparticle shape, size, and surface functionalization on cellular uptake. *Journal of Nanoscience and Nanotechnology* 13:6485-6498.
- Ma ZB, Xu HY, Jiang M, Yang YL, Liu LX, Li YH. 2014. Arsenic trioxide induces apoptosis of human gastrointestinal cancer cells. *World Journal of Gastroenterology* 20:5505-5510.
- Ma ZS, Haddadi A, Molavi O, Lavasanifar A, Lai R, Samuel J. 2008. Micelles of poly(ethylene oxide)-b-poly(epsilon-caprolactone) as vehicles for the solubilization, stabilization, and controlled delivery of curcumin. *Journal of Biomedical Materials Research Part A* 86A:300-310.
- Maeda H. 2012. Macromolecular therapeutics in cancer treatment: The epr effect and beyond. *Journal of Controlled Release* 164:138-144.
- Mahmud A, Xiong XB, Lavasanifar A. 2006. Novel self-associating poly(ethylene oxide)-block-poly(epsilon-caprolactone) block copolymers with functional side groups on the polyester block for drug delivery. *Macromolecules* 39:9419-9428.
- Makino J, Cabral H, Miura Y, Matsumoto Y, Wang M, Kinoh H, et al. 2015. Crgd-installed polymeric micelles loading platinum anticancer drugs enable cooperative treatment against lymph node metastasis. *Journal of controlled release : official journal of the Controlled Release Society* 220:783-791.
- Mancini I, Guella G, Frostin M, Hnawia E, Laurent D, Debitus C, et al. 2006. On the first polyarsenic organic compound from nature: Arsenicin a from the new caledonian marine sponge *echinochalina bargibanti*. *Chemistry-a European Journal* 12:8989-8994.
- Mann KK, Wallner B, Lossos IS, Miller WH. 2009. Darinaparsin: A novel organic arsenical with promising anticancer activity. *Expert Opinion on Investigational Drugs* 18:1727-1734.
- Mao JH, Sun XY, Liu JX, Zhang QY, Liu P, Huang QH, et al. 2010. As4s4 targets ring-type e3 ligase c-cbl to induce degradation of bcr-abl in chronic myelogenous leukemia. *Proceedings of the National Academy of Sciences of the United States of America* 107:21683-21688.
- Markman JL, Rekechenetskiy A, Holler E, Ljubimova JY. 2013. Nanomedicine therapeutic approaches to overcome cancer drug resistance. *Advanced Drug Delivery Reviews* 65:1866-1879.

- Matsumura Y, Maeda H. 1986. A new concept for macromolecular therapeutics in cancer-chemotherapy - mechanism of tumoritropic accumulation of proteins and the antitumor agent smancs. *Cancer Research* 46:6387-6392.
- Miller DM, Thomas SD, Islam A, Muench D, Sedoris K. 2012. C-myc and cancer metabolism. *Clinical Cancer Research* 18:5546-5553.
- Muhammad F, Zhao JY, Wang N, Guo MY, Wang AF, Chen L, et al. 2014. Lethal drug combination: Arsenic loaded multiple drug mesoporous silica for theranostic applications. *Colloids and Surfaces B-Biointerfaces* 123:506-514.
- Nagasaki Y, Kutsuna T, Iijima M, Kato M, Kataoka K, Kitano S, et al. 1995. Formyl-ended heterobifunctional poly(ethylene oxide) - synthesis of poly(ethylene oxide) with a formyl group at one end and a hydroxyl group at the other end. *Bioconjugate Chemistry* 6:231-233.
- Newington JT, Rappon T, Albers S, Wong DY, Rylett RJ, Cumming RC. 2012. Overexpression of pyruvate dehydrogenase kinase 1 and lactate dehydrogenase a in nerve cells confers resistance to amyloid beta and other toxins by decreasing mitochondrial respiration and reactive oxygen species production. *Journal of Biological Chemistry* 287:37245-37258.
- Nguyen DH, Bae JW, Choi JH, Lee JS, Park KD. 2013. Bioreducible cross-linked pluronic micelles: Ph-triggered release of doxorubicin and folate-mediated cellular uptake. *Journal of Bioactive and Compatible Polymers* 28:341-354.
- Nikaido M, Pi JB, Kumagai Y, Yamauchi H, Taguchi K, Horiguchi S, et al. 2003. Decreased enzyme activity of hepatic thioredoxin reductase and glutathione reductase in rabbits by prolonged exposure to inorganic arsenate. *Environmental Toxicology* 18:306-311.
- Ohyashiki T, Mohri T. 1983. Fluorometric analysis of the micelle formation process of surfactants in aqueous-solution .1. Utility of pyrene in determination of the critical micelle concentration. *Chemical & Pharmaceutical Bulletin* 31:1296-1300.
- Otsuka H, Nagasaki Y, Kataoka K. 2003. Pegylated nanoparticles for biological and pharmaceutical applications. *Advanced Drug Delivery Reviews* 55:403-419.
- Park D, Chiu J, Perrone GG, Dilda PJ, Hogg PJ. 2012. The tumour metabolism inhibitors gsao and penao react with cysteines 57 and 257 of mitochondrial adenine nucleotide translocase. *Cancer Cell International* 12:6.

- Pereira DL, Ferreira ACD, de Faria GP, Kwee JK. 2015. Autophagy interplays with apoptosis and cell cycle regulation in the growth inhibiting effect of trisenox in hep-2, a laryngeal squamous cancer. *Pathology & Oncology Research* 21:103-111.
- Piperoudi S, Fatouros D, Ioannou PV, Frederik P, Antimisiaris SG. 2006. Incorporation of peg-lipids in arsonoliposomes results in formation of highly stable arsenic-containing vesicles. *Chemistry and Physics of Lipids* 139:96-106.
- Piperoudi S, Ioannou PV, Frederik P, Antimisiaris SG. 2005. Arsonoliposomes: Effect of lipid composition on their stability and morphology. *Journal of Liposome Research* 15:187-197.
- Price JE, Zhang RD. 1990. Studies of human breast-cancer metastasis using nude-mice. *Cancer and Metastasis Reviews* 8:285-297.
- Qian C, Wang Y, Chen Y, Zeng L, Zhang Q, Shuai X, et al. 2013. Suppression of pancreatic tumor growth by targeted arsenic delivery with anti-cd44v6 single chain antibody conjugated nanoparticles. *Biomaterials* 34:6175-6184.
- Qian WB, Liu JQ, Jin J, Ni WM, Xu WL. 2007. Arsenic trioxide induces not only apoptosis but also autophagic cell death in leukemia cell lines via up-regulation of beclin-1. *Leukemia Research* 31:329-339.
- Ravandi F, Estey EH, Cortes JE, O'Brien S, Pierce SA, Brandt M, et al. 2010. Phase ii study of all-trans retinoic acid (atra), arsenic trioxide (ato), with or without gemtuzumab ozogamicin (go) for the frontline therapy of patients with acute promyelocytic leukemia (apl). *Blood* 116:472-472.
- Ray A, Chatterjee S, Mukherjee S, Bhattacharya S. 2014. Arsenic trioxide induced indirect and direct inhibition of glutathione reductase leads to apoptosis in rat hepatocytes. *Biometals* 27:483-494.
- Rezaei SJT, Amani V, Nabid MR, Safari N, Niknejad H. 2015. Folate-decorated polymeric pt(ii) prodrug micelles for targeted intracellular delivery and cytosolic glutathione-triggered release of platinum anticancer drugs. *Polymer Chemistry* 6:2844-2853.
- Richie JP, Skowronski L, Abraham P, Leutzinger Y. 1996. Blood glutathione concentrations in a large-scale human study. *Clinical Chemistry* 42:64-70.

- Rijcken CJ, Snel CJ, Schiffelers RM, van Nostrum CF, Hennink WE. 2007. Hydrolysable core-crosslinked thermosensitive polymeric micelles: Synthesis, characterisation and in vivo studies. *Biomaterials* 28:5581-5593.
- Robles-Osorio ML, Sabath-Silva E, Sabath E. 2015. Arsenic-mediated nephrotoxicity. *Renal Failure* 37:542-547.
- Roboz GJ, Dias S, Lam G, Lane WJ, Soignet SL, Warrell RP, et al. 2000. Arsenic trioxide induces dose- and time-dependent apoptosis of endothelium and may exert an antileukemic effect via inhibition of angiogenesis. *Blood* 96:1525-1530.
- Rojewski MT, Korper S, Thiel E, Schrezenmeier H. 2004. Depolarization of mitochondria and activation of caspases are common features of arsenic(iii)-induced apoptosis in myelogenic and lymphatic cell lines. *Chemical Research in Toxicology* 17:119-128.
- Rosen BP. 2002. Biochemistry of arsenic detoxification. *Febs Letters* 529:86-92.
- Sahay G, Alakhova DY, Kabanov AV. 2010. Endocytosis of nanomedicines. *Journal of Controlled Release* 145:182-195.
- Salehi R, Rasouli S, Hamishehkar H. 2015. Smart thermo/ph responsive magnetic nanogels for the simultaneous delivery of doxorubicin and methotrexate. *International Journal of Pharmaceutics* 487:274-284.
- Salesse S, Verfaillie CM. 2002. Bcr/abl: From molecular mechanisms of leukemia induction to treatment of chronic myelogenous leukemia. *Oncogene* 21:8547-8559.
- Sanchez Y, Amran D, de Blas E, Aller P. 2010. Arsenic trioxide as an anti-tumour agent: Mechanisms of action and strategies of sensitization. *Journal of Applied Biomedicine* 8:199-208.
- Sarquis M. 1979. Chem-1 supplement - arsenic and old myths. *Journal of Chemical Education* 56:815-818.
- Scholz C, Richter A, Lehmann M, Schulze-Osthoff K, Dorken B, Daniel PT. 2005. Arsenic trioxide induces regulated, death receptor-independent cell death through a bcl-2-controlled pathway. *Oncogene* 24:7031-7042.

- Sercombe L, Veerati T, Moheimani F, Wu SY, Sood AK, Hua S. 2015. Advances and challenges of liposome assisted drug delivery. *Frontiers in Pharmacology* 6.
- Shahin M, Lavasanifar A. 2010. Novel self-associating poly(ethylene oxide)-b-poly( $\epsilon$ -caprolactone) based drug conjugates and nano-containers for paclitaxel delivery. *International Journal of Pharmaceutics* 389:213-222.
- Shao Y, Shi CY, Xu GF, Guo DD, Luo JT. 2014. Photo and redox dual responsive reversibly cross-linked nanocarrier for efficient tumor-targeted drug delivery. *Acs Applied Materials & Interfaces* 6:10381-10392.
- Shen H, Decollogne S, Dilda PJ, Hau E, Chung SA, Luk PP, et al. 2015. Dual-targeting of aberrant glucose metabolism in glioblastoma. *Journal of Experimental & Clinical Cancer Research* 34:11.
- Shen H, Luk PP, Chung SA, Decollogne S, Dilda PJ, Hogg PJ, et al. 2013. Penao, a novel mitochondria-targeted agent, has shown potent antitumor effect on glioblastoma in vitro and in vivo. *Cancer Research* 73:1701.
- Shen JM, Yin T, Tian XZ, Gao FY, Xu S. 2013. Surface charge-switchable polymeric magnetic nanoparticles for the controlled release of anticancer drug. *Acs Applied Materials & Interfaces* 5:7014-7024.
- Shen S, Li X, Cullen W, Weinfeld M, Le X. 2013. Arsenic binding to proteins. *Chemical Reviews* 113:7769-7792.
- Shen SW, Wang C, Weinfeld M, Le XC. 2013. Inhibition of nucleotide excision repair by arsenic. *Chinese Science Bulletin* 58:214-221.
- Shen ZX, Chen GQ, Ni JH, Li XS, Xiong SM, Qiu QY, et al. 1997. Use of arsenic trioxide (As<sub>2</sub>O<sub>3</sub>) in the treatment of acute promyelocytic leukemia (APL). 2. Clinical efficacy and pharmacokinetics in relapsed patients. *Blood* 89:3354-3360.
- Shimobayashi M, Hall MN. 2014. Making new contacts: The mTOR network in metabolism and signalling crosstalk. *Nature Reviews Molecular Cell Biology* 15:155-162.

- Shin ILG, Kim SY, Lee YM, Cho CS, Sung YK. 1998. Methoxy poly(ethylene glycol) epsilon-caprolactone amphiphilic block copolymeric micelle containing indomethacin. I. Preparation and characterization. *Journal of Controlled Release* 51:1-11.
- Sidhu MS, Desai KP, Lynch HN, Rhomberg LR, Beck BD, Venditti FJ. 2015. Mechanisms of action for arsenic in cardiovascular toxicity and implications for risk assessment. *Toxicology* 331:78-99.
- Singh RP, Sharma G, Sonali, Agrawal P, Pandey BL, Koch B, et al. 2016. Transferrin receptor targeted pla-tpgs micelles improved efficacy and safety in docetaxel delivery. *International journal of biological macromolecules* 83:335-344.
- Smith DM, Patel S, Raffoul F, Haller E, Mills GB, Nanjundan M. 2010. Arsenic trioxide induces a beclin-1-independent autophagic pathway via modulation of snon/skil expression in ovarian carcinoma cells. *Cell Death and Differentiation* 17:1867-1881.
- Smith MB, Griffiths EA, Thompson JE, Wang ES, Wetzler M, Freyer CW. 2014. High pseudotumor cerebri incidence in tretinoin and arsenic treated acute promyelocytic leukemia and the role of topiramate after acetazolamide failure. *Leukemia research reports* 3:62-66.
- Song HJ, Zhang J, Wang WW, Huang PS, Zhang YM, Liu JF, et al. 2015. Acid-responsive pegylated doxorubicin prodrug nanoparticles for neuropilin-1 receptor-mediated targeted drug delivery. *Colloids and Surfaces B-Biointerfaces* 136:365-374.
- Soucy NV, Ihnat MA, Kamat CD, Hess L, Post MJ, Klei LR, et al. 2003. Arsenic stimulates angiogenesis and tumorigenesis in vivo. *Toxicological Sciences* 76:271-279.
- Sun GR, Cui HG, Lin LY, Lee NS, Yang C, Neumann WL, et al. 2011. Multicompartment polymer nanostructures with ratiometric dual-emission ph-sensitivity. *Journal of the American Chemical Society* 133:8534-8543.
- Sun H, Guo B, Cheng R, Meng F, Liu H, Zhong Z. 2009. Biodegradable micelles with sheddable poly(ethylene glycol) shells for triggered intracellular release of doxorubicin. *Biomaterials* 30:6358-6366.
- Sun H, Ma L, Hu X, Zhang T. 1992. Ai-lin i treated 32 cases of acute promyelocytic leukemia. *Chinese Journal of Integrated Traditional and Western Medicine* 12:170-171.

- Sun HL, Meng FH, Cheng R, Deng C, Zhong ZY. 2013. Reduction-sensitive degradable micellar nanoparticles as smart and intuitive delivery systems for cancer chemotherapy. *Expert Opinion on Drug Delivery* 10:1109-1122.
- Sun RC, Board PG, Blackburn AC. 2011. Targeting metabolism with arsenic trioxide and dichloroacetate in breast cancer cells. *Molecular Cancer* 10.
- Sun W, Wu JY, Li J, Fang H, Du LP, Li MY. 2012. Boronate can be the fluorogenic switch for the detection of hydrogen peroxide. *Current Medicinal Chemistry* 19:3622-3634.
- Sun Y, Li YP, Huang HL, Wang YZ, Sa ZP, Wang JY, et al. 2015. Ph-sensitive poly(itaconic acid)-poly(ethylene glycol)-poly (l-histidine) micelles for drug delivery. *Journal of Macromolecular Science Part a-Pure and Applied Chemistry* 52:925-933.
- Sun Y, Yan XL, Yuan TM, Liang J, Fan YJ, Gu ZW, et al. 2010. Disassemblable micelles based on reduction-degradable amphiphilic graft copolymers for intracellular delivery of doxorubicin. *Biomaterials* 31:7124-7131.
- Sun Y, Zou W, Bian SQ, Huang YH, Tan YF, Liang J, et al. 2013. Bioreducible paa-g-peg graft micelles with high doxorubicin loading for targeted antitumor effect against mouse breast carcinoma. *Biomaterials* 34:6818-6828.
- Suzuki T, Ishibashi K, Yumoto A, Nishio K, Ogasawara Y. 2015. Utilization of arsenic trioxide as a treatment of cisplatin-resistant non-small cell lung cancer pc-9/cddp and pc-14/cddp cells. *Oncology Letters* 10:805-809.
- Swindell EP, Hankins PL, Chen HM, Miodragovic DU, O'Halloran TV. 2013. Anticancer activity of small-molecule and nanoparticulate arsenic(iii) complexes. *Inorganic Chemistry* 52:12292-12304.
- Szegezdi E, Cahill S, Meyer M, O'Dwyer M, Samali A. 2006. Trail sensitisation by arsenic trioxide is caspase-8 dependent and involves modulation of death receptor components and akt. *British Journal of Cancer* 94:398-406.
- Talelli M, Rijcken CJF, Oliveira S, van der Meel R, Henegouwen P, Lammers T, et al. 2011. Nanobody - shell functionalized thermosensitive core-crosslinked polymeric micelles for active drug targeting. *Journal of Controlled Release* 151:183-192.

- Tangasangasakri M, Takemoto H, Naito M, Maeda Y, Sueyoshi D, Kim HJ, et al. 2016. Sirna-loaded polyion complex micelle decorated with charge-conversional polymer tuned to undergo stepwise response to intra-tumoral and intra-endosomal pHs for exerting enhanced RNAi efficacy. *Biomacromolecules* 17:246-255.
- Tarhini AA, Kirkwood JM, Tawbi H, Gooding WE, Islam MF, Agarwala SS. 2008. Safety and efficacy of arsenic trioxide for patients with advanced metastatic melanoma. *Cancer* 112:1131-1138.
- Thomas DJ, Waters SB, Styblo M. 2004. Elucidating the pathway for arsenic methylation. *Toxicology and Applied Pharmacology* 198:319-326.
- Thornalley PJ, Rabbani N. 2011. Glyoxalase in tumorigenesis and multidrug resistance. *Seminars in Cell & Developmental Biology* 22:318-325.
- Tong R, Tang L, Ma L, Tu CL, Baumgartner R, Cheng JJ. 2014. Smart chemistry in polymeric nanomedicine. *Chemical Society Reviews* 43:6982-7012.
- Tsivgoulis GM, Sotiropoulos DN, Ioannou PV. 1991. Rac-1,2-dicycloxypropyl-3-arsonic acids - arsonolipid analogs of phosphonolipids. *Phosphorus Sulfur and Silicon and the Related Elements* 63:329-334.
- Uchegbu IF. 2006. Pharmaceutical nanotechnology: Polymeric vesicles for drug and gene delivery. *Expert opinion on drug delivery* 3:629-640.
- Ulery BD, Nair LS, Laurencin CT. 2011. Biomedical applications of biodegradable polymers. *Journal of Polymer Science Part B-Polymer Physics* 49:832-864.
- van der Meel R, Vehmeijer LJC, Kok RJ, Storm G, van Gaal EVB. 2013. Ligand-targeted particulate nanomedicines undergoing clinical evaluation: Current status. *Advanced Drug Delivery Reviews* 65:1284-1298.
- Vangeyte P, Leyh B, Auvray L, Grandjean J, Misselyn-Bauduin AM, Jerome R. 2004. Mixed self-assembly of poly(ethylene oxide)-b-poly(epsilon-caprolactone) copolymers and sodium dodecyl sulfate in aqueous solution. *Langmuir* 20:9019-9028.

- Varade D, Joshi T, Aswal VK, Goyal PS, Hassan PA, Bahadur P. 2005. Effect of salt on the micelles of cetyl pyridinium chloride. *Colloids and Surfaces a-Physicochemical and Engineering Aspects* 259:95-101.
- Venugopal J, Prabhakaran MP, Low S, Choon AT, Zhang YZ, Deepika G, et al. 2008. Nanotechnology for nanomedicine and delivery of drugs. *Current Pharmaceutical Design* 14:2184-2200.
- Vuky J, Yu R, Schwartz L, Motzer RJ. 2002. Phase ii trial of arsenic trioxide in patients with metastatic renal cell carcinoma. *Investigational New Drugs* 20:327-330.
- Walker AM, Stevens JJ, Ndebele K, Tchounwou PB. 2010. Arsenic trioxide modulates dna synthesis and apoptosis in lung carcinoma cells. *International Journal of Environmental Research and Public Health* 7:1996-2007.
- Walter I, Schwerdtle T, Thuy C, Parsons JL, Dianov GL, Hartwig A. 2007. Impact of arsenite and its methylated metabolites on parp-1 activity, parp-1 gene expression and poly(adp-ribosylation) in cultured human cells. *DNA Repair* 6:61-70.
- Wang H, Liu Y, Wang X, Liu DH, Sun ZQ, Wang C, et al. 2015. Randomized clinical control study of locoregional therapy combined with arsenic trioxide for the treatment of hepatocellular carcinoma. *Cancer* 121:2917-2925.
- Wang L, Li XL, Liu XY, Lu K, Chen N, Li PP, et al. 2015. Enhancing effects of indirubin on the arsenic disulfide-induced apoptosis of human diffuse large b-cell lymphoma cells. *Oncology Letters* 9:1940-1946.
- Wang W, Sun H, Meng F, Ma S, Liu H, Zhong Z. 2012. Precise control of intracellular drug release and anti-tumor activity of biodegradable micellar drugs via reduction-sensitive shell-shedding. *Soft Matter* 8:3949-3956.
- Wang ZQ, Liu W, Xu HB, Yang XL. 2007. Preparation and in vitro studies of stealth pegylated plga nanoparticles as carriers for arsenic trioxide. *Chinese Journal of Chemical Engineering* 15:795-801.
- Warburg O, Wind F, Negelein E. 1926. Metabolism of tumors in the body. *Klin Wochenschr* 5:829-832.

- Waxman S, Anderson KC. 2001. History of the development of arsenic derivatives in cancer therapy. *Oncologist* 6:3-10.
- Wei XL, Wang YG, Zeng WF, Huang F, Qin L, Zhang CL, et al. 2012. Stability influences the biodistribution, toxicity, and anti-tumor activity of doxorubicin encapsulated in peg-pe micelles in mice. *Pharmaceutical Research* 29:1977-1989.
- Westervelt P, Brown RA, Adkins DR, Khoury H, Curtin P, Hurd D, et al. 2001. Sudden death among patients with acute promyelocytic leukemia treated with arsenic trioxide. *Blood* 98:266-271.
- Wilhelm M, Zhao CL, Wang YC, Xu RL, Winnik MA, Mura JL, et al. 1991. Polymer micelle formation .3. Poly(styrene-ethylene oxide) block copolymer micelle formation in water - a fluorescence probe study. *Macromolecules* 24:1033-1040.
- Williams KJ. 2009. The introduction of 'chemotherapy' using arsphenamine - the first magic bullet. *Journal of the Royal Society of Medicine* 102:343-348.
- Woo SH, Park IC, Park MJ, An S, Lee HC, Jin HO, et al. 2004. Arsenic trioxide sensitizes cd95/fas-induced apoptosis through ros-mediated upregulation of cd95/fas by nf-kappa b activation. *International Journal of Cancer* 112:596-606.
- Woodruff MA, Hutmacher DW. 2010. The return of a forgotten polymer-polycaprolactone in the 21st century. *Progress in Polymer Science* 35:1217-1256.
- Wu GY, Fang YZ, Yang S, Lupton JR, Turner ND. 2004. Glutathione metabolism and its implications for health. *Journal of Nutrition* 134:489-492.
- Wu J, Henderson C, Feun L, Van Veldhuizen P, Gold P, Zheng H, et al. 2010. Phase ii study of darinaparsin in patients with advanced hepatocellular carcinoma. *Investigational New Drugs* 28:670-676.
- Wu JZ, Ho PC. 2006. Evaluation of the in vitro activity and in vivo bioavailability of realgar nanoparticles prepared by cryo-grinding. *European Journal of Pharmaceutical Sciences* 29:35-44.

- Wu XS, Shi JM, Wu Y, Tao Y, Hou J, Meng XQ, et al. 2010. Arsenic trioxide-mediated growth inhibition of myeloma cells is associated with an extrinsic or intrinsic signaling pathway through activation of trail or trail receptor 2. *Cancer Biology & Therapy* 10:1202-1215.
- Wu YK, Yang CL, Lai QY, Zhang Q, Wang W, Yuan Z. 2015. Fabrication of thermo-sensitive complex micelles for reversible cell targeting. *Journal of Materials Science-Materials in Medicine* 26:13.
- Wyman IW, Liu GJ. 2013. Micellar structures of linear triblock terpolymers: Three blocks but many possibilities. *Polymer* 54:1950-1978.
- Xie SL, Yang MH, Chen K, Huang H, Zhao XW, Zang YS, et al. 2015. Efficacy of arsenic trioxide in the treatment of malignant pleural effusion caused by pleural metastasis of lung cancer. *Cell Biochemistry and Biophysics* 71:1325-1333.
- Xiong XB, Ma ZS, Lai R, Lavasanifar A. 2010a. The therapeutic response to multifunctional polymeric nano-conjugates in the targeted cellular and subcellular delivery of doxorubicin. *Biomaterials* 31:757-768.
- Xiong XB, Mahmud A, Uludag H, Lavasanifar A. 2007. Conjugation of arginine-glycine-aspartic acid peptides to poly(ethylene oxide)-b-poly(epsilon-caprolactone) micelles for enhanced intracellular drug delivery to metastatic tumor cells. *Biomacromolecules* 8:874-884.
- Xiong XB, Mahmud A, Uludag H, Lavasanifar A. 2008. Multifunctional polymeric micelles for enhanced intracellular delivery of doxorubicin to metastatic cancer cells. *Pharmaceutical Research* 25:2555-2566.
- Xiong XB, Uludag H, Lavasanifar A. 2010b. Virus-mimetic polymeric micelles for targeted siRNA delivery. *Biomaterials* 31:5886-5893.
- Xu F, Yan TT, Luo YL. 2013. Thermosensitive poly(n-isopropyl acrylamide-co-n,n-dimethyl acryl amide)-block-poly(d,l-lactide) amphiphilic block copolymer micelles for prednisone drug release. *Journal of Bioactive and Compatible Polymers* 28:66-85.
- Yang CA, Tan JPK, Cheng W, Attia ABE, Ting CTY, Nelson A, et al. 2010. Supramolecular nanostructures designed for high cargo loading capacity and kinetic stability. *Nano Today* 5:515-523.

- Yang GF, Li XH, Zhao Z, Wang WB. 2010. Arsenic trioxide up-regulates fas expression in human osteosarcoma cells. *Chinese Medical Journal* 123:1768-1773.
- Yang M, Ding YT, Zhang LY, Qian XP, Jiang XQ, Liu BR. 2007. Novel thermosensitive polymeric micelles for docetaxel delivery. *Journal of Biomedical Materials Research Part A* 81A:847-857.
- Yang XJ, Sun DG, Tian Y, Ling SB, Wang LM. 2015. Metformin sensitizes hepatocellular carcinoma to arsenic trioxide-induced apoptosis by downregulating bcl2 expression. *Tumor Biology* 36:2957-2964.
- Yang YP, Liang ZQ, Gao B, Jia YL, Qin ZH. 2008. Dynamic effects of autophagy on arsenic trioxide-induced death of human leukemia cell line hl60 cells. *Acta Pharmacologica Sinica* 29:123-134.
- Yang ZW, Yang MH, Peng JA. 2008. Evaluation of arsenic trioxide-loaded albumin nanoparticles as carriers: Preparation and antitumor efficacy. *Drug Development and Industrial Pharmacy* 34:834-839.
- Yin G, Chen G, Zhou Z, Li Q. 2015. Modification of peg-b-pcl block copolymer with high melting temperature by the enhancement of poss crystal and ordered phase structure. *Rsc Advances* 5:33356-33363.
- Yin TJ, Wang L, Yin LF, Zhou JP, Huo MR. 2015. Co-delivery of hydrophobic paclitaxel and hydrophilic aurka specific sirna by redox-sensitive micelles for effective treatment of breast cancer. *Biomaterials* 61:10-25.
- Yousefpour P, Atyabi F, Farahani EV, Sakhtianchi R, Dinarvand R. 2011. Polyanionic carbohydrate doxorubicin-dextran nanocomplex as a delivery system for anticancer drugs: In vitro analysis and evaluations. *International Journal of Nanomedicine* 6:1487-1496.
- Yu XF, Yang XQ, Horte S, Kizhakkedathu JN, Brooks DE. 2014. A pH and thermosensitive choline phosphate-based delivery platform targeted to the acidic tumor microenvironment. *Biomaterials* 35:278-286.
- Yu Y, Liao M, Liu R, Chen J, Feng H, Fu Z. 2014. Overexpression of lactate dehydrogenase-a in human intrahepatic cholangiocarcinoma: Its implication for treatment. *World Journal of Surgical Oncology* 12.

- Zagana P, Haikou M, Klepetsanis P, Giannopoulou E, Loannou PV, Antimisiaris SG. 2008. In vivo distribution of arsonoliposomes: Effect of vesicle lipid composition. *International Journal of Pharmaceutics* 347:86-92.
- Zeng LJ, Li JG, Wang Y, Qian CC, Chen YT, Zhang QB, et al. 2014. Combination of sirna-directed kras oncogene silencing and arsenic-induced apoptosis using a nanomedicine strategy for the effective treatment of pancreatic cancer. *Nanomedicine-Nanotechnology Biology and Medicine* 10:463-472.
- Zhai B, Jiang X, He CJ, Zhao DL, Ma LX, Xu LS, et al. 2015. Arsenic trioxide potentiates the anti-cancer activities of sorafenib against hepatocellular carcinoma by inhibiting akt activation. *Tumor Biology* 36:2323-2334.
- Zhang HN, Yang LN, Ling JY, Czajkowsky DM, Wang JF, Zhang XW, et al. 2015. Systematic identification of arsenic-binding proteins reveals that hexokinase-2 is inhibited by arsenic. *Proceedings of the National Academy of Sciences of the United States of America* 112:15084-15089.
- Zhang L, Kim S, Ding WP, Tong YY, Zhang XL, Pan MG, et al. 2015a. Arsenic sulfide inhibits cell migration and invasion of gastric cancer in vitro and in vivo. *Drug Design Development and Therapy* 9:5579-5590.
- Zhang L, Tian W, Kim S, Ding WP, Tong YY, Chen SY. 2015b. Arsenic sulfide, the main component of realgar, a traditional chinese medicine, induces apoptosis of gastric cancer cells in vitro and in vivo. *Drug Design Development and Therapy* 9:79-92.
- Zhang N, Wu Z-M, McGowan E, Shi J, Hong Z-B, Ding C-W, et al. 2009. Arsenic trioxide and cisplatin synergism increase cytotoxicity in human ovarian cancer cells: Therapeutic potential for ovarian cancer. *Cancer Science* 100:2459-2464.
- Zhang Q, Vakili MR, Li XF, Lavasanifar A, Le XC. 2014. Polymeric micelles for gsh-triggered delivery of arsenic species to cancer cells. *Biomaterials* 35:7088-7100.
- Zhang QY, Mao JH, Liu P, Huang QH, Lu J, Xie YY, et al. 2009. A systems biology understanding of the synergistic effects of arsenic sulfide and imatinib in bcr/abl-associated leukemia. *Proceedings of the National Academy of Sciences of the United States of America* 106:3378-3383.

- Zhang XL, Huang YX, Ghazwani M, Zhang P, Li J, Thorne SH, et al. 2015. Tunable ph-responsive polymeric micelle for cancer treatment. *Acs Macro Letters* 4:620-623.
- Zhang XW, Yan XJ, Zhou ZR, Yang FF, Wu ZY, Sun HB, et al. 2010. Arsenic trioxide controls the fate of the pml-rar alpha oncoprotein by directly binding pml. *Science* 328:240-243.
- Zhang XY, Yang SM, Zhang HP, Yang Y, Sun SB, Chang JP, et al. 2015. Endoplasmic reticulum stress mediates the arsenic trioxide-induced apoptosis in human hepatocellular carcinoma cells. *International Journal of Biochemistry & Cell Biology* 68:158-165.
- Zhang YF, Zhang M, Huang XL, Fu YJ, Jiang YH, Bao LL, et al. 2015. The combination of arsenic and cryptotanshinone induces apoptosis through induction of endoplasmic reticulum stress-reactive oxygen species in breast cancer cells. *Metallomics* 7:165-173.
- Zhao LL, Liu YF, Peng LJ, Fei AM, Cui W, Miao SC, et al. 2015. Arsenic trioxide rewires mantle cell lymphoma response to bortezomib. *Cancer Medicine* 4:1754-1766.
- Zhao QH, Zhang Y, Liu Y, Wang HL, Shen YY, Yang WJ, et al. 2010. Anticancer effect of realgar nanoparticles on mouse melanoma skin cancer in vivo via transdermal drug delivery. *Medical Oncology* 27:203-212.
- Zhao WZ, Lu X, Yuan Y, Liu CS, Yang BC, Hong H, et al. 2011. Effect of size and processing method on the cytotoxicity of realgar nanoparticles in cancer cell lines. *International Journal of Nanomedicine* 6:1569-1577.
- Zhao Y, Zhou YX, Wang DS, Gao YJ, Li JW, Ma SJ, et al. 2015. Ph-responsive polymeric micelles based on poly(2-ethyl-2-oxazoline)-poly(D,L-lactide) for tumor-targeting and controlled delivery of doxorubicin and p-glycoprotein inhibitor. *Acta Biomaterialia* 17:182-192.
- Zhao ZH, Wang XM, Zhang ZJ, Zhang H, Liu HY, Zhu XL, et al. 2015. Real-time monitoring of arsenic trioxide release and delivery by activatable t-1 imaging. *Acs Nano* 9:2749-2759.
- Zhao ZH, Zhang H, Chi XQ, Li H, Yin ZY, Huang DT, et al. 2014. Silica nanovehicles endow arsenic trioxide with an ability to effectively treat cancer cells and solid tumors. *Journal of Materials Chemistry B* 2:6313-6323.
- Zhong F, Zhang S, Shao C, Yang J, Wu X. 2010. Arsenic trioxide inhibits cholangiocarcinoma cell growth and induces apoptosis. *Pathology & Oncology Research* 16:413-420.

- Zhou J, Zhang YM, Li JM, Li XX, Hou JX, Zhao YQ, et al. 2010. Single-agent arsenic trioxide in the treatment of children with newly diagnosed acute promyelocytic leukemia. *Blood* 115:1697-1702.
- Zhou XX, Sun X, Cooper KL, Wang F, Liu KJ, Hudson LG. 2011. Arsenite interacts selectively with zinc finger proteins containing c3h1 or c4 motifs. *Journal of Biological Chemistry* 286:22855-22863.
- Zhou XX, Sun X, Mobarak C, Gandolfi AJ, Burchiel SW, Hudson LG, et al. 2014. Differential binding of monomethylarsonous acid compared to arsenite and arsenic trioxide with zinc finger peptides and proteins. *Chemical Research in Toxicology* 27:690-698.
- Zhou ZL, Badkas A, Stevenson M, Lee JY, Leung YK. 2015. Herceptin conjugated plga-phis-peg ph sensitive nanoparticles for targeted and controlled drug delivery. *International Journal of Pharmaceutics* 487:81-90.
- Zhu H-H, Wu D-P, Jin J, Li J-Y, Ma J, Wang J-X, et al. 2013. Oral tetra-arsenic tetra-sulfide formula versus intravenous arsenic trioxide as first-line treatment of acute promyelocytic leukemia: A multicenter randomized controlled trial. *Journal of Clinical Oncology* 31:4215-+.
- Zhu HH, Yalcin T, Li L. 1998. Analysis of the accuracy of determining average molecular weights of narrow polydispersity polymers by matrix-assisted laser desorption ionization time-of-flight mass spectrometry. *Journal of the American Society for Mass Spectrometry* 9:275-281.
- Zhu J, Chen Z, Lallemand-Breitenbach V, de The H. 2002. How acute promyelocytic leukaemia revived arsenic. *Nature Reviews Cancer* 2:705-713.
- Zhu J, Koken MHM, Quignon F, ChelbiAlix MK, Degos L, Wang ZY, et al. 1997. Arsenic-induced pml targeting onto nuclear bodies: Implications for the treatment of acute promyelocytic leukemia. *Proceedings of the National Academy of Sciences of the United States of America* 94:3978-3983.
- Zhu JW, Zheng M. 2012. Verrucous carcinoma due to arsenic ingestion in a psoriasis patient. *Journal of Cutaneous Medicine and Surgery* 16:445-447.
- Zhu L, Torchilin VP. 2013. Stimulus-responsive nanopreparations for tumor targeting. *Integrative Biology* 5:96-107.

Zrazhevskiy P, Sena M, Gao XH. 2010. Designing multifunctional quantum dots for bioimaging, detection, and drug delivery. *Chemical Society Reviews* 39:4326-4354.